Order Number 8821370

Gas exchange in seawater with special emphasis on open-cycle ocean thermal energy conversion

Zapka, Manfred Jürgen, Ph.D.

University of Hawaii, 1988

U·M·I
300 N. Zeeb Rd.
Ann Arbor, MI 48106

PLEASE NOTE:

In all cases this material has been filmed in the best possible way from the available copy. Problems encountered with this document have been identified here with a check mark __✓__.

1. Glossy photographs or pages _____
2. Colored illustrations, paper or print _____
3. Photographs with dark background _____
4. Illustrations are poor copy _____
5. Pages with black marks, not original copy __✓__
6. Print shows through as there is text on both sides of page _____
7. Indistinct, broken or small print on several pages _____
8. Print exceeds margin requirements _____
9. Tightly bound copy with print lost in spine _____
10. Computer printout pages with indistinct print _____
11. Page(s) _____ lacking when material received, and not available from school or author.
12. Page(s) _____ seem to be missing in numbering only as text follows.
13. Two pages numbered _____. Text follows.
14. Curling and wrinkled pages __✓__
15. Dissertation contains pages with print at a slant, filmed as received _____
16. Other _____

_____

_____

GAS EXCHANGE IN SEAWATER WITH SPECIAL EMPHASIS ON OPEN-CYCLE OCEAN THERMAL ENERGY CONVERSION

A DISSERTATION SUBMITTED TO THE GRADUATE DIVISION OF THE UNIVERSITY OF HAWAII IN PARTIAL FULFILLMENT OF THE REQUIREMENTS FOR THE DEGREE OF

DOCTOR OF PHILOSOPHY

IN OCEAN ENGINEERING

MAY 1988

by

Manfred Jurgen Zapka

Dissertation Committee:

Hans-Jurgen Krock, Chairman
Frans Gerritsen
Harold G. Loomis
Gordon L. Dugan
Francis J. Sansone

Acknowledgements

The author wishes to express his appreciation to all committee members for their support and help. Special thanks and deepest appreciation is extended to committee chairman Dr. Hans-Jurgen Krock for his never ceasing help and encouragement. Without his guidance, support, and active interest, the completion of this study would have been impossible. Special thanks also goes to Dr. Frank Sansone for allowing use of his laboratory facilities and for his encouragement and active interest.

The help and support by the staff of J.K.K. Look Laboratory, under the direction of Dr. Hans-Jurgen Krock, and notably the invaluable assistance of senior technician Mr. Henry Ho is deeply appreciated.

The financial support by the Pacific International Center for High Technology Research, under the direction of Dr. Paul Yuen, is greatly appreciated. Special thanks to OTEC project manager Mr. Loyd Trimble for his interest and support.

The financial assistance of the Hawaii Natural Energy Institute, under the direction of Dr. Patrick Takahashi, is appreciated. Special thanks to researcher Mr. Arthur Seki for his interest and friendly cooperation.

The assistance of staff members and students of the Department of Oceanography is greatly appreciated. Special

thanks to research associate Ms. Christine Andrews for her friendly help and patience.

The loan of camera equipment by Dr. Paul D. Snipes, Director of Institutional Resources Service Center, is greatly appreciated.

The assistance of staff members of Pacific Biological Research Center, under the direction of Dr. Robert Kane, is greatly appreciated.

Special thanks to my fellow students Steve Oney, Richard Winkler, and Dayananda Vithanage for their friendly assistance in the experimental work.

Thanks goes also to Dr. Ludwig H. Seidl and to Mr. Peter Rosti for allowing use of their AutoCAD workstations.

To many other, unnamed individuals who contributed to the present study goes the authors warmest MAHALO. Without all the friendly assistance and support so warmly given to the author, this research project would never have been successful.

The author will never forget everybody's kindness.

ABSTRACT

The present study addresses gas transfer in seawater. Special emphasis is on gas transfer processes in connection with Open-Cycle Ocean Thermal Energy Conversion (OC-OTEC) applications.

The evolution of non-condensible gases in the OC-OTEC evaporator and condenser may impose a deterioration of the overall performance. Preliminary tests conducted in part by the author indicated accelerated gas transfer in seawater in comparison to fresh water.

An experimental study was carried out to identify the probable reasons and mechanism for accelerated gas transfer processes in seawater. Furthermore, basic process requirements for an OC-OTEC pre-deaeration procedure were investigated. In order to compare gas transfer in seawater with extensively documented transfer characteristics of fresh water, all tests were done using both seawater and fresh water in the same experimental setting.

The conducted experiments probed the mechanisms regulating gas transfer in bubbles and in a packed column.

By changing the mode of air injection the effect of bubble coalescence and the associated generation of increased interfacial surfaces area were determined. When, by experimental means, bubble coalescence was avoided, the resistance of the liquid-gas interface to gas transfer in

bubble contact was directly measured. Gas transfer in a packed column was used to assess transfer rates of uncontaminated water surfaces by minimizing the effects of the accumulation of surfactants on liquid-gas interfaces on transfer, which is commonly observed in bubble contact transfer processes.

The rise velocity of bubbles in seawater has only been addressed on a very limited basis in the literature. Since the rise rate of a bubble determines its residence time in the water column and, thus, affects the magnitude of liquid-gas interface, rise velocities of various size bubbles were determined in fresh water and seawater. Besides assessing the terminal rise speed of bubbles, the effect of aging of bubbles on the distance of rise necessary to acquire terminal speed was investigated.

Gas transfer characteristics in OC-OTEC subsystems were investigated in the barometric OC-OTEC riser and in a low pressure reservoir. The effect of artificial nucleation on the reinjection of air into the system downcomer was investigated .

The results of these experiments suggested fundamental differences in the magnitude of overall gas transfer processes in seawater and fresh water. Bubble coalescence was significantly less in seawater than in fresh water, which resulted in greater liquid-gas interfacial area and associated higher transfer rates in seawater. If bubbles

did not coalesce the magnitude of overall gas transfer was similar in seawater and in fresh water. The liquid transfer coefficient, which expresses gas transfer rates per unit surface area, for seawater was smaller than or equal to that of fresh water.

Gas transfer rates in bubble aeration were determined to be the same in clean offshore seawater and filtered Hawaiian coastal seawater. Gas transfer in unfiltered coastal seawater was less, which suggested impedance of transfer rates due to higher concentrations of suspended matter or filterable surfactant in coastal seawater.

Gas transfer rates for dissolved nitrogen were determined to be similar to those for dissolved oxygen.

The terminal velocities of bubbles rising in seawater and fresh water were observed to be similar. The rise speed of bubbles in a bubble plume was higher than those for individual bubbles.

Gas liberation in OC-OTEC subsystems was primarily dependent on the system vacuum, residence time of water at low pressure, and amount of bubble seeding. For OC-OTEC applications it was found that deaeration rates were insufficient without active bubble seeding. Even with bubble seeding the total amount of deaeration in the barometric upcomer only was relatively low. Consequently, a reservoir had to be incorporated in the feed water

stream in order to increase the residence time of water at low system pressure.

Reinjection of air in the relatively short test downcomer resulted in small but consistent reabsorption rates for seawater. For fresh water no reabsorption could be detected. The amount of reaeration in seawater was dependent on the residence time of the water in the discharge pipe and on air injection rates, and was therefore higher at small flow rates.

A prototype OC-OTEC deaeration device was conceived from the experimental results. Provided appropriate system conditions are met, an approximately 85% removal of dissolved gases from the OC-OTEC feed stream appears to be feasible.

TABLE OF CONTENTS

LIST OF TABLES

LIST OF FIGURES

CHAPTER I

INTRODUCTION

Human demand for energy is increasing at an accelerated rate. While the population on earth has exceeded the 5 billion mark and is doubling approximately every 35 years, energy consumption is doubling about every 12 years [115]. At present the worlds energy demand is almost entirely met by various forms of fossil fuel. Presently reliable energy technologies based on fossil fuel, which include fuel exploration and transportation, allow little incentive for the pursuit of alternative strategies to meet future demands.

Though the requirement for reliability in energy supply is undeniable, detrimental factors resulting from the present overwhelming reliance on fossil fuels are becoming more and more relevant.

Air pollution caused by automobile exhaust and other domestic and industrial emissions related to fossil fuel use very explicitly underline the vulnerability of the environment to this artificial stress. Acid rain is threatening the existence of vast forest areas in Europe and North America. Carbon dioxide (CO_2) released into the atmosphere from burning fossil fuels restricts the flow of radiation and thereby raises the temperature on a global scale. This is expected to result in dramatic

climatic changes and inundation of precious, densely populated coastal areas from the resultant rise in sea level. Such changes can be expected to have generally detrimental socio-political consequences. Tangible evidence is already at hand to prove that there is an acceleration in the rate of increase of the concentration of carbon dioxide in the atmosphere. Measurements show that the amount of CO_2 has risen from 290 ppm in 1860 to 340 ppm at present [44]. Projections predict a probable increase to 370 ppm by the year 2000 and possibly 660 ppm near the middle of the next century [44].

Environmental concerns are not the only reason for past and present endeavors to explore large scale use of alternate energy forms. The well known oil-embargo of 1973 created sudden, sobering evidence of how severely oil-dependent the world community is. Efforts to fill the oil gap with increased utilization of coal and nuclear energy have resulted in increased acid rain and concerns about nuclear accidents.

The present temporary oil-glut seems to have changed the more prudent approach to energy usage characteristic of the late 70's. Ample supplies and low cost of today's oil are likely to only be a short lived condition. The development and utilization of renewable sources of energy are increasingly recognized as major future challenges of humankind.

There has been, and continues to be, interest in a great number of renewable energy sources such as wind, geothermal, solar thermal, photovoltaic, and tidal, to name a few.

Solar energy has gained perhaps the greatest attention, and a large variety of approaches to harness the sun's power are now in use. However, the major drawbacks to direct usage are intermittent availability and variation in energy density. Large storage facilities are necessary for uninterrupted and steady use of solar power.

A major portion of the total solar radiation reaching the earth is trapped by the surface layer of the tropical oceans thereby creating a vast natural thermal storage reservoir. The heated water masses are contained in a layer some 50-100 m thick which exhibits a relatively constant temperature due to internal convection. Below the thermocline at the bottom of this layer the temperature drops rapidly. Below the thermocline at depths of some 800-1000 meter are water masses which originate at high latitudes and have temperatures of about 5 - 7 ^{0}C . This condition constitutes a temperature differential between the surface layer and the deep water of some 20-25 ^{0}C in the tropical oceans. Although the temperature difference is small in comparison to that usually used in energy generation, the large size of the

thermal reservoir constitutes a resource that is almost inexhaustible.

The French scientist Jacques d'Arsonval [23] first conceived the idea of tapping the stored thermal energy of the tropical ocean using the technology which is now called OTEC, an acronym for ocean thermal energy conversion. It was, however, the French engineer George Claude [23] who actually endeavored to construct the first practical device to utilize this energy source.

There are two general OTEC schemes, the closed-cycle and the open-cycle. In the case of the closed-cycle OTEC system a working fluid which has a low boiling point is evaporated by the warm seawater which is passed through an appropriate heat exchanger. After power extraction by working fluid vapor passage through a turbine, the cold deep water is used in another exchange device to condense the working fluid vapor to its liquid form which is then pumped back to the evaporator to close the cycle. In the open-cycle OTEC scheme water itself is the working fluid. The warm seawater is evaporated by exposure to a vacuum level below its vapor pressure and the resulting steam is passed through a turbine for power extraction and condensed when it comes into direct or indirect contact with the cold water.

A major difference in the components required for closed and open cycle OTEC systems is the need for a heat

exchangers in the evaporator for the closed cycle system. Heat exchangers are prone to corrosion and biofouling and make up a major portion of the closed-cycle OTEC plant's capital costs. Thermal losses associated with the heat exchange through the surfaces therefore make direct contact open cycle in principle more efficient. The reason why open-cycle OTEC development has lagged that of closed cycle is the fact that the latter system has fewer operational uncertainties and difficulties. System components for closed-cycle OTEC can be more easy adapted from available devices. The open-cycle scheme in contrast has more uncertain operational characteristics.

Since open-cycle OTEC is the subject for the present study only this system will be treated in detail in the remainder of this report.

1.1 Concept of OC-OTEC

There are three pertinent power cycle variations of OC-OTEC, namely the lift/foam cycle, the Claude cycle and the hybrid cycle.

Variation of the lift/foam cycle avoid the use of a vapor turbine. The common feature among all the variations is the use of two-phase flow to achieve the required lift. The warm surface water is allowed to partially flash in a vacuum chamber creating a relatively

uniform water-steam mixture. This mixture rises because the steam produced in the flashing of the water drags the droplets upwards. Cold water is sprayed into the top portion of the vessel to condense the generated steam and thereby maintain the upward vapor flow. Shaft power is extracted from a hydraulic turbine which can either be located in the intake or discharge streams.

The obvious advantage of this power cycle is the use of a hydraulic rather than a vapor turbine. Existing high efficiency hydraulic turbines can be easily modified for use in this cycle. Apart of this obvious advantages the lift/foam cycles still exhibit major operational uncertainties.

By far the most popular OC-OTEC scheme is the Claude-cycle, christened after the French engineer George Claude. In 1930 Claude [23] proposed the first OC-OTEC scheme. Warm seawater is used as the working fluid. Warm surface water is admitted to an flash evaporation vessel which has a system pressure less than the corresponding vapor pressure of the water. From the intake water some 0.5% [77] evaporates. The resulting steam expands on a vapor turbine where useful shaft work is extracted. The low pressure steam is then directed to the condenser where condensation of the steam takes place. The fact that the condensate needs not be returned to the evaporator gives rise to this cycle's

name, "open." Optionally a direct contact or a surface condenser can be used. In an OC-OTEC plant with a surface condenser the condensate can be utilized as desalinated water. If direct contact condensation is applied fresh water production is not possible and the condensate cold water is mixed with the discharge stream. Figure 1.1 depicts a schematic of an OC-OTEC system.

One of the main obstacles to overcome in the development of a full size OC-OTEC plant is the design of a large low-pressure gas turbine. Turbines for large scale plants require unusually large diameters. For a 100 MW plant, for example, a turbine of 43.6 m diameter is envisioned [102]. The resulting stress on blades necessitates the development of innovative blade designs and materials. Studies have shown [102] that the use of existing, smaller turbines, such as secondary stages in some conventional or nuclear power plants, might be possible, although losses inherent in this configuration would decrease the overall efficiency.

A power cycle which avoids uncertainties associated with the low pressure vapor turbine is the hybrid cycle. This cycle is an attempt to combine the best features and to avoid the worst features of the open- and close-cycles. A schematic of the OTEC Hybrid Cycle is shown in figure 1.2.

In the hybrid cycle warm surface water is flash

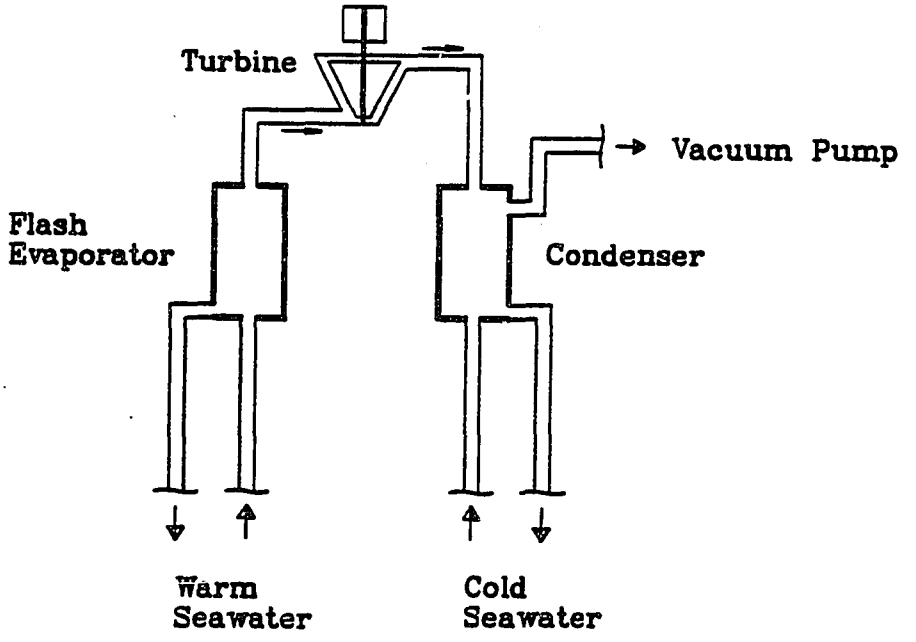

Figure 1.1 Schematic of OC-OTEC [25]

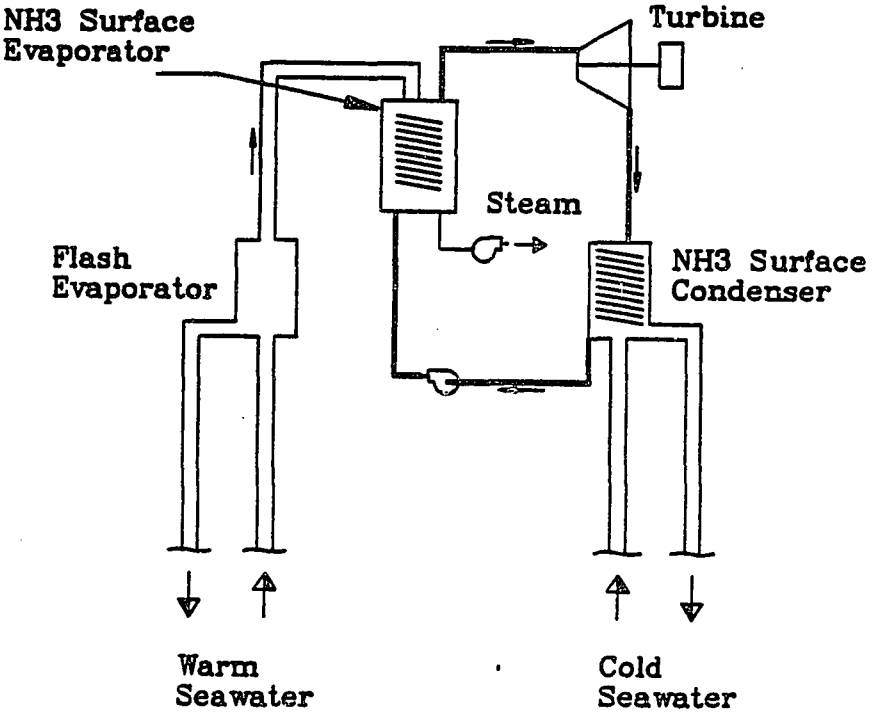

Figure 1.2 Schematic of Hybrid Cycle (from [25])

evaporated as in the open-cycle scheme. The heat in the resulting steam is then transferred to a low boiling point working fluid, such as ammonia, using a conventional surface heat exchanger. The steam condenses to produce potable water. The evaporated working fluid expands on a conventional ammonia turbine and produces shaft power. Downstream of the turbine the low pressure working fluid is condensed by cold deep water using a surface condenser. Employing less troublesome system components than the Claude-cycle, the hybrid cycle produces both energy and potable water. The drawback is that one more heat transfer step is required for the hybrid cycle. The associated thermal losses burden the already small Carnot efficiency of the OTEC cycle.

Although appreciable obstacles have still to be overcome in its development, the open-cycle system has recently received more favorable attention than its, at present, more technically advanced closed-cycle counterpart. The focus is OC-OTEC's ability to produce fresh water and its potentially high thermal conversion efficiency.

Research and development endeavors are presently being carried out world wide to address the main OC-OTEC issues such as effective deployment techniques for the cold water pipe, efficient direct contact and surface heat exchangers, material and methods for heat exchanger

surfaces minimizing biofouling and corrosion, development of effective deaeration devices, to name the most pertinent.

Although the present low energy prices tend to decrease the interest in OTEC development there are other incentives which could make OTEC viable in the relatively near future. The cold water pipe, the unique feature of any OTEC plant, provides access to a vast and unexploited ocean resource. Apart from creating electricity the cold water contains large quantities of nutrients which promote photosynthesis in marine ecosystems. Commercial aquaculture enterprises can potentially blossom where a continuous cold water supply is provided. Future development envisions cold water pumped by OTEC generated electricity to supply large-scale aquaculture operations.

1.2 Previous Research Developments

Claude's design efforts were based on the pioneering work of his teacher and mentor Jacques d'Arsonval. D'Arsonval's conceived power cycle was the closed-cycle using warm sea water to evaporate a low boiling point working fluid. His development, however, never went beyond the conceptual stages and it was left to Claude to successfully demonstrate the OTEC principle.

After successfully operating a demonstration plant in

Belgium, which produced net power, Claude proceeded with a shore based facility at Mantanzas Bay, Cuba. His experimental work proved successful in producing a net power of 60 kW [23]. Unfortunately his facility was short lived, for his cold water pipe was scattered by a storm after only 11 days of operation. Claude proceeded with his OC-OTEC work by conceiving a floating power plant off the coast of Brazil. Loss of the cold water pipe, however, finally stopped his personal endeavors to build an OC-OTEC plant.

In the period following Claude's initial development thrust, French organizations and governmental agencies kept up the interest in OTEC, but progress was rather slow.

In 1978 the French OTEC program gained new momentum with the planning of a 1 MW pilot plant on the island of Tahiti. Preliminary component testing is being conducted using a 30 kW test facility giving favorable results.

Researchers from other countries, namely the U.S. and Japan, have expressed interest in the OTEC concept. Both Japan and the United States developed their own national OTEC research programs.

Japanese OTEC research endeavors were organized by the "Sunshine Project" committee. A major research effort was the conceptual design of a demonstration plant. This effort culminated in the construction of a 100 kW closed-

cycle pilot plant in the Republic of Nauru in 1981 [67]. Recently development efforts have changed an emphasis on closed-cycle OTEC (CC-OTEC) to address OC-OTEC issues. Long term co-operation between Japan and the US has been initiated to specifically strengthen research in OC-OTEC. The U.S. OTEC program started in the early 1970s when OTEC R&D was being funded by the National Science Foundation. Subsequently the Department of Energy became the principal funding agency. Initial research focussed on the closed-cycle scheme since commercialization of OTEC was perceived as being easier. This effort culminated in the at-sea test facilities of Mini OTEC and OTEC-1 which were both short lived but provided valuable experience.

Major institutions which conduct both closed-cycle and open-cycle R&D are the Solar Energy Research Institute (SERI) and Argonne National Laboratory. Hawaiian research institutions include the Pacific International Center for High Technology Research (PICHTR), Hawaii Natural Energy Institute (HNEI), and the University of Hawaii. The Natural Energy Laboratory of Hawaii (NELH) maintains the sea coast test facility on the Kona coast of the Big Island of Hawaii, which supplies cold water on a continuous basis. Experimental work related to heat exchange material selection based on long term corrosion and biofouling tests has been carried out there during the past six years. NELH-based heat and mass transfer

experiments with seawater supplement the results obtained in fresh water tests conducted by institutions on the mainland U.S..

1.3 Effects of Non-condensible Gases in OC-OTEC

Seawater contains dissolved gases, primarily nitrogen and oxygen. Measurements for the ocean near the Hawaiian islands [75] indicate that the dissolved oxygen and nitrogen content of the cold water layer is at or below saturation with respect to air at atmospheric pressure. Warm surface water is generally slightly supersaturated with both nitrogen and oxygen. In figure 1.3 measured dissolved nitrogen and oxygen concentrations are depicted.

In an OC-OTEC plant, dissolved gases will be released in the flash evaporator and direct contact condenser (if used). By accumulating near the condensing surface, the inert gases lower the partial pressure of the steam, hence lowering the saturation temperature of the steam. Reduction of the temperature differential between the saturation temperature and the temperature of the condensing agent lowers the amount of heat flow in the condenser. Simultaneously, these gases raise the condenser pressure. In order to maintain the low

pressure required for operation these gases have to be continuously removed.

The usual plan for the removal of the non-condensible gases is to compress them to atmospheric pressure. This imposes a significant burden on the overall system efficiency since these parasitic losses range from 10 to 15% of the gross power [19], depending on the fraction of non-condensibles which evolve.

There are two methods to handle the non-condensibles, pre- or post-deaeration. Predeaeration occurs upstream of the flash evaporator or the direct contact condenser (if used). It requires additional system components. The advantage of this deaeration strategy is that the evolved gases are ejected from the system at a higher than boiling point pressure. In addition, accumulation of non-condensibles near the condensing surfaces does not occur and the related effects can be avoided. In the post-deaeration method gases are removed from the condenser at the lowest pressure in the system. Removal at this point requires greater compression power than for predeaeration. In post-deaeration, however, no additional components are required and additional hydraulic head losses, which are associated with predeaeration devices, are avoided.

Because of the greater potential efficiency the present study deals only with predeaeration.

1.4 Previous Research Endeavors in OC-OTEC Gas Evolution

Since degasification is a common industrial mass transfer operation there is extensive literature on the subject. Due to the significance of non-condensibles in the OC-OTEC scheme several studies have addressed this particular application.

There are two types of vacuum deaeration techniques for OC-OTEC applications which have been studied, active and passive deaeration.

For the active deaeration concept in OTEC a packed column deaeration was considered. The envisioned packed column apparatus essentially consists of a vertical pipe filled with randomly arranged packing elements of various candidate shapes of some chemically inert material. The liquid enters at the top of the column and trickles over the surfaces of the packing elements. Intimate contact between the water and gas mixture in the tower occurs permitting transfer of gas to or from the liquid, depending on the applied system conditions. An experimental study [44,45] using fresh water investigated the performance of different types of packing in this application. The researchers concluded that using optimum operation conditions significant deaeration efficiency warrants the use of packed-column deaeration for OC-OTEC applications. A subsequent thermoeconomic study [19]

concluded that deaeration using state-of-the-art packed columns is not cost effective. The additional pumping power required was found to be larger than the reduction in compressor power and total parasitic loss.

Passive deaeration introduces little or none of the hydraulic loss associated with active deaeration. Following this strategy, deaeration occurs in the barometric seawater duct to the evaporator and direct-contact condenser. As the water rises in the duct, and is consequently subjected to less and less pressure, it becomes increasingly supersaturated with non-condensibles. Depending on the conditions a fraction of the gases comes out of solution, accumulates in bubbles and is thus expelled from the fluid. Since this deaeration strategy indicates significant reductions in both cost and pumping power [45] barometric leg deaeration is deemed to be a potentially viable OC-OTEC system component.

There have been several recent studies which address active and passive deaeration in connection with OC-OTEC research [76], [37], [45], [46], [47], [84], [109]. Experiments carried out with seawater [76] using a similar system configuration as previous packed column tests [45] revealed mass transfer resistance to be less in seawater than in fresh water. Figure 1.4 shows a comparison between height of transfer units (HTU), an indicator of the rapidity of mass transfer, of seawater and fresh

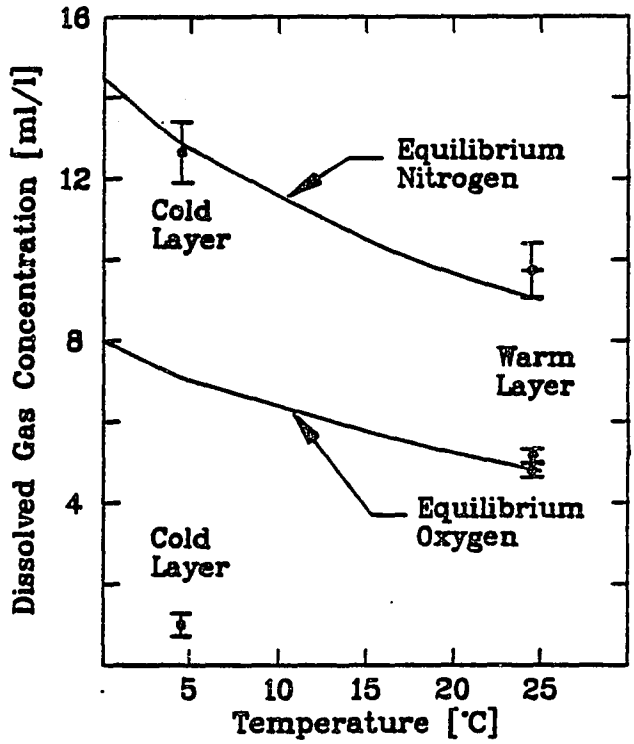

Figure 1.3 Comparison of Measured and Equilibrium Dissolved Gas Concentration (from [75])

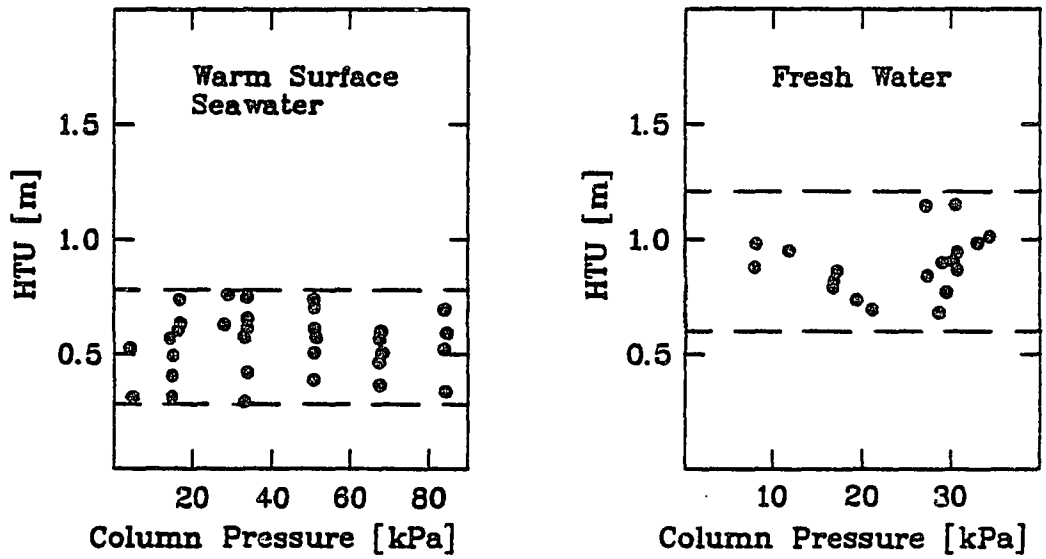

Figure 1.4 Comparison of HTUs of Seawater and Fresh Water in Packed Column Tests (from [76])

water using the same packed column. It should be noted that small HTUs indicate high gas transfer rates.

French researchers [108] predicted from theoretical analysis and experimental heat and mass transfer rates that only 3% of the gas dissolved in the water would be released during evaporation. They concluded therefore that a deaerator ahead of the evaporator or the direct contact condenser (if used) was not necessary. Later French experiments [37] reported gas release measured downstream from the evaporator to be approximately 50% for fresh water and 90% for a 35 g/l brine. Tests conducted in Hawaii using actual seawater showed an even higher evaporator degasification rate for seawater of approximately 95% [76].

These results suggest that gas release caused by the spraying of seawater in a direct contact OC-OTEC heat exchanger is significant. Theoretical predictions indicating only minimum gas release, which would result in only negligible difficulties due to non-condensibles, should therefore be doubted.

The above noted discrepancies in degasification rates in the evaporator can also be found among studies of the rate of gas release in the barometric duct. Tests with fresh water [46, 47] measured the deaeration efficiency of a 5 cm ID barometric duct serving as intake to a packed column. The nuclei contents of natural water was

simulated by the supply water for the tests. With a high nuclei content a maximum deaeration of 30% was observed. Experiments [84] using a 10 cm ID barometric leg system reported seawater deaeration rates which were surprisingly low. Even with artificial seeding of bubbles, with a tested interfacial surface two orders of magnitude large than that found in ocean surface water, a maximum deaeration rate of only 20% was noted. The experiments suggested that most of the gas was evolved within a short distance of the barometric leg where the pressure was the lowest.

The only experiments to date [75] carried out in Hawaii and using natural seawater reported deaeration rates in the barometric leg to be significantly higher than those described before. Gas release in the supply line of a packed column was measured to reach 95%. Vigorous cavitation at a control valve, which generated nuclei and gas transfer surfaces, could be observed. Because of the observed large amount of gas evolution in the intake pipe, a second experimental deaeration system was designed which minimized cavitation in the supply line. Results of deaeration experiments are shown in figure 1.5. Warm surface seawater, cold deep seawater (from approximately 600 m depth), and fresh water were used in these experiments.

Since dissolved oxygen can be readily measured by

means of a sensor while dissolved nitrogen requires a more elaborate analysis method, it has become common practice to use oxygen as an indicator for the overall gas transfer characteristics. Differences in gas transfer characteristics between nitrogen and oxygen are likely to be negligible due to the close similarity in their molecular structure.

Because nitrogen and oxygen together constitute 98% of the total atmospheric gas phase there is no need to look to other gases when dealing with the question of gas volume effects from surface seawater. Cold seawater for OTEC use is taken from the oxygen minimum zone and therefore dissolved oxygen is at a low concentration, leaving nitrogen to represent about 93% of the total dissolved gas phase.

Deaeration rates of nitrogen in deep seawater have been reported to be the same or higher than those of oxygen [75]. The nitrogen measurements were, however, less reliable because of the lack of a gas chromatograph at the site of the experiments.

The observations in Hawaii of degasification characteristics of natural seawater and freshwater indicate that they are significantly different. Also to be considered are the effects of different experimental systems [37,75].

High percentage deaeration of water in the OC-OTEC

direct contact heat exchanger will result in the discharge of waters to the environment with virtually no dissolved oxygen. The magnitude of environmental stress resulting from a large deoxygenated OC-OTEC discharge would be lessened or eliminated by reinjecting air into the discharge pipe, provided that the gas is readily dissolved in the water. Based on the observed rapid gas transfer rates found, a change of the currently accepted design approach for OC-OTEC, incorporating bubble seeding of the intake and gas reinjection into the discharge, was suggested [76]. Figure 1.6 schematically shows the modified OC-OTEC process. Predeaeration units would be included before the evaporator and before the condenser if a direct contact condenser is used. Gas reinjection would occur at a subatmospheric pressure using the downcomer as a barometric air compressor. Another suggested change is the injection of vacuum pump exhaust gases into the upcomer of the predeaeration unit to serve as nuclei.

1.5 Objectives of Present Study

Using available data and theoretical predictions, a strategy is formulated for the present study of gas transfer in seawater. The following topics will be addressed with experimental verification.

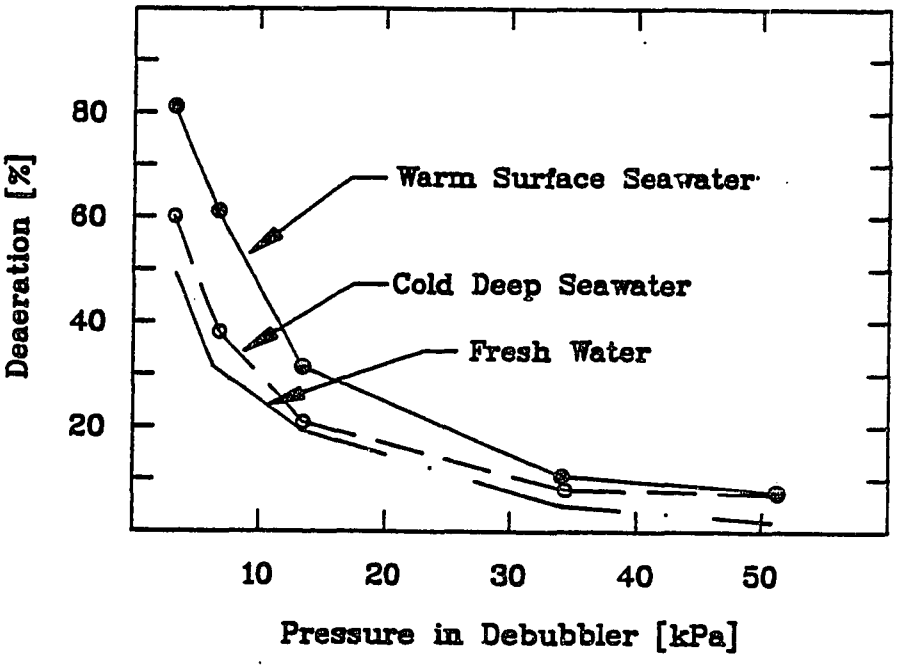

Figure 1.5 Observed Deaeration Rates in Barometric Intake; (data from [76])

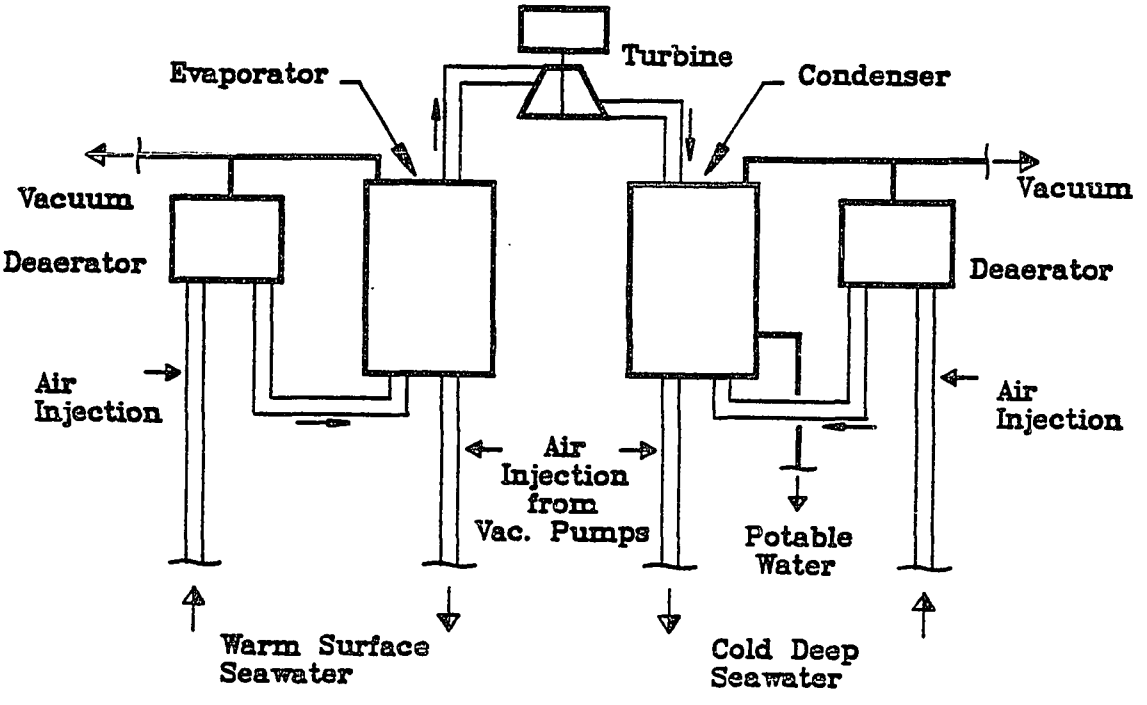

Figure 1.6 Proposed OC-OTEC Process (from [75])

1) Investigate the observed difference in gas transfer characteristics for fresh water and seawater.

Although OC-OTEC operates with seawater, a comparative investigation of operational characteristics using seawater and fresh water is desirable for various reasons. Extensive heat and mass transfer experiments using fresh water have been extensively conducted by several research institutions in recent years. Comparison of fresh water and natural ocean water mass transfer mechanisms allows an assessment of the usefulness of the fresh water data and access to the extensive theoretical treatment of freshwater gas transfer in the literature. Given the same initial system conditions, a comparison of the two types of water is likely to result in important insights.

2) Investigate the observed difference in deaeration rates in the barometric leg.

Recent studies, cited previously, report substantially different deaeration rates. Although the principle of barometric vacuum deaeration was similar in every case, different system configurations and sampling techniques were involved. Identification of possible shortcomings in the experimental procedure would be useful in designing unbiased tests in order to generate more reliable design parameters. A point of interest is the question of what extent deaeration effectiveness is influenced by the

amount of bubble seeding. Though, as noted previously, there are experiments reporting little dependence of deaeration effectiveness on artificial nucleation, other data strongly contradict these findings.

3) Assess the possibility of reaerating the deoxygenated OC-OTEC discharge.

Following an intensive literature search no experiments have been found describing aeration of seawater in a barometric discharge. Experiments should reveal quantitative dependence to flow velocity and air injector design.

4) Examine the gas transfer rates of nitrogen.

Available data describing mass transfer of nitrogen in water is scarce. Frequently nitrogen gas transfer rates are predicted by assuming identical transfer characteristics to oxygen. Although the molecular structure of the non-polar N_2 molecule is similar to that of oxygen, experimental verification of a similarity in transfer rates should be obtained.

The four stated topics of interest constitute the objectives of the present experimental study. It is of course not possible to sharply distinguish between these topics because of the complexity of the problems involved. The necessary experimental approach will have to include various areas of absorption and gas-liquid

reaction in order to establish a reasonably comprehensive strategy.

CHAPTER II

EXPERIMENTAL APPROACH

The experimental portion of this study incorporates a variety of gas transfer experiments related to OC-OTEC research. Existing experimental data from previous experiments and a review of related research endeavors by others in gas absorption and desorption were used to formulate a test strategy for this study.

2.1 Summary of Pertinent Test Data

In order to meet the initial study objective an extensive literature survey was carried out. The pertinent references can be assigned to the following categories:

i) Gas transfer in seawater and electrolyte solutions
ii) Gas transfer in fresh water
iii) OTEC general topics and specific applications
iv) Bubble characteristics in fresh water and seawater
v) Fundamentals of mass transfer, diffusion and solubility

Sources of experimental data and theoretical approaches which were used in defining the test strategy are presented in the following paragraphs.

Deaeration and aeration of seawater are fields which

have received only limited attention in the literature. This may be due to the present lack of large-scale process applications. In one investigation the performance of a packed column in vacuum degasification of seawater [64] was tested. A comparison of fresh water and seawater data showed that seawater degassed at a slightly faster rate. Although the author did not elaborate on these findings he suggested better wetting characteristics of the seawater on the packing elements might be the likely reason for this accelerated gas transfer. The seawater used in this study was transported to the lab facilities using tank trucks. A batch system was used in the experiments.

Packed column vacuum deaeration tests using in-situ seawater were carried out at the Seacoast Test Facility in Hawaii [76]. Surface seawater and deep seawater, the latter extracted from a depth of 600 m, are continuously pumped to this coastal facility. The identical packed column that was used in previous tests for measuring gas exchange rates in fresh water [45] [46] was shipped to Hawaii and connected to the available cold and warm water sources. Although the packed column apparatus and the packing were identical for both studies, the supply piping configuration differed substantially. For the fresh water tests a barometric intake was chosen whereby the available hydraulic head and the column vacuum pressure established

the flow conditions of the supply flow. For the seawater experiments a throttle valve was installed in the supply line to control the flow rate since the required elevation for a barometric intake was not available. Cavitation at this control valve resulted in the generation of a substantial amount of bubbles downstream of the valve. The deaeration characteristics of the intake lines, therefore, differ between the fresh water [45] [46] and seawater [76] packed column experiments. The gas exchange characteristics inside the packed column, which are expressed in HTU, are mainly determined by the liquid flow over the packing. A comparison of the packed column mass transfer rates measured in HTU of fresh water and seawater therefore appears valid and indicates a more rapid deaeration of the seawater (refer to figure 1.4).

As noted earlier, deaeration of seawater was tested in conjunction with OC-OTEC applications [76] [84]. Different liquid flow characteristics prohibited direct quantitative comparisons of the two studies. An additional source of uncertainty for the comparison between the packed column and barometric leg deaeration studies is the varying sampling methodology. Golshani and Chen [45] [46] and Krock and Zapka [76] applied an extraction technique to gather a liquid sample from the subatmospheric process vessel while in operation. Extracting a liquid sample and subsequently measuring its dissolved oxygen (D.O.) content

at atmospheric pressure is necessary since the available D.O. sensors did not operate reliably at subatmopheric pressure [45]. Lindenmuth [84] suggested that sample extraction should be avoided in favor of in situ measurement after the process is stopped and the experimental equipment has been vented to atmospheric pressure.

OTEC-related heat and mass transfer experiments [27] with freshwater and 35 g/l brine using identical test equipment and sampling procedures reported deaeration rates downstream of the flash evaporator of 90% for brine and 50% for fresh water. Here the dissolved oxygen was measured in a discharge well under atmospheric conditions.

In the course of the literature review no references addressing aeration of natural seawater could be found. Aeration processes in electrolyte solutions and related topics, however, have been studied by several investigators. One of these [60] reports on the increased aeration rate of Na_2SO_4 and NaCl solutions when compared to a fresh water system. The experimental procedure involved a batch system where water was stripped of dissolved oxygen by means of injecting nitrogen, and subsequently the degassed water was aerated using a porous stone diffuser. The study showed that the electrolytes investigated increase the aeration rate by as much as 40%. The researcher attributed the observed increased gas

transfer to increased bubble surface due to a reduction in bubble coalescence. Previous investigations were cited which noted a reduction in coalescence with increased electrolyte concentration.

There is abundant literature concerning aeration and deaeration of fresh water, since both processes are extensively used in industrial applications. For this review several frequently cited studies have been chosen out of large number that are available in this area. The selected references describe experimental procedures, the hardware, and types of analyses and operating conditions of packed column and bubble column applications. Of particular interest are those investigations which consider the presence of surface active agents in the process water. Surface active agent (SAA) are generally speaking water constituents (often of organic origin) which alter the characteristics of the liquid-gas interface. Implications to the gas transfer process include a decrease in the rate of gas exchange by augmented surface resistance and, conversely, an increase in the rate of gas exchange by providing more surface by a reduction in coalescence. Several investigators [e.g. 123] describe mechanisms of selective accumulation of water impurities on bubbles rising in polluted water. These accumulations alter bubble characteristics, such as rise speed or the burst mechanism. Similarly to organic

surfactants, some inorganic electrolytes hamper bubble coalescence and, thereby, provide a larger interfacial area for gas transfer.

Static and dynamic characteristics of bubbles have received considerable attention in the literature. Whereas the characteristics of bubble dynamics in fresh water are well understood, such extensive knowledge is not yet available for seawater bubbles. Previous investigations involving various concentrations of electrolytes and SAA revealed bubble characteristics that might be applicable to seawater. Water impurities such as surface-active substances generally lower the rise rate of air bubbles [e.g. 24]. Experiments using brackish water [63] report a similar effect on the rise velocity as was observed in seawater. Presence of surface active agents in the test seawater, however, was inferred, and the influence of other possible seawater characteristics could not be quantified or even identified.

The reduction of the equilibrium gas solubility in the presence of electrolytes is well known and documented [e.g. 30, 59]. Solubility data for seawater of various salinity have been fitted by Weiss [121].

Conclusions about the effects of electrolytes on gas diffusivity differ among authors. It should be noted, however, that all investigations mentioned used compositions of aqueous electrolyte solutions which were

different from the composition of seawater. A review of oceanographic literature revealed the surprising fact that the gas diffusion coefficients for oxygen and nitrogen in seawater have not yet been directly measured. The molecular diffusion values commonly used are based on theoretical assessments and on measurements in fresh water.

2.2 Introduction of Hypothesis

The literature review and the preliminary investigations conducted for this study suggest that the potential causes for the observed increased gas transfer rates in seawater can be classified into two areas. For subsequent treatment these two areas will be termed macroscopic and microscopic. Although there are overlapping mechanisms for these two categories this approach is adopted here for the sake of discussion.

As has been shown, experimental evidence exists that electrolytes diminish bubble coalescence. This means that smaller bubbles and larger numbers of bubbles are present for a given volume of gas in seawater than in fresh water and that this results in greater liquid-gas interfacial area for gas transfer in seawater. On the other hand, accumulation of surface-active agents and electrolytes on the bubble skin in natural seawater may cause greater

resistance to gas-transfer of the surface layer. These two macroscopic mechanisms are likely to control the transfer rate where flow conditions exert little stress on the ascending bubbles. On the other hand, the presence of higher turbulence and resulting shear forces could disrupt the bubble skin and cause frequent renewal of the surface layers. Since reaccumulation of impurities on the surfaces does not happen instantaneously there might be an interval when surfaces with relatively little contamination are involved in the gas transfer process, thus increasing it.

Surfaces without foreign contamination would enable an assessment of the microscopic transfer characteristics of the exposed surfaces. Considering the cluster model for the structure of water, dissolved gas molecules are either contained in "iceberg" like clusters (clathrate structures) or are free, individually moving entities [62]. Introduced ions cause hydration, an accumulation of the polar water molecules around the charged ion. Electrostriction is a process following hydration. The coulombic field of the ions interact with partial charges of the water dipoles. The strength of the attractive force is sufficient to draw the water molecules close to the ions, thereby compressing the solvent in their immediate neighborhood.

Gas diffusion in water is assumed to be a random

process whereby gas molecules are moving about in the empty spaces of the water structure. Binding of a fraction of the free water molecules could reduce the number of collisions and increase the length of free path of the gas molecules. An increase in the molecular diffusion of dissolved gases would be a reasonable result of this thought model of water structure and gas diffusion.

As indicated above, a clear discrimination between macro- and microscopic aspects of gas exchange is not entirely appropriate if interactions between the two are considered. The dynamics of the bubble surface are likely to be influenced by the bulk and interfacial molecululular structures. Bubble coalescence is attributed to some preferred ion attachment onto the surface layers, which causes a repulsion at bubble surfaces.

With the constraint of limited experimental facilities in mind, the emphasis of the present study is on the macroscopic aspects. Two main areas are covered in the experimental endeavors of this study: 1) assessment of the contribution of bubble coalescence inhibition, and 2) determination of the role of surface contamination on gas transfer in seawater.

2.3 Experimental approach

A schematic of the experimental approach is given in figure 2.1. The investigations are divided in two segments. Experiments addressing fundamental aspects of gas transfer in seawater are summarized in the first segment. These involve bubble gas transfer tests, packed column vacuum experiments, and investigation of bubble rise velocities. Gas transfer characteristics important to the OC-OTEC scheme are treated in the second segment .

As a general approach all experiments were conducted using seawater and freshwater with identical experimental settings, although the topic of the present study is explicitly the gas transfer in seawater. The extensive literature review revealed the fact that each gas transfer investigation, including test apparatus and procedure, has its own idiosyncracies. Test procedures and boundary effects for each particular investigation influence gas transfer to varying degrees and make direct quantitative comparison of test data somewhat unreliable. In order to avoid this ambiguity direct comparisons of gas transfer rates of different test waters are best carried out using identical test apparatus and procedures.

The comparison of seawater and fresh water test data is important, since a considerably body of literature exists for freshwater gas transfer. With a literature explanation

Experimental Approach

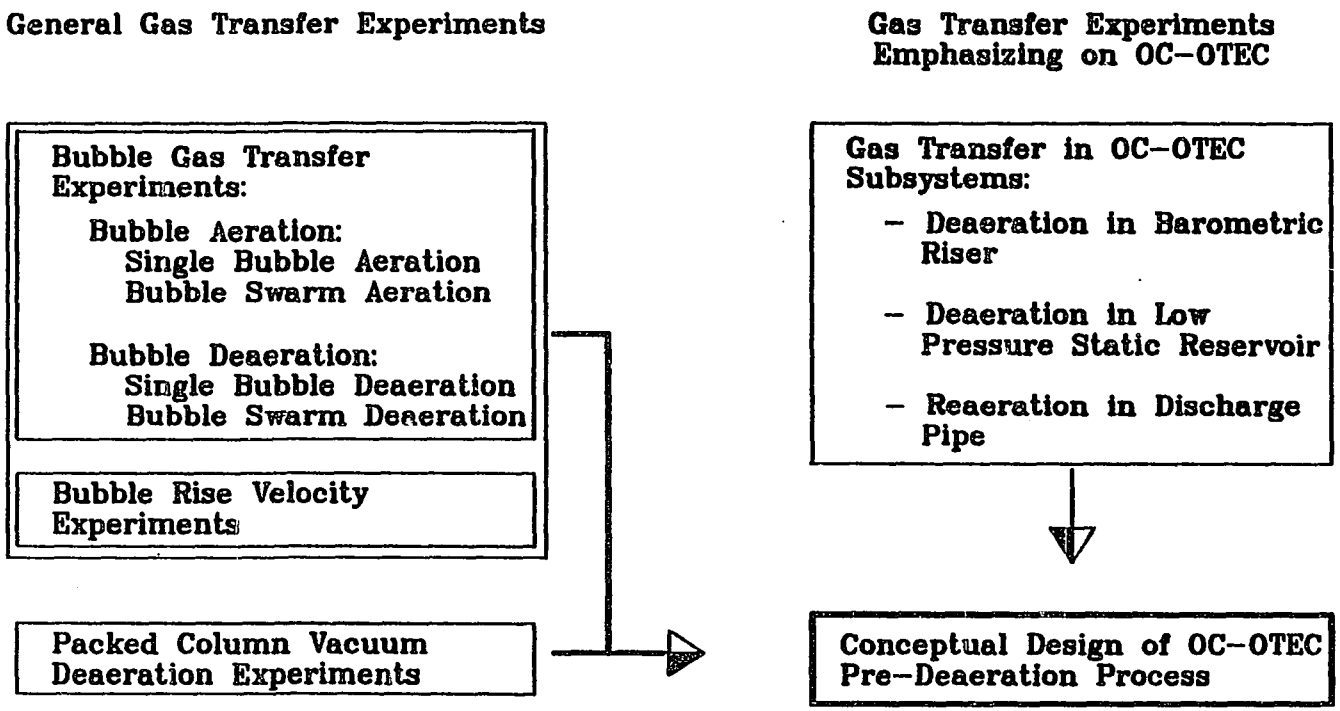

Figure 2.1 Schematic of Experimental Approach

of the pertinent features of fresh water gas transfer characteristics, a comparison to experimental seawater datas should facilitate the identification of gas transfer characteristics in seawater.

Bubble gas transfer experiments are designed to probe the effect of bubble coalescence on the transfer processes. The basic idea is to execute bubble injections in such a manner so that in one case bubble coalescence is avoided and in the other case coalescence is promoted. These two approaches will subsequently be called single bubble and bubble swarm experiments. In single bubble tests bubbles are individually injected into the test water column. Subsequent collisions, which induce agglomeration of bubbles to large bubble entities, are avoided when bubbles do not rise in close proximity of each other.

Bubble swarm experiments promote bubble collisions and thereby provide the opportunity for bubble coalescence. At the point of injection the bubble is generally small and the injection orifices are located close to each other. Bubble collisions may result in coalescence and in bubbles of different sizes, depending on the character of the fluid and on other test conditions.

The bubble gas transfer experiments are further subdivided into aeration and deaeration tests. In bubble aeration experiments of water with air, air bubbles are

injected into degassed water. The dynamics of gas uptake is a function of the test system and of the test water used. Since a large body of literature describing air bubble aeration of fresh water is available the present study can take advantage of past experimental experience and results. Furthermore, aeration occurs under atmospheric pressure and the test apparatus is only exposed to the hydrodynamic water pressure. This condition facilitates the determination of bubble sizes during air injection. In the single bubble tests sizes of individual bubble are determined photographically. For the bubble swarm investigations distributions of bubble sizes are determined, which indicate the extent of bubble coalescence.

Bubble deaeration is a process in which the dissolved gas content is reduced with the aid of the introduction of bubbles of a different gas. This process is called bubble sparging and is a commonly applied laboratory technique. A gas, which is different from the gas to be removed, is injected into the fluid; since the partial pressure of the gas to be removed is below its partial pressure in the injected gas bubbles, the dissolved gas diffuses into the bubble and is removed from the fluid. Simultaneously, some of the carrier gas enters the liquid because its partial pressure is higher in the bubble than in the liquid.

Degasification in the OC-OTEC system occurs under somewhat different conditions. Due to the low liquid pressure the partial pressure of gases in bubbles is lower than that of the water. The batch deaeration experiments were designed to simulate this deaeration mechanism. As in the case of the aeration tests the effect of bubble coalescence is studied by using single bubbles and the bubble swarms.

Bubble gas transfer experiments included evaluation of the exchange characteristics of dissolved nitrogen. Analysis of dissolved nitrogen involves a more elaborate approach as there are no appropriate dissolved nitrogen sensors available at present. Measurements of nitrogen exchange rates are carried out less frequently than those for oxygen because of this difficulty. The available area for gas transfer in a bubble population is determined by the surface area of individual bubbles, their number and their residence time in the water column. Experimental measurements addressing bubble rise velocities in clean tropical ocean water, which can be found in the most likely locations for OTEC use, could not be found in the literature. Bubble rise in freshwater has attracted significant attention in the literature and theoretical explanations exist for the important aspects of this phenomenon. Bubble rise experiments were conducted in this

study with both fresh water and seawater to ensure reliable comparisons.

Previous packed column vacuum deaeration experiments in conjunction with OTEC applications were conducted under significantly different experimental settings. As described earlier, packed column experiments can be used to investigate the effect of surface renewal of the water-air interface on the rate of gas transfer. As a result of its internal flow conditions the packed column reduces gas transfer resistance caused by the accumulation of surface-active agents on the gas-liquid interface. In order to facilitate comparison, identical set up and sampling methodology are applied for both fresh water and seawater experiments; in contrast to previously cited investigations [45 and 76], which compared fresh water and seawater. In these experiments water samples were not extracted from the vacuum environment of the packed column. Instead the system was first vented and samples subsequently taken at atmospheric pressure. Due to the unavailability of a continuous seawater supply the experiments were conducted on a batch basis. After being deaerated in the packed column the test water was reaerated under several experimental conditions.

For the second main segment of the present study gas transfer in a small-scale facility simulating OC-OTEC conditions were investigated. In order to simulate real

OC-OTEC conditions such as pressure distribution in the intake system as close as possible, liquid flow control valves for the intake and discharge were avoided. The hydraulic lay-out of the test set-up allowed variations in liquid flow rates at different system pressures by means of raising and lowering exit and entrance reservoirs. According to the study objectives, the effect of artificial nucleation on barometric leg deaeration and the feasibility of barometric aeration of the discharge flow were investigated. As in the case of the packed column experiments a continuous flow of seawater was not available. Large volume tanks were used to provide appropriate storage capacity. In contrast to previous tests [46] [37], where special processes were applied to the batch test water in order to simulate ocean water nuclei conditions, such processes were not employed and were not necessary for the present study. However, this means that the barometric deaeration rates observed during this study might not necessarily be the same as those that would be observed using in-situ ocean waters. With this experimental constraint in mind the validity of the test system used to investigate the effect of artificial nucleation should be adequate.

The test objectives differentiate between deaeration and aeration tests. The deaeration test are further subdivided into two sections in order to investigate the

feasibility of a proposed OC-OTEC deaeration technique.

There are thus three experimental sections within this test segment.

Deaeration in a static reservoir investigates gas evolution induced by bubble injection into a reservoir subjected to various low pressures. A range of liquid flow rates examines the effect of residence time on deaeration rates. Deaeration in the barometric upcomer assesses the magnitude of gas liberation in the barometric duct leading to a reservoir. Reaeration in the discharge pipe probes the feasibility of aerating the OC-OTEC effluent, which is likely to be essentially void of dissolved gases.

As for all previously described experiments of the present study, this test segment will be conducted using both fresh water and seawater.

CHAPTER III

FUNDAMENTALS OF GAS TRANSFER PROCESSES

Gas transfer phenomena have received great attention in research and development endeavors over the last century. Theoretical tools have been developed and fine tuned to provide a broad understanding of relevant physical and chemical processes.

There are, however, cases when theoretical means fail to predict the rate of transfer from basic data. The processes governing gas transfer for these cases are subject to very complex interactions and transient boundary effects. Theoretical formulations frequently require simplifications which can render the prediction uncertain. In such instances one must rely on empirical approaches.

Before proceeding with the discussion of the experimental part of the present study some basic concepts of the theory of gas transfer are reviewed. Pertinent gas laws and their specific applications are covered. Thermodynamic aspects of dissolved gases and principles of gas diffusion are discussed. Frequently-used models which describe the characteristics of the air-water interface are also covered. Finally, methods to measure dissolved gases in water are introduced. Operational peculiarities of these methods are presented

and their particular implications for the subject study are discussed.

3.1 Review of Gas Laws

3.1.1 Ideal and Real Gas Relationships

The properties of an idealized gas at low densities, termed a perfect gas, are of considerable importance in a variety of scientific and engineering applications. Such a gas provides an understanding of normal behavior which all real gases approach at sufficiently low densities. Even at pressures commonly used in laboratories and process plants the laws of the behavior of an ideal gas are often adequate to describe the behavior of a real gas.

From experimental observations it has been established that the mechanical properties of a gas at low and moderate pressures are closely given by the following equation of state.

$$P * V = m * R * T \qquad (3.1)$$

or

$$P * V = n * R' * T \qquad (3.2)$$

where: P = the absolute pressure; T = the absolute

temperature; V = the volume; m = the mass of a given sample of gas; R′ = the universal gas constant, with:

$$R' = 8.31434 \quad [\ N*m/mol/K\ ]$$

Dividing the universal gas constant by M, the molecular weight, results in a gas constant per unit mass:

$$R = \frac{R'}{M} \tag{3.3}$$

It has been found that the gas constant R′ is almost independent of the nature of the gas if the amount of gas is represented not by its mass, m, but by the number of moles, n.

In order that the volumetric properties of a gas may be compared there are several arbitrarily specified standard states, usually known as standard conditions (S.C.), of temperature and pressure. The most commonly used standard conditions of temperature and pressure are the Universal Scientific S.C. with $0^{O}C$ and 760 mm Hg or their equivalent. Under these conditions the following volumetric data are true for ideal gas applications.

1 mole of gas = 22.414 liters

and

1 mole of gas = 359 cbf

The gas constant R′ becomes entirely independent of the nature of the gas if the temperature scale is defined

by the limiting value of (P*V) at zero pressure. The ratio of two temperatures T_1 and T_2 is then defined by:

$$\frac{T_1}{T_2} = \lim_{P \text{ to } 0} \frac{(P * V)_1}{(P * V)_2} \tag{3.4}$$

Rewriting the above equation the following expression is obtained:

$$\frac{P_1 * V_1}{T_1} = \frac{P_2 * V_2}{T_2} \tag{3.5}$$

This means that gases at low density closely obey the well-known Boyle's and Charles' laws. These laws, of course, were originally based on experimental observations.

If the temperature and pressure conditions deviate from ideal conditions, as with an increase in pressure and/or a lowering of the temperature, the gas no longer can be described by ideal gas laws and its behavior is then according to real gas relationships. This is due to several factors. As the density increases molecules are brought closer together. With reduced intermolecular distances the attractive force between the molecules becomes important. This attractive force between molecules causes the density to assume a greater magnitude than that predicted by the ideal gas relationships, which neglect intermolecular forces and

the fact that individual molecules take up volume. At a sufficiently high pressure intermolecular distances become so small that repulsive forces between the gas molecules become evident.

There are several equations of state for handling real gas relationships. In order to accurately predict the P-V-T behavior of a gas under these conditions, more terms have to be added to the ideal gas relationship.

One of the earliest approaches to formulating a real-gas equation of state was accomplished by van de Waal in 1873. Although not universally accurate the equation illustrates some of the theoretical assumptions used in its development. The effect of the attractive force among the molecules is included by adding a pressure term.

$$\frac{n^2 * a}{V^2} \qquad (3.6)$$

where: n = number of moles; a = a constant, different for each gas; and V = volume.

The effect of the volume of the individual molecules is taken into account by subtracting a term from the volume in the ideal gas law.

These corrections result in the following relationship:

$$\left(P + \frac{n^2 * a}{V^2} \right) * (V - n * b) = n * R * T \qquad (3.7)$$

where: b = a constant.

The constants a and b can be determined by fitting the van de Waals equation to experimental data.

For most practical applications the use of ideal gas relationships are sufficiently accurate at low pressures, independent of the temperature. At pressures double or greater than the critical temperature (see below), ideal gas behavior can be inferred with good accuracy to pressures reaching approximately 10 MPa [124]. For example, the critical temperature of oxygen is 155 K and that of nitrogen is 126 K. At temperature below twice the critical temperature and pressures above very low values, say atmospheric pressure, deviations from ideal gas behavior can be significant. For lighter gases such as oxygen, nitrogen or water vapor deviations are considerably smaller than those for heavier gases like carbon dioxide.

3.1.2 Gaseous Mixtures

The majority of practical problems involve gaseous mixtures rather than a single gas. There are two ideal

gas concepts which can be successfully applied to gaseous mixture. These are:

i) Dalton's law of partial pressures

ii) Amagat's law of partial volumes

Dalton postulated that the total pressure of a gas mixture constitutes the sum of the pressures exerted by molecules of the each component gas. Using this concept it can be assumed that each individual gas of the mixture exerts a "partial pressure". This partial pressure is the same pressure obtained if the identical mass of the individual gas is alone confined in the total volume. The sum of the partial pressures for each gas in the mixture makes up the total pressure. Dalton's law of summation of partial pressures can thus be written:

$$P_T = P_1 + P_2 + P_3 + ... P_n \qquad (3.8)$$

where: $P_T = P_n$ = partial pressure.

At constant volume and temperature the pressure is solely a function of the number of gas molecules. Dividing the ideal gas law of component 1 by that of component 2, and assuming constant temperature and volume, the following expression is obtained:

$$\frac{P_1 * V_1}{P_2 * V_2} = \frac{n_1 * R_1 * T_1}{n_2 * R_2 * T_2} \qquad (3.9)$$

which simplifies to:

$$\frac{P_1}{P_2} = \frac{n_1}{n_2} \qquad (3.10)$$

The ratio of the partial pressure equals the ratio of mole numbers of component 1 and 2.

Substituting the total moles of gas for component 2 results in Dalton's law of partial pressures:

$$\frac{P_1}{P_T} = \frac{n_1}{n_T} = y_1 \qquad (3.11)$$

where: y_1 = mole fraction for component 1

thus:

$$P_1 = y_1 * P_T \qquad (3.12)$$

Amagat developed his relationship of partial volumes in an analogous manner. Amagat postulated that the total volume of a gaseous mixture is equal to the sum of the volumes of the individual gas components, assuming the same pressure and temperature. The individual volumes of the particular components are the partial volumes. Thus the following relationship can be derived:

$$V_T = V_1 + V_2 + V_3 + \ldots V_n \qquad (3.13)$$

where: $V_T = V_n$ = partial volume.

Assuming the same approach as in the derivation of the partial pressure relationship results in the following expression:

$$\frac{V_1}{V_2} = \frac{n_1}{n_2} \tag{3.14}$$

and

$$\frac{V_1}{V_T} = \frac{n_1}{n_T} = y_1 \tag{3.15}$$

thus:

$$V_1 = y_1 * V_T \tag{3.16}$$

Dalton's and Amagat's laws can still be used in cases when pressure and temperature conditions necessitate the use of real gas relationships . The partial pressures and partial volumes of each gas component can be computed with the appropriate equation of state. Individual partial pressures and partial volumes can then be added to give the total pressure and total volume of the system.

3.1.3 Vapor Pressure and Raoult's law

The terms vapor and gas both describe physical matter

existing in a gaseous state. A distinction between the two terms can be made by introducing the concept of critical temperature. A gas above its critical temperature is properly termed a gas while a gas which exists below this particular temperature can condense and is commonly referred to as a vapor. Compression of a vapor at a constant temperature below its critical temperature results in increasing pressure. At a sufficiently high pressure, which depends on the temperature, the vapor starts to condense. Further compression does not increase the pressure but rather increases the fraction of the gas phase which is condensed.

A non-condensible gas is understood to be a gas above its critical temperature or a gas undergoing a process in which it cannot condense.

Condensation and vaporization of a vapor at constant temperature and pressure are equilibrium processes. Vapor pressure is defined as the pressure at which that equilibrium exists. In figure 3.1 the vapor pressure curve of water is shown.

At a given temperature liquid and vapor phases can only exist in equilibrium at the saturation pressure. For a pure substance there is a definite relationship between saturation pressure and saturation temperature.

Another useful term to describe the equilibrium

condition is boiling point. According to figure 3.1 a substance has an infinite number of boiling points. By convention the normal boiling point is the saturation temperature under atmospheric conditions. The expression dew point for the saturation condition is useful if condensation of a vapor is under consideration.

Under saturation conditions a mixture of saturated liquid and saturated vapor is called wet vapor. The weight fraction of the vapor is known as the quality of the saturated vapor.

Vapor pressure of a substance is a function of temperature and pressure. The change of vapor pressure with temperature is frequently expressed by the following equations:

$$\log (P_V) = - \frac{A}{T + C} + B \qquad (3.17)$$

where: T = temperature; A, B, C = constants different for each substance; P_V = vapor pressure.

The change of vapor pressure with changes in pressure at constant temperature is negligible under normal conditions.

Saturation conditions involving the mixture of water vapor and various non-condensible gases are of particular importance in the present study. In the case where a dry gas or gaseous mixture comes into contact with a liquid,

the gas phase will acquire vapor from the evaporating liquid. This process continues until the partial pressure of the vapor equals the vapor pressure of the liquid at the temperature of the system. Once equilibrium is attained no additional vapor will be released into the gas phase. Figure 3.2 illustrates this case for a system at a constant temperature of 50 ^{o}C and a pressure of 101.35 kPa (atmospheric pressure). Starting at time zero water begins evaporating until the vapor pressure reaches the saturation pressure of 12.35 kPa while simultaneously reducing the partial pressure of the dry air immediately above the liquid to 89 kPa.

So far in this discussion, only mechanisms involving pure substances have been considered. With the existence of a solute the vapor pressure of the solvent is depressed. As a consequence the boiling point, which is dependent on the vapor pressure, is increased. An explanation of this vapor pressure decrease involves the number of solvent molecules per unit surface area of the liquid. The vapor pressure of a liquid depends on the number of solvent molecules which can escape from the surface of the liquid. In the presence of solute molecules at the surface the number of solvent molecules is reduced. Consequently, the number of escaping solvent molecules decreases which, in turn, reduces the vapor pressure.

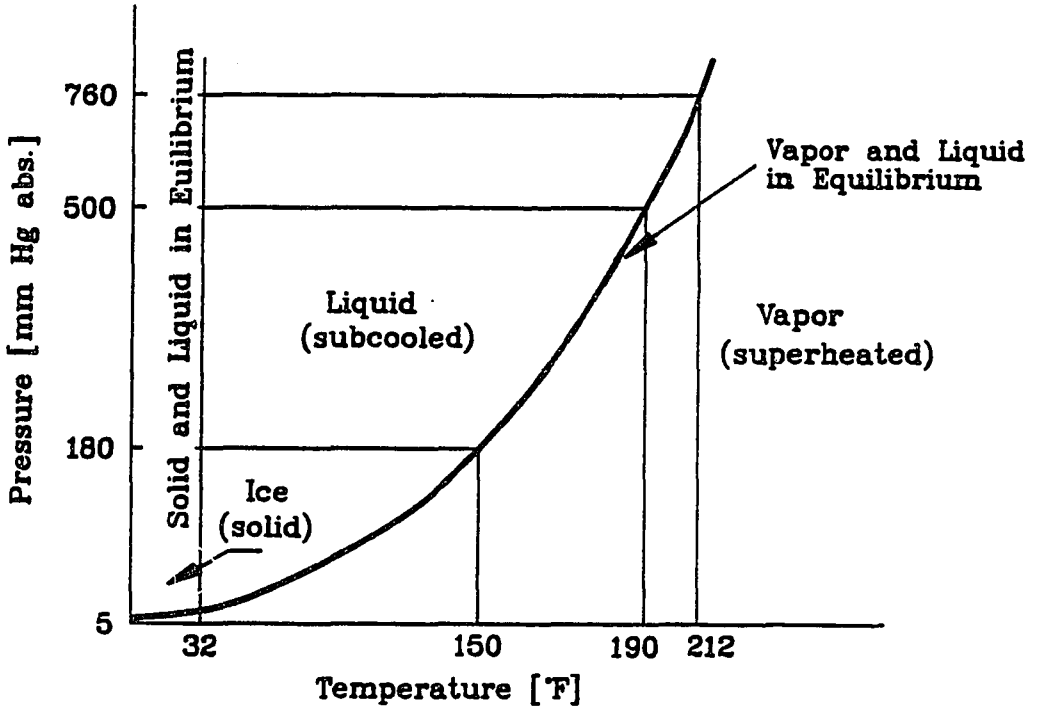

Figure 3.1 Vapor Pressure Curve of Water (data from [58])

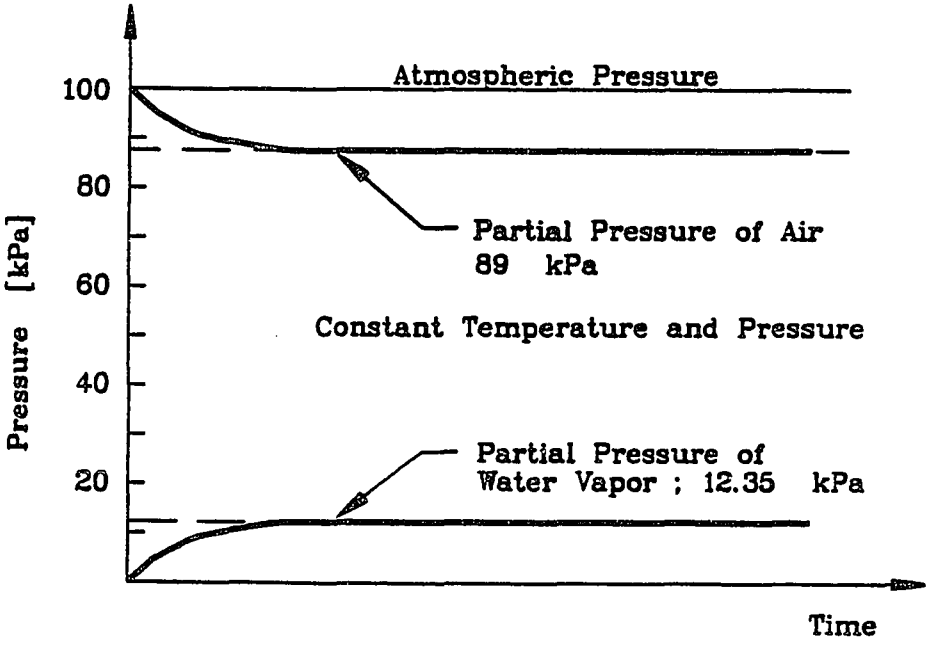

Figure 3.2 Change of Partial Pressure of Air and Water on Vaporization (data from [58])

For very dilute solutions the concentration of the solute is too low to appreciably influence the properties of the solvent vapor. For such solutions Raoult postulated his law which indicates that the vapor pressure of a solvent is inversely proportional to the molar fraction of the solute. Raoult originally named this concept fugacity, a measure of escaping tendencies. If the vapor of the solvent behaves like a perfect gas then the fugacity is equal to the vapor pressure. Raoult's law can be written as:

$$P_1 = P_{10} * x_1 = P_{10} * (1-x_2) \qquad (3.18)$$

where: P_1 = vapor pressure of the solvent; X_1 = mole fraction of the solvent; X_2 = mole fraction of the solute. The value P_{10} is equal to P_1 if $X_1 = 1$.

For more concentrated solutions experimental vapor pressures values depart from those predicted by Raoult's law. Solute-solvent interactions can also have significant effects, particularly charged solute particles in electrolyte solutions. Whereas in terms of molar concentration seawater or a 0.5M NaCl solution appears dilute in Raoult's law, the electrical conductivity results in an effect similar to a much higher concentration [62]. The deviation between ideal solution conditions and the vapor pressure of solutions

with varying electrolyte concentration is shown in figure 3.3.

At a value of 0.5m NaCl, which approximates seawater with 35 ppm salinity, the difference between the measured vapor pressure and that calculated from Raoult's law in 0.4%.

Horne [62] gives the following relationship for the prediction of vapor pressure in seawater (P):

$$P = P_0 * (1 - 0.000537 * Sal) \qquad (3.19)$$

where: P_0 = vapor pressure of pure water; Sal = salinity in $^{o}/_{oo}$.

3.2 Solubility of Gases in Liquid

The solubility of a gas in water depends primarily on four variables: pressure, temperature, concentrations of dissolved electrolytes, and the type of gas.

3.2.1 Pressure Dependence

Using the assumption of a very dilute solution and applying Raoult's law, it is found that the pressure dependence of the solubility of a gas at constant

temperature can be described by the generalized form of Henry's law:

$$f_2 = K * x_2 \tag{3.20}$$

where: f_2 is the fugacity of the solute, X_2 is the mole fraction of the solute and K is a proportionality factor.

Fugacity, the measure of the solutes escaping tendencies, can be set equal to the partial pressure when perfect gas conditions are applicable.

The mole fraction X_A of component A is defined as the number of moles of component A divided by the total number of moles.

$$x_A = \frac{N_A}{N_A + N_B + \ldots N_S} \tag{3.21}$$

For very dilute solutions the sum $N_A + N_B + \ldots N_S$ can be approximated by the number of moles of the solvent, N_S. Furthermore, it can be concluded that in very dilute solutions the mole fraction of solute becomes proportional to the concentration. Thus, with these assumptions, equation (3.20) becomes:

$$P_2 = K_1 * C_2 \tag{3.22}$$

where: P_2 = the partial pressure of the gas; K_1 = a new proportionality constant; C = the concentration of the solute in g/liter or mole/liter.

At constant temperature, the vapor pressure of the solute is proportional to the solute concentration in the solution. Conversely, the equilibrium concentration of a gas dissolved in a liquid is proportional to the partial pressure of the gas above the solution.

In order to obtain equilibrium conditions, the partial pressure of the gas in the liquid must be equal to its partial pressure above the liquid.

Figure 3.4 shows the dependence of oxygen solubility on partial pressure.

Knowing the dissolved oxygen concentration at one particular partial pressure, the gas concentrations for any desired partial pressure can be found by interpolation or extrapolation.

3.2.2 Temperature Dependence

Temperature dependence of the solubility of dissolved gases can be predicted by Le Chatelier's principle. Assuming equilibrium conditions, the solubility decreases with increasing temperatures if the heat of solutions is exothermic (H < 1; heat is released). Conversely, the solubility increases with increasing temperature, if the

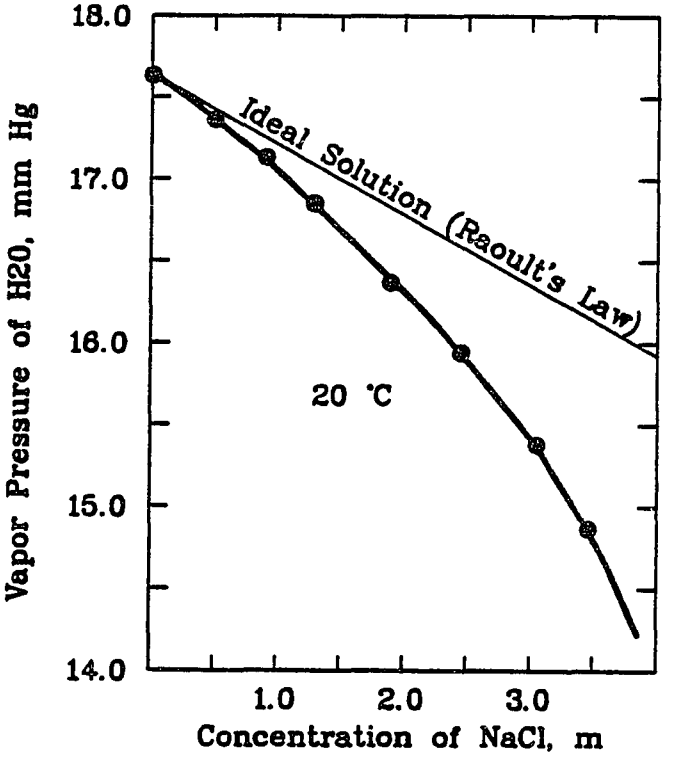

Figure 3.3 Water Vapor Pressure above NaCl Solution (data from [62])

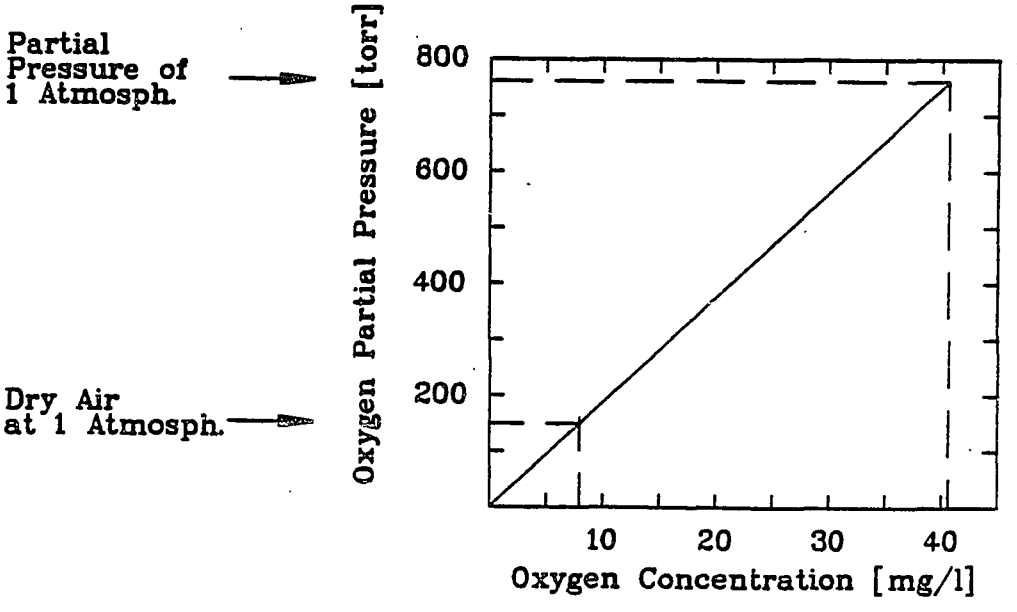

Figure 3.4 The Dependence of Oxygen Solubility on Partial Pressure (data from [59])

heat of solution is endothermic (H > 1; heat is absorbed). Generally, the solution of gases is exothermic. Thus the solubility of gases decreases with increasing temperature, assuming constant pressure. As the temperature of the liquid is raised gas is expelled from the liquid until complete degasification occurs at the boiling point of the solvent.

An equation which strictly holds only for ideal solutions, but which satisfactorily approximates the observed characteristics of dilute solutions is the following:

$$\left[\frac{\partial \ln (x_2'/x_2)}{\partial T} \right]_P = - \frac{H}{R * T^2} \qquad (3.23)$$

where: H = heat of solution at given temperature and pressure; P = total pressure above the solution; X_2 = mole fraction of gas in solution; X_2' = mole fraction of gas in vapor above the solution.

By assuming the heat of solution to be constant over small temperature ranges and X_2'', the mole fraction in the vapor phase, to remain constant, equation (3.23) can be developed to result in the following expression:

$$\ln x''_2 = - \frac{H}{R * T''} + \text{constant} \qquad (3.24)$$

where the double prime denotes a state of the system

different from the initial state and different from an arbitrarily defined reference state.

Equation (3.24) suggests a linear behavior between the variables involved. Experimental values indicate a slightly curved graph which is within $\pm$ 2% of the theoretical value. Equation (3.24) therefore is a first approximation of the solubility of gases as a function of temperature within the temperature range of 0 - 50 ^{o}C [59].

Simple relationships like equation (3.24) fail for the solubility of gases in water . . More complicated relationships have, however, been formulated. But these involve curve fitting and empirical values.

There are two forms of equation (3.24). The first form is obtained by considering the variation of heat of solution with temperature, as in the following power series applies:

$$H = A + B * T + C * T^2 + \ldots\ldots \qquad (3.25)$$

A first approximation neglects all nonlinear terms. The second form of equation (3.24) uses the variation of the Bunsen absorption coefficient, α . This coefficient is defined as the volume of a gas (reduced to S.C.) which is dissolved at the temperature of measurement in one volume of solvent at atmospheric pressure. This form of

equation (3.24) is obtained by fitting a general power series to mean values of a at different temperatures.

$$\alpha = a + b * T + c * T^2 + d * T^3 \ldots\ldots \quad (3.26)$$

For atmospheric pressure figure 3.5 illustrates fresh water solubility of oxygen as a function of temperature.

A useful relationship to calculate the combined effect of temperature and pressure is:

$$S' = S * \frac{P_T - P_V}{P_{AT} - P_V} \quad (3.27)$$

where: S' = the solubility of the gas in question at given pressure P_T; S = the solubility of the gas in question at atmospheric pressure; P_T = pressure above the liquid; P_{AT} = atmospheric pressure; P_V = vapor pressure of liquid.

As can be seen from equation (3.27) the difference ($P_T - P_V$) is the partial pressure of dry air above the liquid.

The dependence of the vapor pressure on temperature has been discussed in section 3.1.3.

3.2.3 Dependence on Electrolyte Concentration

The third major variable which changes the thermodynamic properties of a solution is the

concentration of electrolytes. With increasing electrolyte concentration a decrease in the equilibrium solubility of gases can be observed. This phenomenon is called the salting out effect. As electrolytes are added to the solution, the change in equilibrium solubility of a gas is not directly proportional to the amount added. The concentration of an electrolytic solution, particularly at high concentrations, is not an appropriate quantitative predictor of gas solubility. In general, the solute become increasingly less effective to affecting changes in solution properties if the concentration increases. Consequently an effective concentration rather than an absolute concentration is a more appropriate prediction tool.

In this regard the concept of activity is introduced. The activity α of a solute ion can be expressed using chemical potential or Gibbs free energy:

$$F_1 = \left(\frac{\partial F}{\partial n_1} \right) = F_{10} + R * T * \ln (\alpha) \qquad (3.28)$$

where: F_1 = partial molal Gibbs free energy; F_{10} =Gibbs free energy without presence of ions.

In order to relate the activity to the concentration of the solute the activity coefficient γ is introduced in the following expression:

$$\alpha_I = \gamma_{R,I} * N \qquad (3.29)$$

where: N = mole fraction of solute i

Since the mole fraction is commonly expressed in molar (moles/liter) or molal (moles/kg) units, other expressions are defined. For example:

$$\alpha_I = \gamma_I * m_I \qquad (3.30)$$

where: m_I = molal concentration of solute i.

In applying these concepts to the case of dissolved gases it is necessary to consider the fugacity of the gas. As stated previously, as ideal solution behavior is approached the fugacity and the vapor pressure of a gas become identical. Ideal conditions can be assumed as the partial pressure approaches zero, as indicated in the following expression:

$$\lim_{P \text{ to } 0} \left(\frac{f}{P} \right) = 1 \qquad (3.31)$$

$$\frac{f}{P} = \gamma_E = \text{activity coefficient} \qquad (3.32)$$

A simple relationship has been defined [59] which correlates the solubility of a gas in pure water, S, with

that in an electrolyte solution, S_E, by means of their activity coefficients, as follows:

$$S * \gamma = S_E * \gamma_E \tag{3.33}$$

or

$$\frac{S}{S_E} = \frac{\gamma_E}{\gamma} \tag{3.34}$$

From empirical measurements, the activity coefficients in pure water and electrolyte solutions are related as follows:

$$\ln \left(\frac{\gamma_E}{\gamma} \right) = K_S * I \tag{3.35}$$

where: K_S = a coefficient dependent on the electrolyte species added and the non-electrolyte solution; I = ionic strength.

The term ionic strength takes the charge characteristics of the ionic species into account. It is defined as:

$$I = 0.5 * \Sigma_I \; C_I * Z_I^2 \tag{3.36}$$

where: C_I = concentration of ion; Z_I = charge of that ion

The use of ionic strength is particularly important if

multicomponent electrolyte solutions are treated.
In aqueous solutions, in most cases, the following is true:

$$\frac{\gamma_E}{\gamma} > 1 \qquad (3.37)$$

From equation (3.33) and (3.37) it can be deduced that the solubility of a gas in pure water S is larger than that in ion solutions S_E.

In the case of a single valent solution, such as a sodium chloride (NaCl) solution, the ionic strength equals the molar concentration, C. The expression

$$\ln \left(\frac{S}{S_E} \right) = K_S * C \qquad (3.38)$$

shows a linear relationship between the molar concentration and the logarithmic expression of the ratio S/S_E. In figure 3.6 this ratio is plotted against the molar concentration of the Cl- ion. Measured deviations from the best fit straight line are within a 1% margin.

Seawater represents a complex electrolyte solution of uni- and multi-valent ion species. The desire to express seawater chemically by means of a single parameter has led to the definition of chlorinity and of salinity. For detailed definitions of these extensively used parameters

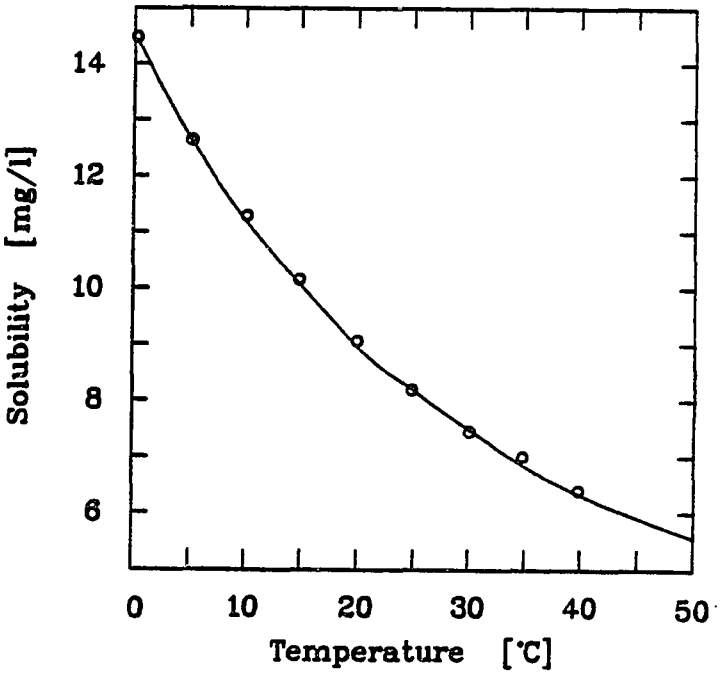

Figure 3.5 Solubility of Oxygen as a Function of Temperature (data from [59])

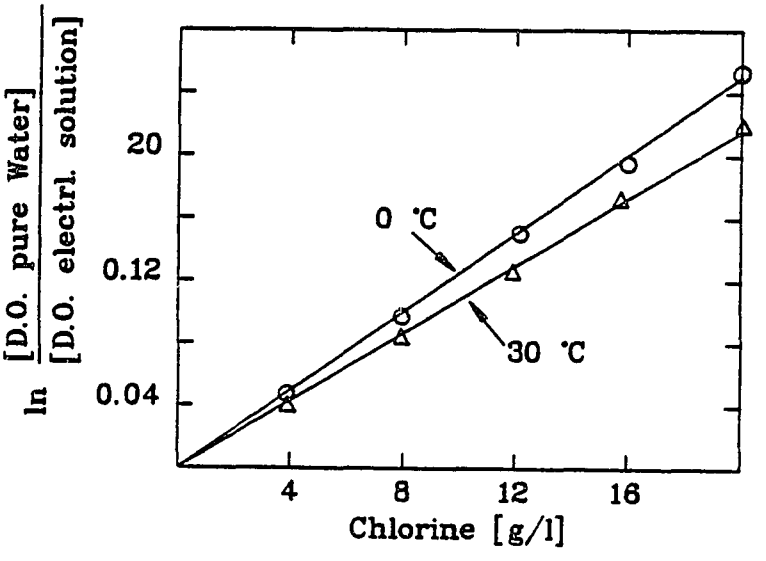

Figure 3.6 Oxygen Solubility in Aqueous NaCl Solutions (data from [59])

refer to standard oceanographic literature [e.g. 62]. Chlorinity (Cl) and salinity (Sal) are expressed in grams per kilogram seawater or ppt. They are related by an empirical expression [62]:

$$Sal = 0.03 + 1.805 * Cl \tag{3.39}$$

Salinity is the more commonly used parameter and denotes, generally speaking, the total salt content of seawater.

There have been numerous attempts to fit existing data of gas solubility in seawater. One of which, used for the present study, was proposed by Weiss [121]. Using a large number of measurements, Weiss curve fitted the data and promulgated the following thermodynamically consistent equation:

$$\begin{aligned} C = {} & A_1 + A_2 * (100/T) + A_3 * \ln (T/100) + \\ & A_4 * (T/100) + Sal * [B_1 + B_2 * (T/100) + \\ & B_3 * (T/100)^2] \end{aligned} \tag{3.40}$$

where: C = solubility of the gas; T = absolute temperature in ^{o}K; Sal = salinity in ppt.

The coefficients A_1 to A_4 and B_1 to B_3 depend on the gas of interest and the dimensions in which the solubility

is expressed. Coefficients for oxygen and nitrogen are listed in table 3.1

3.3 Diffusion

Gas is absorbed by a liquid by first diffusing into the liquid through its surface layer. The process of diffusion of solute molecules in the bulk liquid is due to the random thermal movements of these molecules. These random movements, have the net effect of transport in the direction of lower solute concentration. This phenomena is frequently referred to as driving force, which results in an equilibrium condition of a constant solute concentration throughout the medium. In fact, no such force exists and material transport to regions of low concentration is solely governed by random processes. Diffusion processes can be quantitatively treated by Fick's law of diffusion:

$$R = D * \frac{\partial C}{\partial X} \qquad (3.41)$$

where: R = one-dimensional flow of molecules per unit area normal to the direction of flux per time unit; D = diffusion coefficient; $\partial c/ \partial x$ = concentration gradient in the direction of diffusion.

A partial differential equation relating concentration

Constants	Oxygen		Nitrogen	
	[umole/kg]	[ml/l]	[umole/kg]	[ml/l]
A_1	-173.9894	-173.4292	-173.2221	-172.4965
A_2	255.5907	249.6339	254.6078	248.4262
A_3	146.4813	143.3483	146.3611	143.0738
A_4	-22.2040	-21.8492	-22.0933	-21.7120
B_1	-0.037362	-0.033096	-0.054052	-0.049781
B_2	0.016504	0.014259	0.027266	0.025018
B_3	-0.0020564	-0.001700	-0.003843	-0.0034861

Table 3.1: Constants for Equation (3.40)

with time and location can be developed by considering a differential element of thickness dx, as depicted in figure 3.7.

Applying Taylor's expansion the concentration gradient at the position x + dx is:

$$\frac{\partial C}{\partial X} + dX * \frac{\partial^2 C}{\partial X^2} \qquad (3.42)$$

Assuming further a quiescent liquid, without convective diffusion, and applying the equation of conservation of mass, the accumulation of mass within the control element can be determined. The rate of accumulation of mass can be expressed by the increase of concentration, multiplied by the volume, within the element. The rate of accumulation is the difference between diffusion in and diffusion out, as follows:

$$- D * \frac{\partial C}{\partial X} - \left(- D * \left(\frac{\partial C}{\partial X} + dX * \frac{\partial^2 C}{\partial X^2} \right) \right) =$$

$$dX * \frac{\partial C}{\partial t} \qquad (3.43)$$

thence:

$$\frac{\partial C}{\partial t} = D * \frac{\partial^2 C}{\partial X^2} \qquad (3.44)$$

Equation (3.44) is the basic relationship describing

the diffusion processes in the absence of any reaction. If there is a reaction between solute and solvent during diffusion an additional term, such as r for a first order reaction, has to be introduces in the right hand side of equation (3.44). If the diffusing agent is consumed by the reaction, r is positive.

The proportionality factor D in Fick's law of diffusion is the diffusion coefficient. The diffusion coefficient is a function of the temperature and the diffusing species of interest. The following relation holds:

$$D = D_0 * \exp\left(- \frac{E_A}{R * T} \right) \qquad (3.45)$$

where: D_0 = diffusion coefficient at the reference temperature; E_A = activation energy.

Activation energy is the amount of energy required to produce a chemical reaction. In the case of diffusion it is the energy required for a species to overcome a threshold to diffuse from one site to another. For practical application the dependence of D on temperature is important. In an aqueous solution D changes approximately 2% per degree.

Molecular diffusion of a gas in water happens relatively slowly. If there is convective movement within the liquid the combination of molecular diffusion

and convection result in an overall diffusion rate an order or more of magnitude higher than molecular diffusion alone. Convective diffusion can be expressed by a relationship involving the parameter, Peclet number:

$$P_E = \frac{V_M * L}{D} \tag{3.46}$$

where: V_M = main stream velocity of fluid; L = a characteristics length of the body.

With sufficiently small Peclet numbers molecular diffusion prevails. This occurs with slow fluid velocities and in regions of small dimensions. With increasing Peclet numbers convective diffusion predominates.

Diffusion rates are influenced by the presence of electrolytes. Theoretical formulations for predicting diffusivities in liquid have been established (e.g. [2],[57],[106]). Generally, these relationships contain severely limiting assumptions and are valid only for solutions containing one or two species. In most investigations where gas absorption into liquids containing more than two species of ions takes place, differences in ionic diffusion rates of these species are ignored [30].

Theoretical treatises for single-electrolyte systems

have been carried out. Two of which are presented below [2],[106].

Taking earlier theoretical relations between diffusivity and viscosity as the point of departure various authors have correlated diffusivity data by using the following relationship:

$$\frac{D}{D_W} = \left(\frac{\mu}{\mu_W} \right)^{-n} \qquad (3.47)$$

where: D = diffusivity of aqueous electrolyte solution; D_W = diffusivity of pure water; μ = viscosity of solution; μ_W = viscosity of pure water; n = a constant characteristic for ion-species.

Ratcliff and Holdcraft [106] evaluated n from their data and recommended a single variable for n. They presented their equation as:

$$\log_{10} \left(\frac{D_W}{D} \right) = 0.637 * \log_{10} \left(\frac{\mu}{\mu_W} \right) \qquad (3.48)$$

Figure 3.8 shows the relation between experimental diffusivities of carbon dioxide and the solution viscosity. Properties without subscript refer to electrolyte solutions, properties with subscript water refer to a pure water system.

Building on the concept of free energy of activation,

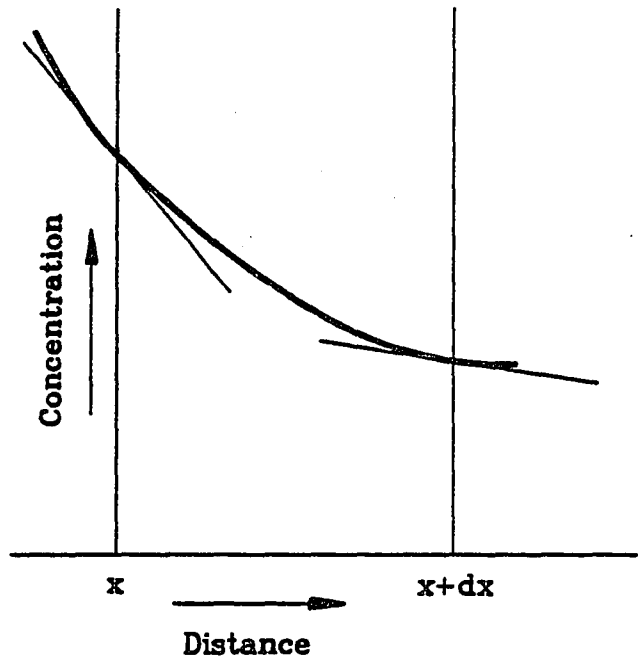

Figure 3.7 Concentration Distribution in Diffusion (from [30])

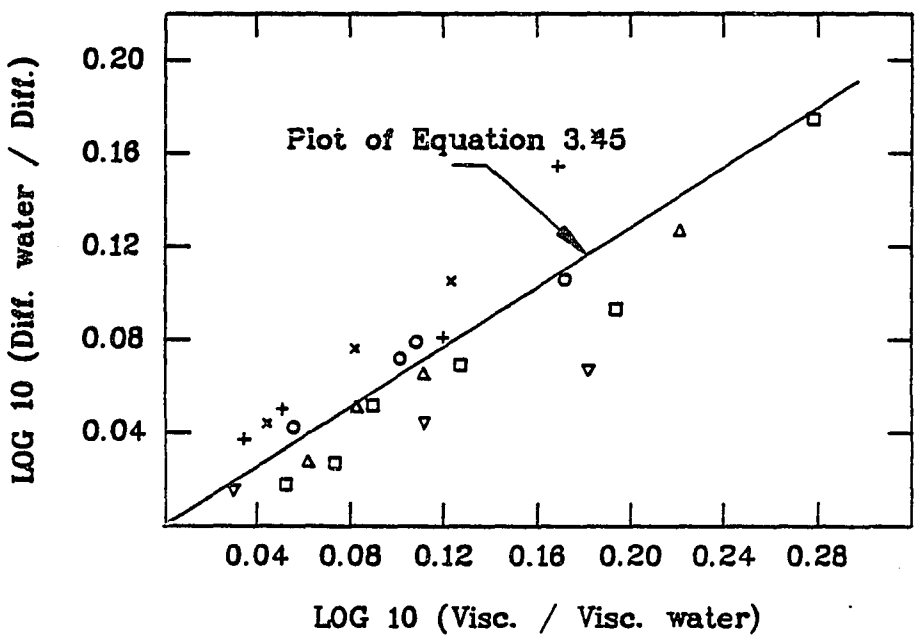

Figure 3.8 Relationship between Diffusivity of Carbon Dioxide and Vicosity of Chlorine Solution (from [106])

introduced in equation (3.45), Akita [2] developed the following relationship:

$$D = \left(\frac{k}{h}\right) * \left(\frac{V}{N_o}\right)^{2/3} * T * \exp\left(-\frac{G}{R * T}\right) \qquad (3.49)$$

where: k = Boltzmann constant; h = Plack constant; R = gas constant; V = molar volume of solution given by $V=1/(C_+ + C_- + C_W)$ where C_+, C_- , C_W are the molar concentrations of cation, anion, and water, respectively; N_0 = Avogadro's number; T = absolute temperature ^oK.

Akita formulated the variable z as follows:

$$Z = X_+ * V_+ = X_- * V_- \qquad (3.50)$$

where: V_-, V_+ = ionic valencies of the anion and cation, respectively; X_-, X_+ = mole fractions of cation and anion, respectively.

In figure 3.9 the experimental diffusivity of oxygen in sodium chloride solutions is plotted against z.

Diffusivities of gases in seawater found in recent oceanographic literature are solely based on theoretical predictions. Given the already noted difficulties of simplifying assumptions, there is an urgent need for experimental verification.

3.4 Gas Absorption

In the following review only physical phenomena of gas absorption are considered. Chemical and biological reactions which might alter the solute are neglected. Also, since the rates of solution of nitrogen and oxygen are primarily under consideration, gas layer resistance is deemed negligible in comparison to liquid layer resistance.

3.4 Gas Absorption into Quiescent Liquids

Although in most real situations turbulent conditions prevail, a study of diffusion into a quiescent liquid reveals important characteristics of gas-liquid exchange. Additionally, much useful information is obtained by experimental investigations conducted under conditions where the liquid can be considered quiescent. Furthermore, various models for the process of absorption of gases into turbulent liquids postulate the existence of a stagnant film where molecular diffusion prevails.

The following situation illustrates the mechanism of gas absorption into a quiescent liquid. The liquid, which for modeling purposes is assumed to be infinitely deep, comes into contact with a gas or a gaseous mixture at $t = 0$. After this initial contact the surface plane

of the liquid is assumed to have acquired its saturation gas concentration, C_S, for the test partial pressure of the gas, in accordance with Henry's law, (equation 3.22). The dissolved gas concentration within the liquid is assumed to be at concentration C_L at t = 0. It is evident that C_S must be greater than C_L for absorption into the liquid body to take place.

The above assumed boundary conditions can be written as follows:

$$C = C_S \text{ at } x = 0 \quad t > 0 \tag{3.51}$$

$$C = C_L \text{ at } x > 0 \quad t = 0 \tag{3.52}$$

$$C = C_L \text{ at } x = oo \quad t > 0 \tag{3.53}$$

where: C = concentration of dissolved gas; x = distance measured from surface of liquid, where x=0; t = time of exposure; C_L = concentration of gas in bulk of liquid; C_S = saturation gas concentration.

As described earlier, the gas absorption process is governed by the diffusion equation (3.44).

$$\frac{\partial C}{\partial t} = D \ast \frac{\partial^2 C}{\partial X^2} \tag{3.54}$$

Fick's law, equation (3.41), defines the rate of transfer of dissolved gas across a unit area normal to the direction of transport as:

$$R = D * \frac{\partial C}{\partial X} \qquad (3.55)$$

Applying the boundary conditions (3.51), (3.52), and (3.53) the solution of equation (3.54) is:

$$C_L = (C_S - C_L) * (1 - erf(\frac{X}{2*(D*t)^{0.5}}) \qquad (3.56)$$

From equation (3.54) and (3.55) it follows that the rate of transfer can be expressed as:

$$R = (C_S - C_L) * (\frac{D}{\Pi * t})^{0.5} \qquad (3.57)$$

or

$$R = k_L * (C_S - C_L) \qquad (3.58)$$

The term k_L is the liquid film mass transfer coefficient [cm/sec].

From equation (3.57) it can be seen that k_L is a function of time. At time t=0 when liquid and gas first come in contact, k_L is assumed infinite. With $t > 0$ k_L decreases with time.

Concentration profiles of a solute gas at successive exposure times are shown in figure 3.10. The molecular diffusion coefficient was assumed to be $2*10^{-5}$ [cm2/sec]

which is a representative literature value [30]. The ordinate represents the ratio of point concentration, C_{point}, over the solubility of solute according to the partial pressure, C_{sat}. The abscissa is distance, x, from the free surface plane.

Discussion, up to this point, of the gas absorption processes has been under the assumption that the resistance to gas absorption is solely a liquid-side phenomena. Gas-side resistance has to be assumed in cases when a gaseous phase consists of a mixture of soluble and insoluble gases. As the soluble gas isreadily absorbed by the liquid, the insoluble gas accumulates near the surface, thereby decreasing the partial pressure of the soluble gas component in the surface layer. A decrease in the rate of solution of the soluble gas results.

A stagnant gas film can be assumed through which the soluble gas travels only by molecular diffusion. Across this film the partial pressure of the soluble gas is linearly reduced from its value in the bulk gas to that at the liquid surface.

Following this argument an overall resistance can be defined as a sum of liquid and gas resistances, as follows:

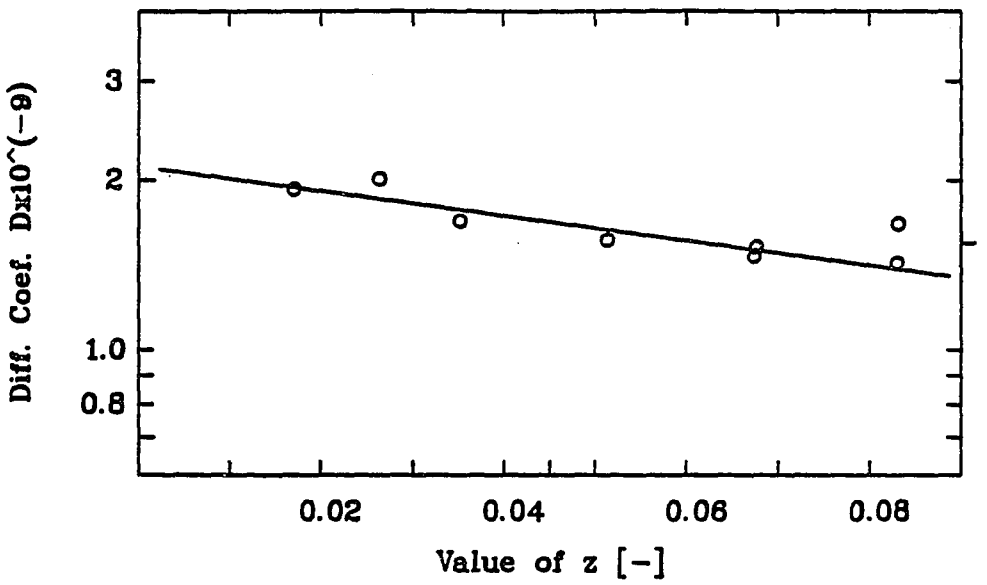

Figure 3.9 Experimental Diffusivities of Oxygen in Sodium Chloride Solutions versus Variable z (data from [2])

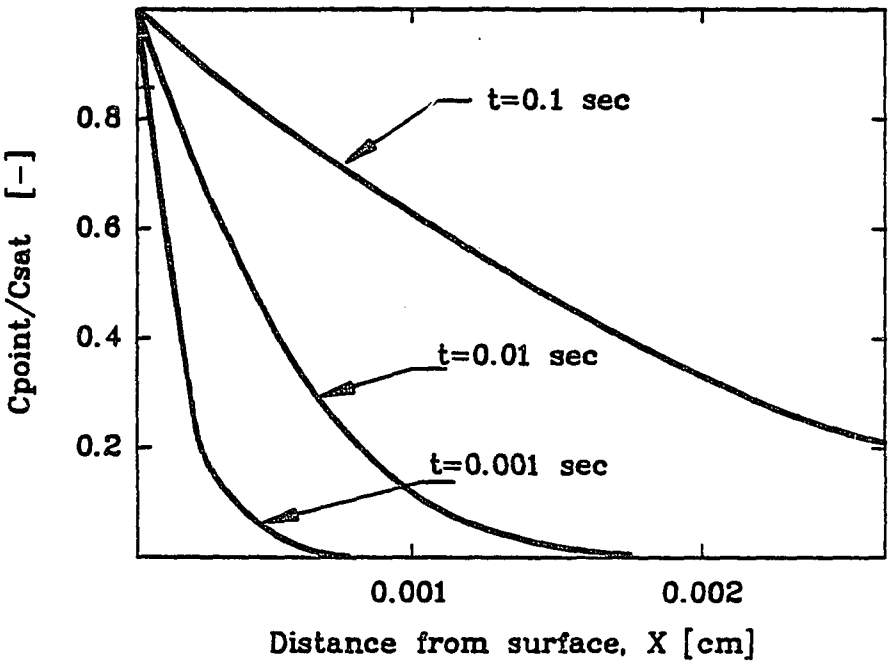

Figure 3.10 Concentration Profiles for the Absorption of Gas into Quiescent Liquid (from [30])

$$\frac{1}{K_L} = \frac{1}{k_L} + \frac{1}{H_e * k_G} \qquad (3.59)$$

where: k_G = gas phase mass transfer coefficient; He = coefficient in Henry's law.

In many practical applications, including water aeration and deaeration, the solubility of gas components are sufficiently similar so that gas phase resistance can be neglected. Consequently, the overall resistance is controlled by liquid-side phenomena.

It should be noted that in the condensation process, in which non-condensibles take the role of non-soluble gases, gas phase resistance is the controlling factor and it is for this reason that the removal of non-condensible gases is a desired pretreatment step.

3.4.2. Absorption into Agitated Liquids

Understanding the gas absorption processes under turbulent conditions is of considerable practical importance. Dissolved gases are transported from the liquid surface layer to the interior of the liquid by convective diffusion.

There are several conditions which may create turbulence :

i) The liquid is sprayed through a gas as drops or jets.

ii) The liquid runs over rough and discontinuous solid surfaces.

iii) The liquid is agitated mechanically.

iv) Gas bubbles are blown into the liquid.

Based on experimental evidence, the rate of absorption of a gas under turbulent conditions, R, can be expressed as follows:

$$R * a = k_L * a * (C_S - C_L) \qquad (3.60)$$

where: a = area of gas-liquid interface per unit volume; k_L = mass-transfer coefficient; C_S = saturation gas concentration; C_L = gas concentration in bulk of liquid. (The importance of the coefficient k_L*a will be discussed in a later chapter.)

There are several models describing the absorption processes. Some of the most prominent are presented in the following paragraphs.

Lewis and Whitman [81] introduced their model in 1924. They postulated a stagnant film in which there is no convection and the gas is transferred only by molecular diffusion. The rest of the liquid is agitated and has a uniform composition. The concentration of a dissolved gas changes from saturation at the exposed surface to

that of the bulk at the interior plane of the surface film. All resistance is assumed to be concentrated in the film. The film coefficient is expressed as:

$$k_L = \frac{D}{L} \tag{3.61}$$

where: D = diffusivity; L = film thickness.

Hydrodynamic characteristics of this system are expressed by the variable L. The film thickness depends on various factors such as the degree of liquid agitation, physical properties of the liquid, etc. As the thickness of the film cannot be predicted, the use of the film theory must be empirical.

Other, more advanced models, depart from the somewhat unrealistic concept of a stagnant film [e.g. 29]. Still liquid models propose absorption to take place from a solid surface into a moving turbulent fluid. Transport is assumed to progressively change from molecular diffusion to convective diffusion with increasing distances from the surface.

A surface rejuvenation model envisions the initial transfer to happen in a stagnant film. After a certain time of exposure a convective disturbance replaces the film into the bulk liquid to a certain depth. This model is deemed a fairly good description of what happens when liquid flows over packing [29].

Surface renewal models propose that elements of liquid at the surface are replaced by liquid from the interior after various time intervals. While at the surface the liquid is exposed to the gas phase and absorption happens as if the liquid were quiescent. Surface liquid elements are exposed at the surface for different length of time, or have different ages. Consequently, absorption rates of liquid elements are different.

Descriptions of liquid surface layer ages differ among variations of this model. The original Higbie model assumes each element to be exposed to the gas for the same length of time. The Dankwerts model [29] modified the Higbie theory by assuming a constant rate of surface renewal. Based on this model and on the rate of absorption into quiescent liquid, equation (3.57), the mass transfer coefficient is defined as:

$$k_L = (D * s)^{0.5} \qquad (3.62)$$

where: s = fraction of the area of surface replaced with fresh liquid per time interval.

Although stagnant film models convey a not entirely realistic impression, they do incorporate essential features of the real system. Predictions made with this model are usually remarkably similar to those obtained by more sophisticated models. Due to its simplicity, the

stagnant film model is frequently used for treatment of the absorption processes under turbulent conditions.

3.5 Dissolved Gases Measurement Techniques

Since in the present study only dissolved oxygen and nitrogen are measured, a review of commonly used analysis methods is limited to these two gases.

3.5.1 Dissolved Oxygen Sensor

Introduction of the membrane covered polarographic detector by Clark in 1956 has appreciably facilitated the measurement of dissolved oxygen. Numerous variations have been developed from Clark's original conception .

The basic design of the detector consists of two electrode cells with a membrane separating the electrodes in an electrolyte solution from the liquid to be measured. The membrane is made of a gas permeable material. Oxygen from the liquid to be measured diffuses through the membrane into the electrolyte solution covering the cathode. Thence it diffuses through the solution and reaches the cathode where it is reduced. The cathode is at such a negative potential that it reduces all of the arriving oxygen. This results in a current flow. The magnitude of the current is proportional to the oxygen

available for reduction, which is proportional to the oxygen concentration in the liquid to be measured.

Figure 3.11 illustrates the distribution of oxygen concentration in the vicinity of the membrane. The concentration of oxygen in the bulk liquid, C_L, is assumed to be constant up to the outer edge of the membrane. With steady state at the liquid-membrane interface a linear relationship exists between the liquid gas concentration C_L and the corresponding concentration within the membrane C_M. Similarly, at the inner boundary of the membrane a relationship exists between C_M and the concentration of oxygen within the electrolyte solution C_E. These two equilibrium relationships can be expressed as:

$$C_M = K_1 * C_L \tag{3.63}$$

and

$$C_M = K_2 * C_E \tag{3.64}$$

where: K_1 and K_2 are appropriate coefficients.

As shown in figure 3.11 the concentration distribution in the membrane and the electrolyte solution varies from t=0 (start of electrolysis) until acquiring steady state (here denoted with oo) is achieved. The situation

immediately following start of oxygen reduction on the cathode is characterized by a high flux of oxygen and a steep concentration slope in the electrolyte layer. With time the concentration profile is continuously modified until steady state is reached.

A relationship which correlates the production of current with the concentration gradient at the electrode can be written as follows [59]:

$$i = n * F * D_E * \left(\frac{\partial C_E}{\partial X} \right)_{X=-a} \qquad (3.65)$$

where: F = Faraday constant; n = number of electrodes per electrode reaction; D_E = diffusivity of electrolyte solution.

Further developments of this relationship and definition of permeability of the membrane P_M can be expressed as:

$$P_M = D_M * \frac{K_1 * C_L - K_2 * C_{E,X=0}}{C_L - C_{E,X=0}} \qquad (3.66)$$

where: D_M = diffusivity of membrane.

This gives the current, i, as a function of the oxygen concentration of the liquid, C_L, as follows:

$$i = n * F * C_S * \frac{P_M}{b} \qquad (3.67)$$

where: b = thickness of the membrane.

In the presence of electrolytes in the sample liquid, activity takes the place of concentration in equation (3.67). The oxygen detector responds to the difference in activity across the membrane rather than to a concentration difference. Equation (3.67) can thus be written:

$$i = n * F * a_S * \frac{P_M}{D} = n * F * \gamma_{LE} * C_{LE} * \frac{P_M}{b} \qquad (3.68)$$

where: subscript LE denotes a liquid sample electrolytes.

One important operational feature of the oxygen detector is the required flow over its membrane. In the previous theoretical derivation it was assumed that the liquid bulk concentration is constant up to the outer boundary of the membrane. In order to maintain such a constant concentration, the sample has to be continuously stirred. Oxygen diffuses through the membrane than is replenished from the bulk of the liquid. As a consequence, depletion of oxygen occurs in the liquid close to the membrane surface and erroneous measurements result.

Figure 3.12 shows the influence of stirring on the sensitivity of the oxygen detector; sufficient stirring is obtained when the liquid flow across the membrane is equal or above 0.30 m/sec.

3.5.2. Winkler Method

The Winkler method is the most commonly used chemical method for analyzing dissolved oxygen. The method involves oxidizing Mn(II) to Mn(III) in an acid solution. Iodine is then titrated, with starch being used as an indicator [62]. With careful technique the precision of this method is better than $\pm$ 0.1 mg/l.

Due to potential interferences from various ions and other chemical species (especially in seawater) a number of modifications of the basic method have been developed to correct for these interferences. The Azide modification [59] was used in previous gas transfer experiments (conducted by the author) to calibrate the polarographic detector used in the present study.

3.5.3 Gas Chromatography

Chromatography is based on separating a mixture into its components by taking advantage of different diffusion and sorption characteristics of the component substances.

In gas chromatography a mixture of gases is separated as it is pushed through an analytical column by a carrier gas. The column is coated with a powder. As the mixture is transported through the column its gas constituents establish equilibria with the packing material. The rates

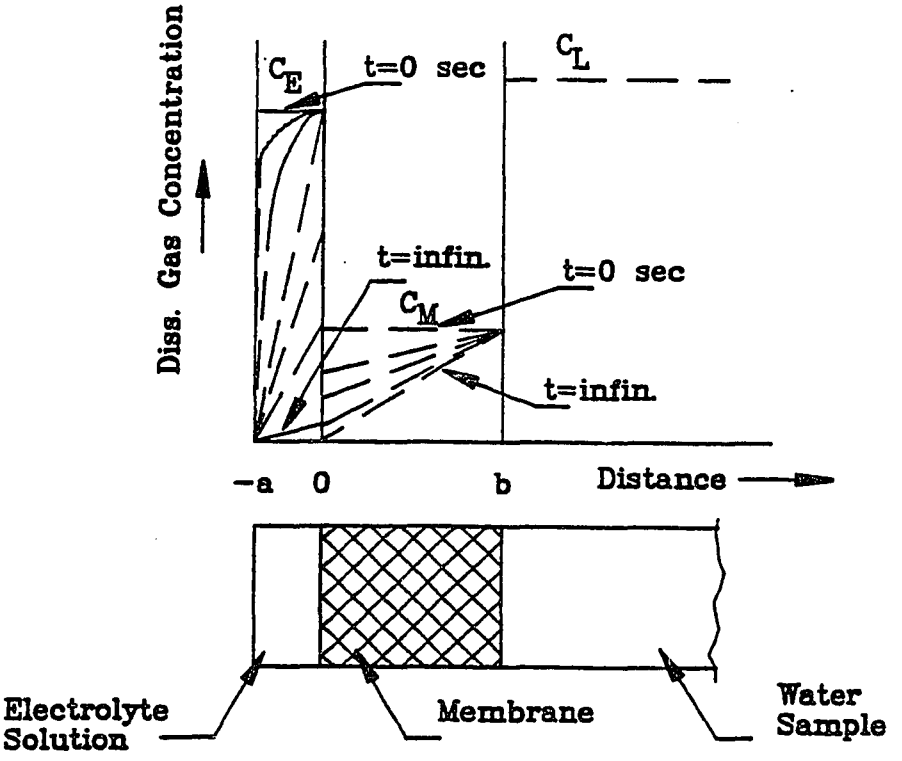

Figure 3.11 Concentration Profiles in the Vicinity of Detector Output (from [59])

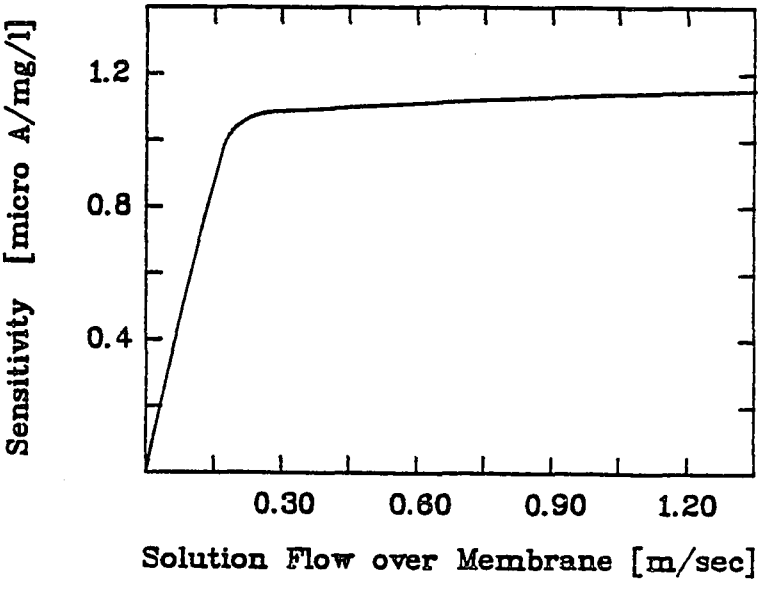

Figure 3.12 Effect of Stirring on Oxygen Detector Output (from [59])

of such reactions are characteristics of each specific gas. As a result the gas mixture is partitioned into chromatographic zones, one for each gas. The zones move with different speeds thereby separating the gas mixture into its individual gases. When individual chromatographic zones reach a detector, a signal is generated which is proportional to the gas content in the mixture. A standard gas mixture of known composition is used for calibrating the gas chromatograph. From the recorded signals of the standard gas the quantitative compositions of similar gas mixtures can be determined. Gas chromatography allows simultaneous analysis of several gases in a test sample.

The gases dissolved in liquids have to be separated from the liquid phase before separation in the gas chromatograph column can occur. A suitable means for this is stripping of the liquid sample with carrier gas in an in-line stripping device.

CHAPTER IV

BUBBLE GAS - TRANSFER EXPERIMENTS

4.1 Review of Pertinent Bubble Properties

The purpose of this section is to introduce some important aspects of the dynamic and physical properties of bubbles. Pertinent bubble characteristics, introduced here, are used as points of departure for the discussion of bubble gas transfer experiments.

4.1.1 Formation of Bubbles

The generation of bubbles is of great importance in a wide range of phase-contacting experiments and technical equipment. Bubbles can be formed in a variety of ways. The most important methods are by means of air injection, falling water jet entrainment, and spontaneous growth (nucleation) in thermodynamically unstable systems. Although the third method plays a significant role in the OC-OTEC heat and mass transfer processes, only bubble formation in water due to air injection will be treated at this point.

Bubbles are formed by forcing gas through orifices or porous sparging devices into the water column. Although for practical purposes a single orifice normally would not

be used to form bubbles, an understanding of the bubble formation process at a single orifice is necessary for the discussion of more complex methods of air injections.

Bubble formation at an orifice is a surprisingly complex phenomenon. Some of the principal factors which affect the diameter d_B of a formed bubble are:

i) diameter of the orifice
ii) liquid density and viscosity
iii) gas density and viscosity
iv) surface tension of the liquid
v) volumetric gas flow rate through the orifice
vi) contact angle for the liquid with orifice surface plane
vii) shape of the orifice
viii) submergence of the orifice
ix) flow conditions near the orifice
x) pressure drop across the orifice

At some point all of these factors have been used in the many models proposed to predict bubble formation in liquids. In the following discussion the models used are based on sequences of events suggested by photographic observations.

There are basically two categories of theoretical models, namely one-stage models and multi-stage models. One-stage models assume that bubbles grow smoothly at the orifice until buoyancy exceeds attachment forces and

detachment occurs. Multi-stage models predict basic changes in the growth mechanism during the formation process.

Due to the complexity of the bubble formation process, models are valid only under restrictive assumptions and thereby exhibit inherent limitations. Some of these limitations are:

i) resident turbulence in the liquid and up-draught due to the wake of the preceding bubble are generally ignored.

ii) expressions used for drag and added mass are at best only approximate.

iii) bubbles are assumed to remain spherical

In order to illustrate bubble formation processes, the simplest mechanism is used in the following discussion. Consider a bubble forming very slowly in a vertical tube. The bubble grows until its buoyancy exceeds the surface tension force. (figure 4.1) Assuming the bubble to be spherical and of diameter d_B at the moment of release, the two forces involved can be expressed as follows:

$$F_R = \text{retarding surface tension forces} \qquad (4.1)$$

$$= \pi * d_o * \sigma$$

$$F_A = \text{acting buoyancy forces} \qquad (4.2)$$

$$= 1/6 * \pi d_B^2 * \Delta\rho * g$$

where: d_o = orifice diameter; σ = surface tension; $\Delta\rho$ = density difference between liquids and gas; g = acceleration due to gravity; d_B = bubble diameter.

Setting the two forces equal results in the following equation:

$$\pi * d_o * \sigma = 1/6 * \pi * d_B^2 * \Delta\rho * g \qquad (4.3)$$

solving for d_B

$$d_B = \left(\frac{6 * \sigma * d_o}{\Delta\rho * g} \right)^{1/3} \qquad (4.4)$$

By knowing the surface tension of the liquid and the density difference, the resulting bubble diameter d_B is found to be a function of the orifice diameter d_o only:

$$d_B = (0.446 * d_o)^{1/3} \qquad (4.5)$$

for water @ 22°C; σ = 72.4 [dynes/cm]

Blanchard et.al. [16] carried out bubble formation experiments to test the validity of equation (4.5). The results of these tests are shown in figure 4.2, where generated bubble radii are plotted against the radius of the capillary tube. Good agreement between experiment and theory can be observed. The researchers, however, detected several factors which altered bubble formation

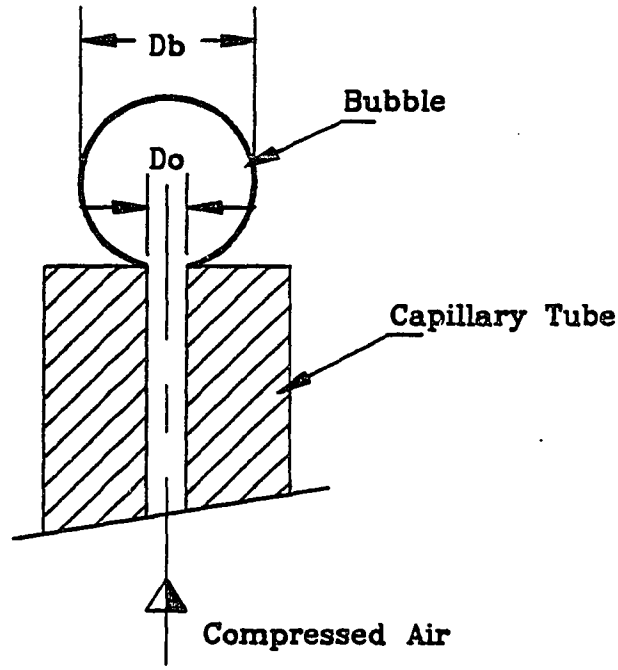

Figure 4.1 Air Bubble on Orifice

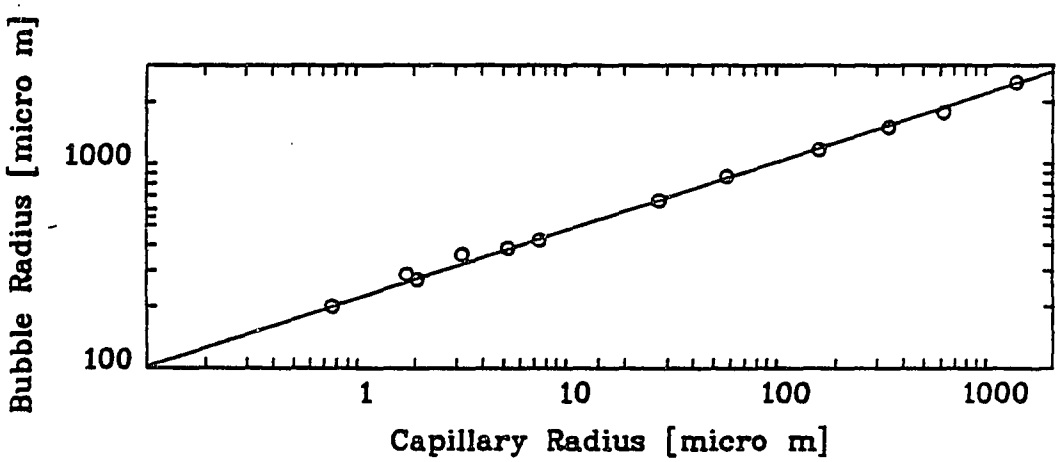

Figure 4.2 Comparison of Theory and Experiment for the Size of a Bubble Produced by a Capillary (data from [16])

and gave rise to deviations from theoretical predictions. If the plane of the tip was more than a few degrees from the vertical axis of the capillary tube, significant differences between theory and experiment were found. If bubble forming was too rapid, the bubbles tended to be larger than predicted.

Given these limits, the experiments suggested remarkably good agreement with theoretical predictions. Using equation (4.5), the capillary tube diameter necessary to produce a small bubble of predetermined size can be calculated readily.

Blanchard described further the intricate procedure of fabricating glass capillaries with extremely small orifice diameters. This procedure was applied in the present study to produce some capillary tips for the bubble rise experiments.

By increasing the gas flow through the orifice the bubble diameter initially remains constant while the frequency of bubble generation increases. At higher gas injection rates the frequency of bubble formation becomes constant while the bubble diameter increases. By increasing the flow further, single bubbles are no longer formed. Instead, there is a considerable spread of bubble sizes with bubble breakup resulting in production of numerous small bubbles.

Several procedures can be used to generate small

bubbles. The method described above, in which small bubbles are produced from capillary tubes, has the disadvantage of requiring considerable pressure differentials across the capillary. In practical applications two methods are commonly applied. In one case, bubbles are produced by means of a porous air stone or fritted disk. In the second case, water moves perpendicular to relatively small orifices. Due to the shear of the moving water bubbles are prematurely released.

4.1.2 Forms of Bubbles

Although bubbles are often axisymmmetrical, bubbles are spherical only under special circumstances. Depending on the external flow regime bubbles tend to alter their forms when subjected to normal and shear stresses. Possible shapes are determined by the force balance of external stresses and interfacial reactions.

If bubbles are prevented from moving freely and instead adhere to solid surfaces they are called static bubbles. Pendant bubbles are those attached to a surface with gravity forces trying to pull them away. Sessile bubbles are hindered from moving under the influence of gravity by solid surfaces and form at the underside of these surfaces.

Moving bubbles can be grouped into three categories according to their shapes [e.g. 83]. In figure 4.3 regimes of characteristic bubble shapes are described by two dimensionless parameters:

$$R_e = \frac{\rho * dE * U}{\mu} = \text{Reynolds Number} \qquad (4.6)$$

and

$$E_o = \frac{g * \Delta p * d_E^2}{\sigma} = \text{Eotvos Number} \qquad (4.7)$$

where: ρ = density of continuous phase; d_E = diameter of volume-equivalent sphere; U = rise velocity; μ = dynamic viscosity; g = acceleration due to gravity; Δp = excess pressure in bubble; = interfacial surface tension.

Shapes of spherical bubbles can be closely approximated by spheres if the ratio of their minor to major axis is within 10% of unity [29]. Here viscous forces and interfacial tension are more important than inertial forces.

Ellipsoidal bubbles are generally described as oblate spheroids (described below). Their shapes are subject to continuous change during bubble rise and undergo periodic or random wobbling.

Spherical-cap bubbles are bubbles which are greater than approximately 1.7 cm [119]. They assume a semi

spherical cap shape with a flat and indented base. In their appearance they resemble cut-off sections of spheres or oblate spheroids. Larger bubble species often develop wakes in which smaller bubbles are dispersed.

The presence of containment walls affect the movement and shape of rising bubbles. If the bubble is sufficiently large slug flow is encountered whereby the bubble takes up a large fraction or the entire cross-sectional area of the containing vessel.

For the present study spherical and ellipsoidal bubbles are of particular interest since the bubble sizes encountered here are below the values where spherical-cap bubbles start to form. Since the geometrical description of spherical bubbles is self-evident, terms describing geometrical features of fluid particles are given only for ellipsoidal bubbles.

Ellipsoidal bubbles very frequently are described as axisymmetrical spheroids. A spheroid is an ellipsoid of revolution, generated by rotating an ellipse about one of its principle axes. If this is the minor axis, the body is referred to as oblate, otherwise the spheroid is prolate.

The aspect ratio E is defined as the ratio of the axis of symmetry to the maximum diameter normal to that axis [29]. Therefore an oblate spheroid has an aspect ratio of $E < 1$ whereas $E > 1$ for prolate spheroids. The

dimensions of a spheroid are illustrated in figure 4.4.

If a and b are the major and minor semi-axis, respectively, the area A and volume V of an oblate spheroid can be expressed as:

$$A = 2 * \pi * a^2 + \pi * (b^2/e) * \ln \left(\frac{1 + e}{1 - e} \right) \quad (4.8)$$

$$V = 4/3 * \pi * a^2 * b \quad (4.9)$$

where: e = eccentricity of ellipse.

There is a variety of empirical factors to describe the geometry of ellipsoidal bubbles and to correlate flow characteristics. The approach used in this study is based on volumetric expressions. The diameter of a volume equivalent sphere d_E, used in equation (4.6) and (4.7), is derived by setting the volume of the spheroid equal to the volume of sphere with diameter d_E:

$$4/3 * \pi * a^2 * b = 1/6 * \pi * d_E^3 \quad (4.10)$$

$$d_E = (8 * a^3 * b)^{1/3} \quad (4.11)$$

4.1.3 Effects of bubble contamination

Even small amounts of surface active contaminants in the liquid have a significant effect on the hydrodynamic

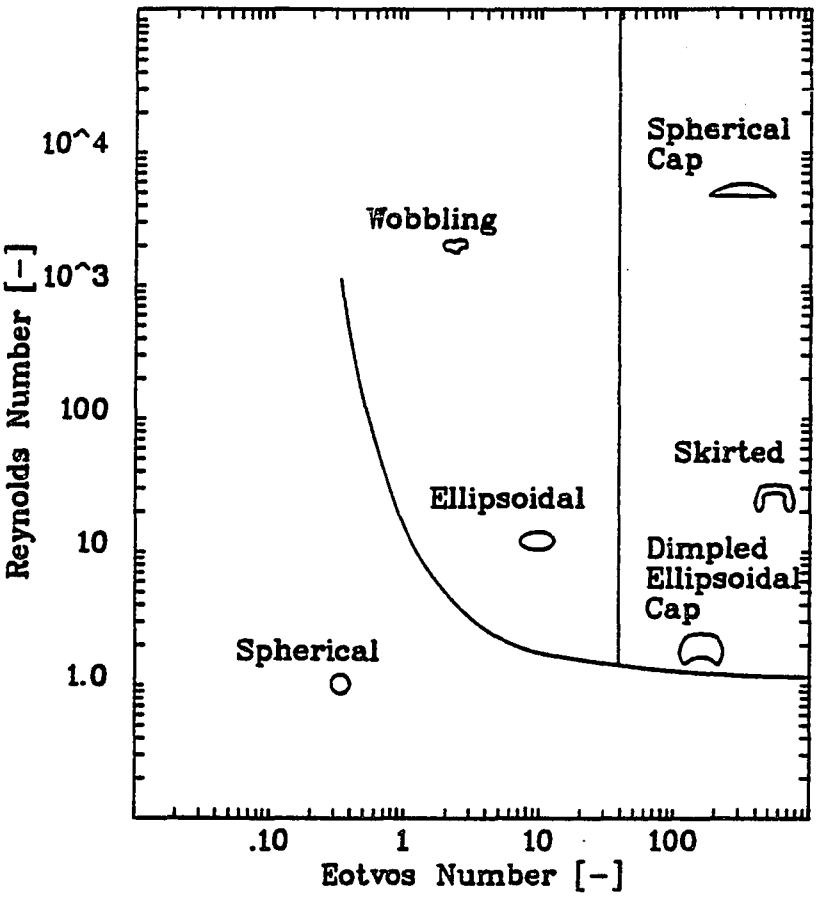

Figure 4.3 Shape Regimes for Bubbles in Free Motion (from [24])

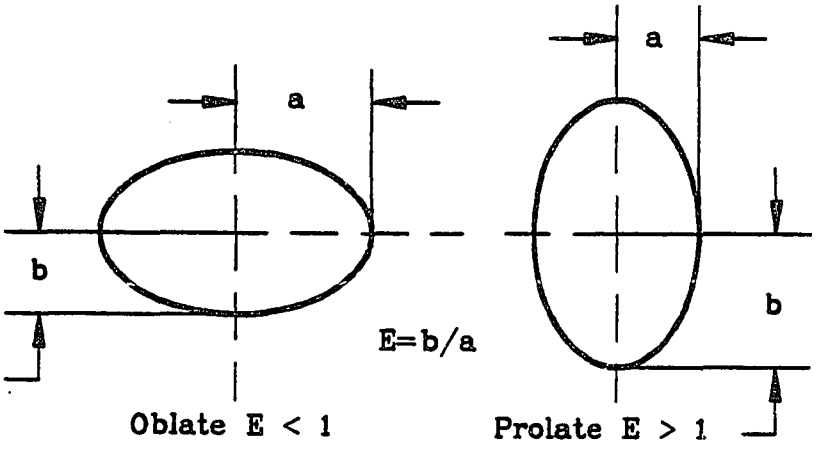

Figure 4.4 Dimensions of a Spheroid

behavior of bubbles. The contaminant can drastically increase the drag of a bubble and reduce the overall mass and heat transfer rates. Systems with high interfacial tension, such as air-water systems, are particularly prone to such interferences.

The effect of the contaminant depends on its chemical nature, on its concentration in the continuous phase and on the size of the bubble. By considering the air-water system of the present study, effects of surface contaminants on the transfer coefficients of dissolving bubbles can be categorized as follows:

1) In contaminated water the mass transfer coefficient of any bubble is usually found to be less than in pure water. In particular, small bubbles with a diameter range of 0.5-5 mm diameter are affected. As a bubble is injected into the fluid there is a period when contaminants accumulate on the bubble surface. This process is referred to as bubble aging. The transfer coefficient decreases from its pure fluid value while the bubble ages. The rate of decrease is higher for low bubble ages.

2) Fluid particles with internal circulation have a small wake, which has little influence on the mass transfer. Surface contaminants change the flow behavior of bubbles to that of solid spheres or spheroid which develop an appreciable wake.

3) The presence of a fixed amount of interfacial contaminants leads to a time dependent transfer from the bubble. While the bubble is rising, however, more impurities are accumulated and this variation introduces a further element of time dependence on transfer rates.

4) If external flow conditions are such as to cause large interfacial shear forces, surface contaminants are likely to cause a much lower influence on interfacial transfer. Large bubbles and systems with high turbulence are influenced to a lesser degree than small bubble systems.

Estimating the influence of surface contaminants is made difficult by the fact that both the magnitude and the nature of the contamination determine its effect.

The above-mentioned effects apply to surface active contaminants. These additives that are absorbed at the interface and tend to reduce the surface tension. Inorganic electrolytes, however, increase the surface tension of water.

Electrolytes have a profound effect on bubble coalescence. (See chapter 4.1.6). There has been much speculation about the physicochemical mechanism involved and to date no unanimously accepted theory exists. Furthermore, there is dispute as to what effect electrolytes have on mass transfer other than via coalescence. According to some theories, in a system

where gas transfer is liquid-side controlled, the ratio of the rate of transfer in pure water to that of sea water is in exact proportion to the ratio of the solubility of a gas. Thence, gas molecules encounter the same resistance in each situation. Bubble gas transfer experiments [80], however, report that mass transfer coefficients increased significantly with electrolyte concentration. These authors suggest that the resistance is affected by the presence of the ions, and that some ions, enhance the ability of gas molecules to dissolve in water. Other aeration investigations [6] state that NaCl did not change the mass transfer of a bubble.

4.1.4 Spherical Bubbles

Two terms which are frequently used in the following chapters are noncirculating and circulating fluid particles. Non-circulating, rigid fluid particles are those in which no internal motion of fluid exists relative to a particle bound coordinate system. Circulating, mobile fluid particles move relative to such a coordinate system.

For flow regimes with low Reynold numbers analytical solutions have been developed for mobile and rigid spheres. Perhaps the most important analytical solution for mobil spheres was independently developed by Hadamard

and Rybczynski [24]. The fluid sphere is assumed to have an interface, which is completely free from surface-active contaminants. Resulting streamlines are plotted in figure 4.5. As can be seen from figure 4.5 the streamlines are not closed. The solution predicts that the outer fluid is entrained along with the moving sphere. The form drag coefficient is obtained by integrating the fore-aft unsymmetrical pressure over the surface. For gas bubbles the drag due to shear is zero. By setting the drag force equal to the buoyancy force, the terminal velocity for a mobile spherical gas bubble at creeping flow can be developed as follows:

$$U_T = 1/3 * \frac{g * a^2 * \Delta\rho}{\mu} \qquad (4.12)$$

where: a = radius of sphere; μ = viscosity.

The flow behavior of rigid spheres at low Re is described by Stokes's solution. The streamlines are shown in figure 4.6. The total drag coefficient is given by Stokes's Law.

$$C_D = \frac{24}{R_e} \qquad (4.13)$$

Of the total drag two thirds is due to skin friction and one third from form drag. The terminal velocity is described by:

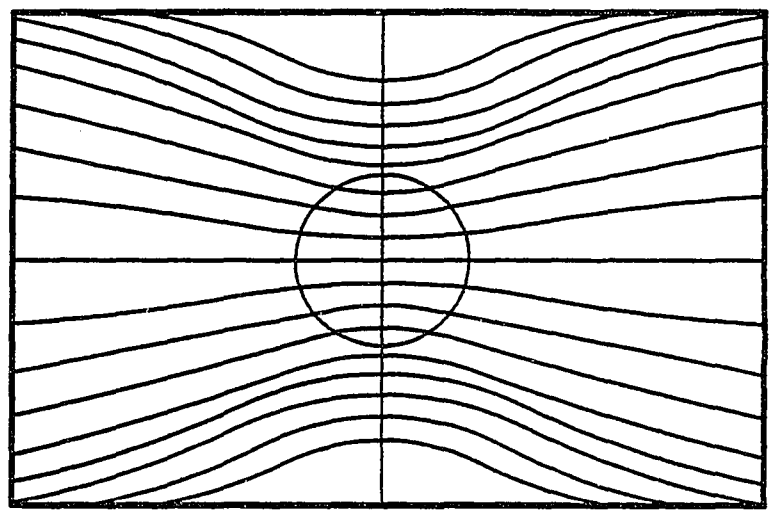

Figure 4.5 Streamlines for Motion of Fluid Spheres through Fluid at low Re (Hadmard-Rybczynski Solution)

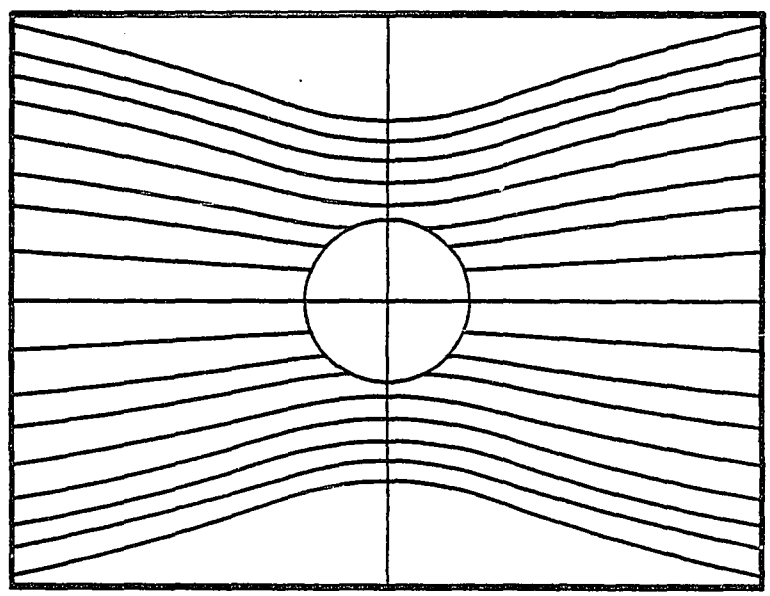

Figure 4.6 Streamlines for Motion of Fluid Spheres through Fluid at low Re (Stokes Solution)

$$U_{TS} = 1/18 * \frac{g * d_B^2 * \Delta\rho}{\mu} \qquad (4.14)$$

The Hadamard-Rybczynski theory gives the terminal velocity of a mobile bubble as up to 50% higher than the velocity of a rigid bubble with the same volume and density. Experimental data, however, indicate that small bubbles generally follow Stokes's solution. Furthermore, internal motion was observed to be absent. There are several hypotheses for these differences.

The most reasonable explanation for the absence of internal circulation suggests the existence of a stagnant cap at the downstream face of the moving bubble. Surface-active substances tend to accumulate at the bubble surface, thereby reducing surface tension. While the bubble is traveling through the liquid, absorbed contaminants are swept to the rear of the bubble, thereby leaving the front of the bubble relatively uncontaminated. A gradient of contaminant concentration results in a tangential gradient of surface tension which causes a tangential stress strong enough to suppress surface motion.

This mechanism of surface contamination theory implies that bubbles, including very small species, exhibit internal circulation if the continuous phase is sufficiently free of surface active contaminants.

Experimental investigations, in which great care was taken to purify the sample water, revealed excellent agreement with predictions made by the Hadamard-Rybczynski theory [29].

According to the stagnant cap model a relationship can be developed to correlate terminal velocities calculated by Hadamard-Rybczynski and by Stokes's solution. Such a terminal velocity is:

$$U_T = U_{TS} * k\ (\ \beta\ ) \qquad (4.15)$$

where: β = stagnant cap angle, measured from the nose of the bubble; k = a constant varying with .

In figure 4.7 the effect of the stagnant cap angle on the terminal velocity of a bubbles is shown. A cap angle of 180 degrees refers to uncontaminated liquid; an angle of zero indicates conditions of a rigid sphere.

The stagnant cap model illustrates the processes involved in the complex relationship of surface-active contamination with the hydrodynamic behavior of bubbles. The stagnant cap model has been used on several occasions as a point of departure for the interpretations of hydrodynamic and mass-transfer mechanism.

The effect of surface contaminants on mass transfer is hydrodynamic and molecular in nature. Contaminants decrease the mobility of the interface in the absence of

mass transfer. In the presence of mass transfer the motion at the interface may be increased. Concentration gradients due to non-homogenous mass transfer establish local surface tension gradients which, in turn, stimulate the movement at the interface. Interfacial convection results in higher mass transfer rates. If interfacial turbulence is important for the mass transfer of a system, the addition of surfactants can cause significant reductions in the transfer rate. In specific systems, the contaminants themselves constitute a significant resistance to mass transfer.

Analytical solution are not available for flow regimes with higher Reynolds numbers . Instead, experimental observations, numerical solutions and boundary layer approximations have to be used to predict hydrodynamic and transfer properties of such a system.

As shown in figure 4.8, streamlines for flow past a solid sphere are increasingly asymmetric as Re increases. Only a steady flow with very low Re shows fore-aft streamline symmetry. With Re = 10 asymmetry is recognizable in the streamlines. Re = 20 marks the onset of separation. Flow separation first takes place at the near-stagnation point. With Re increasing above 20, the separation point moves forward. The attached recirculating wake increases in breadth and length. As R_e is increased beyond about 130, vortex shedding begins.

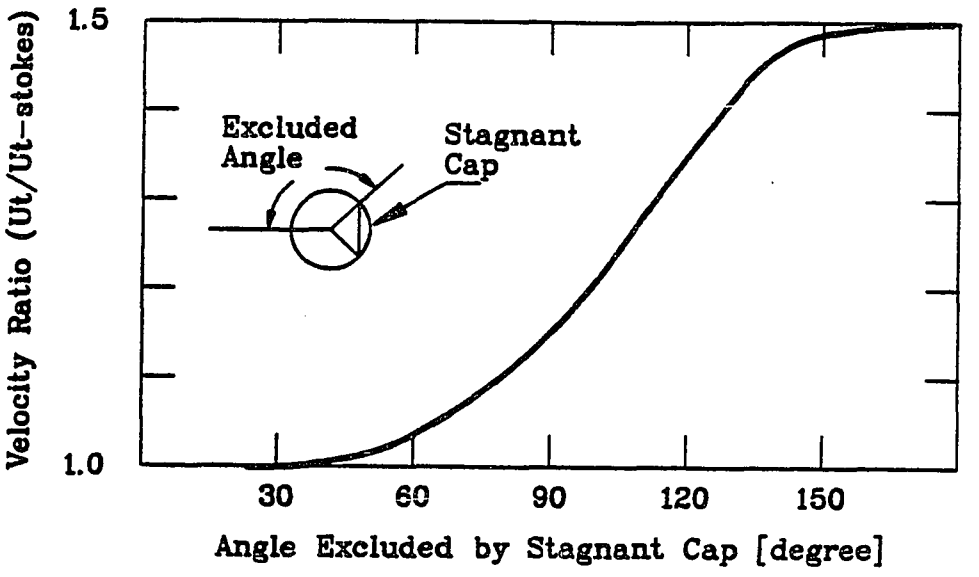

Figure 4.7 Effect of Stagnant Cap on Terminal Velocity of Bubble (from [24])

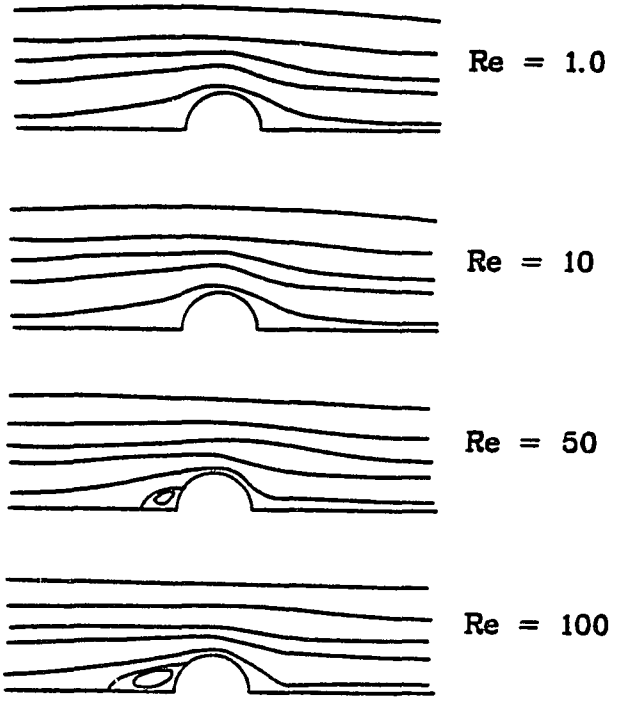

Figure 4.8 Streamlines for Flow Past a Sphere at Various Re-Numbers (from [24])

Form drag becomes increasingly important in this region while skin friction becomes negligible once Re > 150.

In the case of mobile spheres, interfacial movement delays the beginning of flow separation and wake formation. Generally, movement of the surface in the same direction as the passing fluid delays boundary layer separation. Mobile bubbles exhibit much lower values of both form drag and skin friction than a rigid sphere. A boundary layer exists on the mobile surface, but it is of a rather different kind than that of a rigid body. The boundary layer is much thinner and remains attached longer to the surface than in the case of rigid fluid particles.

Mass transfer behavior of a rigid sphere follows closely the already noted hydrodynamic features. Even in creeping flow concentration contours are symmetrical. Concentration gradients at the surface are largest at the upstream stagnation point and decrease to the rear of the fluid particle. The diffusing matter is transferred downstream and accumulates at the rear end of the bubble, forming a region of high concentration.

Although there is no physical flow separation, a concentration wake exists downstream of the fluid particle. When separation occurs and a recirculating wake is established downstream of the point of separation, the concentration wake becomes thinner. Furthermore, the concentration gradients at the surface are distorted by

the recirculation vortices [24]. The mass, which is transferred from the section of bubble surface where the recirculating wake exists, is transferred to the external flow. Fluid elements of the wake move away from the bubble, thereby carrying mass from the rear of the bubble to the external stream which ultimately moves it downstream. As Re is increased further vortex shedding begins. The mass transfer rate downstream of the separation point starts to oscillate.

There are few experimental data for mass transfer of mobile spheres due to the fact that even traces of surface-active agents significantly reduce interfacial movement.

4.1.5 Ellipsoidal Bubbles

Ellipsoidal bubbles are often approximated as oblate spheroids. In many cases, however, bubbles in this regime lack fore- and -aft symmetry.

The flow pattern and mass transfer of solid bubbles at low and intermediate Re depend on their orientation to the external flow. The total drag force is a summation of drag components acting parallel to the principal axis. Since the resulting drag force is generally not parallel to the direction of motion, a fluid particle moves

vertically only when it possesses a certain orientation or a certain symmetry.

Axisymmetric fluid particles move vertically if the axis is vertically oriented. A particle with fore-and-aft symmetry also moves vertically if the axis is horizontal.

A bubble rises steadily only if two conditions are met. First, the total drag force must be directed vertically to counterbalance the buoyancy force. Second, there must be no external moment induced by drag and weight. This means that the total drag force must go through the center of mass of the particle. Bubbles without fore-and-aft symmetry generally rise with a tumbling motion.

Analytical solutions exist for spherical bubbles and useful approximations can be deduced for the drag force. A drag ratio, D_R, can be expressed as the ratio of the resistance of the spheroid to that of a sphere with identical dimensions of the major semiaxis, a. In figure 4.9, drag ratios for spheroids in axissymmetrical flow are shown. With increasing E the surface area of the spheroid will increase. Figure 4.9 indicates that the major drag force is due to skin friction.

Numerical solutions can be computed for a rigid spheroid at intermediate Re. In figure 4.10, streamlines for spheroids with varying aspect ratio, E, are shown for Re = 100. With increasing E, the particle becomes

streamlined. The wake is smaller, than in the case of an oblate spheroid. Generally, the separation point is located aft of the horizontal plane. For aspect ratios greater than 0.2, the wake is reasonably steady even for higher Re. Experimental data supports the results of the numerical calculations. As for low Re regimes, the total drag of a spheroid contains friction and form drag components. The ratio of skin friction and form drag is proportional to the aspect ratio, E. This is illustrated in figure 4.10, where the wake is more developed for oblate spheroids, which have low aspect ratios.

The mechanisms for mass transfer is basically the same as that of rigid spherical bubbles at low Re. Minimum transfer occurs downstream from the separation point. For oblate spheroids, regions of high transfer rates are located at the upstream face near the edge.

Bubbles acquire ellipsoidal shape within an intermediate size region where the equivalent bubble diameter d_E (see below) typically has values between 1 mm and 15 mm. For this higher Re regime there exist numerous experimental investigations which have determined the terminal velocity for air bubbles rising in water (e.g., [94], [88], [66]) . In figure 4.11 terminal velocities of bubbles are shown for the ellipsoidal range. Although some data scatter is due to the different experimental procedures, the predominant cause of data spread is the

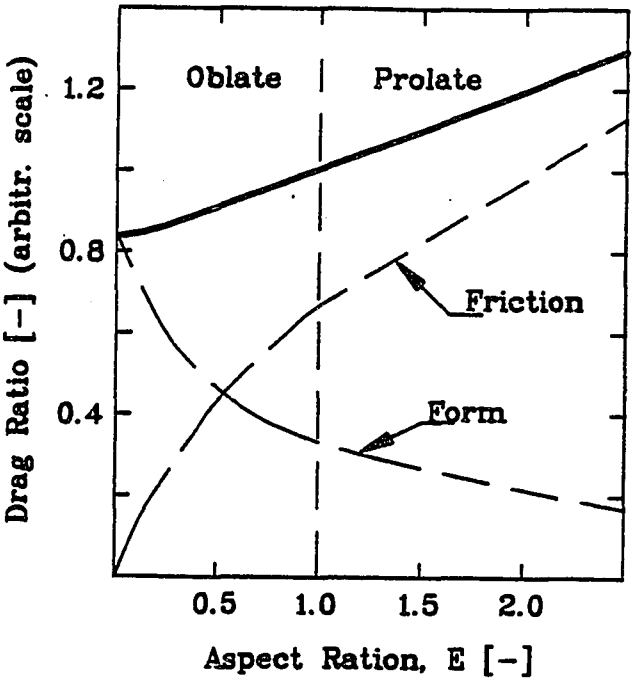

Figure 4.9 Drag Ratio for Spheroid (from [24])

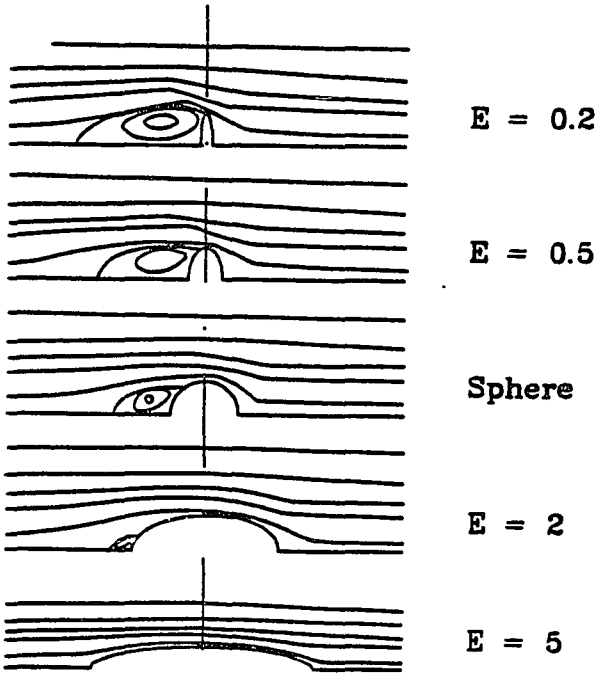

Figure 4.10 Streamlines of Flow past a Spheroid for Re=100 (from [24])

effect of surface contamination. Air bubbles in water exert little viscous resistance to surface movement. Therefore,drag and terminal velocity are greatly influenced by the presence of surface-active contaminants.

The upper and lower curves in figure 4.11 are for pure water and water containing significant amounts of surface active material, respectively. At low Re the curves converge. This is due to the fact that even highly purified water generally contains traces of contaminants, which are sufficient to suppress surface movement. The two curves also converge at the high Re end of the intermediate bubble regime. Surface tension forces cease to be important for large bubbles. The region between the convergences represents the ellipsoidal regime where surfactants have great influence on rise velocity.

In summary, contaminants are particularly important in systems characterized by high surface tension, such as air-water systems. Contaminant accumulation causes the formation of rigid surfaces which suppress internal motion. The influence of contaminants is at its greatest at the point of onset of oscillation. Internal motion can greatly affect the wake of the bubble by delaying boundary layer separation and the vortex shedding.

The mass transfer mechanism in ellipsoidal bubbles is greatly affected by the hydrodynamic characteristics of the bubble, such as outlined above. Contamination of

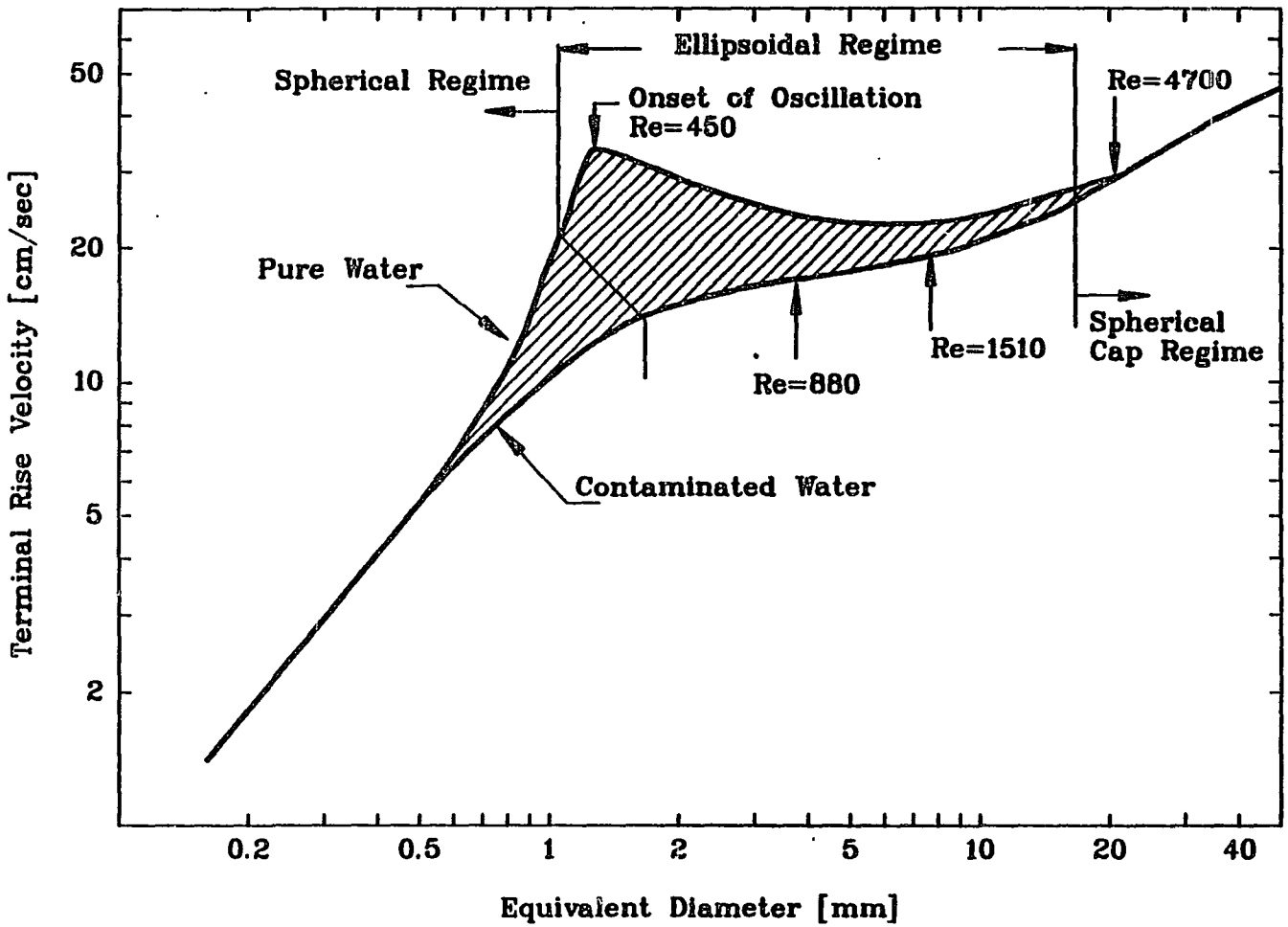

Figure 4.11 Terminal Velocity of Air Bubbles in Water (from [24])

bubble surface has a significant influence on the transfer mechanism. Generally speaking, the resistance to transfer always decreases when a bubble oscillates.

In pure systems, bubbles circulate freely. In contaminated systems, spherical and ellipsoidal bubbles are practically rigid. At Re > 200 vortex shedding and shape oscillation occurs. As a result interfacial movement is stimulated. This variety of flow conditions indicates a complex dependence of transfer rates on the flow characteristics of bubbles and on the rate of system contamination.

4.1.6 Bubble Coalescence

Bubble coalescence is hindered by the presence of electrolytes, surface active substances, or impurities. The reduction of bubble coalescence means that more surface area is available for mass transfer.

Interfacial areas measured in aeration tests with NaCl solutions are indicated in figure 4.12. [6] The ratio a/ao refers to the ratio of surface area per unit volume of electrolyte solution over that measured in fresh water. As can be seen from figure 4.12 the surface area increases to a value six times that of fresh water with increasing solute concentration. With yet higher NaCl concentrations the surface curve levels off and indicates

a somewhat asymptotic behavior for such concentration regimes. Another investigation [30] reported interfacial area in pure water to be 1.5 to 3 times smaller than those of a 0.8 M Na2SO3 solution, using a similar test set-up as the tests previously cited.

In distilled water, bubbles which are brought together coalesce as soon as they are in contact. In order to asses bubble coalescence behavior in electrolyte solution, investigations under tightly controlled conditions were conducted by Lessard [80]. Bubbles were simultaneously generated by two microsyringes in close proximity to each other. As the bubbles were brought into contact, their coalescence rate was determined by photographic means. If salt was added to the water a concentration was reached at which a drastic reduction in coalescence occurred [80]. The concentration at which this transition happened was characteristic of the salt species. Figure 4.13 shows coalescence rates for various salts. A dependence of coalescence on the valence combinations can be inferred. The electrolyte species under investigation can be grouped into three categories, according to the valence-combination.

The effect of temperature on coalescence was investigated using seawater [80]. It was reported that coalescence rates decreased with lower temperatures.

For coalescence to occur between two bubbles, they must

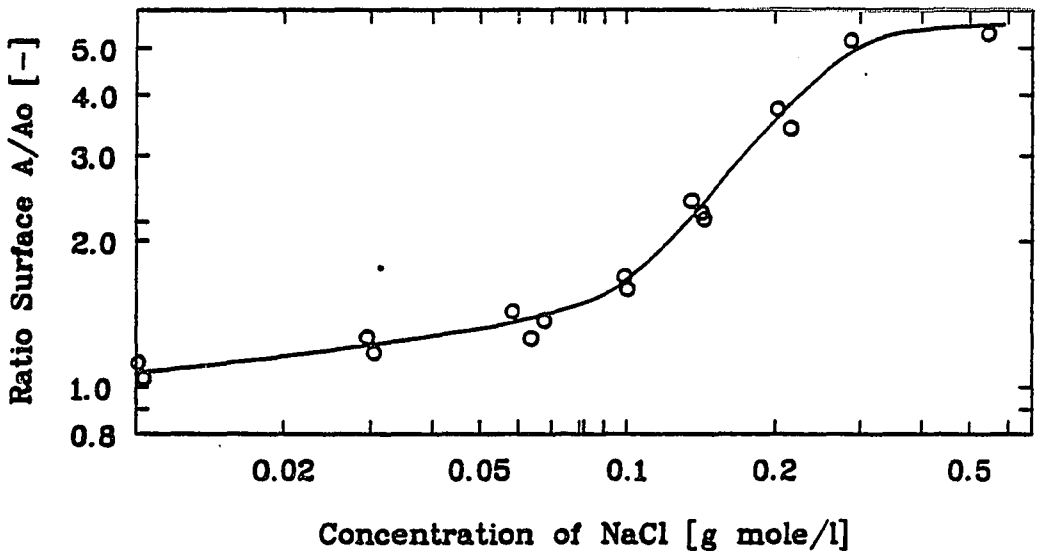

Figure 4.12 Interfacial Area in NaCl-Solution (from [6])

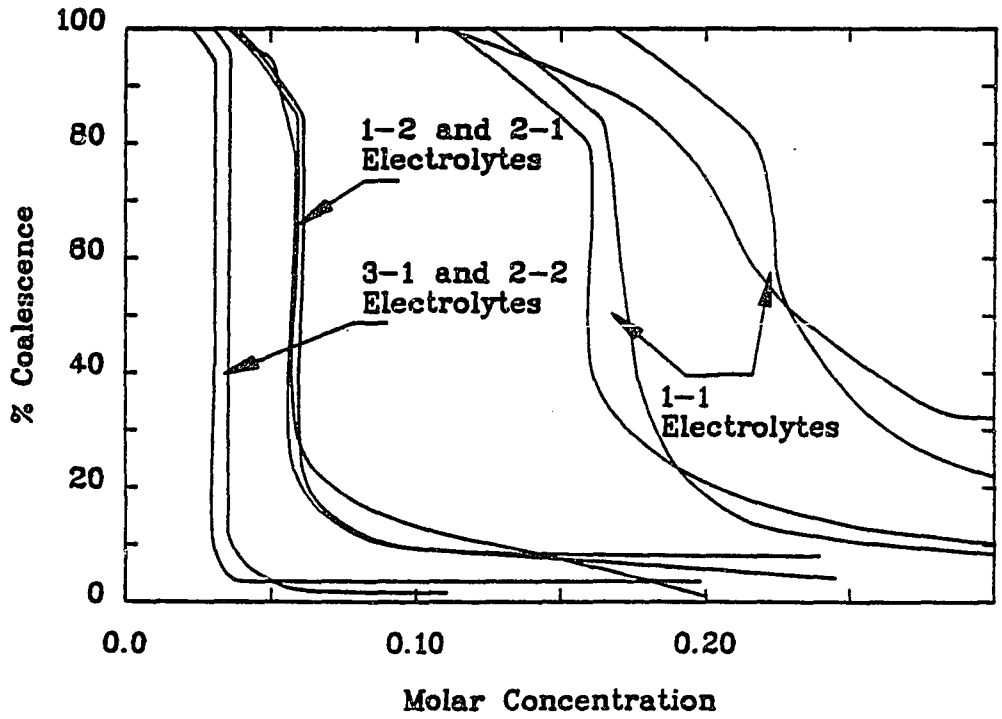

Figure 4.13 Coalescence Behavior of Different Electrolyte Species (from [80])

first come into close proximity. As a result of severalfactors, such as inertial forces and pressure differencesdue to unequal surface curvatures, the bubbles squeeze out the liquid film which separates them. The film must drain to a certain thickness before it can rupture. Interfacial tension gradients generate a resistance to the drainage of the film. The larger the gradient, which a contaminating species generates, the less likely the coalescence.

There are several theories to describe the effect of electrolytes on coalescence. One of them, introduced by Schnurman in 1929, suggests that the rate of coalescence is a function of viscosity, and decreases in more viscous liquids. Investigations previously cited [80] showed that viscosity cannot be the only parameter affecting coalescence in electrolyte solutions. KCl solutions which actually reduce the viscosity of water were found to effectively reduce coalescence at sufficiently high concentrations. The researchers indicated, however, that viscous effects cannot be ignored since a qualitative correlation between coalescence and viscosity could be observed for other salt solutions. It was concluded that a combination effect of charge and viscosity may be involved. It was further pointed out that, although the charge effect can account for the valence dependence of coalescence, it fails to explain the temperature

dependence, which can be readily interpreted by the viscosity effect.

4.1.7 Effect of Secondary Motion

There are two types of secondary motion for bubbles of intermediate size.

A) Movements performed by the entire fluid particle

B) Motions of the bubble surface relative to a bubble bound coordinate system.

The first type of motion is a function of the type of ascent, such as a zig-zag or a spiral bubble path. The second type of motion is usually referred to as oscillation and manifests itself in period- or random-shape fluctuations. Often these two types of motion are superimposed to produce a highly complex motion for the ascending bubbles.

Bubble oscillations are most likely to be caused by wake shedding, because the onset of oscillations coincides with the onset of wake shedding.

The natural frequency of a fluid particle is approximated by:

$$f_N = \left(\frac{48 * \sigma}{2 * d_E^2 * \rho * (2 + 3 * \gamma)} \right)^{1/2} \qquad (4.16)$$

For an air-water system, where the density ratio can be

neglected, equation (4.16) is plotted in figure 4.14. Measured oscillation frequencies were reported to be smaller than those obtained by equation (4.16) [24]. A typical range for this frequency reductions was 10-20% in contaminated water and 20-40% in pure systems [29]. The amplitude of oscillation is larger in a pure systems, which could explain the reduction in frequency.

Assuming a single-degree-of-freedom damped system with a wake frequency, f_W, the shape oscillation of a bubble can be estimated to follow a combined pattern of oscillation of frequency, f_1, with the amplitude modulated at f2 [24]. Where $f_1 = (f_W - f_N)/2$ and $f_2 = (f_W + f_N)/2$. Although somewhat oversimplified, this approach provides a conceptual understanding of certain features related to surface oscillation. For example, if f_W and f_N approach equal values, resonance can be expected which, in fact, is deemed to be responsible for bubble breakage [24].

Generally, oscillating bubbles follow zig-zag or spiral ascent trajectories. It is certain that the type of ascent trajectory is influenced by the mode of release [94].

Secondary motion has a great effect on drag and on mass transfer. It increases the mean drag. A particle which undergoes secondary motion, tends to have a vertical terminal velocity smaller than that of a rigid sphere. Secondary motion also promotes mass transfer. Harbaum

[54] investigated the effect of vibration on the rate of gas absorption in water. Increases in mass transfer rates were reported for the entire range of vibration frequencies of 20-20000 [c/s] used for these tests. The greatest effect was noted near the resonance frequency when the transfer rate was 70% higher than that without vibration. The author attributed the effect of vibration on gas transfer as due mainly to an increase in gas hold up, i.e., the reduction of ascent velocities of excited bubbles. Some instances were observed, however, in which the vibration caused the bubble to disintegrate into a number of smaller ones, which in turn increased the available interfacial area.

4.2 BATCH AERATION EXPERIMENTS

Before presenting single bubble and bubble swarm aeration experiments, theoretical aspects of aeration are introduced.

4.2.1 Theoretical Aspects of Aeration

As introduced in section 3.4.2., the two-film theory of Lewis and Whitman [81] has found widespread attention and has been generally adopted to describe gas transfer in bubble aeration. In cases with negligible gas film resistance the overall gas transfer coefficient equals the liquid film transfer coefficient k_L. The fundamental gas absorption equation can therefore be expressed as:

$$\frac{1}{A} * \frac{dW}{dt} = k_L * (C_I - C_L) \qquad (4.17)$$

where: W = weight of solute dissolved; A = area of liquid-gas interface; C_I = gas concentration at the interface; C_L = gas concentration in bulk liquid at time t.

For equation 4.17 to apply exactly, gas transfer has to take place under conditions of constant temperature and pressure, and in the absence of chemical reactions. At the liquid-air interface, equilibrium conditions are

assumed. The gas concentration at the interface, C_I, is thus determined by the partial pressure of the gas component of interest according to Henry's law. Since the gas concentration, C_I, is the saturation concentration at the interface, it will subsequently be referred to as C_S. Thus with multiplication by A:

$$\frac{dW}{dt} = k_L * A * (C_S - C_L) \qquad (4.18)$$

Dividing both sides of equation (4.18) by the volume, V, of the system:

$$\frac{1}{V} * \frac{dW}{dt} = k_L * \frac{A}{V} * (C_S - C_L) \qquad (4.19)$$

The term W/V represents the gas concentration in the bulk liquid at time t, C_L. Thus:

$$\frac{dC_L}{dt} = k_L * \frac{A}{V} * (C_S - C_L) \qquad (4.20)$$

Furthermore, the term A/V represents the liquid-air interface area per volume, and is subsequently referred to as the specific interfacial area, a:

$$\frac{dC_L}{dt} = k_L * a * (C_S - C_L) \qquad (4.21)$$

The term dC_L/dt represents the instantaneous rate of

change of gas concentration in the liquid. It is not possible to apply the instantaneous rate for any appreciable time length because the value of (C_S-C_L) changes with time. Equation (4.21) is integrated in order to describe the concentration change for any given time, . The corresponding integration limits are 0 and t for time and C_o and C_L for concentration. Here C_o is the initial concentration at t=0. With separating of variables:

$$\int_{C_o}^{C_L} \frac{1}{(C_S - C_L)}\, dC = k_L * a * \int_0^t dt \qquad (4.22)$$

$$- \ln \left(\frac{C_S - C_L}{C_S - C_o}\right) = k_L * a * t \qquad (4.23)$$

$$\ln \left(\frac{C_S - C_o}{C_S - C_L}\right) = k_L * a * t \qquad (4.24)$$

From these equations it can be deduced that the rate of gas transfer is determined by the following parameter.

1) The transfer rate at any instance is proportional to the difference between the saturation concentration, C_S and the actual concentration in the bulk water, C_L.
2) The transfer rate is directly proportional to the gas transfer coefficient, k_L, which depends on the diffusivity, D, and film thickness, L (See equation 3.61)
3) The transfer rate is directly proportional to the

specific liquid-gas interfacial area

For further developments the following assumptions are made:

1) The gas obeys the perfect gas laws. The magnitudes of the pressures and temperatures which usually prevail, allow the use of perfect gas relationships.

2) Isothermal conditions apply. Since the temperature of the gas and surrounding water does not vary significantly, isothermal conditions can be assumed.

3) Bubbles have a geometrically defined shape: Smaller bubbles, to about 1.5 mm diameter, tend to assume a spherical shape. Large air bubbles, to a size of about 10 mm diameter, can be reasonably approximated by oblate spheroids.

4) The excess pressure due to surface tension is negligible. For a bubble to sustain its shape, its internal pressure, P_O, has to be large enough to withstand the external liquid pressure, P_L, plus the pressure resulting from surface tension. The excess pressure due to surface tension is calculated from the relationship:

$$P = \frac{2 * \sigma}{R} \qquad (4.25)$$

where: $P = (P_O - P_L)$; σ = surface tension ; R = radius of bubble.

In air-water systems it has been shown [80] that for

bubbles equal or greater than 1.0 mm diameter, the surface tension pressure is a negligible portion of the total bubble pressure.

5) There is no temporal variations of C_S and a. Though C_S and a were assumed to be independent in time in order to execute integration of equation (4.21), both variables exhibit a complex variation with time. These variations are not only restricted to the time span it takes a bubble to travel through the entire water column, but C_S and a also vary over the total aeration time.

As a bubble rises from the point of release to the surface of the water column, its internal pressure decreases due to two processes. As the bubble rises the hydrostatic pressure and, therefore, the pressure in the bubble decreases. Additionally, gas dissolves from the bubble into the water during its ascent. These phenomena occur at any given instant of the aeration period. At the beginning of aeration, the gas content of the water is low. High gas transfer rates result. As aeration progresses the water approaches the saturation concentration and the rate of gas transfer decreases. These two processes have to be combined to obtain the actual time dependence of C_S.

The foregoing considerations can be readily applied to explain the time dependence of the air-liquid interfacial area. As C_S, the area, a, varies during both the

retention time of the bubble in the water column and the duration of aeration process. Because the bubble size changes due to decreasing hydrostatic pressure and gas absorption.

Bubble expansion due to decreasing hydrostatic pressure and contraction due to gas loss from dissolution are compensatory in character. With increasing aeration time, the effect of decreasing hydrostatic pressure becomes much larger in comparison to the effect of gas loss due to gas absorption.

According to Carver [28], attempts have been made to express the time dependences of C_S and a. The author states, however, that no adequate functional relationship has been developed so far to describe the complex processes involved.

For relatively small water depths, such as those used in the present experimental study, the variations of C_S and a, with time are small enough to permit averaging of these variables [28]. Accordingly, the saturation pressure is calculated for the pressure conditions at the midpoint of the water column to account for the effects of hydrostatic pressure variations.

Following the derivation of equation (3.27), the midpoint saturation concentration, C_S, for the gas component of interest can be calculated as follows

$$C_S = C_{S0} * \left(\frac{P_M - P_V}{P_{AT} - P_V} \right) \qquad (4.26)$$

where: C_{S0} = saturation concentration of gas component at atmospheric pressure and constant temperature; P_M = pressure at midpoint of water column; P_{AT} = atmospheric pressure; P_V = vapor pressure.

For large bubbles, P_M is the sum of P_{AT} and the hydrostatic pressure at the midpoint. For very small bubbles the excess pressure due to surface tension has to be added.

As evident from equation (4.24) k_L*a represents the slope of the plot of time versus the left hand side logarithmic term. Having the saturation concentration, C_S, determined, and knowing the initial gas concentration, C_o, values of C_L can be obtained for various values of t from the corresponding aeration curve.

A typical aeration curve obtained from an aeration test using oxygen bubbles is shown in figure 4.15 [66]. Additionally, the semi-logarithmic plot of relative concentrations is shown. As can be seen, the gas absorption rate diminishes in the course of aeration. Similarly, the plot of relative concentration, calculated by equation (4.24), deviates from linear behavior with increasing aeration time. Maximum values for k_L*a are obtained by considering the slope of a plot of relative

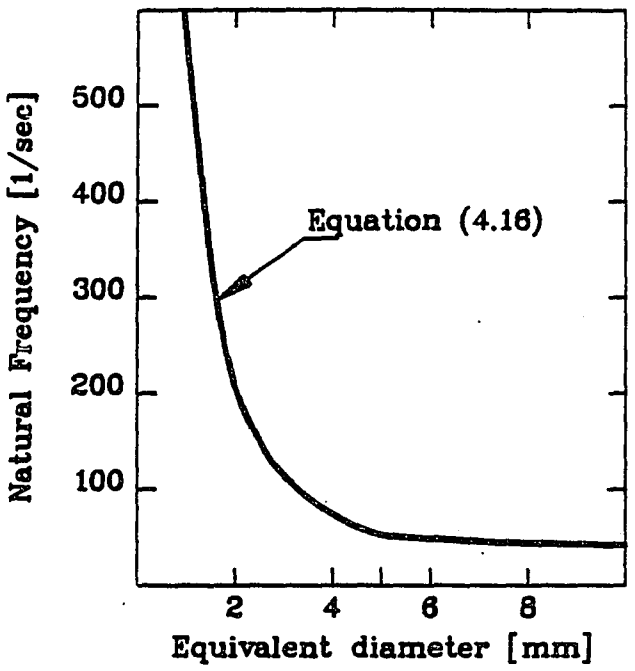

Figure 4.14 Natural Vibration Frequency of Air Bubble in Water

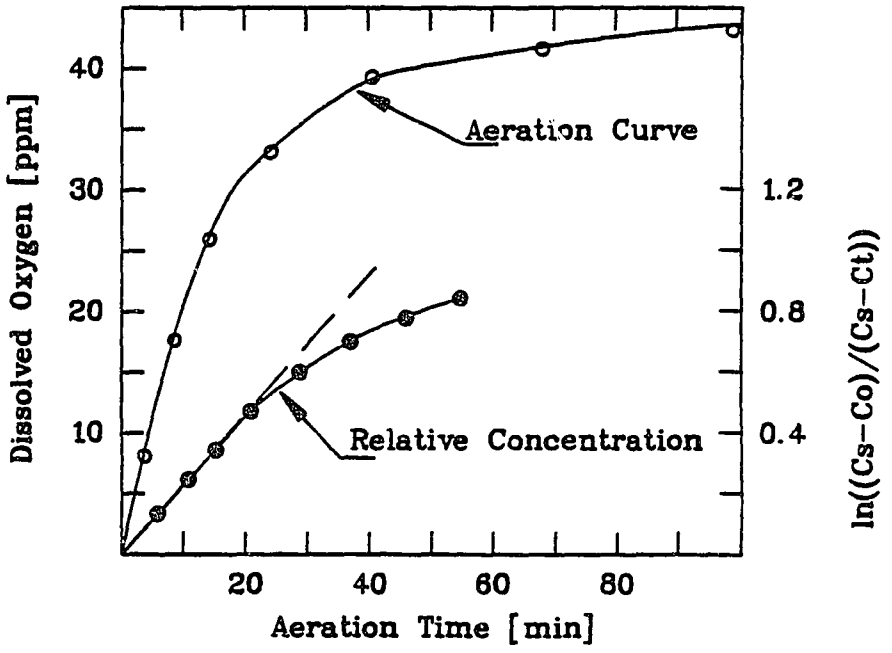

Figure 4.15 Typical Oxygen Aeration Curve and Semilogarithmic Plot of Relative Concentration in Fresh Water (from [66])

concentration at the beginning of the aeration experiment.

The term k_L*a expresses the overall gas transfer characteristics of the aeration process. It incorporates, however, the contributions of the effect of film resistance, k_L, and the effect of the amount of liquid-air interface, A. By identifying the instantaneous surface area in the water column, the mass transfer coefficient, k_L, can be readily obtained.

Various techniques have been employed to assess the instantaneous interface area via the size and ascent velocity of bubbles in a two-phase flow regime. Barczweski [9] reviewed presently-used techniques, such as bubble impact probes (based on optical or resistance methods), hot film anemometry, laser doppler measurements, gamma ray attenuation, and photographic observations. The author identified the shortcomings and error sources of these techniques. According to his findings he concluded that photographic means are well suited for bubble size and ascent measurements. The advantage of optical measurement is that the flow regime is not disturbed by intruding probes. Photographic observations fail if the bubble swarm becomes too thick. Bubbles located at the outer edge of the plume do not necessarily represent the true size distribution of the swarm and obstruct the inner view field.

If the surface area cannot be determined, the overall

transfer coefficient, k_L*a, is frequently used to express the transfer efficiency of a system. The term α has been defined as follows as the ratio of gas transfer in a test solution to the transfer of pure water:

$$\alpha = \frac{(k_L * a)}{(k_L * a)_o} \qquad (4.27)$$

where: $(k_L*a)_o$ = the overall transfer coefficient of pure water.

By defining the stagnant film theory [81], an analogy was made to the flow of heat in materials. With such an analogy in mind the mass transfer coefficient k_L corresponds to the coefficient of heat conductance, which is a property of the particular material.

Strictly speaking, the transfer coefficient, k_L, is not characteristic of the liquid-gas media, but is dependent on the concentration distribution of the liquid layer in the vicinity of the interface. Therefore, k_L can be understood as to reflect the ability of gas to penetrate the liquid film which surrounds the bubble. As discussed in section 4.1, the hydrodynamic characteristics of the liquid film is a function of the rise trajectory of the bubble and the purity of the liquid.

It has been indicated [66] that k_L varies during the rise period of a bubble. Three phases of gas transfer were proposed, starting with the formation of the bubble

at the capillary and ending with the bursting of the bubble at the surface. The intermediate phase takes place as the bubble rises through the column. The intermediate phase can be characterized as more or less steady state, whereas the first and third phases have transient features.

The formation phase is characterized by high transfer rates. During the bubble's growth, its surface continuously increases and the concentration gradient in the liquid film is high, thus the transfer rate is high. Immediately after detaching from the orifice, the bubble experiences acceleration resulting in high turbulence adjacent to the interface. These high turbulences increase the transfer rate. If contaminants are present, accumulation on the bubble surface alters the flow conditions, causing a reduction in transfer.

During subsequent bubble rise the transfer remains more or less constant. Deviations from steady state conditions are due to variations in the ascent behavior of the bubble.

During the third phase, the bubble bursts at the water surface. Water from the well-aerated film surrounding the bubble remain at the surface as the gas escapes upon bursting. Furthermore, the bursting process causes vigorous undermixing of saturated surface water. As a consequence of the downward currents produced by the

rising bubbles, water with high gas content is transported to the interior of the water column.

Since the first and final phases of bubble transfer are more effective than the intermediate phase, in which the transfer occurs at a somewhat constant rate, the magnitude of k_L is larger for smaller column heights.

4.2.2 Single Bubble Aeration

4.2.2.1 Experimental Apparatus and Test Procedure

The test set-up used for single bubble aeration is shown in figure 4.16.

The aeration column, shown in figure 4.17, was a 5 cm ID plexiglass pipe with a 6.4 mm thick wall. Its lower end is cemented to a plate which, in turn, is supported by four brass rods. The plate has a tapered hole to accommodate a rubber stopper. A retaining circular plate was bolted into the under-side of the plate to hold the rubber stopper in place. Suitable holes were drilled into the rubber stopper to allow insertion of different sized capillaries. The upper end of the column was cemented to a plate to allow the attachment of a water reservoir. As shown in figure 4.17, a 7 cm long pipe section was cemented to a 4.0 cm thick plate. In the middle of this plate a hole of 1.5 cm was drilled. The diameter of this

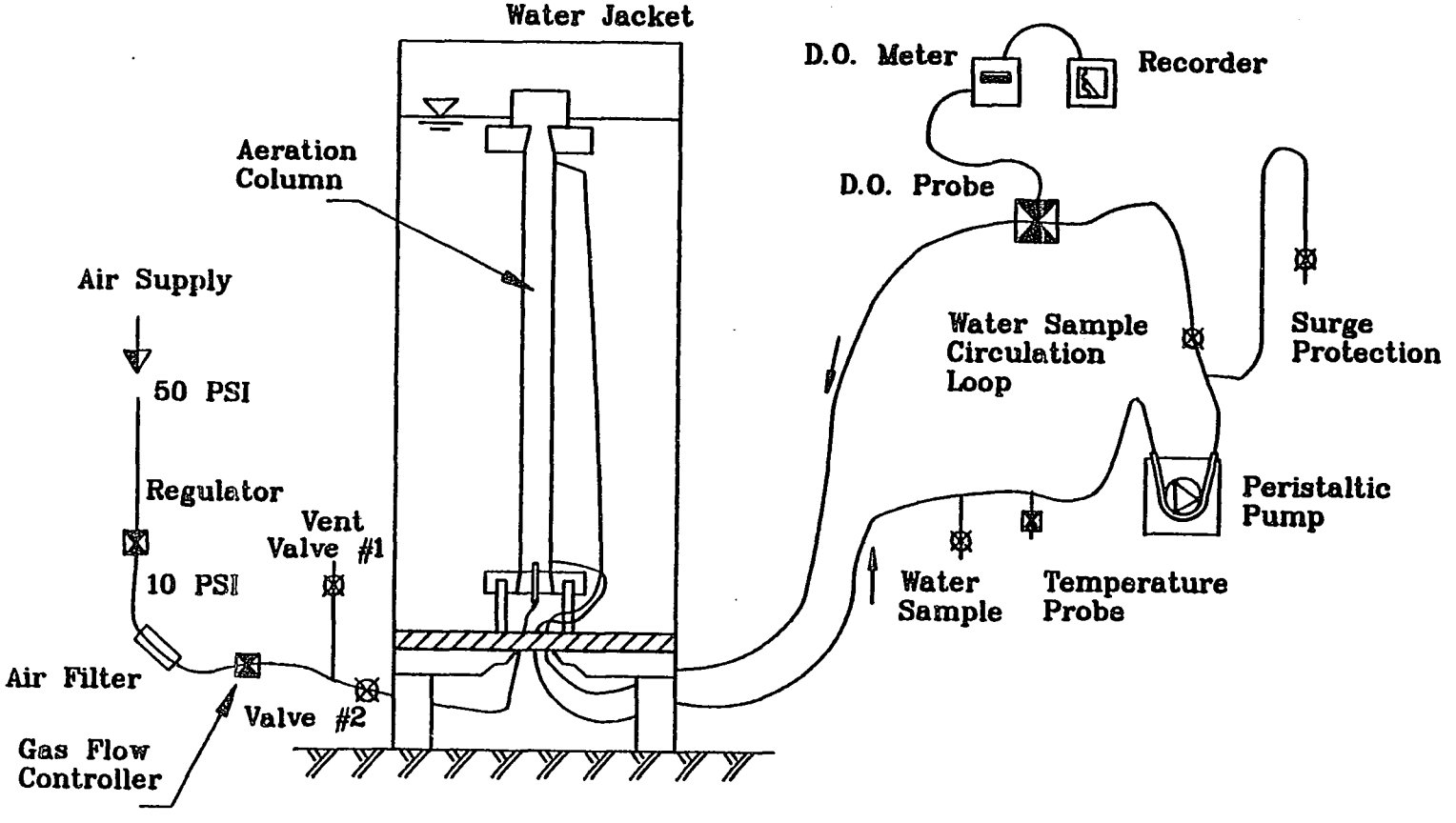

Figure 4.16 Flow Scheme for Single Bubble Aeration

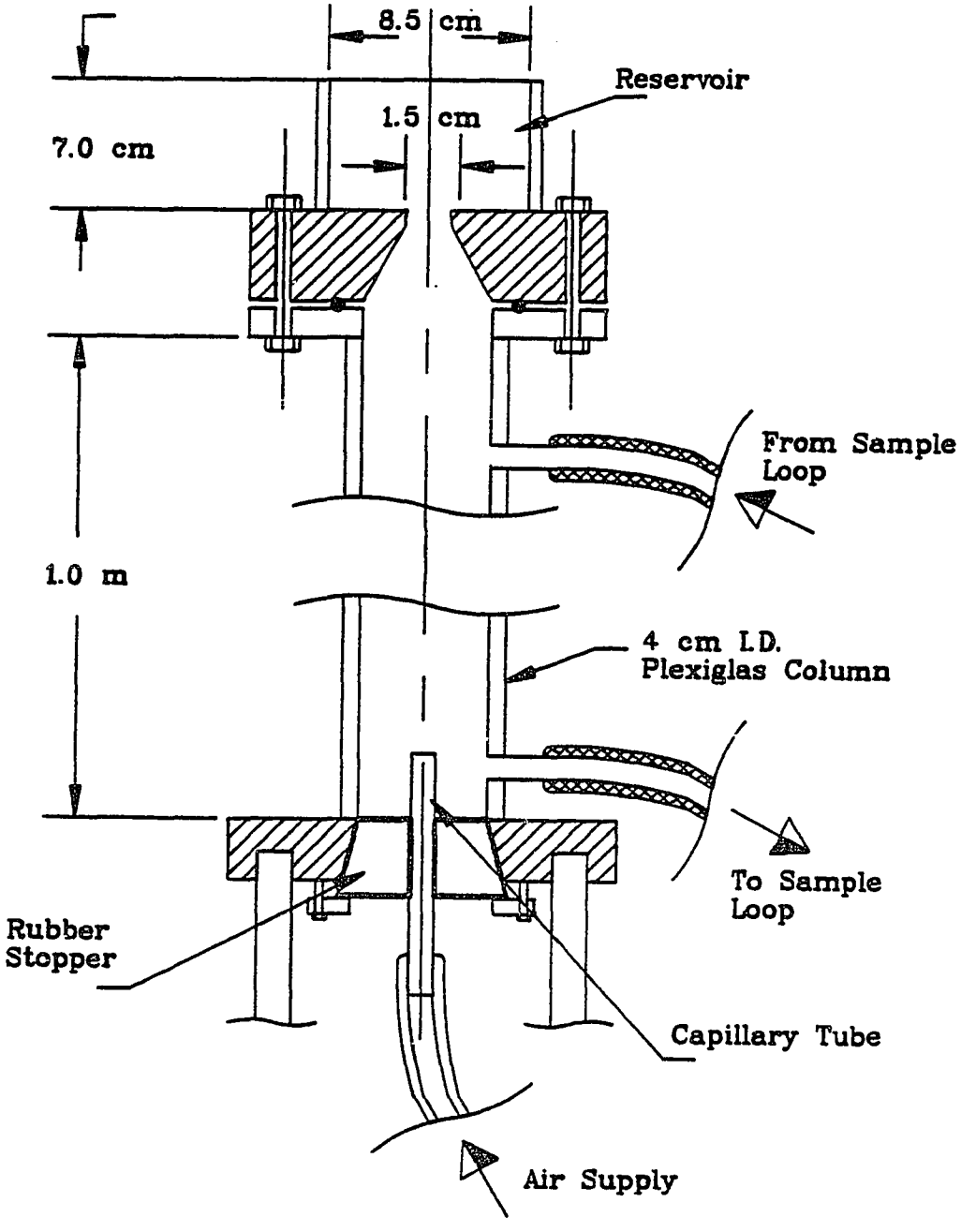

Figure 4.17 Aeration Column (for Single Bubble Aeration Experiments)

orifice gradually increased downward.At the underside of the plate, the diameter of the tapered section coincided with the inside diameter of the column. An o-ring, placed between the two plates, seals the structural junction. During aeration, the reservoir was always filled to its rim, thereby providing a constant hydrodynamic pressure head.

The overlying reservoir has several functions. By placing an inverted graduated cylinder over the bottom hole allows easy air flow calibration . Its principle function, however, is to minimize the aeration process by bursting bubbles. These effects were discussed in section 4.2.1. The reservoir assembly was designed to avoid the mixing of reservoir water with water from the aeration column below. The slope of the tapering is such as to avoid bubble adhesion to its walls and to smoothly guide the bubbles out of the aeration column.

Between aeration periods, water was circulated throughout the system. Water entered the column at the top and flowed downward. For the reservoir assembly to perform properly it is necessary that there be only a minimum or no interchange with the column water. Observations, both during aeration and water circulation, showed no significant water mixing.

The aeration column is located in a square plexiglass tank 35 cm on a side. In order to allow undistorted

photography of objects inside the circular aeration column, a water-filled observation box with square sides surrounds the column. In addition to this function, the water jacket not only provides a thermal insulation but also prevents air leaks at the connections to the aeration column.

Air was injected into the aeration column through a capillary tube. The single aeration experiments were grouped into three segments. In each of these segments a different capillary was used to produce bubbles of different sizes. The air source was the laboratory compressed air supply. A regulator reduced the air pressure from 50 to 10 psi. An air filter was installed to remove particles and oil residues in the air stream. The magnitude of air flow was regulated by means of a gas mass flow controller. Calibration tests showed that the air flow rate could be accurately maintained if the line pressure upstream of the flow controller was held constant. On its path to the capillary tube the air passed through a glass vessel, which was partially filled with water. The water was discharged from the column through the capillary tube when the pressure within the glass vessel was not high enough, i.e., between aeration periods. Air entered the vessel and rose through the water to the surface. On its way through the water, the air received additional cleaning. It is reasonable to

assume that the air in the vessel was water-saturated and had attained the temperature of the water in the glass vessel. From the glass vessel, the air flowed upwards to the capillary tube.

To determine the D. O. concentration, water was circulated in a small tubing loop (see figure 4.16). The flow was driven by a peristaltic pump. Temperature of the water was measured using a direct-reading thermistor thermometer (YSI-400 series; accuracy +- 1% of full scale). A surge protector, consisting of two valves, was placed upstream of the peristaltic pump to smooth out the pressure pulses generated by the pump.

Since no flow-through cell was commercially available for the D. O. probe, the device shown in figure 4.18 was designed and built. The cell consists of three plexiglass plates held together by bolts and sealed with O-rings. Sample water enters the reservoir through the middle plate and leaves the cell through the tapered exit port at the top. The middle plate was machined to provide a threaded orifice to accommodate the D. O. probe. Once the probe is in place, its membrane establishes flush alignment with the interior wall of the reservoir. As discussed in section 3.5.1, a minimum flow velocity across the membrane is required to prevent both oxygen depletion of the membrane and erroneous measurements. A sufficient water flow across the membrane is achieved by

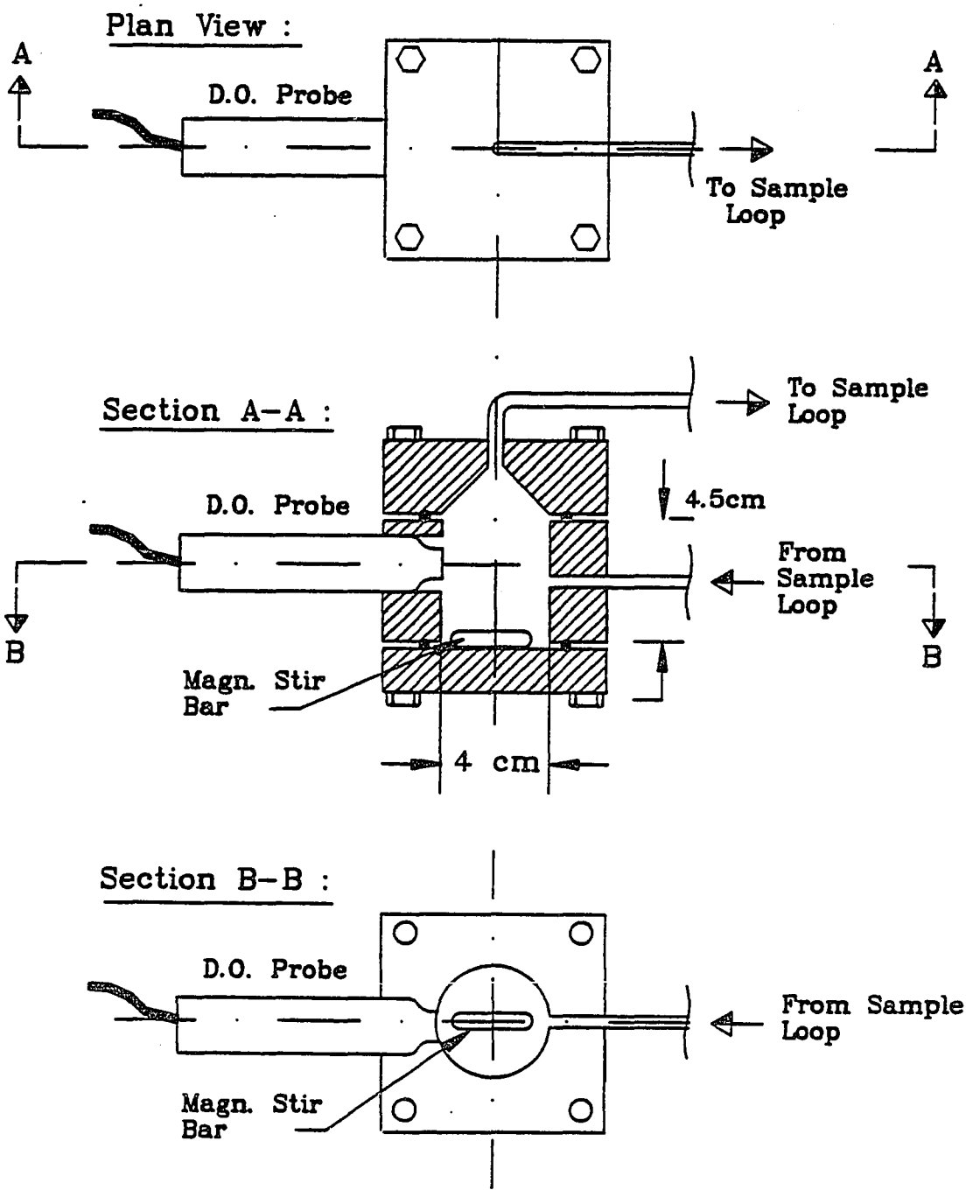

Figure 4.18 D.O. Probe Flow-Through Cell

means of a magnetic stirring bar on the bottom of the reservoir, which is driven by a magnetic stirrer. The sensor output is read visually on the D.O. meter. In addition, a strip chart recorder continuously documents the signal. D.O. measurements are carried out with a polarographic probe (YSI 5521 probe) and monitored with a temperature compensated D. O. meter (YSI 57; accuracy +- 0.1 ppm).

The water to be aerated is stripped of dissolved gases by means of a vacuum deaerator. The packed column (figure 4.19) assembly consists of a 5 cm ID transparent pipe section of some 1.5 m length with connecting tubing. The column is filled with 1.5 cm plastic ring packing and two identical carboys serve as both the water supply and receiving well. In figure 4.19 carboy II is the receiving well. Its rubber stopper accommodates connections for two lengths of tubing; one to the discharge of the packed column and the other to the vacuum pump.

When a partial vacuum is established in the column and in carboy II, water is lifted from carboy I, runs over the packing elements and is finally collected in carboyII. After carboy II is filled, the assembly is vented. Carboys I and II were interchanged and the process was repeated. To obtain sufficient deaeration of the water, this procedure usually had to be done four times.

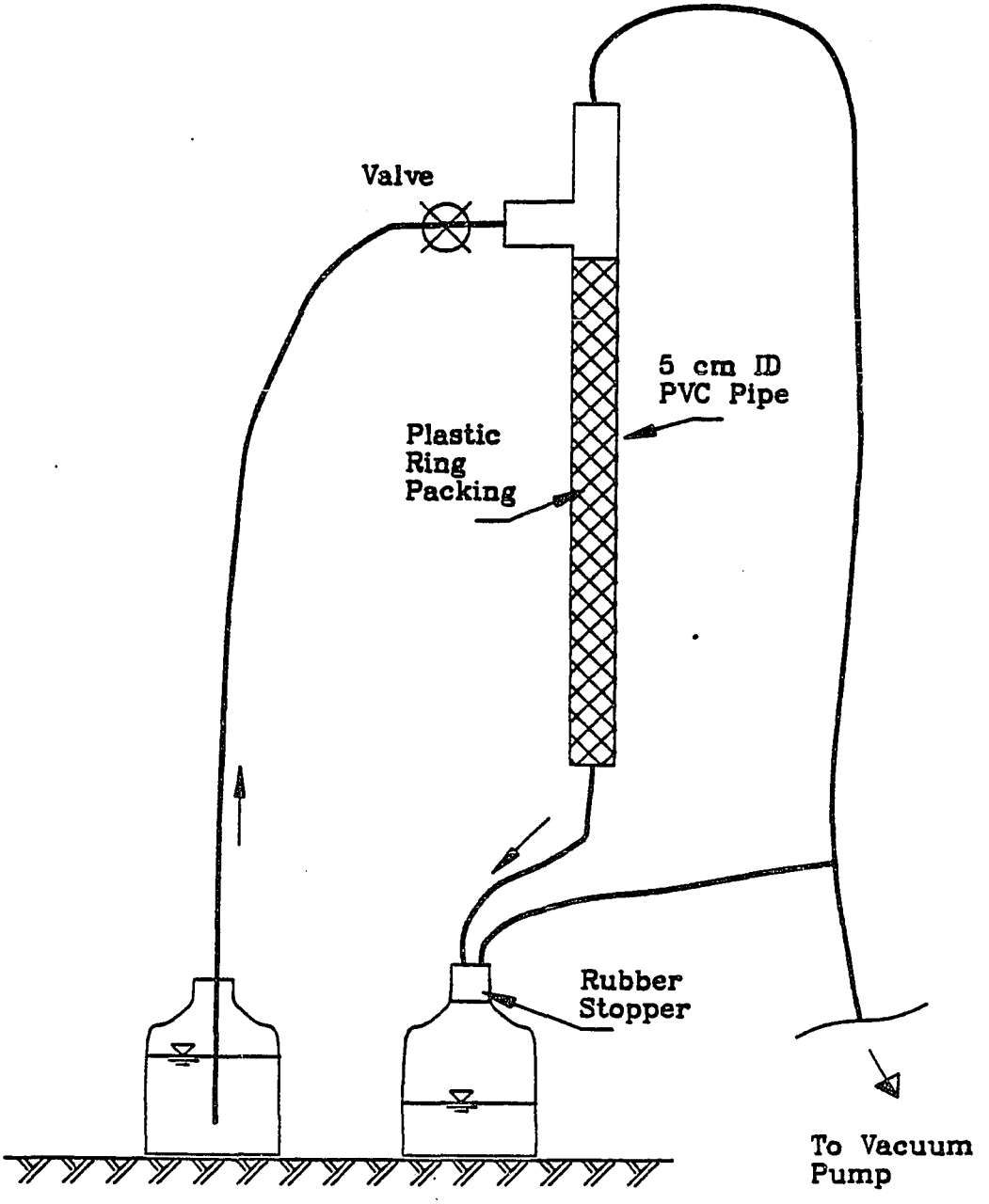

Figure 4.19 Packed Column for Sample Water Degasification

Experimental procedure:

In order to avoid organic contaminations usually found in near-shore waters seawater samples were collected from the ocean some 2.5 miles offshore . The seawater was pumped from a 10 m depth and stored in dark plastic carboys. The subsurface sampling was designed to eliminate contamination by any possible organic surface films. The carboys were subsequently placed in the laboratory where the experiments were conducted. This allowed the water to acquire the ambient temperature. Fresh water was taken from the laboratory tap water supply and also stored in carboys.

Before each experiment, the desired air flow was regulated and calibrated. According to the particular experiment, the aeration column was filled with either seawater or fresh water. Air was admitted and bubbles rose through the water column. A graduated cylinder was filled with water, turned over 180° with the opening covered, and placed in the column reservoir in an inverted position. The graduated cylinder was then pulled over the bottom orifice of the reservoir. The time needed for the ascending bubbles to displace the water in the inverted cylinder was noted. With this method the air flow could be accurately adjusted. Repetitive calibration runs were conducted until three consecutive measurements showed variations of not more than +- 1%. With the desired flow

rate adjusted, valve II (figure 4.16) was closed and valve I opened in order to allow venting of air until the start of the aeration test. The deaerated water then filled the aeration column. With the calibrated D. O. probe and temperature probe in place, the water was circulated for 30 min. before starting aeration. This was done to rid the system of potential air pockets and to equilibrate the water temperature with ambient conditions. At the end of this 30 min period the D. O. concentration was recorded as the initial condition. The aeration commenced by closing valve I and opening valve II.

After a variable aeration interval aeration was stopped. The sample was circulated in the sample loop and the D.O. concentration and the temperature were recorded. Initial aeration test runs determined the circulation time needed. Shown in figure 4.20 is a typical D. O. curve during the circulation interval.

After an initial peak, the D.O. leveles out to a final concentration. Some 12 minutes of circulation are required to achieve this plateau. From figure 4.21, it can be inferred that the water in the aeration column was not well mixed during aeration. Lower water layers absorbed more oxygen than those at higher elevations. Mixing of the water obviously occurred in the D.O. cell reservoir. Mixing was evidently accomplished after the 12 minute circulation interval. The D.O. concentration at the end of

the circulation interval was recorded as the characteristic concentration.

Figure 4.21 shows the aeration curve for one of the initial test runs. At the beginning of these experiments, the aeration period was about two minutes long. Subsequently this was increased from 2 to 4 minutes, to 8, and finally to 12 minutes. A semilogarithmic plot of relative concentrations is shown in figure 4.22. The distribution indicates similar behavior to the curve in figure 4.15. With increased aeration time, deviation from a linear relationship can be observed.

In figure 4.23 the semi-logarithmic plot was calculated using the concentration profile of only the first ten minutes of aeration. Least-square fit of these data indicates excellent linear correlation.

Due to the above findings subsequent aeration tests were relatively short. For the three test sequences, the lengths of experiments were between 6 and 10 minutes.

Photographic procedure:

Bubble size and bubble hold-up were determined by photographic means. A 35mm camera , equipped with a macro lens (1:2 magnification), was placed in front of the square water basin and the lens focussed on the midpoint of the aeration column. At the side of the aeration column, a scale was attached facing the camera. Focusing on an object, which was situated in the vertical

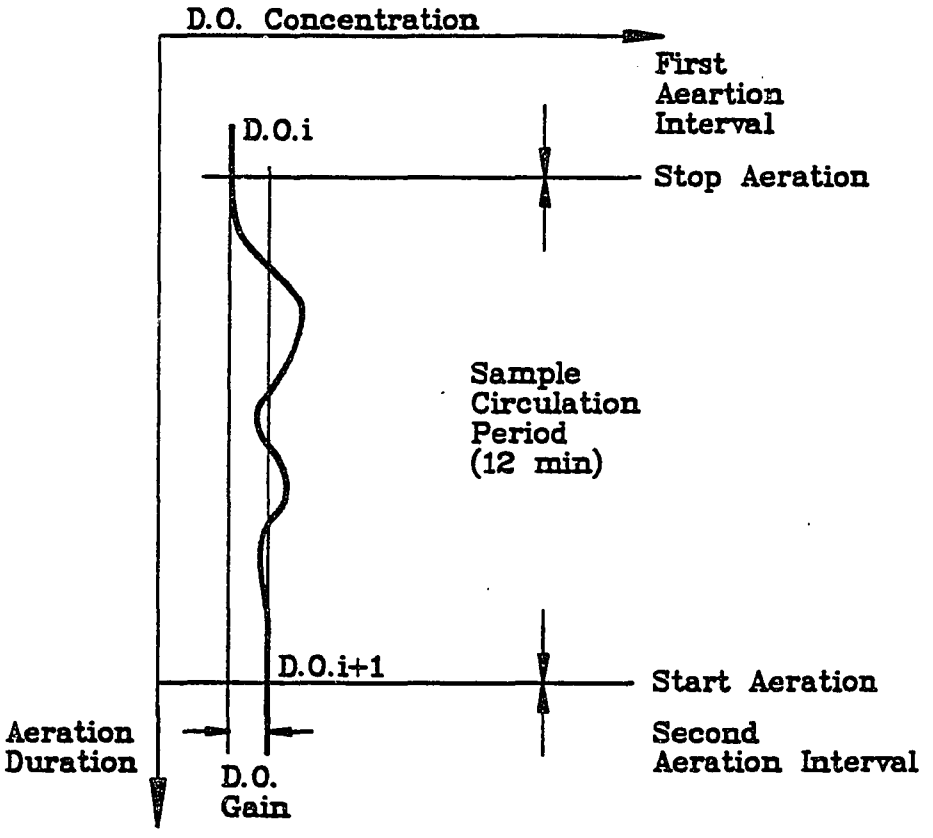

Figure 4.20 Typical D.O. Record During Sample Circulation

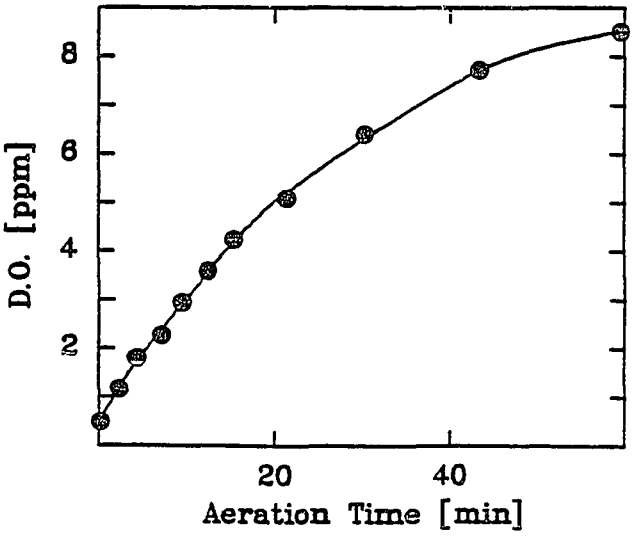

Figure 4.21 Typical Aeration Curve for Tests

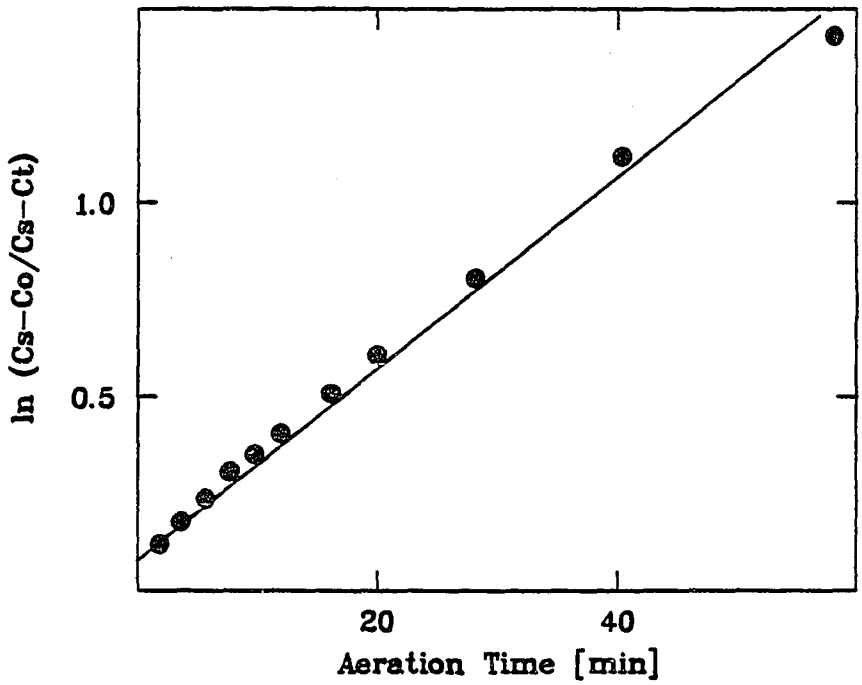

Figure 4.22 Semilogarithmic Plot of Relative Concentrations

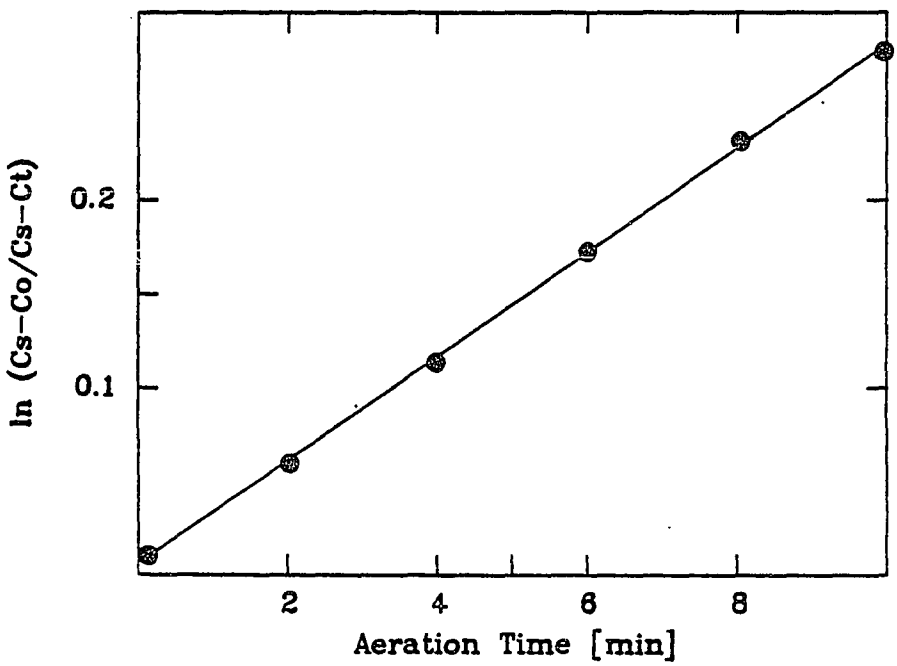

Figure 4.23 Semilogarithmic Plot of Relative Concentrations - only Initial Phase Considered

axis of the column, the entire width of the aeration column including the scale, was within the view field. Test photographs showed that the dimensions of a calibration object in the column were accurately represented by the section of the attached scale.

A synchronized electronic strobe was used for the bubble photographs. Lighting was perpendicular to the lens axis. A dark background was found to be the most appropriate. Bubble photographs were taken during several aeration periods of each test segment. The resulting slides were projected on a wall with a magnification of 10. Individual bubbles were traced on paper along with the aeration column walls and the attached scale. Measurements of the major and minor axes of the traced bubble shape were noted.

The number and concentration of bubbles was determined by photographing an 18 cm long section of the aeration column. The bubbles included in this section were counted from projected slides. The total number of bubbles in the aeration column was calculated by dividing the number of counted bubbles by the fraction the 18 cm section represented of the entire column. For each test sequence some 40 bubble count pictures were taken for both seawater and fresh water. In each case, the obtained number of bubbles was averaged to give a representative value.

4.2.2.2. Results and Discussion

Results: Experiments with single bubble aeration were carried out in three test sequences. In each sequence bubbles were generated by a specific capillary tube. In table 4.1, test numbers are associated with the test sequence and the water type tested.

For the first 16 tests of sequence I (No. 3-18), considerable scatter of the overall transfer coefficient, k_L*a, was observed, as can be seen in figure 4.24. For those tests the peristaltic pump kept circulating the water during the aeration periods. Close observation of suspended particles in the aeration column showed pulsed settling movements during the circulation period, which coincided with the frequency of the peristaltic pump. It was assumed that vibrations induced by the pressure pulses of tubing pump were responsible for secondary motions of the bubbles. Effects of secondary motion on the overall mass transfer are described in section 4.1.7. In subsequent tests the peristaltic pump was turned off during the aeration period. As can be seen in figure 4.24, data scatter was considerably less without pumping.

The sizes of capillary tubes and the air flow rates for the three test sequences are listed in table 4.1. For test sequences I and II, glass capillaries were used to produce 3 mm and 4 mm bubbles. Consistent generation of

Test Sequence	Test Run #	Water Tested	Air Flow Rate [ml/min]	Capillary Bore ID [mm]	$\overline{Kl*a}$ [1/min]	$\overline{Equival.\ Diam.}$ [mm]	$\overline{Bubble\ Area}$ [mm^2]	$\overline{No.\ of\ Bubbles}$	Area in Column [cm^2]	Kl [cm/ sec]
I	19-30	FW	20.0	0.4	0.0312	2.98	20.1	100	20.1	0.0421
I	31-42	SW	20.0	0.4	0.0371	3.04	20.8	106	22.07	0.0455
II	43-53	FW	65.0	0.8	0.095	4.02	27.66	119	32.92	0.078
II	54-62	SW	65.0	0.8	0.080	4.05	29.14	138	40.3	0.0536
III	65-72	FW	6.3	0.25	0.0304	1.46	9.37	212	19.9	0.0413
III	73-82	SW	10.3	0.25	0.0371	2.03	12.93	240	31.03	0.0323

Table 4.1 Summary of Single Bubble Aeration Experiments

smaller bubbles was a a major difficulty, since capillary glass tubes smaller than 0.4 mm I. D. were not readily available. (At the time of these experiments neither the author and nor his technician were aware of the special manufacturing procedures for glass capillaries, as outlined in section 4.1.1). A syringe needle of 0.2 mm I.D. was finally used to produce the desired bubble size of some 2 mm diameter for test sequence III.

Two aspects of bubble formation had to be considered to select an appropriate air injection rate. High air discharge from an orifice results in bubble break-up and very distorted shapes. Air flow rates, which are too low, cause intermittent bubble formation. Depending on the magnitude of such low air injection rates, bubbles are formed in a rather random manner and in groups. Air flow rates used in each test sequence were determined with preliminary injection tests. The flow rate was increased to a point where the intermittent bubble generation ceased and a continuous string of bubbles was obtained. For test sequences I and II, these air flow rates were identical for both seawater and fresh water. In test sequence III, the required minimum air injection rate was larger for seawater than for fresh water.

An average of 10 experiments were conducted for each the fresh water and the seawater test sequence. Water temperature generally did not vary more than 0.3 degree

Celsius over the length of each aeration experiment. Under these conditions the saturation oxygen concentration was considered to be constant at the average temperature. Overall mass transfer coefficients, k_L*a, were averaged and the standard deviation calculated. If an individual test showed a substantial deviation from the calculated mean, the experiment with the greatest deviation (greater than two standard deviations) was excluded. It is obvious that such a procedure could only be applied once, otherwise all data would have to be rejected. In those cases when the aeration curve showed very erratic behavior, systematic measurements errors had to be inferred, and the experiment was repeated.

The mean equivalent bubble diameter, d_E, and the number of bubbles in the aeration column were estimated from photographs. Bubble shapes with clear, defined edges were considered to be within the depth of field of the photograph and were traced for subsequent measurements. An average of 250 bubbles were analyzed for each setting. The calculated area, A, and equivalent diameter, d_E, were averaged and used as the representative values. With the average value of overall transfer coefficient, k_L*a, and the average interface area per volume, a, the transfer coefficient, k_L, could be readily calculated.

Figure 4.25 presents a typical frequency distribution of number of bubbles in the count section of the aeration

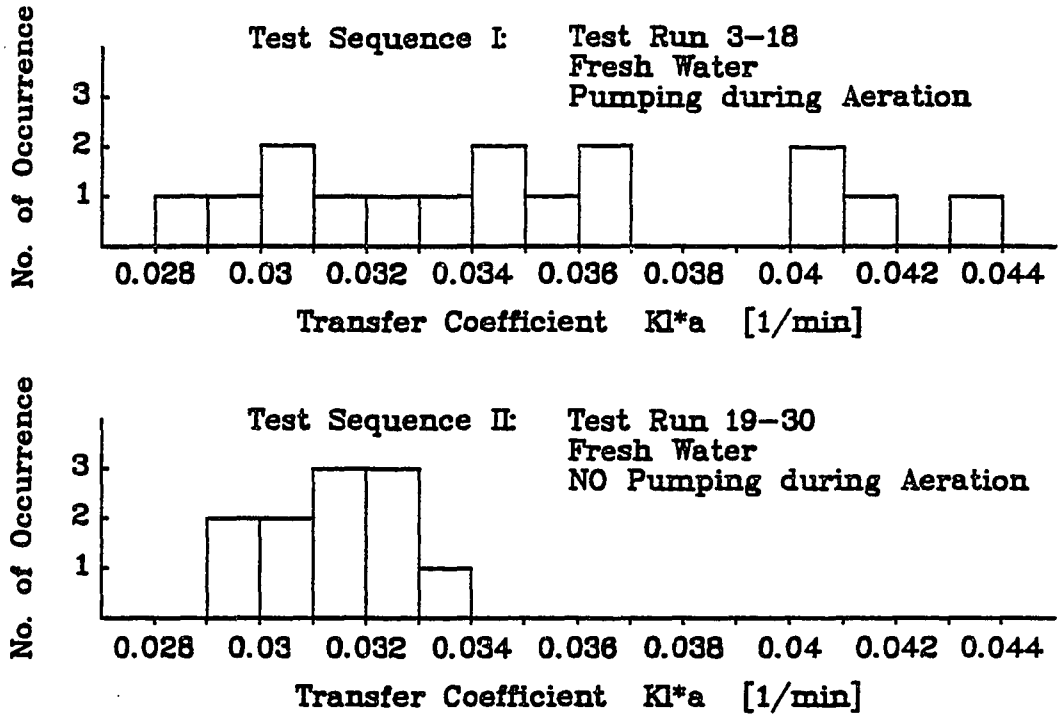

Figure 4.24 Effect of Vibration on Overall Mass Transfer

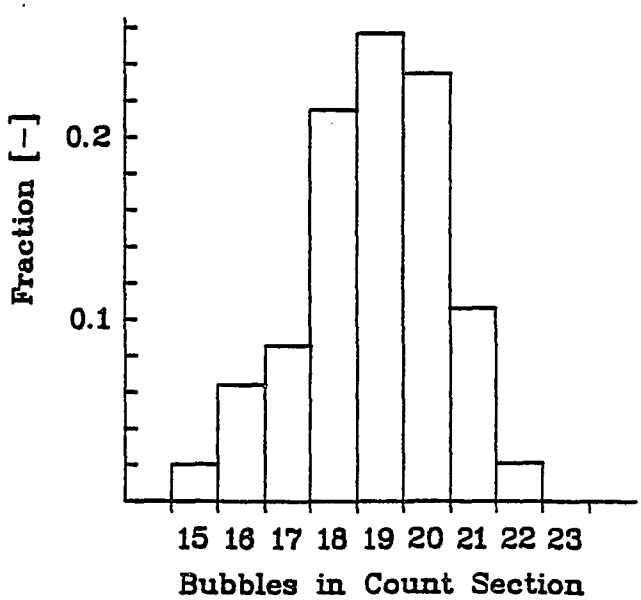

Figure 4.25 Typical Frequency Distribution of Bubbles in Column Count Section

column. Overall, 47 photographs were taken from which the number of bubbles was recorded. The average value in this caes is 18.85 bubbles in the 17.5 cm long view section. Assuming steady state bubble generation, the total number of bubbles in the column is:

$$Nt = 18.85 * 98.5/17.5$$

(here 98.5 = length of water column above the orifice)

$$Nt = 106 \text{ [bubbles]}$$

The calculated mean area per bubble was 20.82 [mm^2]. The total instantaneous interfacial area in the column was:

$$A = 106 * 20.82 = 2207 \text{ [}mm^2\text{]} = 22.1 \text{ [}cm^2\text{]}$$

The volume of aeration plus sample loop was measured to be 1620 [cm^3]. Finally, the gas transfer coefficient K_L can be calculated:

$$k_L * a = k_L * (A/L) = 0.0371 \text{ [}min^{-1}\text{]}$$

$$= 0.618 * 10^{-4} \text{ [}sec^{-1}\text{]}$$

$$k_L = 6.18 * 10^{-4} * 1620 / 22.1 = 0.0455 \text{ [cm/sec]}$$

The measured values of k_L*a generally showed good repeatability. Relative errors (standard deviation divided by the mean) were smaller than or equal to 5% in sequences I and II, and smaller than 6.7% in sequence III. Figures 4.26 and 4.27 show the semilogarithmic plots of relative concentration for all fresh water and seawater tests, respectively. Calculated transfer coefficients, k_L, for all settings along with pertinent calculation variables are presented in table 4.1. Finally,

coefficients k_L*a and k_L are plotted as a function of equivalent diameter, d_E, in figures 4.28 and 4.29, respectively.

Discussion: The photographic technique used in this study provided sharp images of bubbles rising in the aeration column. Testing confirmed that the square plexiglass water basin resulted in undistorted images of objects inside the circular aeration column. The method for estimating the bubble population size resulted in a reliable measure of the instantaneous interfacial area.

After correcting some initial difficulties, the experimental aeration procedure gave repeatable results for the overall transfer coefficient, k_L*a. The magnitudes of the relative error for Kl*a are equal to or better than those reported in the literature.

The overall transfer coefficients, k_L*a, (figure 4.28) indicate similar gas transfer in seawater and fresh water in single bubble experiments. Values in figure 4.29 suggest that the transfer coefficient, k_L, for seawater is equal to or smaller than that of fresh water. A surprising feature is the different number of bubbles in the aeration column for seawater and fresh water. Generally, when the aeration column was filled with seawater, more bubbles were present at any given instant. Since the air flow rate was always calibrated before each test and measured to be steady, the bubble rise velocity

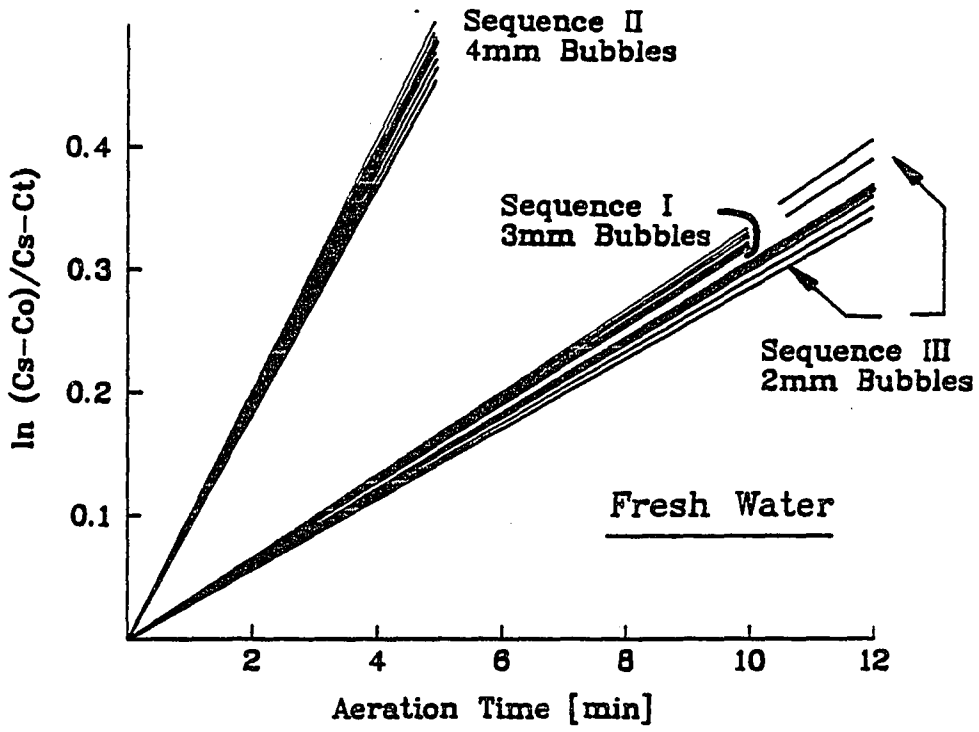

Figure 4.26 Semilogarithmic Plot of Relative Concentrations for all Fresh Water Tests

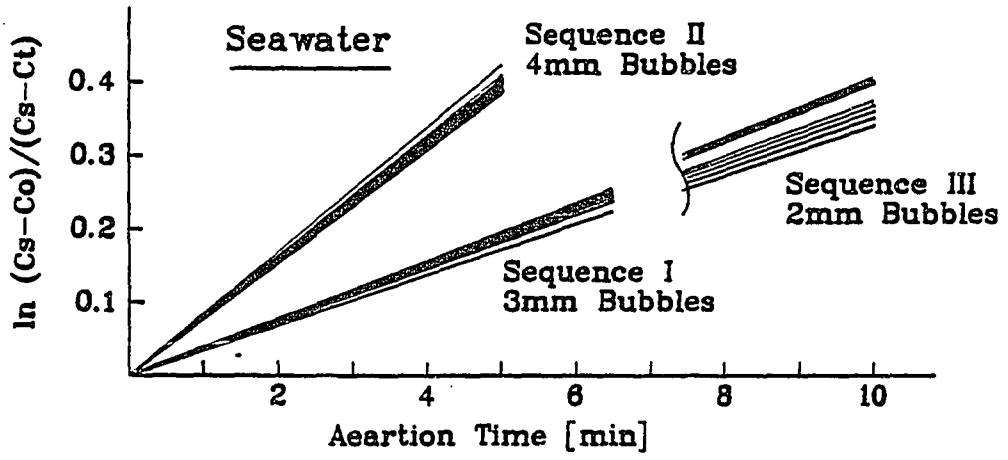

Figure 4.27 Semilogarithmic Plot of Relative Concentrations for all Seawater Tests

Tests

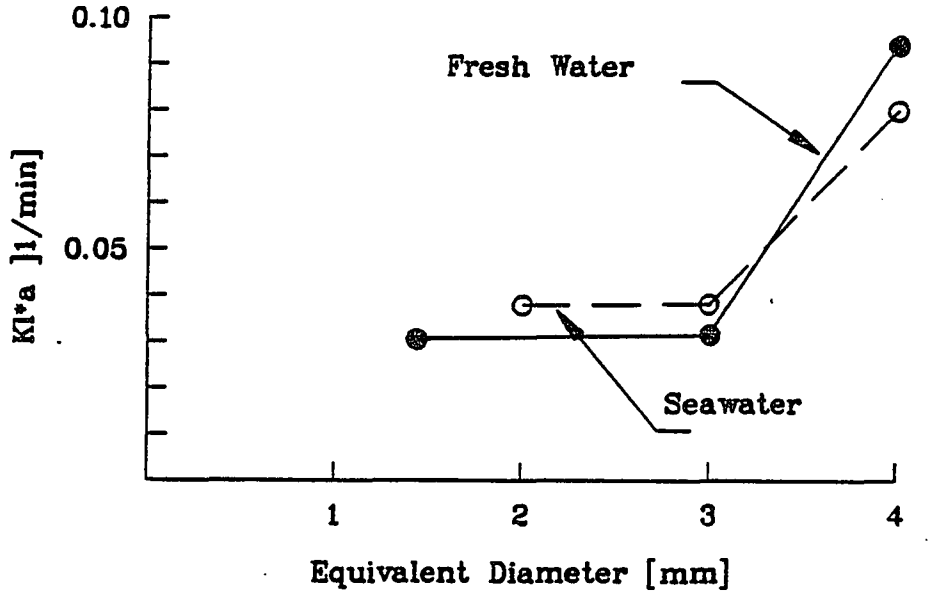

Figure 4.28 Plot of $k_{L}*a$ Versus Bubble Diameter

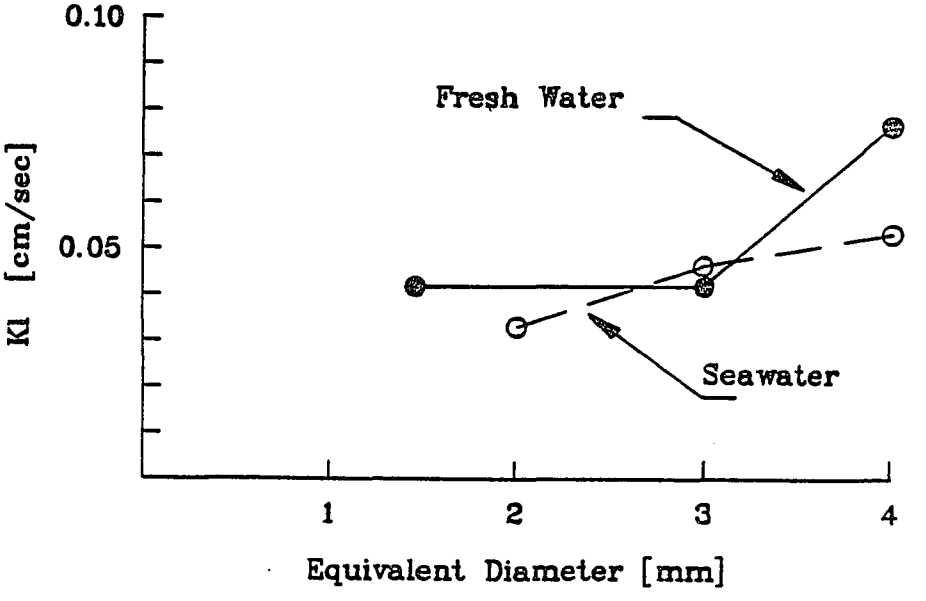

Figure 4.29 Plot of k_{L} Versus Bubble Diameter

had to be different for seawater and fresh water.

Bubble rise velocity in the aeration column was estimated by measuring the time a bubble needed to rise a certain distance. Two marks a distance of 50.8 cm apart were made on the outside of the aeration column. Air injection occurred under a controlled setting in sequence I for both seawater and fresh water. Shortly after formation, individual bubbles were identified and the time determined for them to traverse the 50.8 cm column section. These measured rise velocities are presented in table 4.2. As can be seen, relatively good repeatability was obtained with this somewhat simple method, due to the large number of observations. Generally, it could be seen that bubble in seawater rose at velocities about 10% slower than in fresh water. This observation prompted an extensive literature search for bubble rise velocities in seawater. Subsequent tests are described in section 4.4.

In figure 4.30, measured values of fresh water, k_L, are compared with values reported by Valentine [119]. An excellent fit of Kl values for bubble diameters 1.5 mm and 3 mm was found. The k_L measured for a bubble diameter of 4.0 mm, however, differs substantially from the reference. These observations suggest the following conclusions.

For smaller bubbles, the experimental procedure gave values of k_L, which were very similar to previously reported values. For the larger bubbles the present

Water Type in Aeration Column	Number of Observed Rising Bubbles	Rise interval for 50.8cm		Rise Velocity [cm/sec]
		Average [sec]	Stand. Dev. [sec]	
FW	76	2.038	0.115	24.9
SW	143	2.312	0.09	22.0
SW	119	2.330	0.082	21.8
SW	109	2.304	0.073	22.05
SW	124	2.310	0.086	21.99

Table 4.2 Rise Velocities of Bubbles in Single Bubble Aeration Column (Mean Bubble Diameter 3 mm)

investigations, k_L values are substantially higher. Therefore, the validity of tests in sequence II are questionable. The air flow rate used in sequence II was more than three times that of sequence I. Frequent collisions of bubbles with other bubbles and with the column wall were observed. It is expected that these collisions had a significant effect on the gas transfer processes. The literature was consulted during the design of the aeration test apparatus to assess potential wall effects. As indicated in figure 4.31 the retarding effects of column walls on the terminal velocity of bubbles is a function of the ratio d_E/D, where D is the diameter of the column. Consequently, a 4mm bubble should be minimally affected in a 4 cm column. The observed vigorous bubble collisions in test sequence II, however, indicate a more severe wall effect than previously noted in the literature.

4.2.3 Bubble Swarm Aeration

4.2.3.1 Experimental Apparatus and Test Procedure

Test set-up: For bubble swarm experiments a 14 cm I.D. plexiglass column 122 cm long replaced the smaller aeration column used in previous tests. The flow scheme

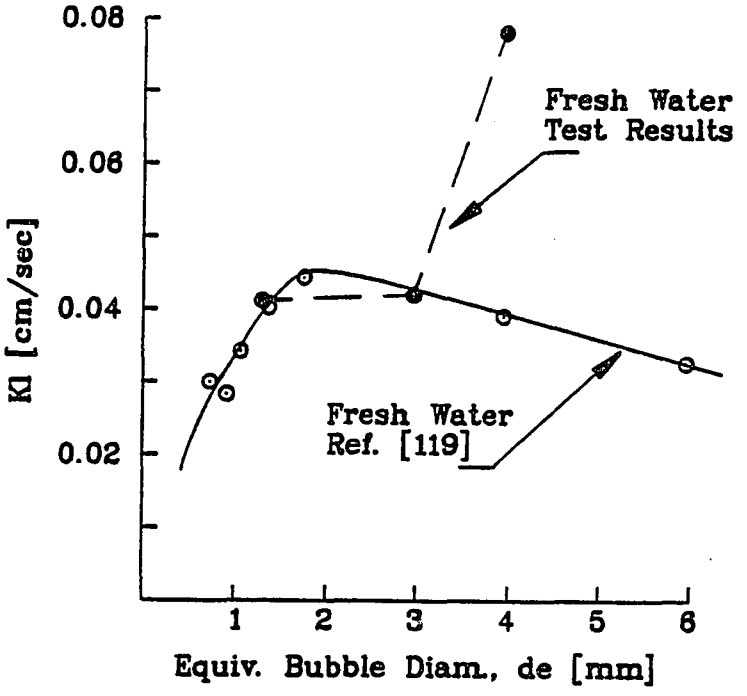

Figure 4.30 Comparison of Measured k_L with Literature Values

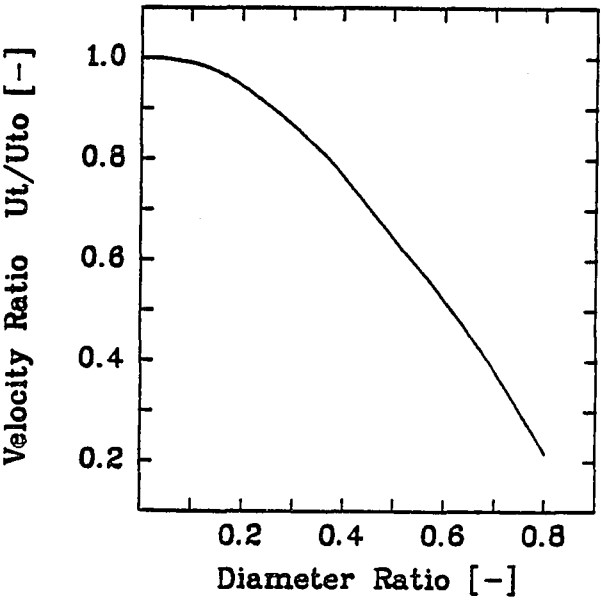

Figure 4.31 Wall Effects on Bubble Rise

of the sample loop and the air supply was the same as indicated in figure 4.16.

The aeration column used in this test sequence is shown in figure 4.32. The top portion of the column had a similar configuration as the top configuration of the aeration column for single bubble aeration. Water to be circulated in the sample loop was extracted at the midpoint of the column through a 0.95 cm O.D. copper tube. After being pumped through the sample loop, water was reinjected into the bottom of the aeration column. Air injection occurred by means of a fritted disk. A variety of fritted disks and aeration stones had been tested previously. The type selected was chosen because it produced the desired homogeneous swarm of small bubbles approximately 2 cm in diameter. As measured immediately above the horizontally oriented stone plane.

One of the main objectives of this test segment was to investigate the effect of bubble coalescence on gas transfer. Since bubble collisions are imperative for successful coalescence, a method was incorporated to augment the collision rate of bubbles after formation. An inverted plastic funnel was suspended above the fritted disk as indicated in figure 4.33. Bubbles generated by the fritted disk rose and impinged on the inclined walls of the funnel. They were then guided to the funnel orifice, which had a diameter of 1.5 cm. Water which left

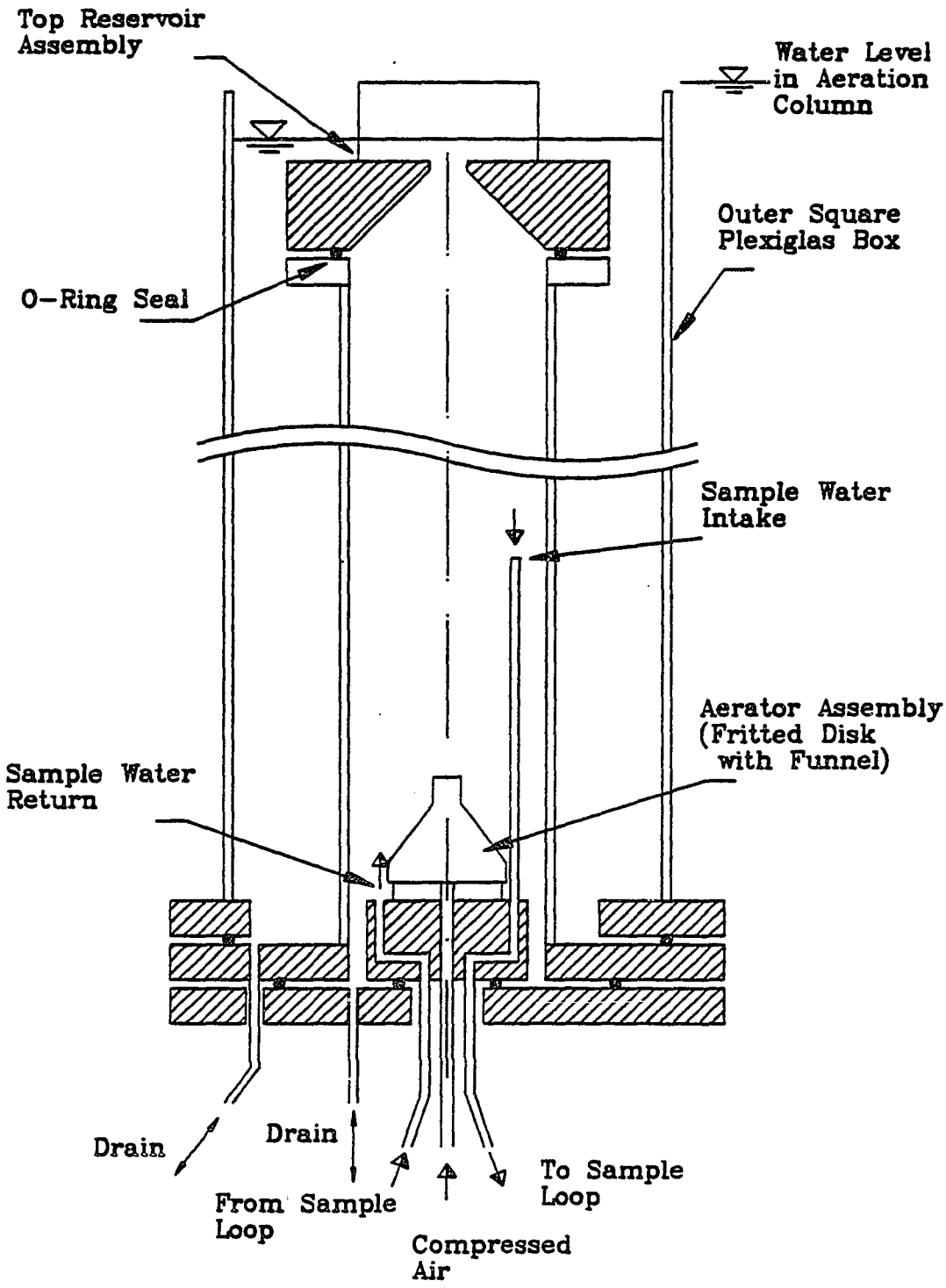

Figure 4.32 Aeration Column for Bubble Swarm Aeration Experiments

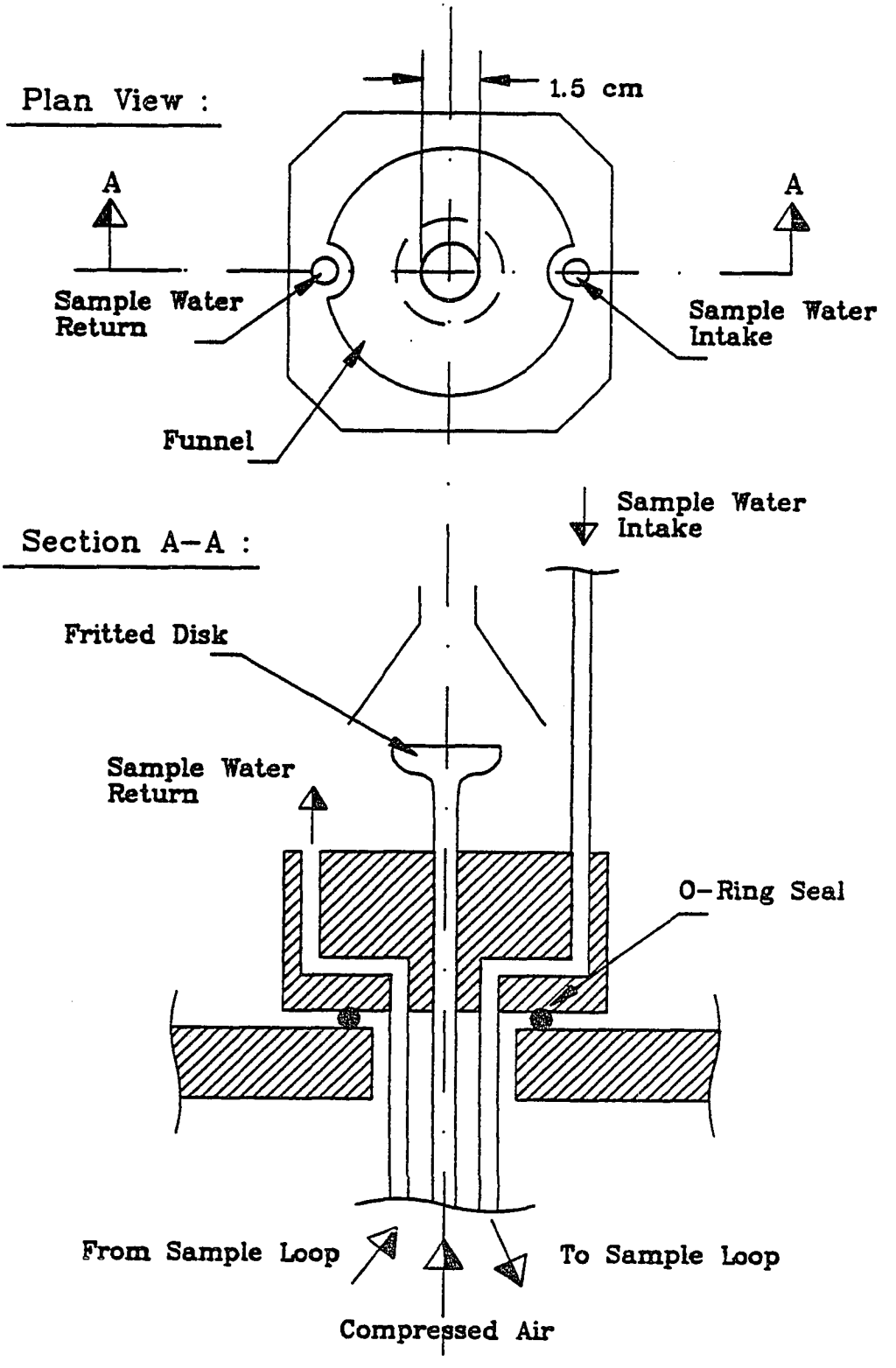

Figure 4.33 Fritted Disk Air Injector Configuration for Bubble Swarm Aeration Experiments

the funnel with the ascending bubble stream was replenished by water entering from the open spaces underneath the funnel. Air flow regulation and adjustment were carried out in the same manner as described in section 4.2.2.1..

Due to the large volume of the aeration column, water mixing within the sample loop was not feasible. Water had to be mixed in the column before measurements with the D.O. probe could be accurately carried out. Consequently, a stirrer was used to mix the water. The stirrer consisted of two moveable blades, which swung out when rotated. The stirrer could, therefore, be inserted for mixing and removed for aeration. Initial test runs indicated, however, that the bubble swarm alone produced vigorous mixing of the water. Consequently, the stirrer was used only to mix the deaerated water prior to the first aeration period of an experiment.

Seawater was collected from the ocean approximately 4.5 km offshore. The water was pumped from a depth of about 10 m into a storage tank of 600 l capacity. The tank was subsequently transported to an air-conditioned room, close to the laboratory where aeration tests were conducted. Seawater was stored in the dark and used within eight days. In addition, two seawater batches were obtained from PBRC, a coastal laboratory facility which continuously pumps seawater from 300 m offshore at a depth

of approximately 10 m. One of these nearshore seawater batches was filtered using a 5 micron polypropylene cartridge. Fresh water was taken from the laboratory tap water supply.

Water batches of some 25 l were partially degassed for the aeration experiments by means of a packed column configuration similar to that shown in figure 4.19. Water was lifted under vacuum into the packed column deaerator and flowed down over the packing elements. Deaerated water was transferred to the aeration column by gravity flow.

Test procedure: Before the first aeration period the test water was mixed thoroughly for a short while and then circulated through the sample loop for an average period of about 20 min. The D. O. concentration measured at the end of the 20 min period was taken as the initial concentration, C_o. The air flow rate was calibrated prior to the day's first aeration test. Calibration was checked periodically to verify steady flow rates.

During aeration periods the peristaltic pump was turned off. After the aeration interval was completed water was circulated through the sample loop. Figure 4.34 shows a typical D.O. record during circulation. D.O. values increased until they approached a constant value after approximately 3 minutes. When the measured D.O. value was steady the next aeration run could be started.

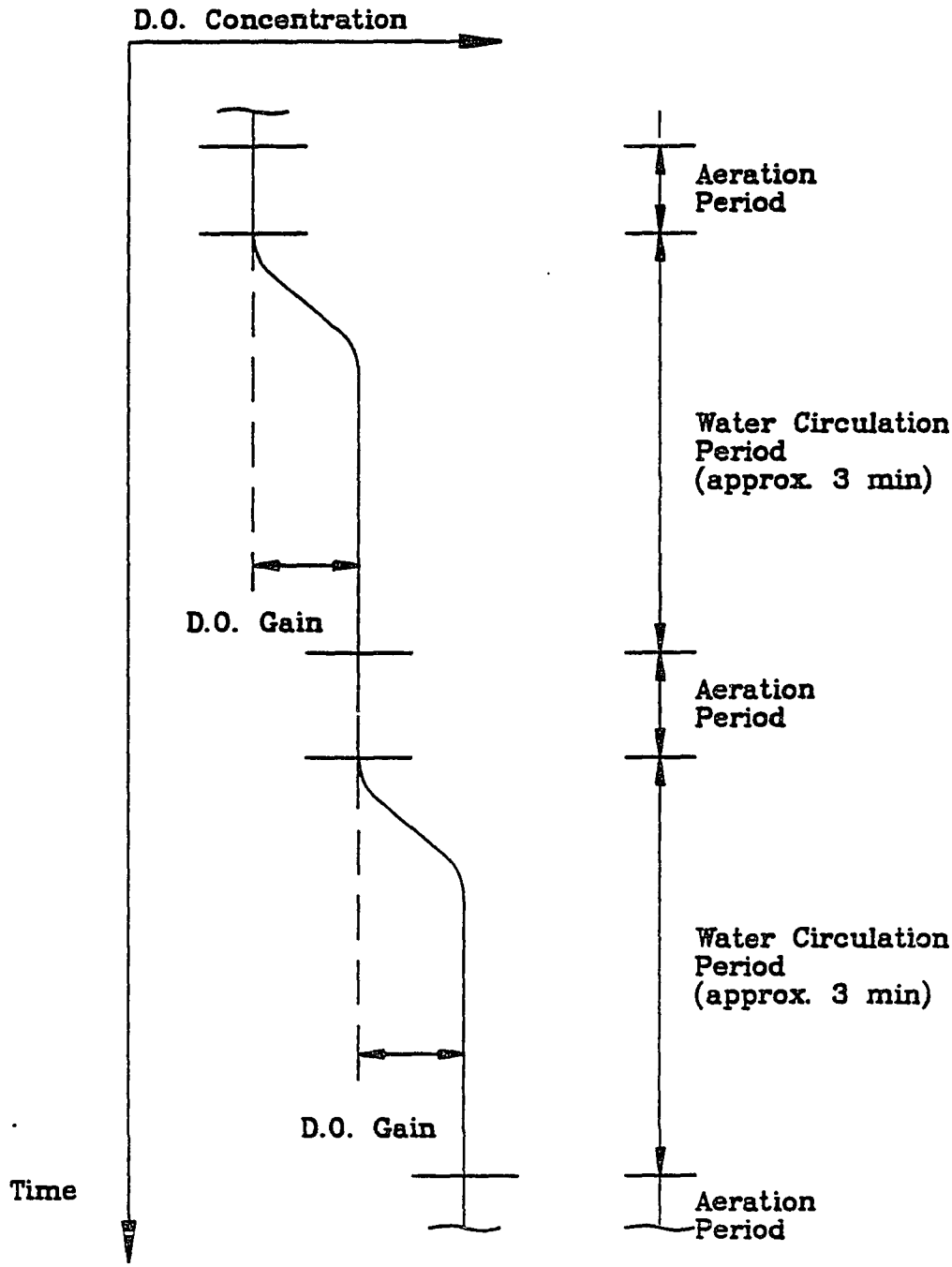

Figure 4.34 Typical D.O. Record for Bubble Swarm Aeration

As in the single bubble aeration experiments, bubble size and bubble hold-up measurements were required to calculate the transfer coefficient, k_L. Initial tests revealed that the photographic technique that was previously used, was not suitable in this configuration. The bubble plume was relatively broad and it was observed that large bubbles were predominantly located on the outside portion of the plume. Smaller bubbles were most abundant within the plume center. Since the depth of field of the macro lens was relatively short, it was possible to focus either on the center or the outside of plume but not on both. For these reasons only the overall mass transfer coefficient, k_L*a, was determined for the experiments of this segment.

Bubble size distribution: Although the magnitude of the interfacial area for calculating k_L was not determined, a qualitative estimate of the bubble size distribution was obtained in order to estimate the degrees of coalescence in seawater and in fresh water. In order to do this, a special viewing device was constructed to replace the aeration column. Air injection occurred with the same fritted disk configuration and under the same air flow calibration conditions as with the aeration column.

Since the total bubble plume was too wide to allow satisfactory photographic recognition of single bubbles the swarm had to be photographed in a narrower section.

In order to seperate such representative portion of the bulk swarm, a viewing device was built (figure 4.35).

This device was designed to collect a cut section of the axial bubble swarm by means of a downward facing opening of a small thickness. The two thickness used were 2.5 cm for fresh water and 1.25 cm for seawater. The width of the opening was 23 cm to cover the entire breadth of the bubble plume. Bubbles not entering the viewing device impinged on bubble deflector baffles, which guided the ascending bubbles to either side of the square water tank, away from the observation window. Bubbles ascending inside the collection box appeared in the observation window after passing through a tapered section, which decreased the width of the box from 23 to 14 cm. Small baffles located at the upper ends of the tapered section ensured that all bubbles were deflected into the viewing area of the observation window.

The deflector device was positioned in such a way that its vertical centerline coincided with the opening of the inverted funnel. Pictures of the bubbles were taken through the window. An electronic strobe, which was synchronized with the camera shutter, illuminated the side opposite the camera lens. A shutter speed of 1/30 and an aperture of 1/5.6 f was used. The film was an Ektachrome 100 ASA.

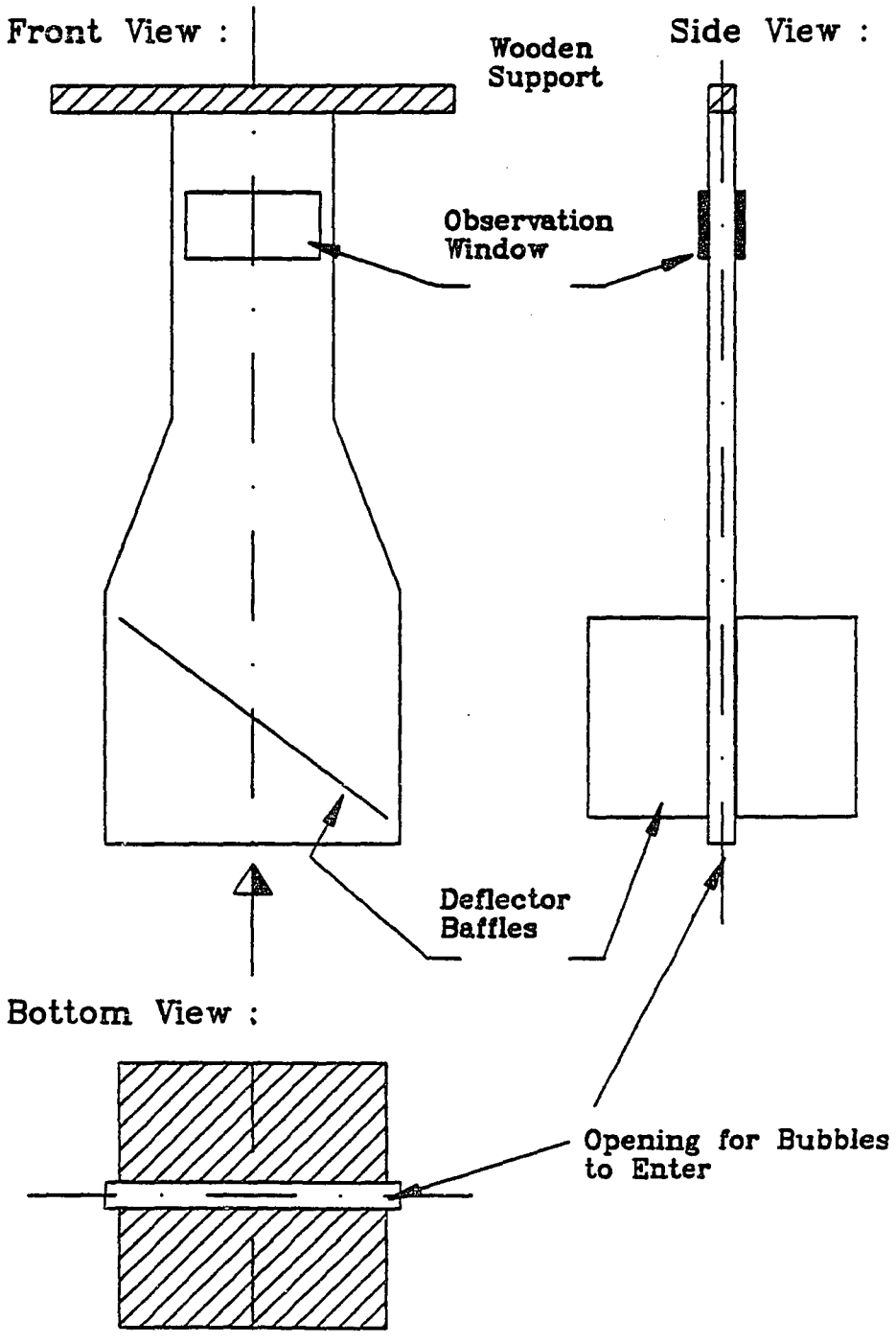

Figure 4.35 Viewing Device for Bubble Size Distribution Assessment

The resulting slides were projected with a magnification of 4. Bubble images were traced on paper along with the boundaries of the observation window. A scale was located on the window boundaries to facilitate accurate measurements.

Methods for measuring and counting the traced bubbles differed for fresh water and seawater photographs. In the case of fresh water, all large bubbles (>1.5 mm) were traced and counted. Smaller bubbles were traced only for a representative section of the window (typically some 45% of the entire window area). For seawater no distinction was made between larger and smaller bubble groups. All bubbles inside a designated area (typically some 10-20% of the window area) were traced and counted.

4.2.3.2 Results and Discussion

Aeration Tests: Aeration experiments for seawater and fresh water were carried out with three air flow rates: namely 100, 200 and 300 ml/min. In addition to offshore water, two batches of coastal seawater were tested, one of which was filtered. The test procedure gave good repeatability, as can be seen for example in the case of the 200 ml/min air injection experiment in figures 4.36-4.37. In these figures the aeration curves of representative test runs, along with semilogarithmic plots

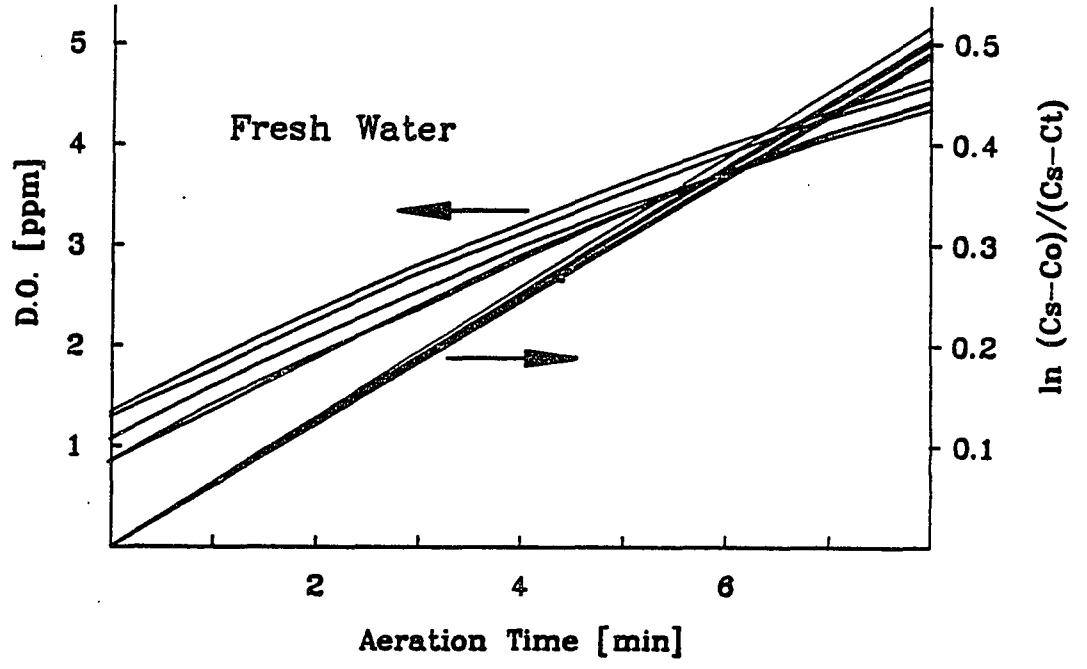

Figure 4.36 Aeration Curves and Semilogarithmic Plots (Fresh Water; 200 ml/min Air Injection)

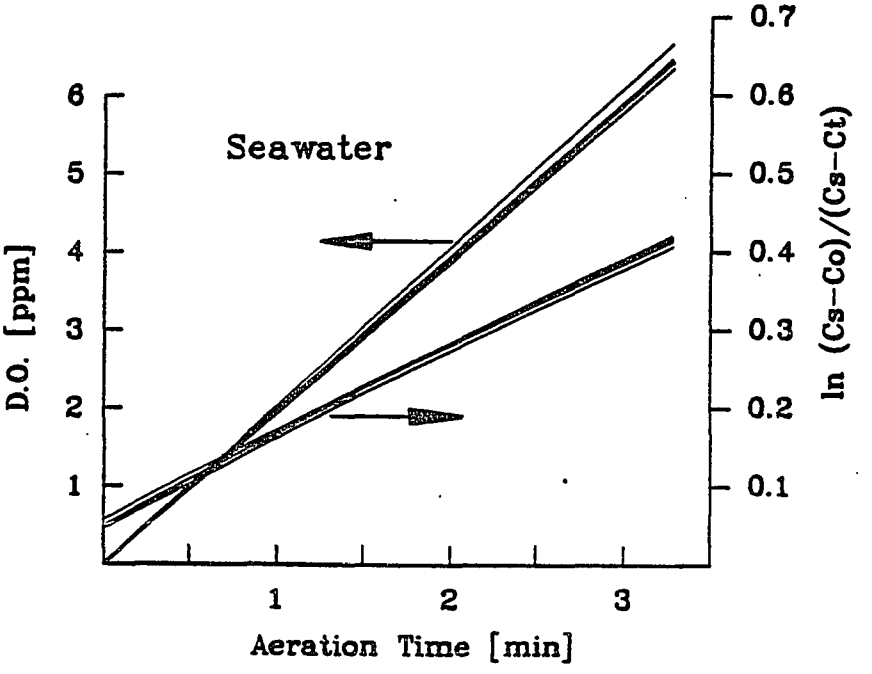

Figure 4.37 Aeration Curves and Semilogarithmic Plots (Seawater; 200 ml/min Air Injection)

of relative concentration, are presented.

During these experiments the water temperature changed only slightly, having a maximum overall deviation of 0.3 ^{o}C. The saturation D.O. concentration was determined for the average temperature and for the elevation of half of the water column above the fritted disk. The overall transfer coefficient was readily calculated from the semilogarithmic plots of figures 4.36 - 4.37.

Mean k_L*a values for seawater and freshwater are plotted in figure 4.38 as a function of air injection rate. Figure 4.39 presents the k_L*a values of the three different seawater batches used in the aeration tests.

As indicated in figure 4.38, seawater gas transfer rates were significantly higher than fresh water values. The k_L*a ratio of seawater to fresh water increased from 2.7 at 100 ml/min air injection to 3.7 at 300 ml/min. Obviously, the increase in K_L*a with increasing air flow is significantly higher for seawater. Results in figure 4.39 suggest that there is no significant difference in k_L*a values between offshore and filtered coastal seawater. Unfiltered coastal water, however, has water impurities which evidently decrease the rate of the gas transfer processes.

Bubble size distribution:

Tracing of bubbles and subsequent measuring and counting of the recorded images proved to be a very time-

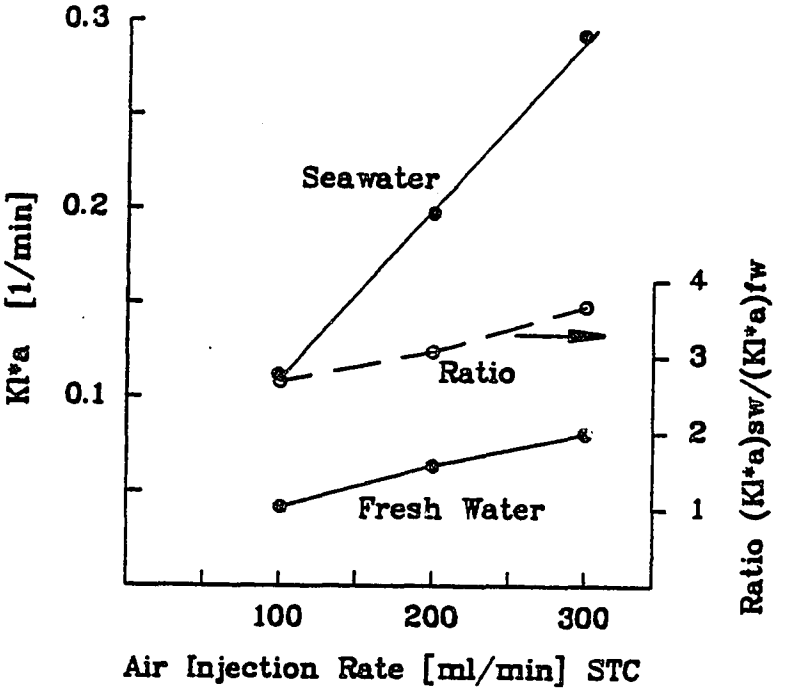

Figure 4.38 Fresh Water and Seawater $k_{L}*a$ Values Versus Air Injection Rates

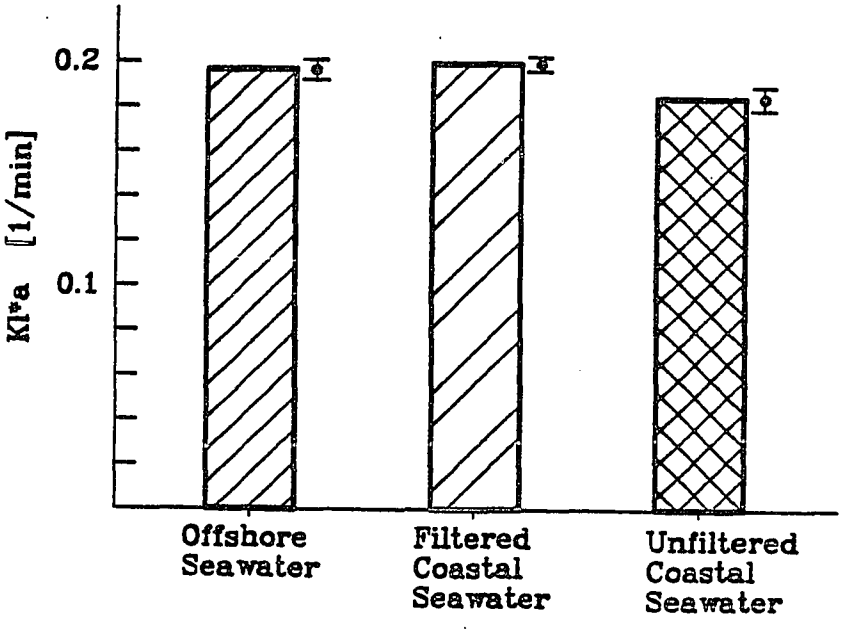

Figure 4.39 Comparison of Offshore and Coastal Seawater Gas Transfer Characteristics

consuming endeavor. Consequently, only four pictures perinjection rate were analyzed for both fresh water and seawater.

If a bubble was ellipsoidal, its major and minor axes were measured and its surface area determined by equation (4.8). The equivalent diameter d_E was calculated using equation (4.11). The bubble surface area was also calculated and this value placed into one of 13 bins, which spanned a diameter range from <0.25 - 4 mm. The resulting areas of each bin were multiplied with appropriate correction factors to account for the fact, that only a certain fraction of the window area was analyzed. The sum of corrected bin areas gave the total surface area in the window. The areas of every bin could in turn be expressed as a fraction of the total area.

The distributions of area fraction versus equivalent diameter are shown in figures 4.40 and 4.41 for fresh water and seawater, respectively. As stated previously, a distinction between small bubble and larger bubble groups was made in the case of fresh water. The fraction of total area provided by the small bubble group diminished with increasing air flow. Consequently, more surface area was provided by larger bubbles at higher air flow rates.

In the case of seawater, only one group of bubbles was observed; namely, that covering the diameter range from <0.25 to approximately 1.2 mm. As can be seen in figure

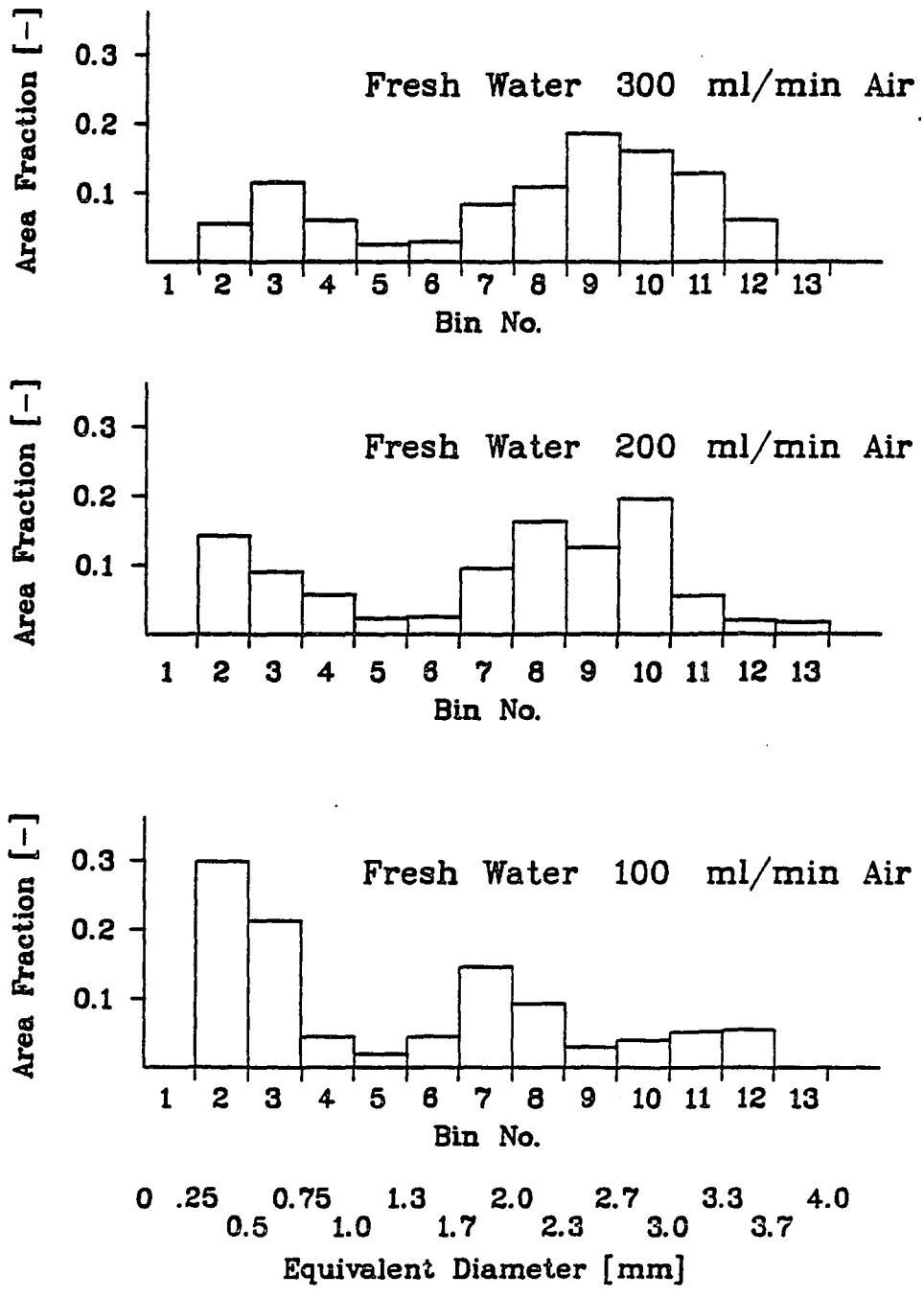

Figure 4.40 Surface Area Fractions for Bubble Size Ranges (Fresh Water)

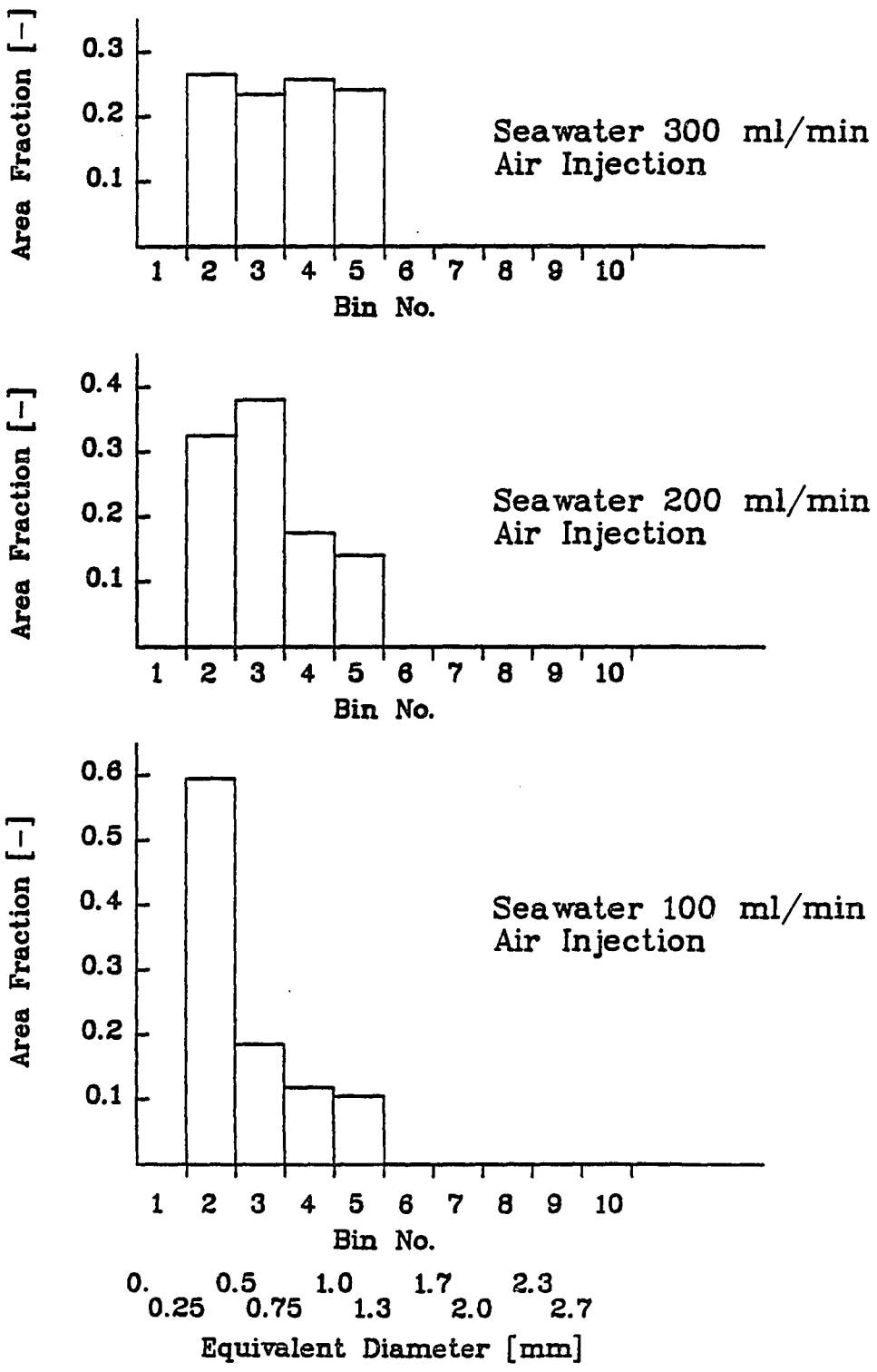

Figure 4.41 Surface Area Fractions for Bubble Size Ranges (Seawater)

4.41 a peak was established by bubbles in the 0.25 to 0.5mm range. With increasing air injection rate, the peak declined and a more even distribution resulted.

The fractional area distributions indicate intensities of bubble coalescence which are significantly different in fresh water and seawater. In fresh water, a large percentage of bubbles coalesce, producing bubbles, which grew in this case to a maximum size of 3.5 mm. At higher air flow rates, more bubbles collide and the fraction of area presented by the larger bubble group increases. A similar, but much less pronounced, mechanism is suggested for seawater. Here, increased air injection also causes higher coalescence rates. The maximum observed diameter, however, never surpassed about 1.3 mm.

In certain cases data scatter was considerable. Attempts to quantify the absolute surface area in the plume by correlating the portion of the captured bubble had to be rejected as reliable because of the magnitude of the data scatter. However, as a qualitative indication of the relative degree of coalescence processes in fresh water and in seawater, these distributions provide valuable information.

While designing the viewing device, an attempt was made to minimize disturbance to the bubble plume caused by the device. It could not be determined whether the data scatter was due to flow alteration of the box or due to

instabilities of the plume itself. It was observed, however, that with the viewing device in place the plume deviated from its vertical position in a somewhat swinging mode. Consequently, bubbles entrained in the viewing device were likely to represent several different sections of the plume.

4.3 BATCH DEAERATION EXPERIMENTS

4.3.1 Theoretical Aspects of Desorption

For gas desorption to occur the concentration of dissolved gas in the bulk liquid must be greater than that of the liquid gas interface. Thus, the partial pressure of the dissolved gas, which would be in equilibrium with the bulk of liquid, is greater than the partial pressure at the surface. In those instances where the difference between the partial pressure in equilibrium with the bulk liquid and the partial pressure at the surface is somewhat larger, bubbles form in the interior of the liquid and a large fraction of the gas escapes the liquid by diffusing into these bubbles .

The process of bubble formation due to supersaturation requires of bubble nucleation. In a liquid medium nucleation can take place in two ways; namely, as homogeneous or as heterogeneous nucleation. The point of departure for discussing these forms of nucleation is the force balance on a submersed spherical bubble, this way treated previously in section 4.2.1.. According to equation (4.25), the excess pressure required for bubble sustenance is:

$$p = \frac{2 * \sigma}{R} \qquad (4.28)$$

It is evident that with decreasing bubble radius the necessary excess pressure increases. With very small bubbles the required pressure inside the bubble becomes prohibitively high and bubbles are hypothetically not able to exist. An equilibrium radius can be defined for the liquid of interest in order to quantify a threshold size below which bubbles cannot exist.

Homogeneous nucleation is the process in which bubbles form from inhomogeneous sites in the bulk of the liquid. There are several hypothesis of the origin and methods of generation of these liquid inhomogeneities. One hypothesis starts with a stochastic assumption that due to thermal fluctuations in the liquid, clusters of gas molecules come together to from "embryo" voids of a size corresponding to the equilibrium radius. In natural water another hypothesis assumes that the accumulation of contaminants on the bubble surface can establish cage-like structures around shrinking bubbles, thereby generating small voids whose stability is not determined by the liquid film surface tension. [83]

Whatever the origin of the "embryo" voids, these nuclei are the necessary first step for the formation of larger bubbles.

Heterogeneous nucleation describes the process whereby bubble formation is initiated on container surfaces or surfaces of foreign matter. These foreign bodies can be

either stationary or, for example, the walls of a container, or suspended in the bulk liquid.

As discussed earlier, surface tension increases the internal pressure of free bubbles. According to Lieberman [83], on a hydrophobic surface the effect of surface tension can reverse, and surface tension is then able to act opposite to the aqueous pressure, thereby reducing the total pressure. The curvature of the aqueous surface lets the surface tension oppose the pressure in the bulk of the liquid. Whenever these opposing pressures are equal, the dissolution of the gas stops and the gas void can persist indefinitely.

Gas transfer to bubbles formed in supersaturated liquids is a process, which is very different from the absorption process, in which the area of the available surface is determined by external factors and not by the absorption process itself. In addition to bubble formation due to nucleation, bubbles can be introduced externally to augment the available interfacial surface. Since the transfer rate is a function of surface area, gas transfer will be increased by such external bubble seeding.

Assumptions used to derive the expressions for absorption (section 4.2.1) can be equally applied to desorption. The difference is that in gas release, the gas concentration in the liquid, C_L, is greater than the

saturation concentration at the liquid-gas interfaces, C_S.

Assuming that gas release is negative, absorption equation (4.21) can be revised as follows:

$$- \frac{dC_L}{dt} = k_L * a * (C_L - C_S) \qquad (4.29)$$

Integrating equation (4.29) with appropriate limits gives:

$$\ln \left(\frac{C_L - C_S}{C_o - C_S} \right) = - k_L * a * t \qquad (4.30)$$

Equation (4.30) can be readily rewritten to give the expression:

$$\ln \left(\frac{C_o - C_S}{C_L - C_S} \right) = k_L * a * t \qquad (4.31)$$

The overall mass transfer coefficient for the present deaeration experiments is calculated using equation (4.31).

4.3.2. Bubble Swarm Deaeration

4.3.2.1. Experimental Apparatus and Test Procedure

Test set-up: The experimental configuration was modified

for the bubble swarm deaeration tests. The top section of the previous aeration column was modified as indicated in figure 4.42. Now a round plexiglass plate rested on the top column flange with an O-ring providing the vacuum seal. Two orifices were drilled in the plate, one of which was connected to a mercury manometer to monitor the pressure in the deaeration column. The other orifice accommodated connectors to the vacuum holding system and the vent line.

The same fritted disk injector was used. For these deaeration experiments, however, the inverted funnel was removed. Observations had shown that bubbles were generated over the entire area of the fritted disk stone. As bubbles rose from the disk surface, the plume's diameter narrowed to about one half of the initial width, some 4 cm above the disk. The plume increased steadily in width from the point of the smallest diameter upwards. It was assumed that the intensity of collisions in the initial plume contraction was sufficient to cause coalescence.

The modified test set-up is shown in figure 4.43. As in previous experiments the circular column was surrounded by a square water-filled box. The water level in the aeration column was lower than in previous aeration tests. Water intake for the sample loop was located at half-column height. Because of the new top configuration, the

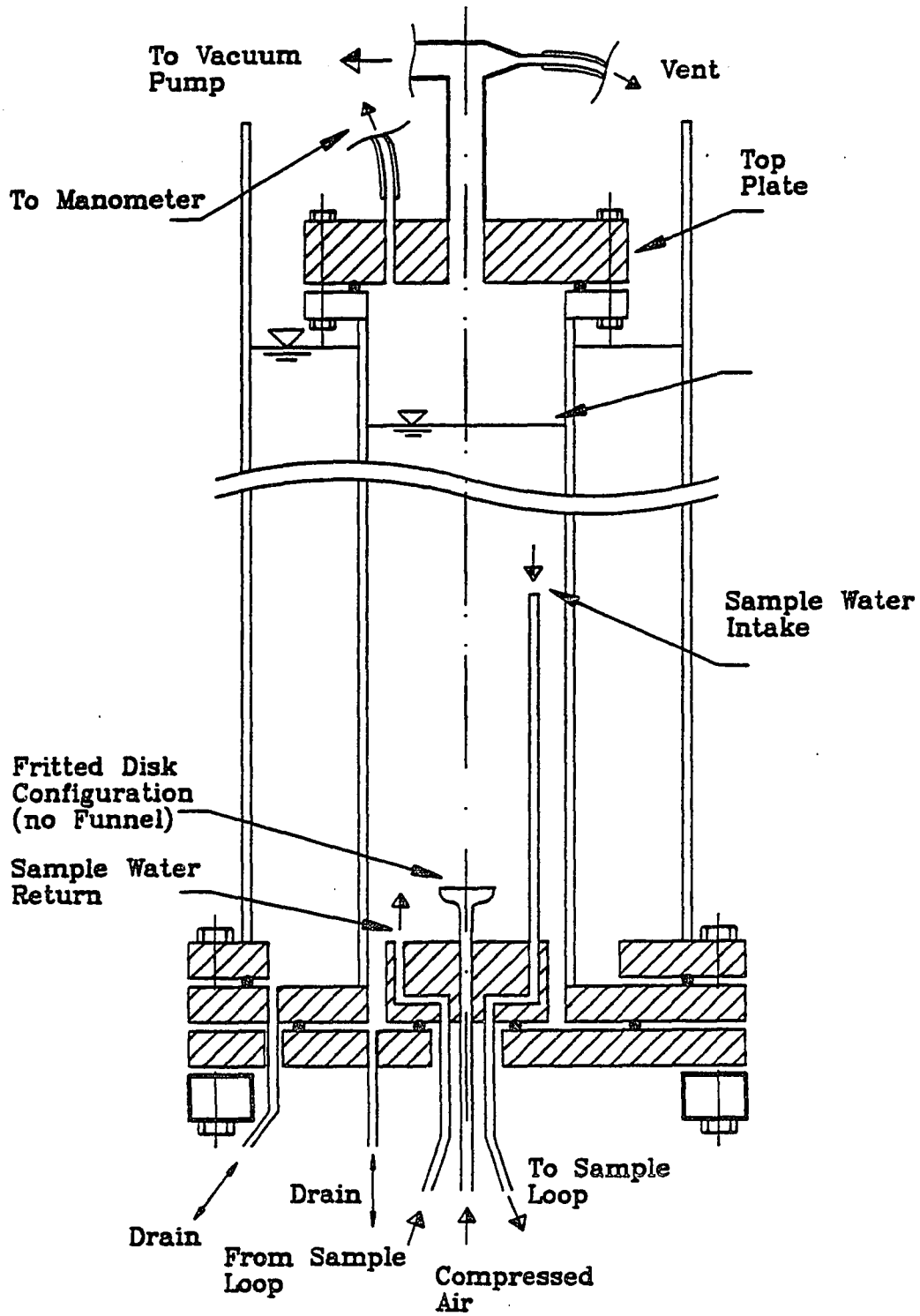

Figure 4.42 Deaeration Column

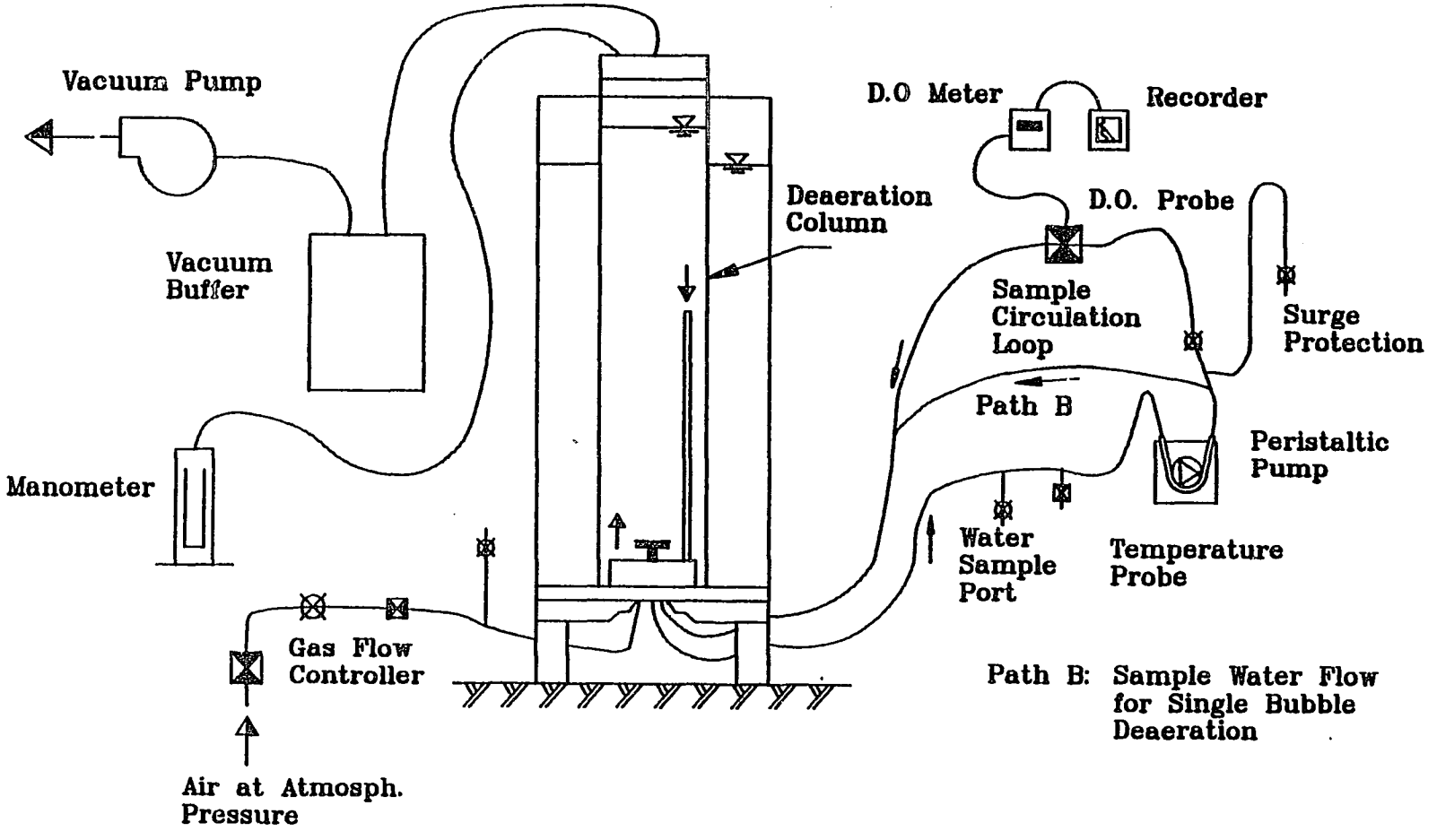

Figure 4.43 Flow Scheme for Deaeration Experiments (Flow Modification for Single Bubble Deaeration)

exposed water surface extended over the entire column's cross-sectional area.

The top plate connected the vacuum holding system. A needle valve was located upstream of the vacuum buffer vessel, which, in turn, was connected directly to the vacuum pump.

Air, for injection into the subatmospheric deaeration column, was admitted from the atmosphere. Air flow rate was regulated by means of the gas flow controller used in the aeration experiments. A rotameter was used to measure the air flow rate. The upstream opening of the rotameter was exposed to the atmosphere. Thus, the indicated flow rate was essentially measured at atmospheric pressure. A thermistor probe was located near the intake of the rotameter to determine the temperature of the air.

Two valves, valve I and II in figure 4.43, were included in the sample circulation loop in order to separate the D. O. probe during deaeration runs.

The results of previous aeration tests had suggested that there is little difference in overall gas transfer between offshore seawater and filtered coastal seawater (section 4.2.2.2). Filtered seawater was thus used for the dearation experiments. A batch of seawater was transported to the laboratory and stored in the dark in a 600 l tank. Individual seawater batches were used for

the experiments normally within three days. Fresh water was obtained from the laboratory's tap water supply.

Test procedure: Before a deaeration test was conducted, the column was filled with water and the desired air flow rate was adjusted for that particular test settings. The intial fill water was then drained and a new water batch admitted. Water was circulated in the sample loop for approximately 20 min. At the end of this period the D.O. concentration and the water temperature were recorded as initial values. During the run the peristaltic pump was stopped and valves I and II (figure 4.43) were closed. The desired partial vacuum was then established in the deaeration column. Air injection commenced as the air valve was opened with column pressure being maintained by regulating the needle valve upstream of the vacuum buffer. After the test deaeration interval was completed, the air flow was stopped. The system was held at the test vacuum pressure until the bulk of the bubbles had risen to the water surface. The deaeration vessel was then vented.

After opening valves I and II, water was pumped through the sample loop for approximately 3 minutes. The D.O. concentrations was measured with the in-line D.O. probe. A typical record is shown in figure 4.34. After the D.O. concentration and water temperature were obtained, the pump was stopped and valves I and II closed. A new deaeration interval could then be started.

4.3.2.2. Results and Discussion:

Bubble deaeration experiments were carried out with fresh water and with seawater. Four air injection rates were used; namely, 47.5, 95, 142.5, and 190 ml/min (all at 21 ^{o}C; 760 mm Hg). Two vacuum pressures, 50 and 100 mm Hg abs, were applied as system pressures inside the deaeration column.

Experimental procedures were fine tuned in initial trial runs . According to previous deaeration experiments [76], the magnitude of vacuum pressure exerted on the free water surface in the deaeration vessel was the most important parameter for gas transfer experiments. Accurate pressure settings during air injection was thus imperative. During the initial trial runs, the technique of vacuum adjustment, by means of the vent and valve upstream of the vacuum buffer, was rehearsed. During later experimental work, pressure could be accurately maintained using this technique.

After valves I and II had been closed and the vacuum applied, but before air was injected, bubbles formed in the liquid bulk and on the column walls. After successive deaeration runs fewer bubbles formed when the system was subjected to vacuum.

The water temperature did change slightly during these deaeration tests, consequently, the saturation

concentration, C_S, was calculated for the average temperature. The hydrostatic pressure considered for calculating C_S was half the water column pressure. The overall mass transfer coefficient, k_L*a, was calculated using equation (4.31). In those cases with high deaeration rates, only the first part of the deaeration curve was needed to calculate k_L*a.

The calculated values of k_L*a generally showed good repeatability. Seawater deaeration at 50 mm Hg abs. pressure, however, showed considerable data scatter. In figures 4.44 - 4.47 typical D. O. curves for one air flow setting are presented for both seawater and fresh water. As can be seen by comparing the fresh water and seawater curves, seawater deaeration occurred at a substantially higher rate.

Figure 4.48 presents the overall transfer coefficient, k_L*a, as a function of the air injection rate. The strikingly higher gas transfer rates for seawater are evident. Seawater transfer rates increased rapidly as a function of the air injection rate. Conversely, fresh water rates increased only moderately with higher air flow. As indicated in figure 4.48 the data scatter increased for seawater with higher air injection rates and lower system pressures. The reason for increased data scatter in these cases was most likely the rapidity of gas desorption. When air injection was started, several

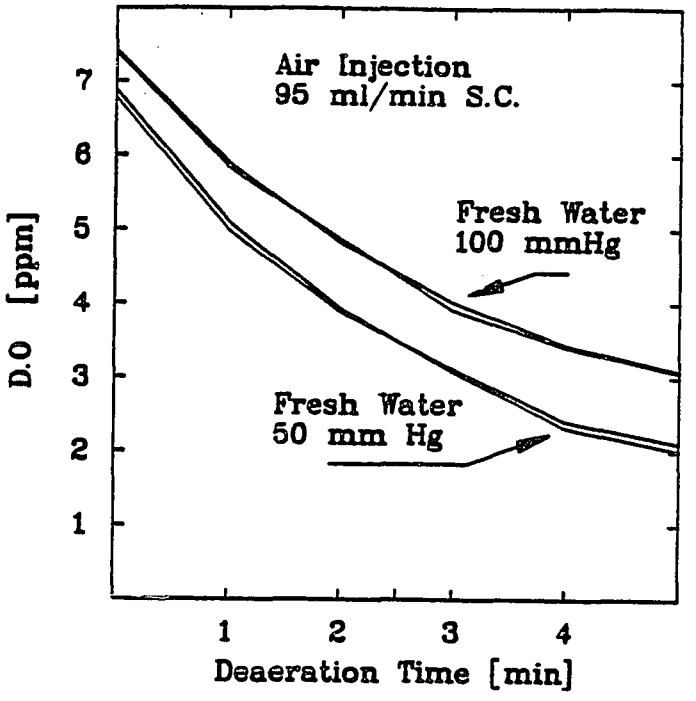

Figure 4.44 Deaeration Curves for Bubble Swarm Air Injection

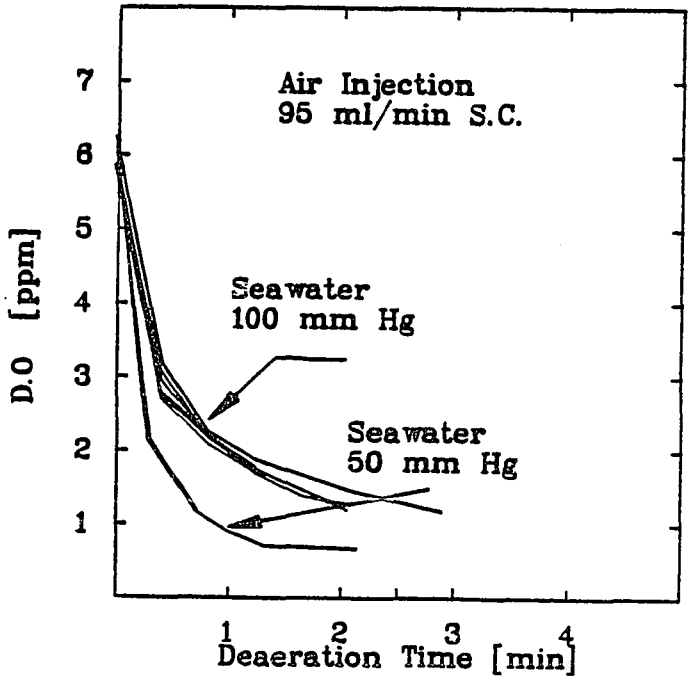

Figure 4.45 Deaeration Curves for Bubble Swarm Air Injection

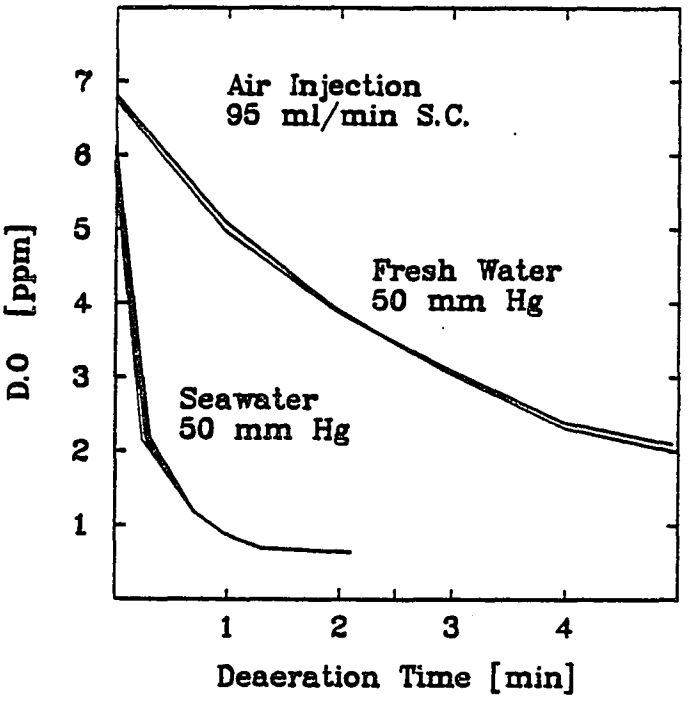

Figure 4.46 Deaeration Curves for Bubble Swarm Air Injection

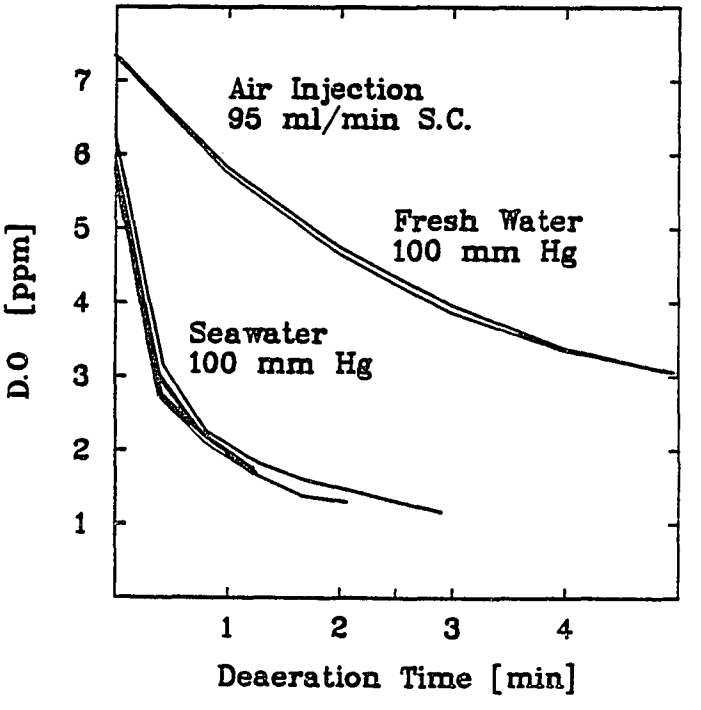

Figure 4.47 Deaeration Curves for Bubble Swarm Air Injection

seconds passed until steady state bubble formation was obtained. At high air flow and low pressures the length of the air injection period was extremely short; namely, between 12 and 20 sec. Due to the initial unsteady bubble formation period, a well-defined start of the air injection interval was hard to determine. Timing of the air injection interval became approximate. The resulting variable durations of deaeration are thought to be the cause of the data scatter.

4.3.3. Single Bubble Deaeration

4.3.3.1 Experimental Apparatus and Test Procedure

Test set-up: For single bubble deaeration experiments the following modifications of the previous test set-up were made. The fritted disk injector was replaced by a capillary injection device, which is shown in figure 4.49. Five glass capillaries with 0.4 mm bore were inserted in a rubber plate. The plate was sandwiched between an aluminum retaining ring and the plexiglass body of the device. The plexiglass was machined to have an internal diameter of some 6 cm. Capillaries were spaced sufficiently far apart to avoid interference among bubbles. The air supply tube extended into the interior of plexiglass body. This avoided flooding of air intake

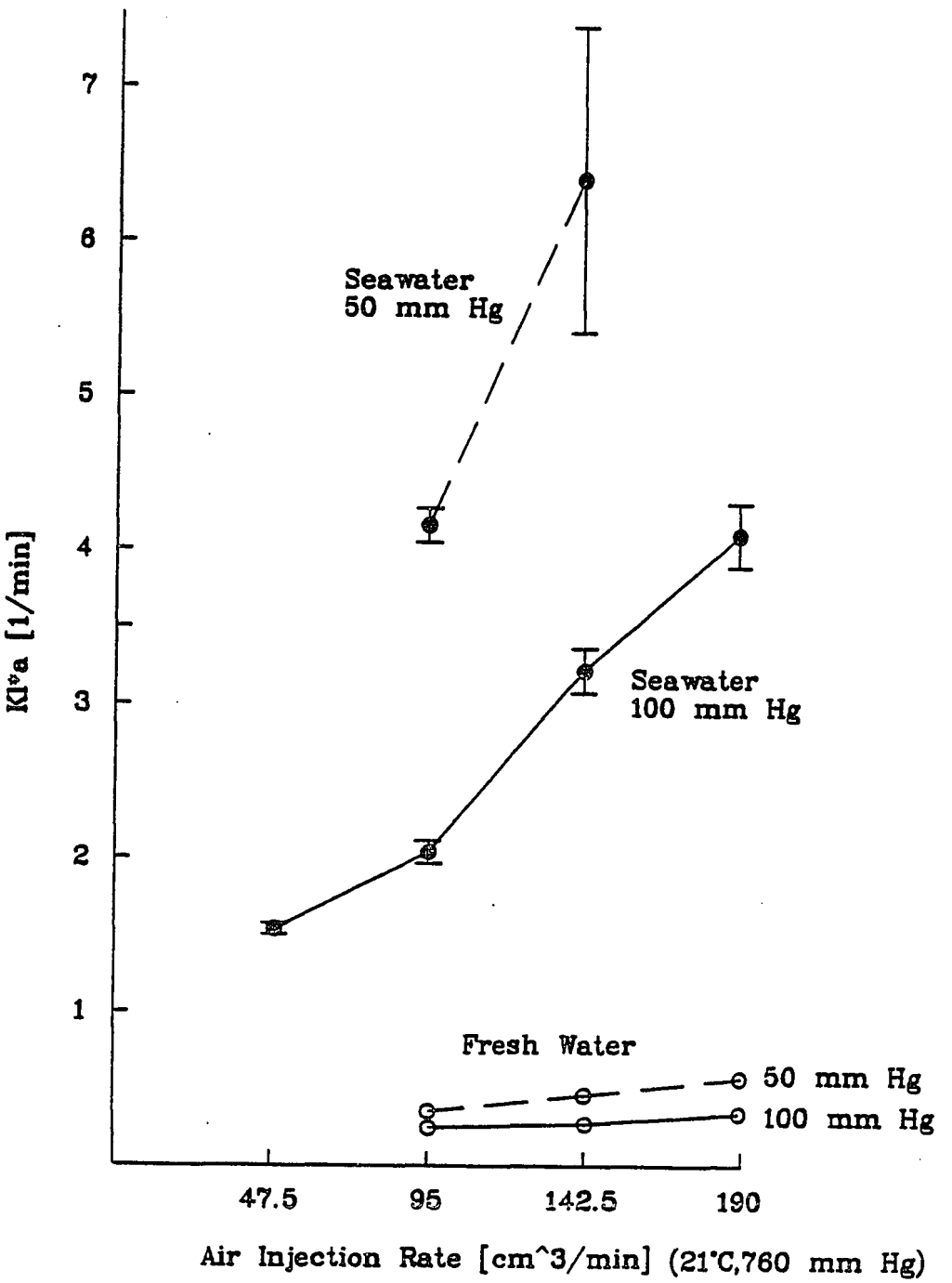

Figure 4.48 Overall Transfer Coefficient $k_{L}*a$ for Fresh Water and Seawater Deaeration

hose. Between deaeration intervals capillaries discharged water into the plexiglass reservoir if hydrostatic pressure was higher than internal pressure. Entrained water obstructed subsequent air injection as it caused uneven discharge of the capillaries. The injection procedure was improved by draining the water before each air injection test. By adjusting the gas flow controller air flow was started and simultaneously the drain valve of the reservoir was opened. Entering air displaced the accumulated water in the capillaries. After enough water was drained, the drain valve was closed and air injection commenced without interference.

As indicated in figure 4.43 the flow path of the sample loop was also modified. The D.O. probe was by-passed and water circulation was limited to enable temperature readings and water sampling. Water samples were analyzed with a gas chromatograph.

Chromatographic analysis was conducted as follows. Calibration of the instrument occurred prior to the first sample of the day. Verification of calibration was done at the end of analysis and, if the analysis periods were long, at intermediate time intervals.

Helium carrier gas flowed through the packed chromatographic column at a rate of 20 ml/min. The chromatographic column was usually held at 60 ^{o}C. For calibration purposes, standard mixtures of helium-oxygen

and helium-nitrogen were used. The concentrations of oxygen and nitrogen in these mixtures were such as to correspond with atmospheric conditions.

During calibration runs, the standard mixtures were injected into the chromatograph one at a time. The recorded peak areas were averaged for successive calibration runs and the mean areas were then used to determine the dissolved oxygen and nitrogen contained in the water samples.

Water from each sample B.O.D. bottle was slowly sucked into transfer syringes. This liquid sample was then injected into a sample loop of known volume. Special care had to be taken to exclude air bubbles at this step, since otherwise erroneous measurements were obtained. Upon injection, the water sample was pushed by the carrier gas to an in-line sparging device where the dissolved gases were separated from the liquid sample. Further downstream the gaseous flow passed through a drying column filled with layers of Drierite and through a molecular sieve, before entering the chromatographic column. A thermal conductivity detector finally recorded the quantitative signals from the passing oxygen and nitrogen chromatographic zones.

Experimental procedure: The main features of the experimental procedure in this section were the same as for the bubble swarm experiments. Water circulation in

the shortened sample loop, however, was different. The water was circulated for 10 minutes before the start of a deaeration run,. After air injection was completed the deaeration column was vented and the water was circulated for approximately three minutes. The water temperature was then measured and two liquid sample were slowly withdrawn. Water samples were collected in 300 ml/BOD bubbles. Plastic caps were placed on the tops of these bottles to avoid drying of the water seal. The sample bottles were stored in the dark until sample analysis was carried out within 24 hours.

4.3.3.2. Results and Discussion:

Preliminary experiments were conducted to determine the suitable time period for air injection. In these experiments dissolved oxygen concentrations were measured with a D.O. bottle probe. The results of these tests are shown in figure 4.50. Three experiments were done with intermittent air injection. A deaeration period of 10 minutes was chosen since the D.O. loss averaged approximately half of the initial oxygen concentration. Three tests were subsequently done with one air injection interval extending over the entire 10 minutes length of the deaeration experiment, in order to compare the desorption rate with previous results. In this case the

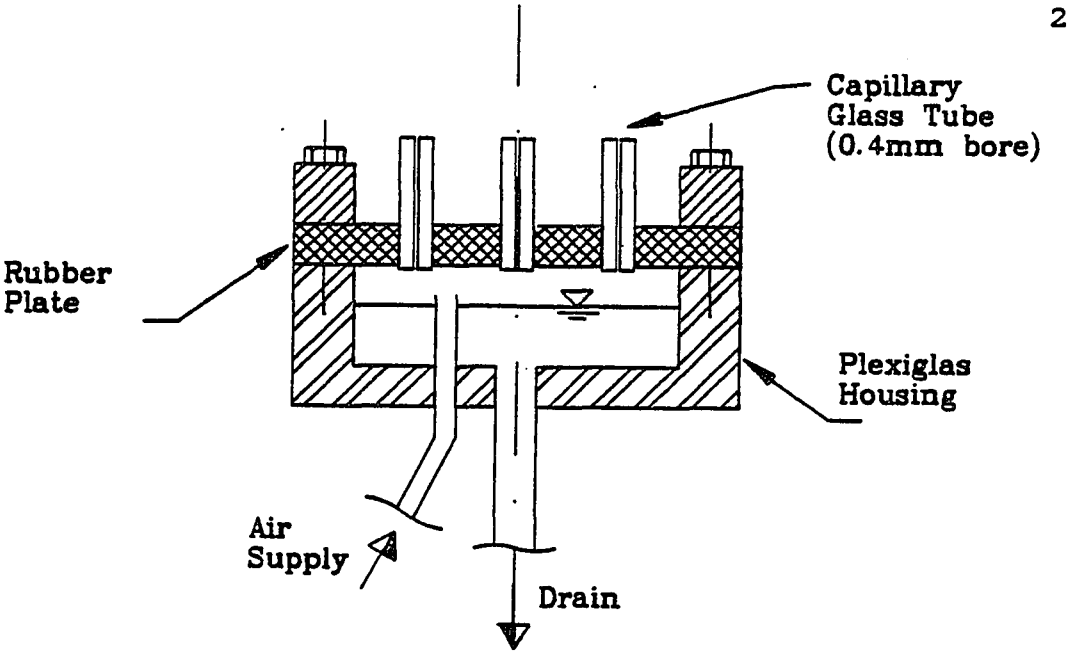

Figure 4.49 Capillary Air Injection for Deaeration Experiments

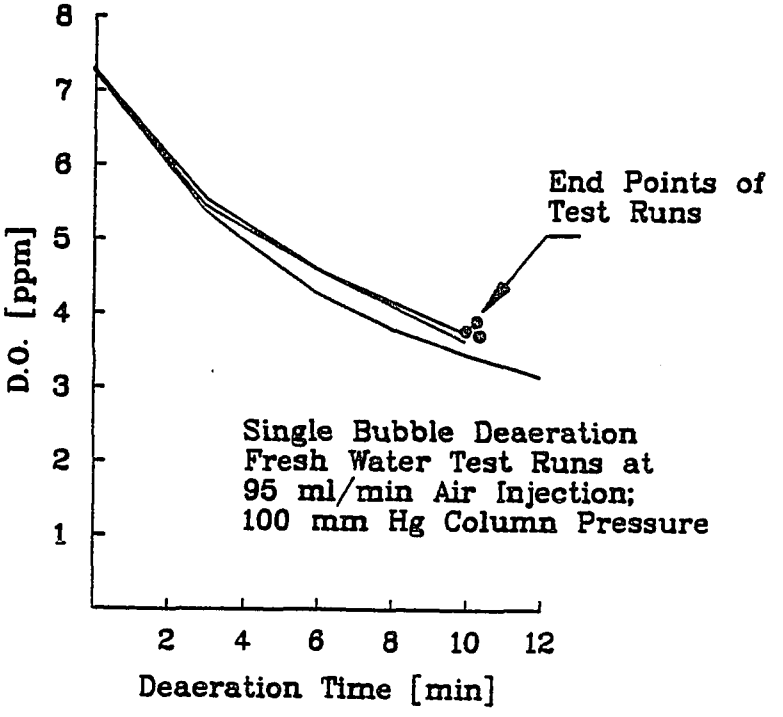

Figure 4.50 Single Bubble Deaeration (Fresh Water Pre-Test Runs)

air injection rate was 95 ml/min (@21.1^{0}C, 760 mm Hg abs.)and the pressure inside of deaeration column was 100 mm Hg abs.

Seven deaeration experiments were done for each freshwater and seawater. The saturation concentrations for both oxygen and nitrogen were calculated using measured test temperatures and equation (3.40). From each sample bottle multiple subsamples were injected into the gas chromatograph. The number of multiple injections was dependent on the repeatability of the results from previous injections. Mean sample concentrations for nitrogen and oxygen were then obtained by averaging the injection results.

In order to compare calculated saturation concentrations for nitrogen and oxygen with measured values, a seawater sample was vigorously shaken in a partly filled flask at atmospheric pressure. Subsequently the seawater in the open flask was stirred with a magnetic stirrer for several hours. The temperature was measured and this water was used to completely fill test B.O.D. bottles. Gas chromatographic analysis revealed a very good fit with theoretical predictions obtained from equation (3.40).

By having the initial and the end point concentrations, the overall mass transfer coefficients were calculated for nitrogen and oxygen. The results are present in figure

4.51. The repeatability of these measurements varied with the gas species and with the type of water. However, results for transfer coefficients are too close to suggest clearly defined differences in mass transfer behavior between gases and water types.

An attempt to photographically determine bubble sizes failed due to the obstructed view of the column interior. As pressure inside the column was lowered bubbles formed on the walls of the column due to heterogeneous nucleation. A method was conceived to brush the inside walls with a metal bar coated with a sponge which was to be moved from the outside by means of a magnet. Removal of bubbles, however, was insufficient as bubble regeneration was quite fast.

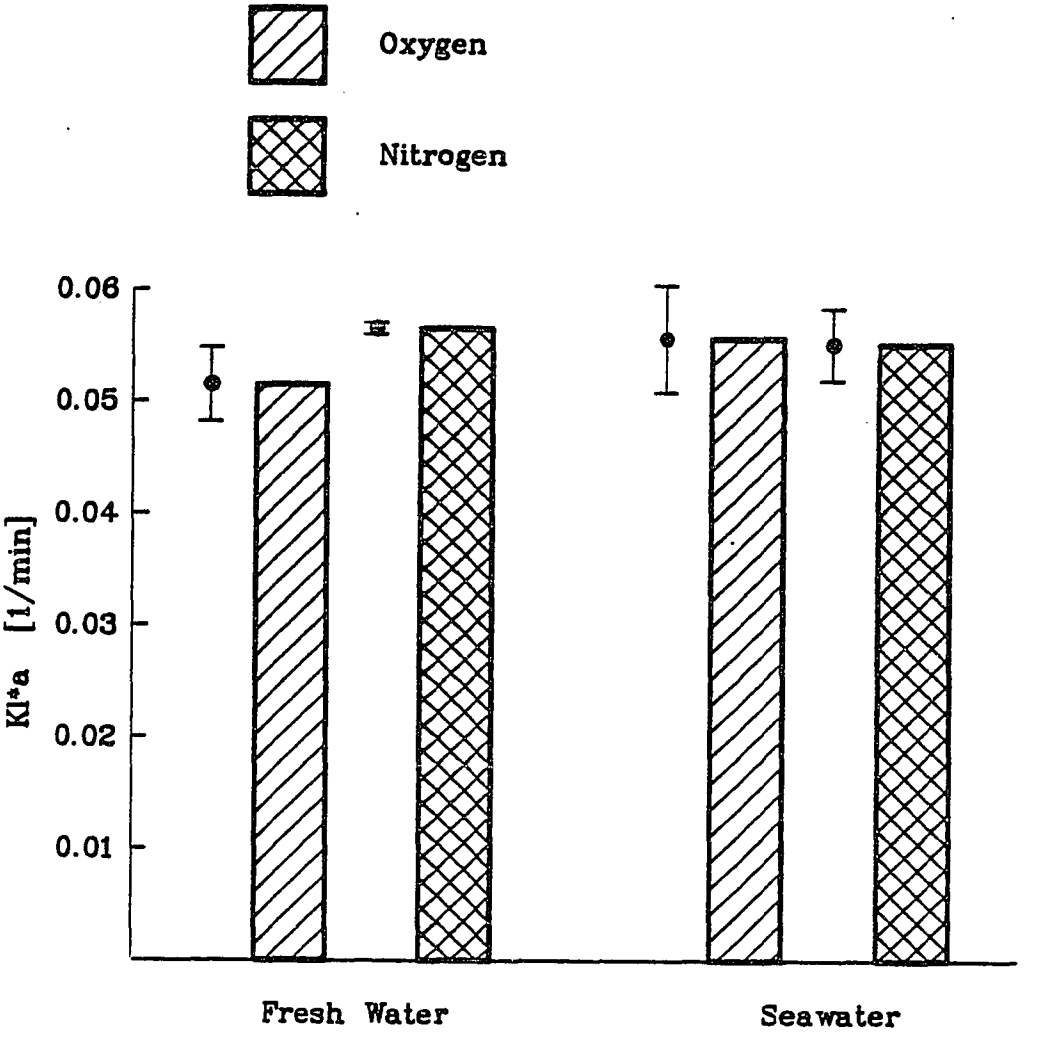

Figure 4.51 Overall Transfer Coefficient k_{L*a} for Nitrogen and Oxygen

4.4 Bubble Rise Velocities

In section 4.1 some important properties of bubbles and how these affect the rise rate through water were introduced. In the following review of some theoretical aspects of bubble rise, pertinent features of air bubbles in water systems will be summarized and further developed.

4.4.1 Theoretical Aspects of Bubble Rise

The forces which act on a rising air bubble can be classified as those due to surface tension, those due to buoyancy, and the retarding force due to the resistance of surrounding water.

The surface tension tends to keep the bubble spherical and thus tending to make the surface area of the bubble as small as possible. This effect of surface tension is most pronounced for small bubbles. Flow resistance tends to deform the bubble. When the bubble is large, the effect of surface tension diminishes in comparison to viscous and hydrodynamic forces. The bubble then tends to display a flattened shape which is far more unstable than a spherical shape. The deformed bubble changes its shape momentarily due to oscillations which are somewhat periodic or completely random. The flattening to an approximately oblate spheroid increases the drag compared

to a sphere of equal volume. With still larger sizes the bubble assumes the shape of a so-called spherical cap. Here viscous forces and surface forces are small compared to hydrodynamic forces.

Under steady state conditions the forces are in equilibrium and the equation of motion of a rising bubble is as follows:

$$\text{Drag} + \text{Buoyancy} = 0 \tag{4.32}$$

Due to the complexity of bubble motion completely satisfying theoretical descriptions are rather limited. For the majority of cases of practical importance empirical equations are therefore used to describe bubble motion.

Assuming the bubble has attained terminal velocity, equation (4.32) can then be used to express its motion. Using the convenient length parameter of the equivalent spherical diameter the drag force is

$$F_D = 1/2 * C_D * \rho_L * A * U^2 \tag{4.33}$$

or

$$F_D = 1/2 * C_D * \rho_L * \frac{\pi * d_E^2}{4} * U^2 \tag{4.34}$$

where: C_D = drag coefficient; A = cross-sectional area normal to the direction of rise; $_L$ = liquid density; U = rise velocity.

The buoyancy force is given by equation (4.2). Thus by setting the drag force equal to the buoyancy force the drag coefficient, C_D, is defined:

$$C_D = \frac{4}{3} * \frac{g * d_E}{U^2} \qquad (4.35)$$

For small Re the drag coefficients obtained by Stokes and Hadamard-Rybczynski solution are, respectively:

$$C_D = \frac{24}{R_e} \qquad \text{(solid sphere)} \qquad (4.36)$$

$$C_D = \frac{16}{R_e} \qquad \text{(mobile sphere)} \qquad (4.37)$$

The above relationships hold strictly only for bubbles which move in a more or less quiescent fluid. If bubbles move close to one another flow disturbances from nearby bubbles can significantly alter the flow resistance. Haberman [51] reported that bubbles rising in close proximity showed an increase in rise velocity of 9 % to 39%. The presence of wakes in the liquid evidently resulted in higher rise velocities for these bubbles. This effect, frequently referred to as the chimney-effect,

might not be accurately quantifiable because of the complexity involved.

There are three types of trajectories for rising bubbles, namely rectilinear motion, motion in a helical path, and rectilinear zig-zag motion.

Spherical bubbles generally show either rectilinear or helical motion. Ellipsoidal bubbles can move with any or all three types of motion. According to Haberman [51] there is a dependence of the type of motion on the Reynolds number. At Re < 300 the motion is rectilinear. With increasing Re spiraling begins and increases in amplitude and frequency until a maximum is reached. With Re > 3000 spiraling motion ceases and only rectilinear motion with rocking prevails. Depending on conditions during bubble formation or release the helical trajectory can either occur clockwise or counter-clockwise.

If a bubble could maintain a regular symmetrical shape the rise path would be a vertical line. However, due to initial disturbances, which can be very slight, symmetric shapes almost never exist. Consequently, this deformation from symmetry invokes a deviation from the vertical rise path of bubble.

Observation [51] revealed that the major axis of ellipsoidal bubbles was always perpendicular to the direction of motion. An explanation of such motion behavior was suggest by Miyagi [94]. As shown in figure

4.52 a bubble starts at position A and moves on an inclined path towards B, due to some initial disturbance. Resistance acting upon the front face of the bubble hampers its motion and tends to make it flat normal to the A-B direction. The bubble temporarily stops at position B. The course of the bubble changes towards C when it glides sideways and is accelerated by its buoyancy. Retarding forces again change its shape with the flattened surface facing C, where the bubble again stops. Subsequently, this motion pattern repeats itself again. Such a trajectory can be described by a simplified two-dimensional model. In a three-dimensional fluid the bubble does not go through stopping points at B, C etc. but continues its motion around the vertical axis X-Y.

The motion of a bubble immediately following their formation and before attaining constant, terminal velocity is very much influenced by the presence of surface-active agents. The flow of fluid around the bubble pushes accumulating material to the rear of the bubble where a quasi rigid cap begins to grow upstream the stagnation point of the bubble. Resulting surface tension gradients oppose the motion of fluid around the body and, in due course, reduce the rise velocity. The effect of such a stagnant cap on velocity of spherical bubbles can be quantified for the portion of bubble coated by the cap (figure 4.7.). As a function of flow conditions the cap

can grow to cover the entire bubble surface or can reach an equilibrium size before this occurs [34]. For larger ellipsoidal bubbles a dynamic boundary layer develops which makes the drag more difficult to quantify.

Immediately following the formation of a bubble, contaminants accumulate on its surface and increase the drag until equilibrium conditions are reached and the bubble travels at its terminal velocity. This process is frequently referred to as "bubble aging" (section 4.13). Bubbles must rise a considerable length of time or, equivalently, a considerable distance until terminal velocity is attained. This interval of time or distance, is a function of the bubble size and the purity of the water. A larger bubble has to travel further than a small one and all bubbles reach terminal velocities more quickly in more contaminated water. In a letter to the author [18] Blanchard referred to experiments where rise speed was determined to be a function of age. As shown in figure 4.53 the rise velocity of 0.8 mm bubbles decreased from a value of about 20 cm/sec (immediately after leaving the capillary tip) to a terminal speed of about 10 cm/sec. As can be seen from figure 4.53 it took about 10 sec for the bubble speed to reach equilibrium. With an average speed of 15 cm/sec Blachard suggested that it takes a bubble about 1.5 m to reach terminal speed. Commenting on the present author's estimation of bubble rise in the test

aeration column, Blanchard suggested that the column length of less than a meter might be too short for bubbles to reach their terminal speed. He, however, added that his investigation used a "poor-man's seawater", and that with natural waters the required distance could be less.

4.4.2 Terminal Rise Velocities

4.4.2.1 Experimental Apparatus and Test Procedure

The test configuration used in this section is shown in figure 4.54. A plexiglass observation vessel, available from a previous investigation was used. This had an overall length of about 90 cm and inside dimensions of approximately 10 x 8 cm. Its top and bottom faces were machined to receive a 5 cm (2 inch) ID male pipe adapter. A 1.8 m long transparent pipe section was attached to the bottom orifice thereby providing the required rise distance for bubble aging.

The bottom end of the pipe had a configuration as illustrated in detail B on figure 4.54. Rubber stoppers, which each held different capillary glass tubes, were inserted into the downward facing pipe and secured with a retaining ring. A tubing connector at the lower end of the pipe attached tygon tubing to fill and empty the apparatus. Air could be injected into the pipe by means of

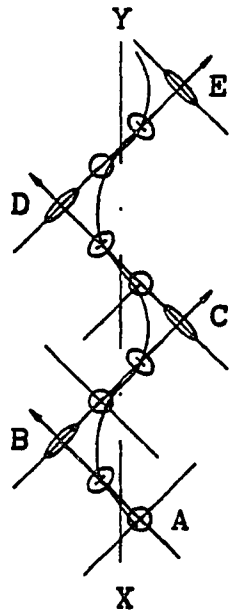

Figure 4.52 Rise of Ellipsoidal Bubble (from [94])

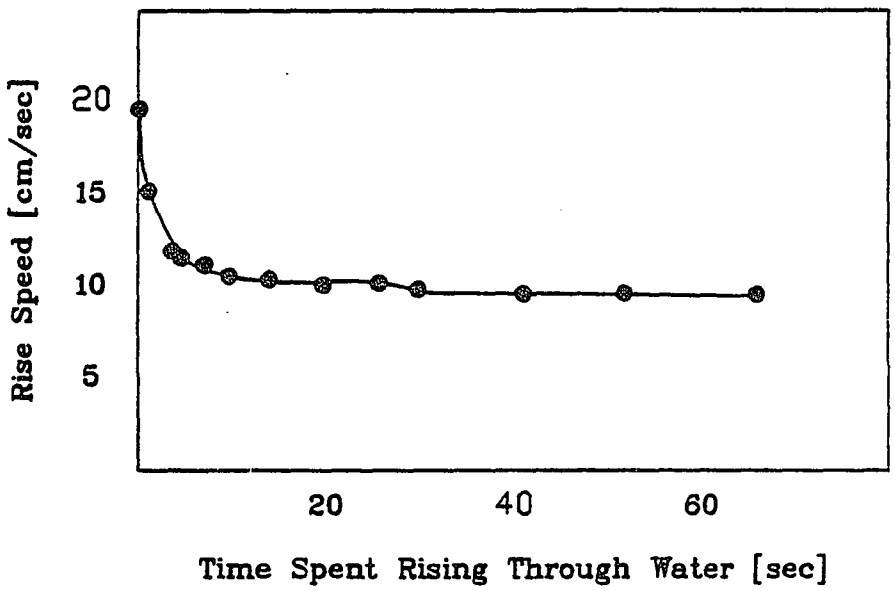

Figure 4.53 Rise Speed as a Function of Age in 3% NaCl-Distilled Water Solution (from [15])

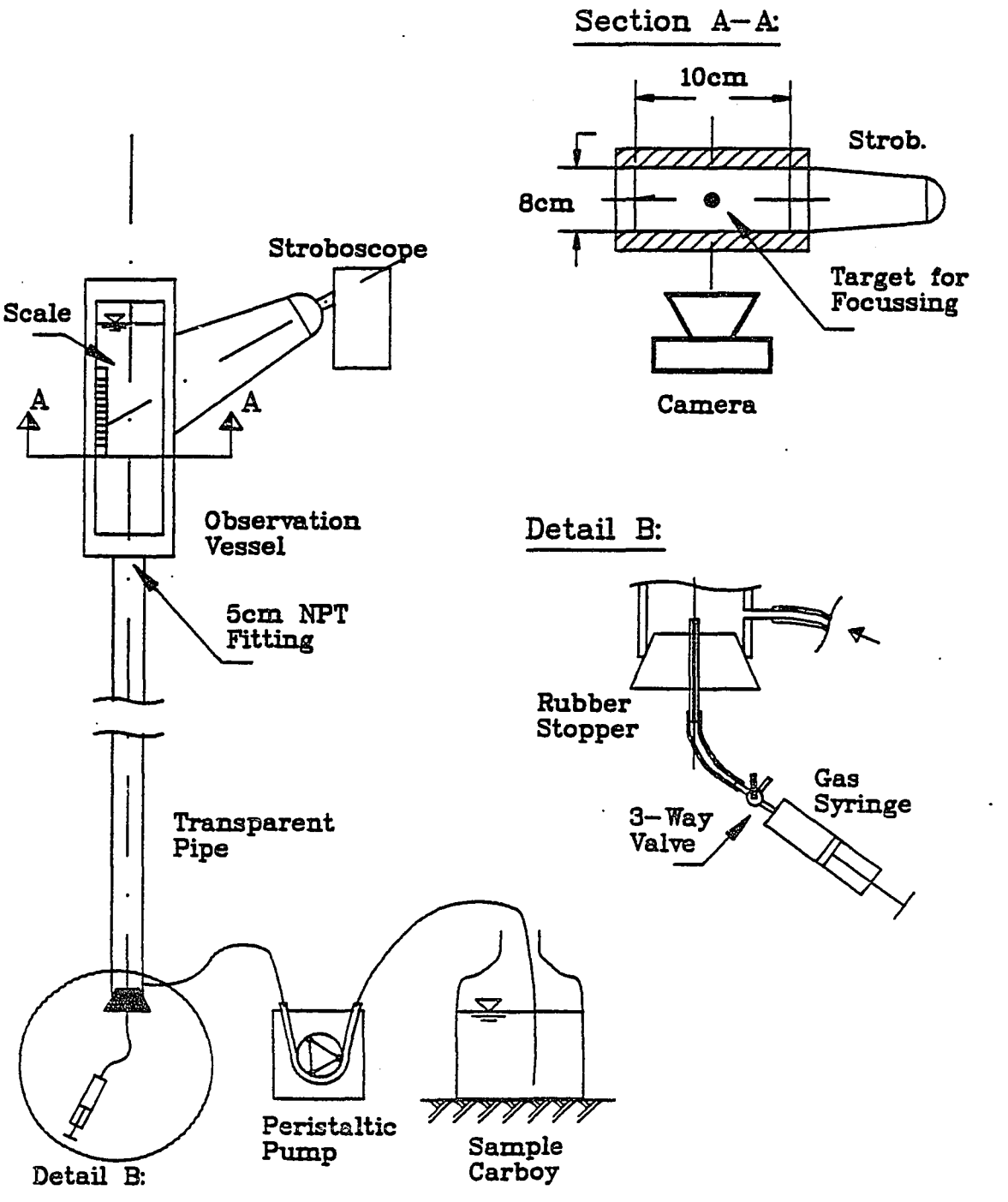

Figure 4.54 Experimental Set-Up for Terminal Bubble Rise Velocity

a gas syringe as indicated in detail B. A stroboscope was used to illuminate bubbles rising in the observation vessel. The strobe beam was directed at one side of the observation vessel at an angle of 20° downward from the horizontal plane. In order to increase the intensity of illumination inside of vessel, a cardboard cone with a reflecting interior was used to focus the strobe beam. Along the inside wall of the vessel, opposite the strobe, a scale having 1/2 mm increments was attached, as can be seen in detail A. The free vertical side of the scale pointed slightly away from the camera in order to increase lighting by the strobe. Interior walls of the observation vessel perpendicular to the camera axis were covered with aluminum foil, except for the opening for the strobe beam. The wall opposite the camera was black. Trial photos showed that a dark background gave better quality photos than a bright background.

The photographic equipment used was a Minolta 35mm camera with a macro lens (magnification 1:2), magnetic remote-shutter release and adjustable tripod. The film was 200 ASA Ektachrome/daylight.

Seawater for these experiments was collected at a 4 km offshore site. The collection procedure was the same as that for single bubble aeration. Fresh water and seawater batches were stored in the laboratory prior to experiments in order to attain ambient temperature. Water for each

experiment was pumped from storage carboys into the test apparatus. The temperature of the water was noted before and after the experiment. The average temperature for both fresh water and seawater was 19.5°C.

The camera was focused at the midpoint of the observation vessel. A target was suspended at the desired location to facilitate focusing. The scale at the side of observation vessel was included in the view field with scale graduations appearing in sharp focus.

The electronic stroboscope was a Gerneral Radio Company model 1531-A . Calibration of the stroboscope was done using the electric power supply grid frequency of 60 Hertz. With the stroboscope in calibration mode, an adjustment dial was turned until an indicator light was emitting a continuous light signal. The documentation for the strobe lamp indicated that upon calibration the accuracy of flash lamp frequency was equal to or less than +- 0.1 % of the flash frequency.

In order to verify the repeatability of the flash frequency several tests were conducted using a pendulum of 1.75 m length. According to classical theory the natural frequency of the pendulum was calculated to be:

$$T = \frac{2 * \pi}{(g/l)^{1/2}} \qquad (4.38)$$

where: T = pendulum period; l = pendulum length.

Measurements with a stopwatch gave an average period of 2.62 sec. with a standard deviation of 0.1 sec. The governing equation of a mathematical pendulum is:

$$m * l * \ddot{\lambda} + m * g * \sin (\lambda) \qquad (4.39)$$

where m = mass of pendulum.

For small angles of deflection $\lambda = \sin (\lambda)$.

The solution of equation (4.39) is then:

$$\lambda = \lambda_o * \cos ((g/l)^{1/2}) * t \qquad (4.40)$$

The maximum velocity at the bottom of the pendulum arc is then the product of angular velocity , $\dot{\lambda}$, and the length of the pendulum, L.

Photographic studies were taken of the swinging pendulum, which was illuminated by the stroboscope. These slides were projected and the distance travelled by the pendulum weight per flash interval was determined. This test was very repeatable having a relative error of 1%. The frequency of the stroboscope could then readily be obtained by dividing the maximum horizontal velocity of pendulum by the mean distance travelled by the pendulum.

Tests, as outlined above, were carried out three times during bubble rise experiments. The results for the stroboscope flash frequency were very close to each other.

It, therefore, was assumed that the stroboscope frequency was accurate and steady.

Injection of bubbles into the water was performed using the arrangement shown in detail B of figure 4.54. The capillary was connected to a three-way valve by a flexible tygon tube. A gas syringe was held in another receptacle of the three-way valve. By connecting the path to the capillary the syringe was filled with air. Compression by the syringe piston caused bubbles to form at the capillary. The valve was then turned to close the capillary side.

The motion of small bubbles in the vicinity of capillary tip served as an indication of residual turbulence in the liquid. After sufficient time, the motion of these small bubbles became regular thereby indicating that the residual turbulence was small. Approximately one minute usually passed between pressurizing the tubing (which produced bubbles) and the start of individual bubble generation. In order to produce individual bubbles, the tygon tubing was slowly squeezed until the newly formed bubble detached from the capillary tip. It was found that this procedure was easier than generating a bubble by using a micro syringe.

Rising bubbles were observed as they approached the viewfield of the camera. The shutter was opened before the bubbles entered the viewfield and closed after the

bubbles had left the viewfield. The resulting pictures portrayed successive bubble images as the bubble rose through the viewfield of the camera and were illuminated by the strobe. Photographs were projected using a magnification of ten. Changes in bubble volume due to differences in hydrostatic pressure were minimized by measuring the displacement of the bubble per flash over a vertical displacement of less than 5 cm. The rise velocity of bubbles was determined by multiplying the mean vertical distance of ascent per cycle by the total number of flash cycles of the stroboscope per time interval.

A typical trace from bubble rise photograph is shown in figure 4.55. Rather than tracing the exact shape of an ellipsoidal bubble, the approximate orientation of both axes were outlined, along with the intersections of the bubble edge with these axes. These, in turn, indicated the major and minor axis. Vertical rise distance per stroboscope flash was determined by averaging the distances between successive bubble images.

4.4.2.2 Results and Discussion

Some 100 bubble rise photos were taken for each fresh water and seawater experiments. Bubble sizes and terminal rise velocities were calculated following the procedures outlined in section 4.4.2.1.. In figures 4.56 and 4.57

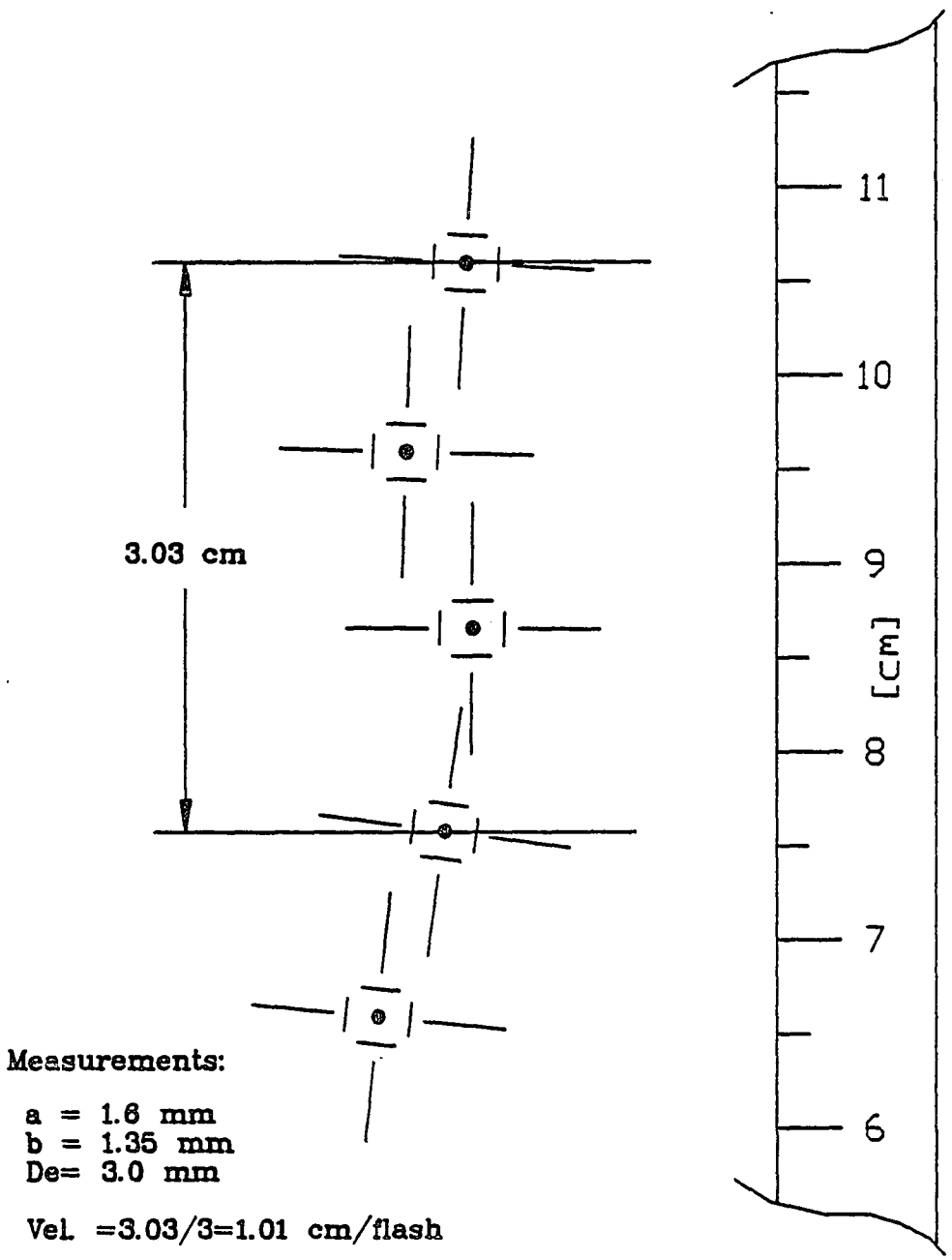

Figure 4.55 Typical Images from Bubble Rise Photography

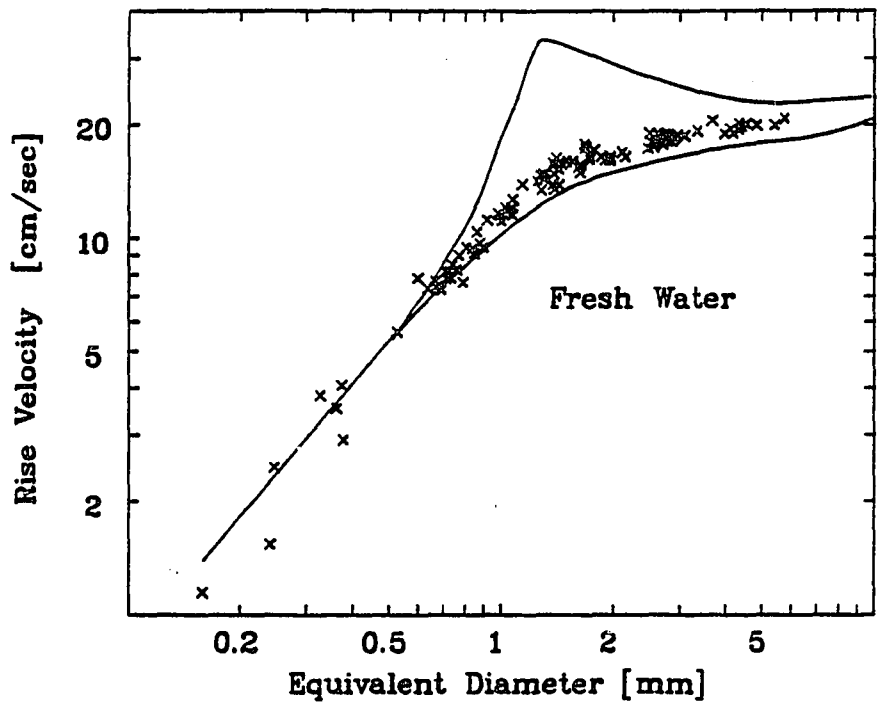

Figure 4.56 Terminal Velocities of Bubbles Rising in Fresh Water

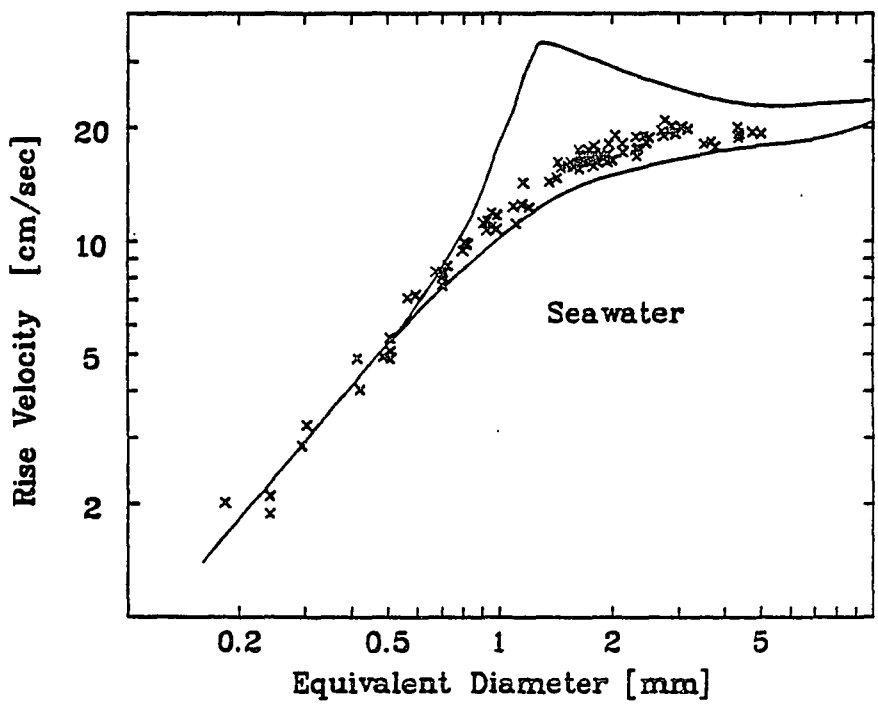

Figure 4.57 Terminal Velocities of Bubbles Rising in Seawater

rise velocities are plotted versus equivalent diameter, d_E, for both fresh water and seawater. The two solid curves in these figures were obtained from figure 4.11. They represent limiting values for bubble rise in the diameter range 0.5 mm to 15 mm. Rise velocities of bubbles within this range should therefore be located between those limits if the test water is partly contaminated. As shown in figures 4.56 and 4.57 bubble rise velocities were very similar in fresh water and seawater tests. In both cases the measured values were located in the lower portion of the curve envelope.

In general the repeatability of data was good compared to investigations reported in the literature. It appears, from the literature review, that due to the complexity of bubble rise phenomena such data scatter is an inherent feature of this sort of investigation. For small bubble diameters more scatter was observed. Bubbles of this size were produced by the breakup of larger bubbles during formation. As the larger bubbles rose quickly to the surface small bubbles ascended slower. The time between large and small bubbles passing the view field of the camera was of such a magnitude that residual turbulence might not have significantly influenced the trajectories of the small bubbles. Furthermore, because of the unavoidable glare from the strobe determination of the diameter of very small bubbles was less accurate.

Seawater bubbles between approximately 3.5 and 4.5 mm exhibited a reduction in rise velocity as compared to adjacent bubble sizes (figure 4.57). This is very likely not a result of data scatter. Interestingly, this bubble range coincides with bubbles sizes for which a range of rise velocities were measured during the single bubble experiments.

Using equation (4.35) the drag coefficient, C_D, was calculated. Results are plotted in figures 4.58 and 4.59. The solid curves were taken from experiments by Haberman [51]. The curve labelled "with SAA" refers to experiments in which organic surface active agents were added to the water. As can be seen from figures 4.58 and 4.59, there is a relatively good fit of the present data to previous results. Drag coefficients for seawater were generally lower in the approximate range of $500 < Re < 700$. As in the case of rise velocities, there was data scatter at the lower end.

Equations (4.36) and (4.37) represent theoretical velocities for solid spheres and mobile spheres, respectively. As noted earlier, bubbles rising at low Reynolds numbers approach the Stokes solution of rigid spheres. However, even thoroughly purified water contains trace concentration of surface active contaminants. These minute concentrations are enough to cause very small bubbles to behave like solid spheres.

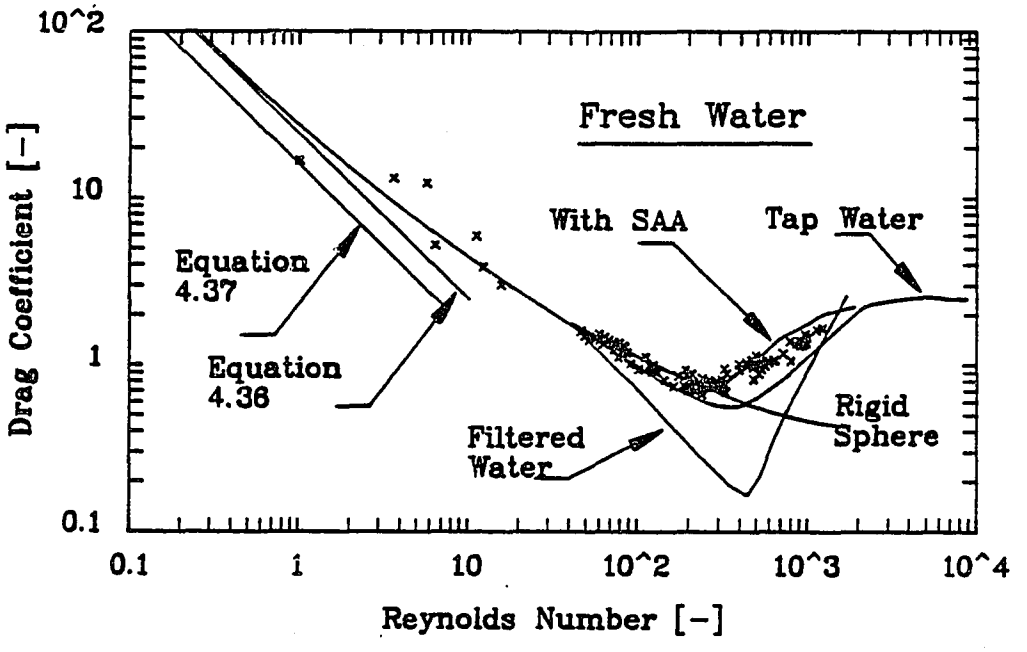

Figure 4.58 Drag Coefficients for Bubbles Rising in Fresh Water

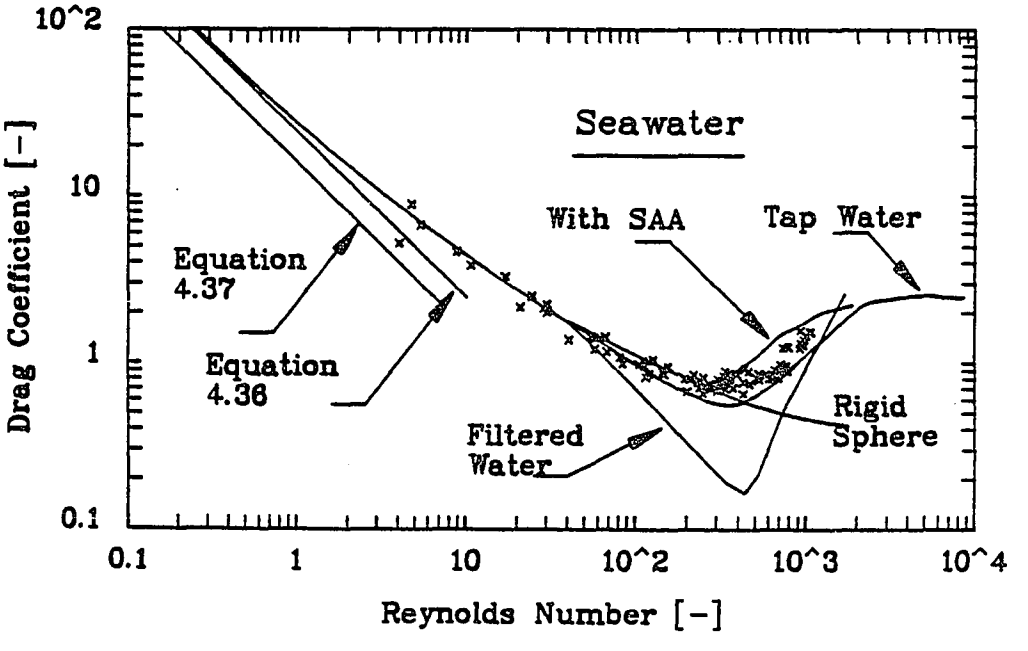

Figure 4.59 Drag Coefficients for Bubbles Rising in Seawater

Considering these factors it appears certain that both the fresh water aund the seawater used for bubble rise experiments had characteristics indicative of partial contamination. From the rise velocities and drag coefficients measured in this study it is suggested that the behavior of a single bubble rising in freshwater and in seawater is very similar.

4.4.3 Partial Bubble Rise

4.4.3.1 Experimental Apparatus and Test Procedure

For this experiment the test set-up shown in figure 4.61 was modified in the following manner. The 1.8 m long transparent pipe was replaced by pipe sections of different lengths, depending on the desired distance between focal point of the camera lens and the point of release of the bubble. Bubble rise distances were varied between 6 cm and 91 cm. Bubble production and photographic procedures were the same as for the terminal velocity tests.

With the camera focused at a particular height in the observation vessel, bubbles were released and traveled through the view field while the camera shutter was open. Three capillary tips were used to produce bubbles of three diameter groups, subsequently referred to as small,

medium and large bubble groups. Due to the reduction in hydrostatic pressure, the bubbles expanded during their upward path. Measured diameters of bubbles of one size group varied with elevation. There was not, however, a systematic increment of diameter increase with increased elevation. Rather, fluctuations of bubble sizes were observed. Consequently, the diameters of the bubble generated were not uniform within the bubble group. Variation of diameter were generally in the order of 5-15%.

An average of five photographs were taken at each elevation per bubble group.

4.4.3.2 Results and Discussion

Tests with three bubble size groups were conducted using seawater. For comparison, tests were conducted with the medium bubble size group using fresh water.

The results for seawater are given in figures 4.60-4.62. The error bars indicate the relative error. For seawater the required ascent distance to obtain terminal velocity increases with increasing diameter. This finding is in agreement with predictions discussed in section 4.1.

A comparison of values measured here with the results presented by Detwiler [34] is made by using the small

bubble group of seawater (figure 4.60). Blanchard [10] indicated by citing Detwilers experiments that a distance of 1.5 m was needed by a 0.8 mm bubble to attain terminal rise speed. Blanchard further indicated that the liquid was an artificial seawater (3% NaCl - distilled water solution) and that conditions in natural seawater might be different. The results in figure 4.60 indicate that the bubbles in the present experiment decelerated at a much quicker rate. After only about 21 cm a value was obtained which was close to the assumed terminal velocity. A remarkable observation was the high rise speed immediately above the capillary tip. A value of 30 cm/sec was measured. This rise speed is about that for a bubble of that size in pure water, as can be seen in figure 4.11. It should be noted that the bubble generation technique was the same in all cases, namely bubbles grew slowly by compressing the tygon feed tube and the bubbles detached themselves when a critical diameter was reached. The high rise velocity is therefore not a consequence of high gas injection velocities.

The results for partial bubble rise in fresh water are presented in figure 4.63. In this case, after an initial drop the rise velocity increased again. Such a distribution of rise speed was not observed in the other experiments. The reason for the drop and subsequent rise in speed is unknown. Ignoring this feature, the general

results suggest that for the tap water used in this experiment the terminal speed is reached relatively quickly.

In summary, it can be concluded from this study that bubbles in fresh water and seawater reach the terminal velocities much faster than in the distilled water solutions reported in the literature. The required distance the bubble has to travel in order to attain terminal velocity is a function of the shear forces which act on the bubble, and is longer for larger bubbles.

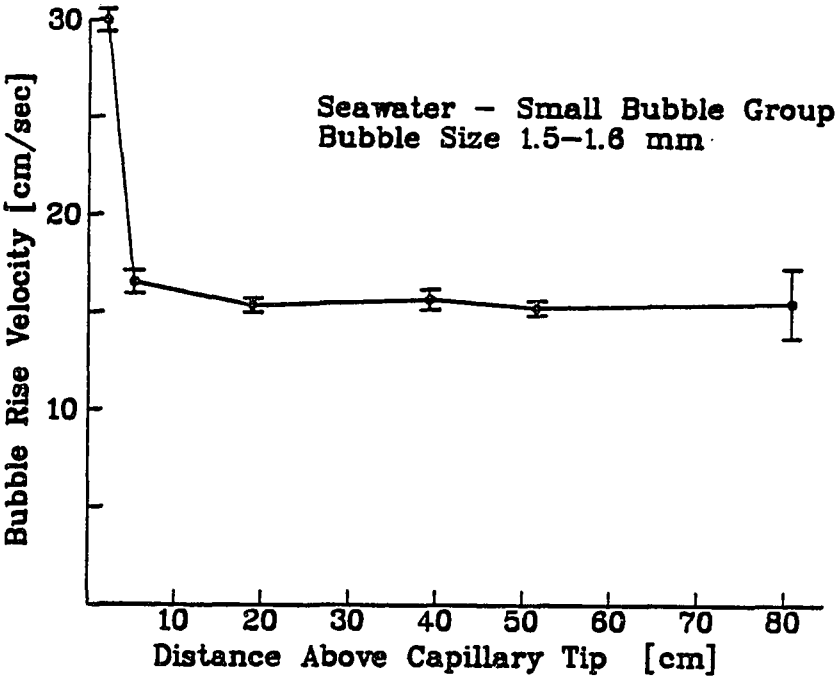

Figure 4.60 Bubble Rise Velocity as a Function of Aging

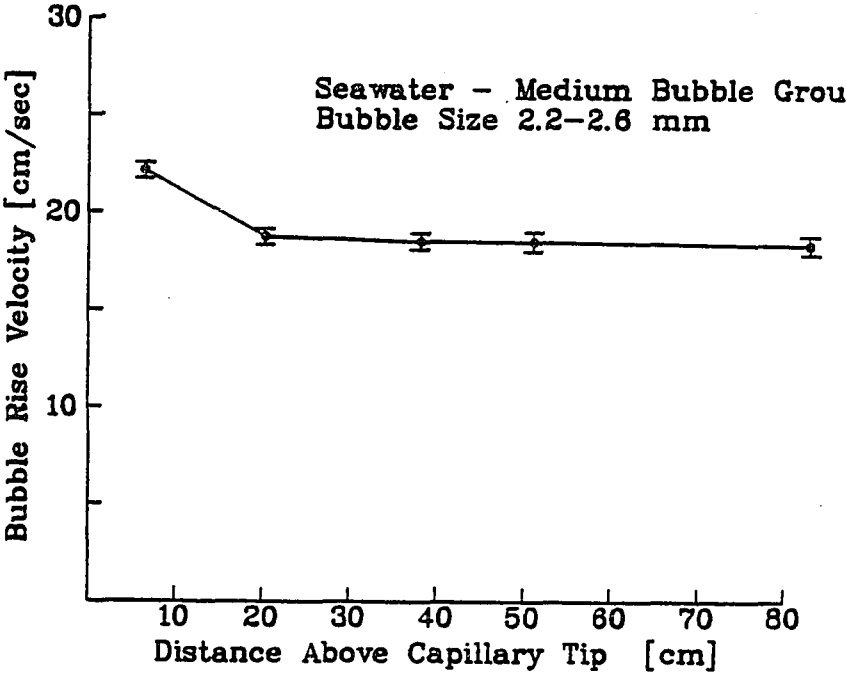

Figure 4.61 Bubble Rise Velocity as a Function of Aging

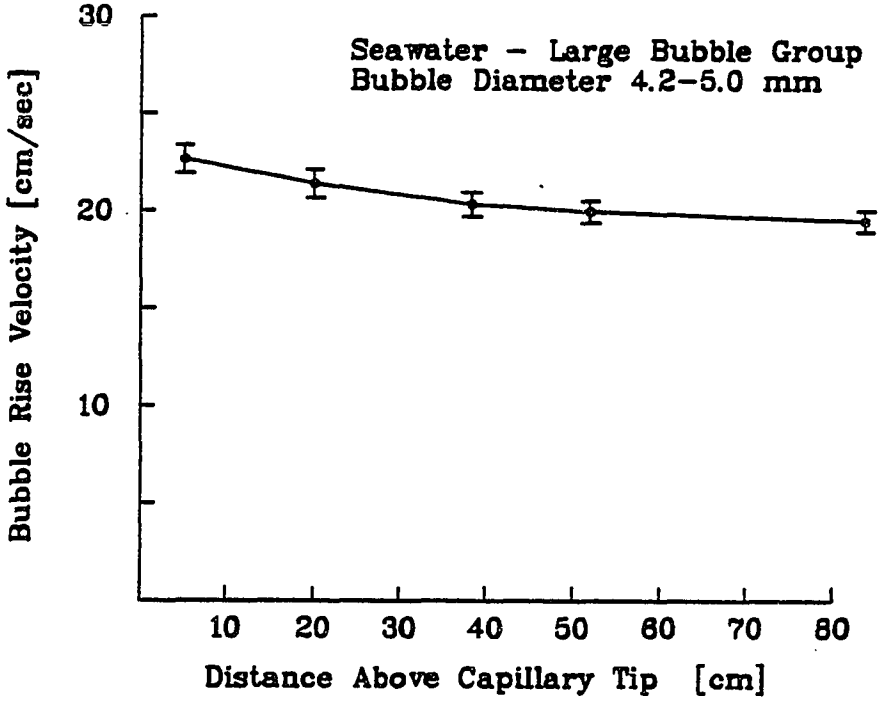

Figure 4.62 Bubble Rise Velocity as a Function of Aging

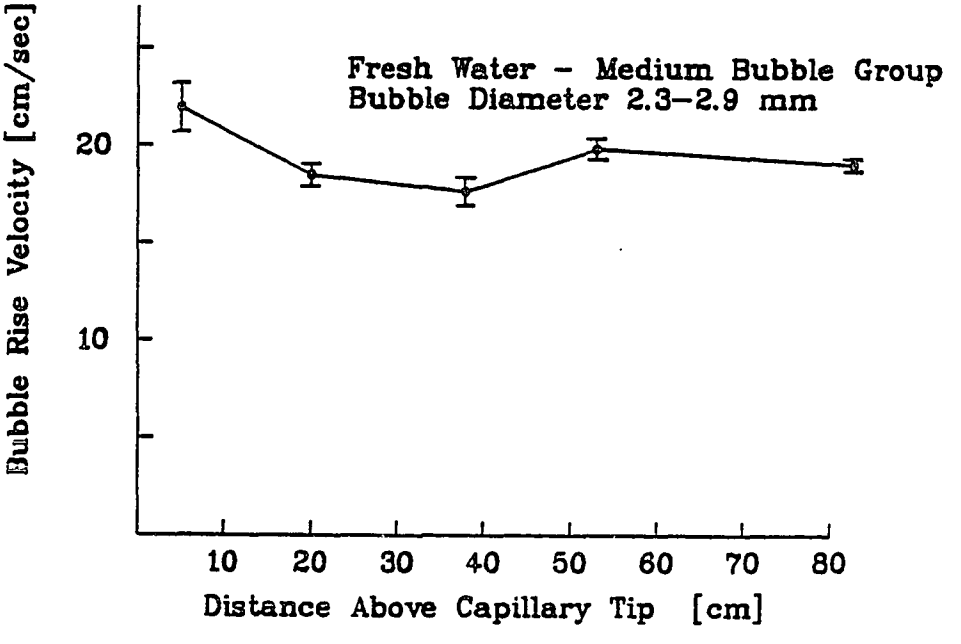

Figure 4.63 Bubble Rise Velocity as a Function of Aging

CHAPTER V

PACKED COLUMN EXPERIMENTS

5.1 Theoretical Aspects of Packed Column Deaeration

In a properly functioning packed-column deaeration device, the liquid is evenly distributed over the surface packing elements, runs evenly down the elements in the body of the column and leaves at the bottom.

The spatial orientation of packing elements is random. It is therefore assumed that the effective area of packing per unit volume is the same in all parts of the column. Furthermore, it is assumed that the volume of liquid per unit volume of space, or liquid hold-up, is uniformly distributed in the column. In actual practice, however, liquid tends to collect at the walls if the height of the column is more than a few times its diameter. There, however, is not a complete segregation between the liquid at the wall and that on the packing elements. Packing elements which touch the walls of column partially redirect the flow on the walls to the interior of the packing. The overall magnitude of redirection of wall flow, and thus the tendency for the wall-layer to remix, is dependent on the individual alignments of elements in the vicinity of column wall. The liquid hold-up in the packing during irrigation is a function of the superficial

velocity of the liquid in column, L, (cm^3/cm^2) and of the nominal diameter of the packing elements, D. Hold-up generally increases with higher L and decreases with larger packing elements. There is, however, a finite hold-up in a wetted packing even when the flow rate is zero.

Mass transfer between the gas phase and the liquid occurs as the liquid flows over the packing . As discussed previously, the overall resistance to gas transfer consists of liquid-film and gas-film resistances. The individual film transfer resistances are added to give the overall resistance. In the present case of oxygen and nitrogen desorption, gas film resistance is neglected since the solubility of both gases is fairly similar [30].

Instead of the coefficients and resistances for liquid-film and gas-film, the alternate concept of a transfer unit can be employed. This approach is useful for interpreting and correlating mass transfer processes. The gas transfer in a packed column is expressed by two parameters, namely the number of transfer units (NTU) and the height of transfer units (HTU). The parameter NTU is indicative of the difficulty of transfer and is solely dependent on concentration and concentration driving forces. (Mechanism related to the term driving force are described in section 3.3) Height of transfer unit, HTU,

is a measure of the effectiveness of the column packing and is actually the depth of packing material required by a single transfer unit. These quantities are related as follows:

$$H = (NTU) * (HTU) \qquad (5.1)$$

where: H = total height of the packed column.

The transfer unit is derived as follows:

$$NTU = \int_{C_{IN}}^{C_{OUT}} \left(\frac{1}{(C_L - C_S)}\right) * dC = \ln \left(\frac{C_{OUT} - C_S}{C_{IN} - C_S}\right) \qquad (5.2)$$

The quantities (HTU) and (NTU) are related as:

$$\frac{1}{NTU} = \frac{d(NTU)}{dH} = \frac{\ln \left((C_{OUT}-C_S)/(C_{IN}-C_S)\right)}{(H + H_{END})} \qquad (5.3)$$

where: H = actual height of the packing; H_{END} = the additional packing height that would produce the mass transfer which takes place in the inlet distribution and all other parts of the column except the packing.

According to Dankwerts [30] the transfer in a packing element of infinitesimal depth, dh, can be expressed as:

$$\left(\frac{1}{C_L - C_S}\right) * dC_L = \left(\frac{k_L * a}{L}\right) * dH \qquad (5.4)$$

where: C_L = concentration in bulk of liquid;

L = superficial liquid velocity (volume of liquid per cross-sectional area of column).

Applying appropriate boundary conditions equation (5.4) can be integrated to give:

$$\ln \left(\frac{C_{OUT} - C_S}{C_{IN} - CS}\right) = \frac{k_L * a}{L} * H \qquad (5.5)$$

The term (k_L*a/L) on the right hand side of equation is equal to the quantity HTU, assuming H to include the contributions of end effects.

The advantage of using H.T.U. for quantification of the mass-transfer process is its simple visualization. Heights of transfer units (HTU) are given in length whereas dimensions of mass transfer coefficients are more complex.

The flow of a liquid over the packing elements can be divided into turbulent and laminar parts. A laminar layer of liquid always exists adjacent to the surface. Underneath this layer the liquid is turbulent and always completely mixed. The shear force acting on a portion of such a laminar layer can be assumed to be of the order of the weight of the layer itself, which is very small. For a typical thickness of the laminar layer of about 0.004 cm there can be no appreciable shearing motion within the layer. Rather, the layer slides over the liquid as an elastic body. From the viewpoint of absorption the layer

behaves somewhat like a solid body until it is intermixed with the rest of the liquid.

The Lewis-Whitman theory [81] describes the transfer coefficient, k_L, as the ratio of diffusivity over the stagnant layer thickness. The penetration theory by Higbie (e.g. [30]) gives a coefficient which approaches infinity as the time of exposure is shortened indefinitely, as can be readily seen from the following equation:

$$k_L = 2 * \left(\frac{D}{\pi * t_E}\right)^{1/2} \qquad (5.6)$$

where: D = diffusivity; t_E = time of exposure between surface renewal.

5.2 Experimental Apparatus

The system configuration shown in figure 5.1 was utilized for the packed column deaeration experiments . The following features had to be considered for this experiment .

1) A continuous seawater supply was not available at the laboratory; instead, seawater had to be transported batch-wise from a coastal pump station nearby.
2) Water samples at the packed column intake and the

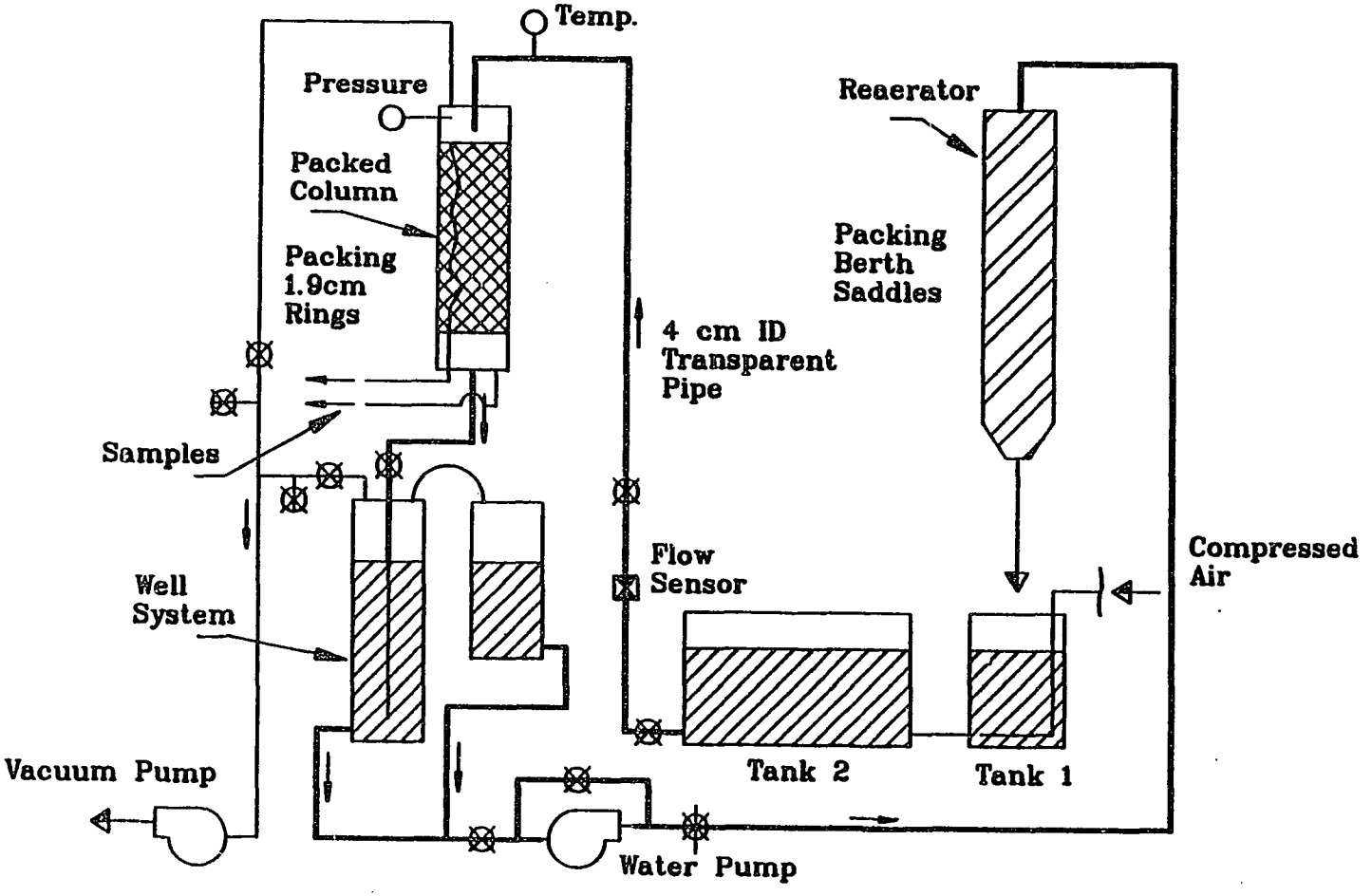

Figure 5.1 Packed Column Deaeartion Test Set-Up

discharge had to be extracted after the pressure vessel was vented.

3) The flow path and process conditions had to be identical for freshwater and seawater tests.
4) The systems had to be able to be operated by one person

The resulting test system is described below.

Vacuum was established in the pressure vessels of the system which included the packed column and two well vessels. After opening the intake valve water rose from the well reservoir tanks to the top of the packed column. Water overflowed the distribution plate, ran through the packing section and collected in a reservoir at the bottom of the packed column. Another overflow in this reservoir discharged the water to the well system where it was stored for the duration of the test run. When the test was completed pressure vessels were vented and water samples were collected. The water in the wells was lifted to the top of a packed reaerator by means of a centrifugal pump. After running through the packing of the reaerator the water ran into tank I. This completed the flow cycle.

The individual system components are described below.

Tank System: Water was held in two tanks having a total volume of about 2,500 liters. If fresh water was used the water was taken from the laboratory tap water supply. Seawater was obtained from a nearby coastal pumping

station which continuously extracted seawater from a depth of 10 m some 300 m offshore. The seawater was filtered by means of an in-line filter using a 5 micormeter pore-size polypropylene cartridge.

Tank I had a volume of 430 liters. In addition to aeration taking place in the packed reaerator water passing through tank I was aerated by an air injector. The injector was made out of 1.9 cm ID PVC pipe with some fifty 2 mm orifices drilled into the horizontal pipe sections.

Packed column: The packed column used in this experiment is shown in figure 5.2. The pressure vessel was a 1.50 m long 20 cm ID PVC pipe section. Plastic flanges with grooves to accommodate 0.6 cm O-rings were cemented to both ends of the pipe. Metal blindflanges accommodated a vacuum line and an intake pipe at the top and a discharge pipe at the bottom of the packed column. The packing consisted of 1.6 cm plastic rings which were supported by a plastic bottom plate, which, in turn, was supported by four galvanized rods and was located some 23 cm above the bottom blindflange. The bottom plate had fifteen 1.3 cm diameter holes to allow the water to drip into the underlying well. The small packing elements were chosen because the ratio of individual element to column diameter had to be smaller than eight in order to avoid uneven liquid distribution in the packing [45]. Water

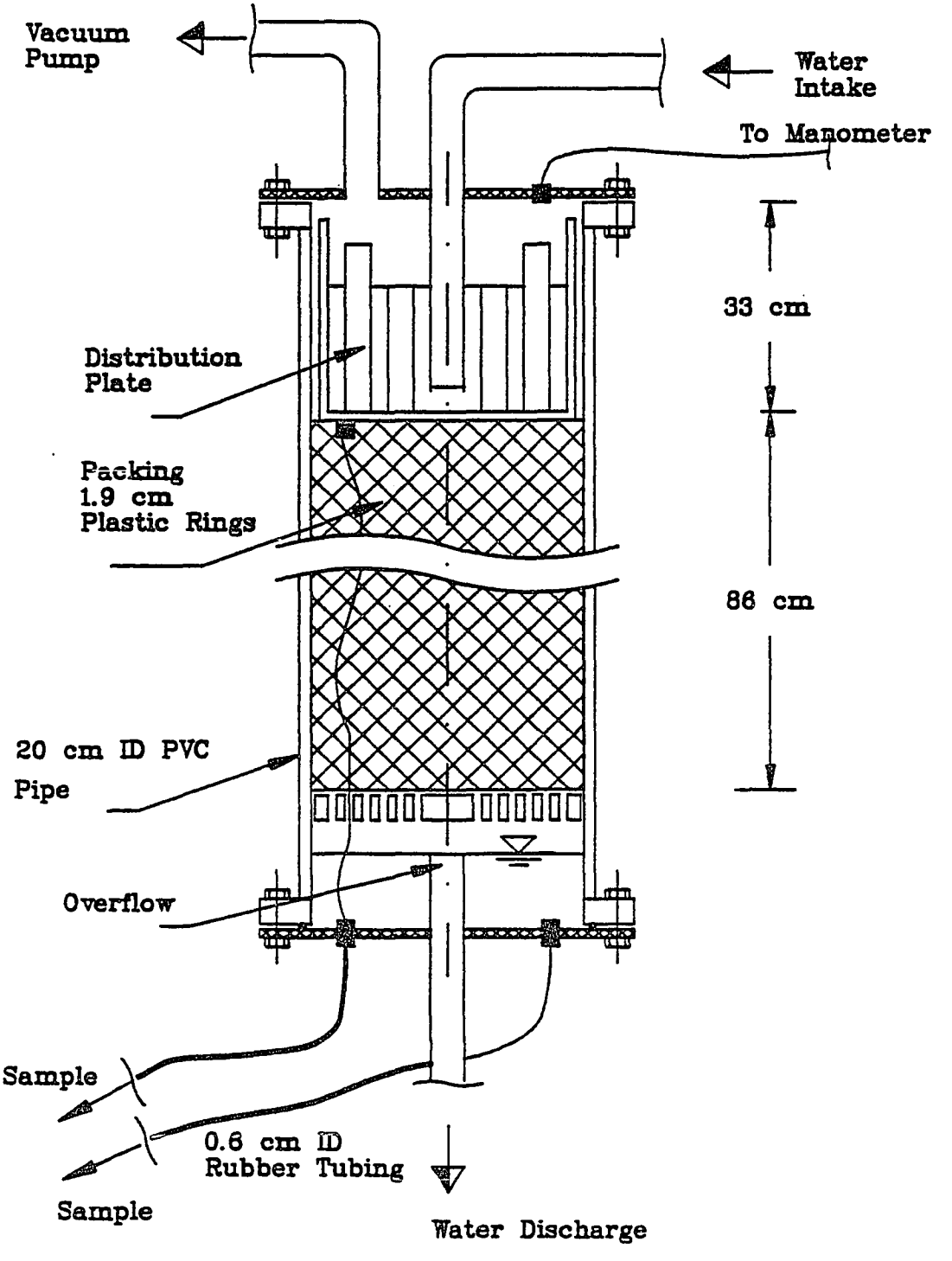

Figure 5.2 Packed Column Configuration

collected in the reservoir and was held at a constant depth of 19 cm by means of an overflow.

Vacuum was established in the column by the vacuum source via a 3.8 cm ID PVC connection pipe. Column pressure was measured with a mercury manometer which was connected by a 0.6 cm ID tygon tube to the top of the column.

Water entered the column through a 3.8 cm PVC pipe and was discharged into a reservoir established by the distribution plate. This distribution plate rested loosely on the packing. Since the configuration of the distribution plate was important for the performance of the column, the design of the plate is described in more detail.

Distribution plate: The method of liquid distribution over the top of the packing was chosen according to several factors. Water entering the packed column had to be evenly distributed over the underlying packing in order to avoid partial starvation or excessive irrigation with consequent non-uniform gas transfer within the packing. Gas transfer occurs at liquid interfaces if the water is not in equilibrium with the surrounding gas phase. The design goal was to reduce these effects at the column ends by minimizing the area of exposed water surfaces, thus by minimizing splashing, spraying and dripping of the incoming water.

Evolved non-condensible gases have to be able to escape to the top of the column from where they are discharged by the vacuum pump. The gases must escape through the distribution plate. Suitable gas paths had to be provided in order to avoid significant pressure losses and associated uneven pressure distributions throughout the packed column.

Samples of incoming water were taken just before the water impinged on the packing elements. A sufficiently large reservoir for collecting water samples had to be available which could be sampled after the column was vented.

The above mentioned design features were implemented in the design of the distribution plate of present study. In addition, apparatus configurations of previous experiments (eg. [29], [3], [45], [74], [105]) were consulted for the present design.

The distribution plate is shown in figure 5.3. A 33 cm long 15 cm ID PVC pipe section was used for the side walls of the water reservoir. A top ring and the actual distribution plate at the lower end of pipe section had outside diameters of 20 cm. Assembled, the entire device could be inserted into the packed column pressure vessel where it rested loosely on the packing elements. Six threaded rods compressed a rubber gasket between the 15 cm ID pipe and the bottom plate of the distribution plate

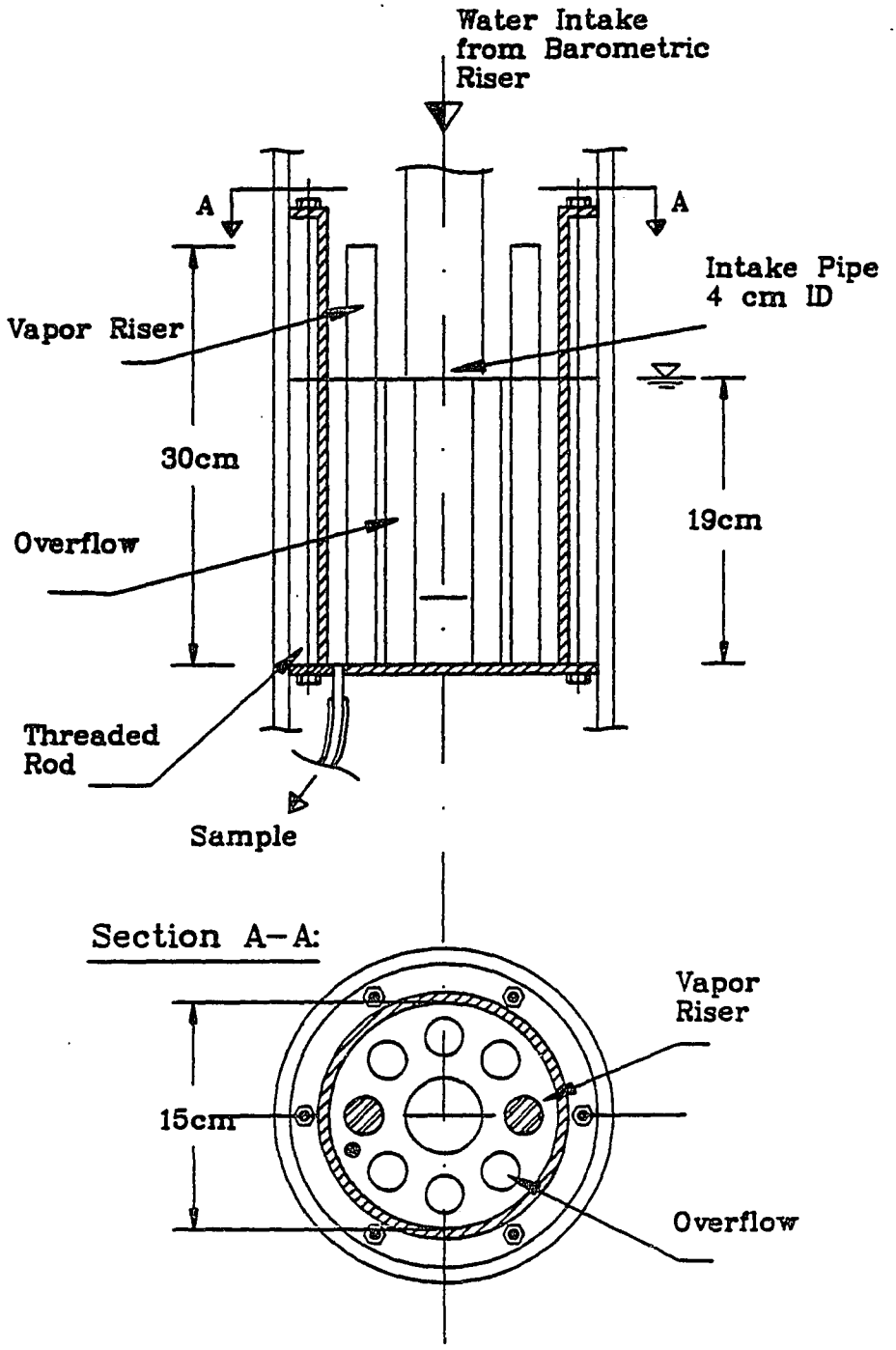

Figure 5.3 Distribution Plate

assembly. The distribution plate accommodated eight 1.9 cm ID pipes which were cemented to the upper side of bottom plate. Six of which had a length of 19 cm and served as water overflow pipes. The remaining two pipes were vapor risers and had lengths of 30 cm. This length was selected so as to avoid water discharge through these orifices. Since the gas flow was very small, pressure loss was negligible and the pressure was deemed constant throughout the packed column.

The discharge opening of the 3.8 cm ID water inlet pipe was located some 5 cm above the distribution plate and was thus submerged throughout the test runs. Water sample withdrawl took place through tubing which was attached to the underside of the bottom plate.

Well System: After overflowing the discharge reservoir in the packed column, water ran into the well system. Pressure in the well was identical to that in the column.

Two connected 30.5 cm ID pipes with lengths of 2.0 and 1.5 meter made up the well reservoir. Vacuum and vent lines for the well were separated from those serving the packed column. This provided the possibility of venting the wells independently from the packed column. The shorter pipe section was raised so that the upper flanges of both pipe sections were at the same elevation. Asbestos gaskets between flanges and blind flanges were used as vacuum seals. The discharge pipes of the well

vessels were connected with each other and branched to the centrifugal pump. A valve separated the wells from the pump.

The combined volume of the wells was about 300 l. The water level in the well could be monitored by two stand pipes.

Water pump: A centrifugal water pump lifted water from the well discharge to the top of the packed reaerator. In the original design it was desired to lift the water from the well system under vacuum conditions to achieve a continuous flow scheme. The shaft of the pump, however, caused extensive leakage which destroyed the pump's suction. Replacement of the shaft and packing did not alleviate the problem.

Due to these difficulties it was deemed necessary to change the original set-up design to the present configuration.

Reaerator: Water lifted by the water pump reached the top of the reaerator. A 6 meter long 35 cm diameter pipe section was suspended vertically above tank I. Packing, consisting of 5 cm Berth saddles, filled the entire pipe. At the lower end a short tapered section was attached which accommodated a discharge pipe. The reaerator discharged into tank I.

Vacuum pump: The vacuum source used for these

experiments was the same as used in the previous batch deaeration experiments.

Sampling Station: Samples of the water entering and leaving the packed column were collected. In addition, samples of the water in tank II were taken periodically.

Water collected in the reservoir of the distribution plate was extracted by 0.6 cm rubber tubing which was connected to the bottom of the distribution plate. The tubing crossed through the packing and the packing support and was fixed to a suitable connector at the inside of the lower packed column blindflange. A feed-through connected the flow path to the outside of the column, from where an additional rubber hose connected to a sample valve. Water which collected in the bottom reservoir of the packed column was extracted by a rubber hose which was connected to a sample valve and tubing connector on the lower blind flange. A sample of the water from tank II was simply siphoned.

Instrumentation: The dissolved oxygen meter, vacuum gauge and temperature sensor were the same as used for the batch aeration and dearation experiments and have been previously described.

A water flow sensor was installed in the packed column intake pipe immediately downstream of the tank II outlet. A Signet MK515 paddle wheel sensor was housed in a 3.8 cm installation fitting. Four permanent magnets, imbedded in

the rotor blades, spun past a coil in the sensor body, producing a signal directly proportional to the flow rate. Accuracy was +- 1% of the full scale. The vendor specified minimal head loss and no cavitation caused by the device. Flow rate was displayed by a Signet MK 576 flow rate indicator whose display repeatability was given as +- 0.5% of full scale. The measurable flow range was 0-100 gpm (0-6.3 l/sec).

5.3 Test Procedure

A test run started by bringing the packed column and the well to the desired pressure. Pressure settings for each run were chosen randomly by drawing a card containing that particular setting from a predefined total group of test configurations to be examined. When the desired pressure was achieved the intake valve (refer to figure 5.1) was opened and water started to flow into the packed column. For every test run a water flow rate between 19 and 20 liter/min was maintained by adjusting the intake valve. The length of experiments averaged 12 minutes; by that time the water had filled the well to capacity. The intake valve was closed, thereby stopping the intake flow. The system was held under the present vacuum pressure for some 20 seconds after flow had been stopped. Bubbles that might be suspended in the top and bottom

reservoirs of the packed column could thus rise to the respective surfaces. Following this procedure, reaeration of the water upon venting, due to air contained in these bubbles, was avoided.

The packed column discharge valve was closed and the packed column was separately vented, following the procedure outlined above. Samples were immediately extracted. Two 300 ml BOD bottles from both the intake and the discharge water were collected. The D.O. concentration of the samples was measured following each experimental run.

The well system was vented and the water pumped to the top of the reaerator. The circulated water was then available for the next run.

5.4 Results and Discussion

An average number of 35 tests were conducted for each fresh water and seawater. The following parameters were measured to quantify the gas exchange processes:

1) Dissolved oxygen concentration of the packed column intake and discharge
2) Vacuum pressure in the packed column
3) Liquid flow rate
4) Temperature of the water in the system

Since the water level of the exit reservoir was

regulated by the overflow, the depth of useful packing was always constant. At no instance were parts of the packing flooded. Therefore the entire packing length of 86 cm was effective.

The determination of end effect is commonly carried out by flooding parts of the packing and measuring the resulting gas transfer. When this procedure is executed a linear relationship of NTU and packing height is obtained. At zero packing height zero NTU should be obtained. If, however, at zero effective packing height there is a residual NTU value the magnitude of end effects can be readily determined.

For the present case this procedure to determine the magnitude of end effects could not be carried out due to the particular system configuration. Instead values obtained in previous investigations were reviewed and the present end-effect conservatively was estimated at 5% of the packing height.

In order to calculate values of HTU by equation (5.3) the following assumptions were made:

1) Pressure and temperature are uniform within the packed column
2) Pressure losses from vapor risers are negligible
3) Temperature in the column is equal to that of the intake water.
4) ideal gas law conditions prevail

Calculated values of NTU and HTU are presented in tables 5.1 and 5.2. Results for HTU are plotted as a function of column pressure in figure 5.4 and 5.5 for fresh water and seawater, respectively. It is apparent that the HTU appears to be independent of vacuum pressure. The values of HTU range between 0.55 and 0.7 m for fresh water and between 0.48 and 5.75 m for seawater. Comparing the mean values of both ranges, seawater HTUs are approximately 20% smaller than those of fresh water.

Packing Height 0.863 m

End Effects 0.04 m

Run #	Pressure [mmHg]	Temp [°C]	Cin [ppm]	Cout [ppm]	NTU [-]	HTU [m]
302	180	25.8	6.20	2.5	1.60	0.57
303	180	25.9	6.5	2.6	1.56	0.58
304	160	25.9	6.9	2.5	1.58	0.57
305	160	25.9	6.9	2.6	1.50	0.61
306	160	25.9	7.0	2.6	1.51	0.60
307	160	25.0	3.2	2.4	1.57	0.58
308	160	25.1	6.7	3.2	1.08	0.84
309	160	25.0	6.6	2.7	1.38	0.66
310	140	25.0	6.9	2.5	1.47	0.62
311	140	25.0	7.0	2.5	1.49	0.61
313	140	25.1	6.9	2.7	1.33	0.68
318	120	25.2	7.3	2.8	1.24	0.73
319	120	25.3	7.4	2.7	1.34	0.67
320	100	24.8	7.0	2.3	1.44	0.63
321	100	24.9	7.1	2.3	1.43	0.64
322	100	24.9	7.1	2.3	1.46	0.62
323	100	24.8	7.2	2.3	1.48	0.61
324	80	24.9	7.0	2.1	1.44	0.63
325	80	24.9	7.2	2.2	1.44	0.63
326	80	24.9	7.2	2.2	1.44	0.63
327	80	24.9	7.2	2.2	1.40	0.65
328	60	24.9	6.7	1.8	1.49	0.61
329	60	25.0	6.9	2.2	1.26	0.72
330	60	25.1	7.0	1.8	1.57	0.58
331	60	25.1	7.1	1.7	1.61	0.54
332	60	25.1	7.0	1.8	1.56	0.58
333	180	25.2	7.6	3.0	1.45	0.63
334	180	25.3	7.5	3.1	1.36	0.67
335	180	25.4	7.4	3.0	1.40	0.65
336	120	25.4	7.3	2.3	1.55	0.58
337	120	25.5	7.7	2.6	1.42	0.64
338	140	25.6	7.7	2.9	1.36	0.67
339	140	25.6	7.7	2.8	1.39	0.65
340	160	25.7	7.8	3.2	1.27	0.71
341	160	25.8	7.7	2.8	1.48	0.61

Table 5.1: Packed Column Deaeration Experiments-
Fresh water Results

Packing Height 0.863 m

End Effects 0.04 m

Run #	Pressure [mmHg]	Temp [°C]	Cin [ppm]	Cout [ppm]	NTU [-]	HTU [m]
350	80	24.8	5.0	1.5	1.54	0.59
351	140	24.8	5.7	1.8	1.81	0.50
352	120	24.8	5.9	1.6	1.86	0.49
353	140	24.8	6.0	1.9	1.76	0.52
354	120	24.8	6.0	2.2	1.35	0.67
355	100	24.8	6.0	1.7	1.67	0.54
356	60	24.8	5.3	1.2	1.71	0.53
357	100	24.8	6.0	1.6	1.73	0.53
358	160	25.0	6.2	2.1	1.71	0.53
359	180	25.0	6.2	2.3	1.64	0.55
360	80	25.1	5.8	1.3	1.85	0.49
361	100	25.1	6.0	1.6	1.72	0.53
362	120	25.2	6.2	1.8	1.69	0.54
363	180	25.2	6.3	2.3	1.67	0.54
364	160	25.2	6.0	2.0	1.78	0.51
365	140	25.3	5.9	1.8	1.84	0.49
366	60	25.4	4.8	1.0	1.86	0.49
367	120	25.4	6.0	1.7	1.81	0.50
368	80	25.4	5.8	1.4	1.79	0.51
369	180	25.4	6.1	2.1	1.78	0.51
370	140	25.4	5.9	1.8	1.84	0.49
371	160	24.6	5.5	2.0	1.69	0.54
372	180	24.6	6.0	2.2	1.67	0.54
373	160	24.6	6.3	2.2	1.65	0.55
375	100	24.5	6.0	1.5	1.83	0.49
376	140	24.5	6.1	2.0	1.67	0.54
377	160	24.4	6.3	2.2	1.60	0.57
378	80	24.4	5.7	1.3	1.86	0.49
379	60	24.4	5.3	1.1	1.85	0.49
380	100	24.4	5.8	1.6	1.75	0.52
381	80	24.5	5.5	1.3	1.88	0.48
382	120	24.4	6.1	1.7	1.80	0.50
383	60	24.4	2.3	1.1	1.91	0.48
384	180	24.4	6.2	2.2	1.78	0.51

Table 5.2: Packed Column Deaeration Experiments-
Seawater Results

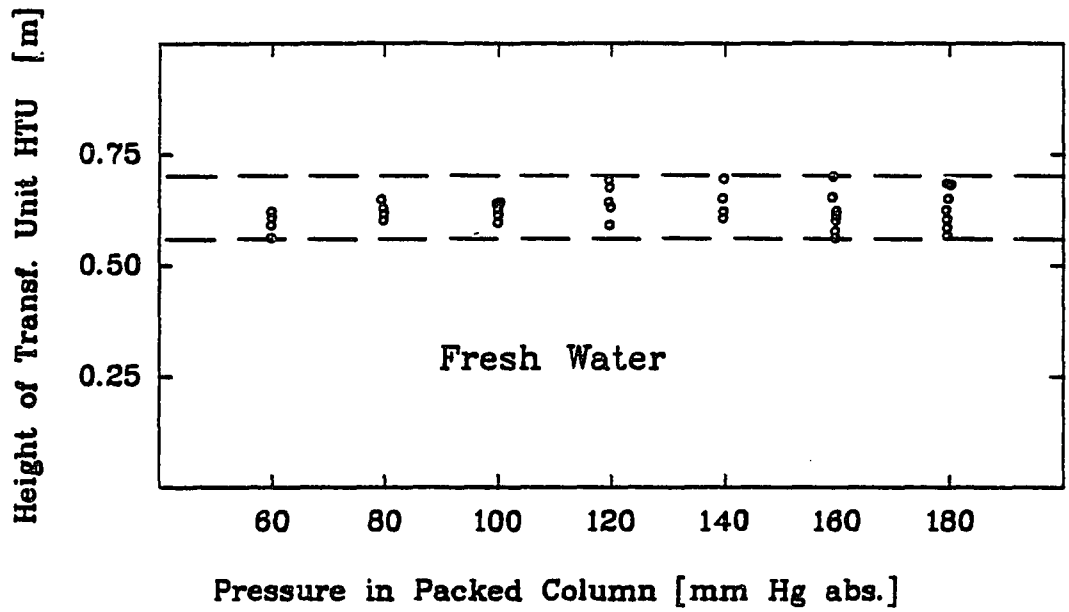

Figure 5.4 HTU Versus Column Pressure for Fresh Water

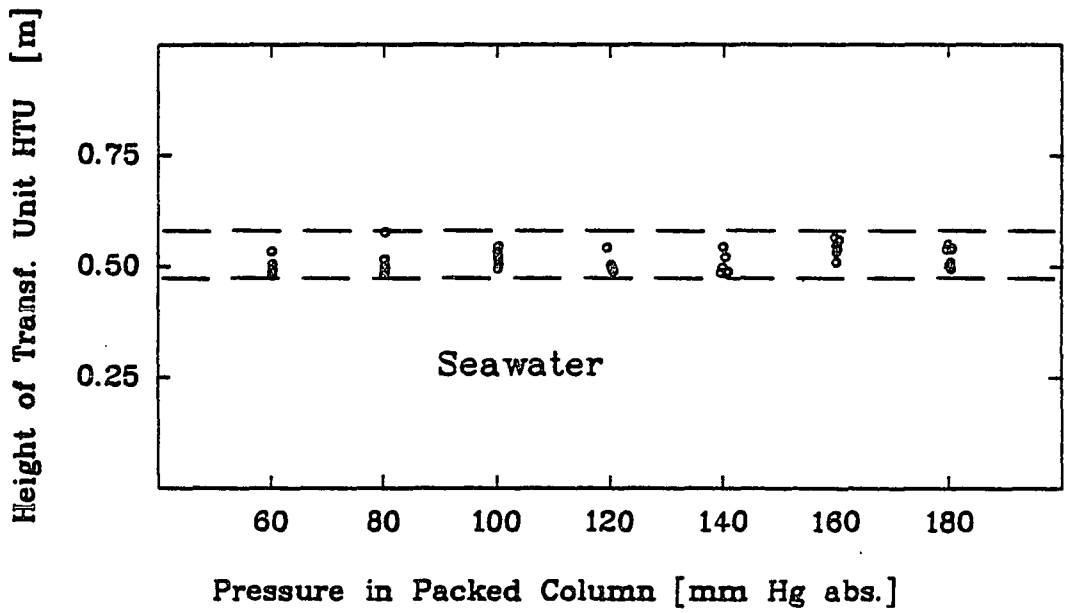

Figure 5.5 HTU Versus Column Pressure for Seawater

CHAPTER VI

GAS TRANSFER IN OC-OTEC SUBSYSTEMS

6.1 Review of Previous OC-OTEC Gas Transfer Investigations.

6.1.1 Desorption Tests

Four recent investigations which studied degasification in OC-OTEC system components are discussed below.

Lindenmuth [84] investigated the rate of deaeration of water in an OC-OTEC riser leg. The test loop flow path is shown in figure 6.1. Water from a 6 m^3 air-saturated feed tank was drawn into a 10 cm diameter clear pipe. After rising some 10m, the flow passed through a horizontal pipe section and then moved downward to a circulation pump.

As the water moved upwards it became increasingly supersaturated with gases due to loss of hydrostatic pressure head. The amount of gas evolution was determined by measuring the initial oxygen concentration in the feed tank and that in the riser at locations of low pressure. Experiments were done with waters having different nuclei content in order to simulate actual OC-OTEC process conditions. Warm surface seawater usually has a great number of nuclei which are generated by a variety of

biological and physical processes. The cold deep water is known to have a negligible amount of nuclei.

Nuclei were seeded by injecting small air bubbles at the base of the vertical riser. The bubble injection arrangement consisted of a porous tube which was embedded in an outer solid tube. Water flowed across the porous tube surface as the air was forced out of the porous material. The shear exerted by the flowing water detached bubbles before they were fully formed and thus small bubbles could be generated.

The rate of deoxygenation was measured to be a function of nuclei content and of water flow velocity through the riser. At 100 mm Hg above vapor pressure the deaeration rate was 4-8%. A maximum of 11-25% of the available air was removed at about 75mmHg above vapor pressure.

Experiments conducted by Golshani and Chen [46] investigated the amount of gas released in fresh water in a 5cm diameter intake pipe of a packed column. The barometric intake configuration is schematically shown in figure 6.2. When vacuum was applied to the packed column, water was lifted from the water tank into the packed column pressure vessel. The liquid flow rate was a function of column pressure and water level elevation in the tank. The percentage of evolved gases was determined by measuring the oxygen concentration in the water tank

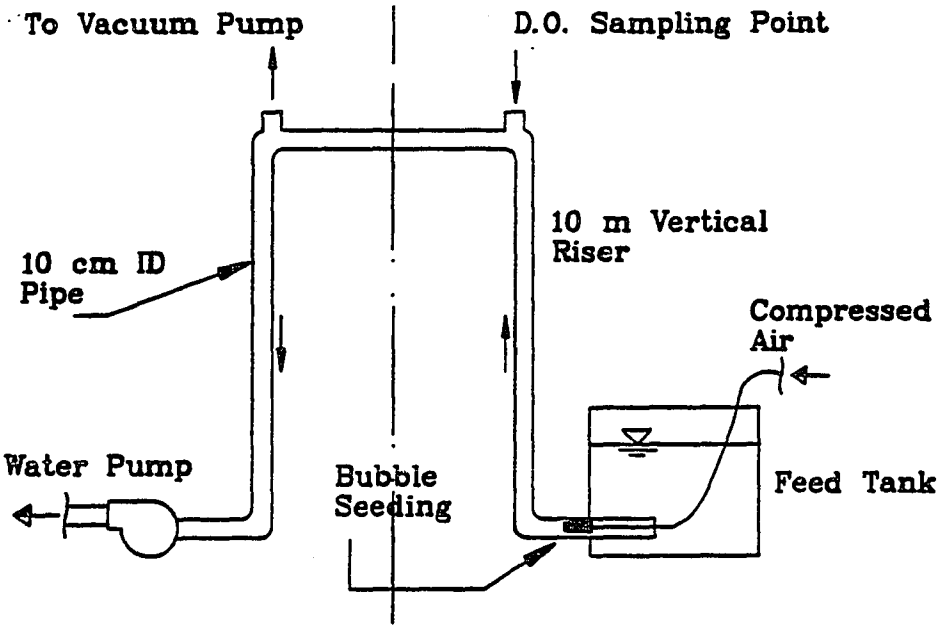

Figure 6.1 Set-Up of Previous Deaeration Tests (from [84])

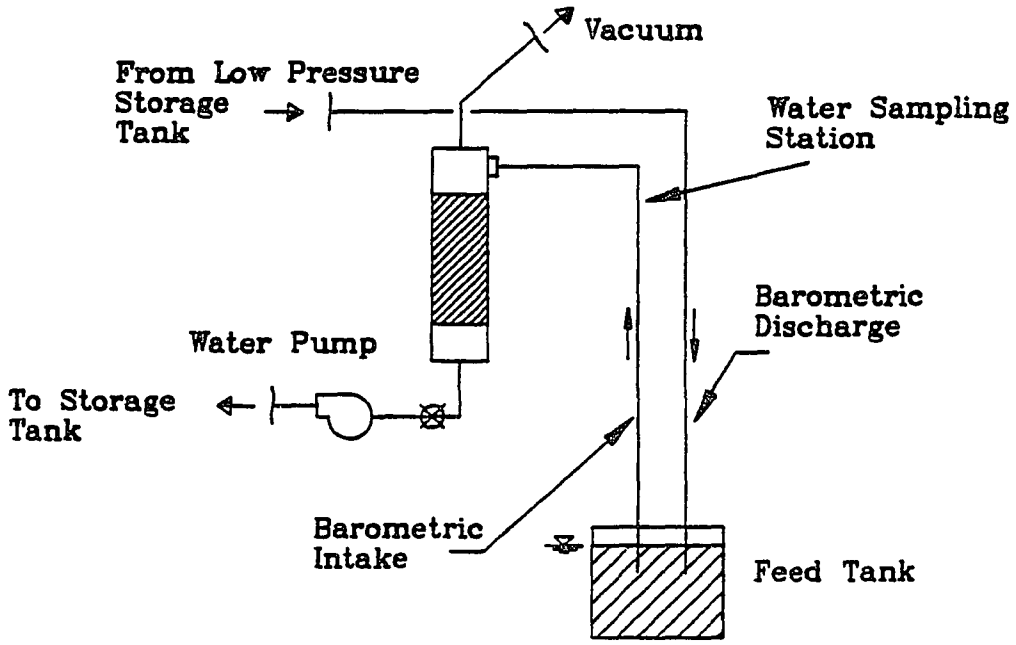

Figure 6.2 Set-Up of Previous Deaeration Tests (from [46])

and that of a sample extracted at the in-line sampling station.

Similarly to the experiments by Lindenmuth [84], the nuclei content of the feed water was taken as a variable for the deaeration tests. When a low nuclei content water was used, the test water was left overnight to eliminate as many bubble nuclei as possible. The loop then operated only in a once-through mode. Moderate nuclei content was obtained by aerating a tank which in turn fed the intake water tank. In the case of high nuclei content water, aeration occurred in both tanks.

Deaeration was found to be affected by such parameters as the vacuum pressure in the packed column vessel, the liquid flow rate in the barometric riser, and the existence of nuclei in the water. Maximum oxygen removal was 27% at a liquid flow of 1.8 m/sec with high nuclei content.

Experiments carried out by Fournier [37] were designed for heat transfer tests of OC-OTEC spout evaporators. The system, however, incorporated measurement of dissolved gases. The test set-up is shown in figure 6.3. The loop operated in an open cycle configuration with the feed water being prepared in the tank. From the tank the water flowed to the evaporator and was discharged via a drain well. In addition to fresh water, a 35% brine was used which represented seawater. The water was aerated in order

to simulate in-situ conditions. The prepared water could either be fed directly to the evaporator or could reach the evaporator via a resorber well. The resorber well was a U-tube of 25 m depth. Its function was to dissolve suspended microbubbles and, thus, to provide a water of lower nuclei content. Valves for controlling the liquid flow were located in the intake and discharge pipes.

Gas release in the system was determined by measuring the oxygen content in the feed tank and in the discharge tank. Values of gas desorption were 35% for fresh water and 90% for the 35 g/l brine. The author attributed the high gas release to processes happening at the evaporator spout exit. Release in the barometric riser was estimated to be less than approximately 6%.

The only OC-OTEC gas evolution study to date using natural seawater was carried out by Krock and Zapka [76]. Deaeration was studied with two experimental test set-ups. One of these determined deaeration in the intake pipe of a packed column. The system configuration is depicted in figure 6.4. Both warm surface seawater and cold deep seawater were continuously extracted from the ocean. Seawater was pumped into header tanks from where it was distributed to laboratory facilities. Water from the header tanks entered the packed column via a throttle valve. In order to adjust the liquid flow rate, the valve had to be manipulated in response to the vacuum pressure

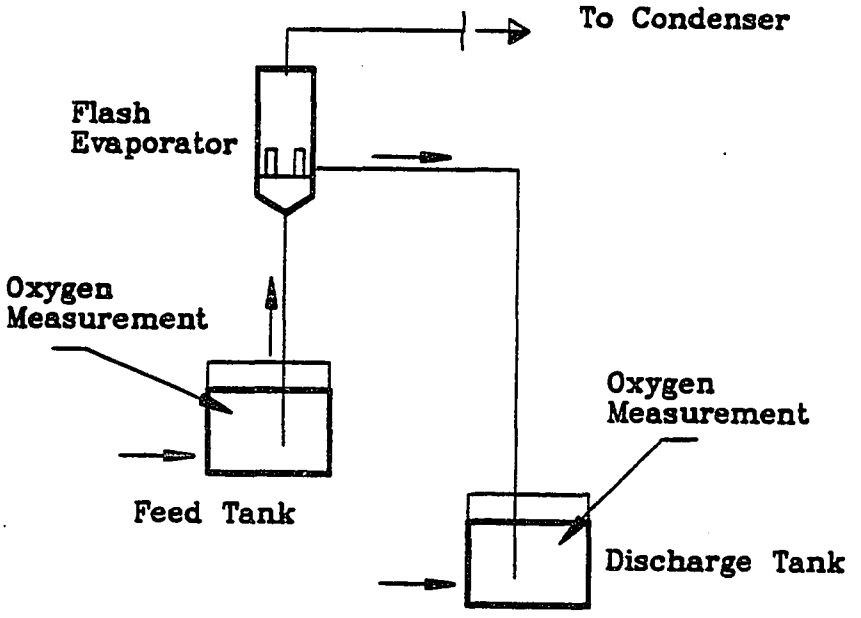

Figure 6.3 Set-Up of Previous Deaeration Tests (from [37])

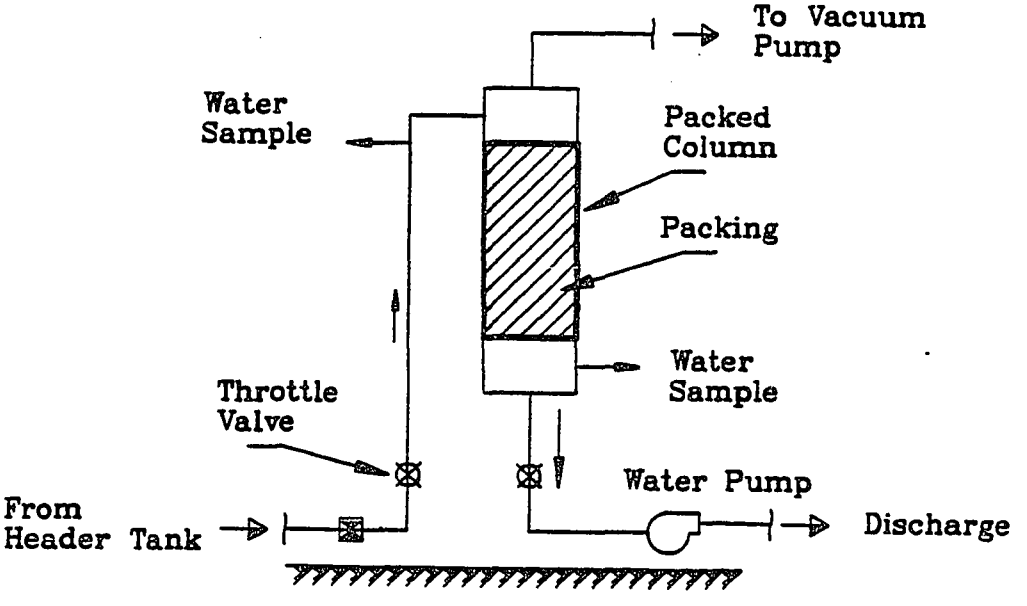

Figure 6.4 Set-Up of Previous Deaeration Tests (from [76])

in the packed column. As a consequence the valve had its smallest opening at relatively high vacuum. Considerable cavitation could be detected downstream of the throttling valve. This valve thereby served as a source of nuclei for bubble formation in the low pressure section of the upcomer.

Deaeration was determined by measuring the oxygen concentration in the water entering the system, in the intake pipe upstream of the packed column and in the water exiting the packed column. Deaeration rates were found to be primarily a function of the vacuum pressure within the packed column. At a column pressure of 50 mm Hg abs. the maximum oxygen desorption rate was measured to be 95%. Nitrogen evolution was determined to be 90%.

Because of the large amount of gas evolution observed in the upcomer of packed column, a second deaeration system was designed. This system, depicted in figure 6.5, was simply a bubble trap. As in the packed column experiments, seawater was taken from an elevated tank. Water flowed through the intake riser into the debubbler where a low pressure was maintained. Bubbles which had formed in the intake pipe rose to the water surface in the debubbler and were thus separated from the liquid stream. The water was then discharged by a pump. A flow control valve was placed on the intake line. However, care was taken to minimize cavitation by placing this valve low

on the upcomer and by locating the flow turbine meter on the discharge side. Tests were conducted using warm surface seawater, cold deep seawater, and fresh water. The operational test variables were flow rate and vacuum pressure in the debubbler.

Considerably less cavitation was observed in the upcomer as compared to the previous experiment with the packed column. The degree of deaeration in the surface seawater was significantly higher than in fresh water. Deaeration rates in deep seawater were less than those of surface seawater. Maximum dearation rates were 80%, 60%, and 50% for surface seawater, deep seawater, and fresh water, respectively (refer to figure 1.5).

6.1.2. Reaeration

Injection of air into the OC-OTEC discharge has been suggested by several authors [e.g. 76, 47]. There are several advantages associated with injection of process gases into the discharge stream.

1) Reinjection redissolves non-condensible gases which evolved during evaporation and direct-contact condensation and, therefore, makes OC-OTEC application environmentally more acceptable.

2) Reinjection utilizes a part of the kinetic energy contained in the effluent flow in order to condense the

steam contained in the vacuum exhaust.

3) Injection of vacuum exhaust occurs at a subatmosheric pressure; therefore the hydraulic compression reduces the power required for the OC-OTEC vacuum system. The fact that an hydraulic air compressor is technically far more simple than a mechanical one supports the cost effectiveness of this approach.

4) Reinjection not only reoxygenates the effluent but also prevents discharge to the atmosphere of significant quantities of carbon dioxide from the cold seawater stream if a direct contact condenser is used.

The concept of reinjection originates from two, relatively old technologies, namely hydraulic air compression and U-tube aeration. Hydraulic air compression was widely used to supply compressed air to mines in the late nineteenth century. Its working principle is illustrated in figure 6.6. Water flows downward, horizontally through a separation chamber, and then again upwards. In the intake, air is entrained in the water flow. In the downpipe air bubbles mix with water and are compressed as the hydrostatic pressure increases. In the air chamber, bubble which contain air of approximately ambient pressure are separated from the liquid. The water passes out of the chamber and rises upward. Due to compression and hydraulic losses, the

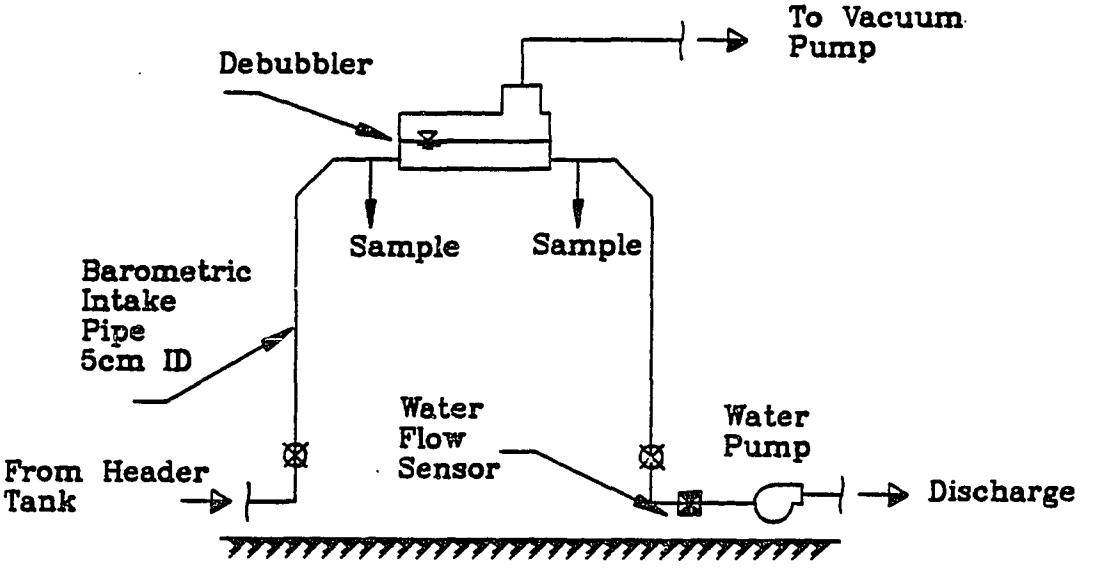

Figure 6.5 Set-Up of Previous Deaeration Tests (from [76])

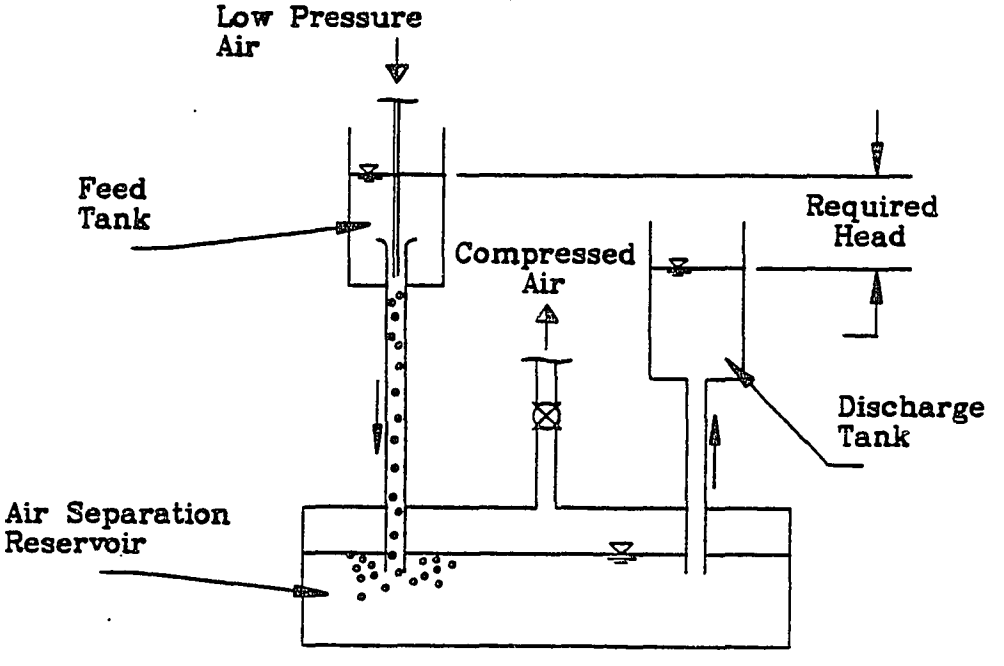

Figure 6.6 Principle pf Hydraulic Air Compression

power consumption is equal to the headloss between the intake and exit water.

Golshani and Chen [47] investigated the power consumption of a hydraulic air compressor. They correlated test data with results from an analytical model. Their test set-up is schematically depicted in figure 6.7.. Water entered the downpipe and was barometrically discharged into a well of constant water level. Air was injected at a location below the water entrance. Bubbles were moved downward with the liquid flow and were compressed as the pressure increased. The power required for compression was simply the increment of water column above the air injection location. When there was no air injection, the free water surface was maintained by applying vacuum pressure at the top of the discharge pipe. In this investigation the authors did not determine the degree of reaeration of the previously deaerated feed water.

U-tube aeration is an effective concept for aerating water (figure 6.8). The water to be aerated passes through an appropriate device which allows it to entrain air. The air-water mixture passes downward through a pipe, changes the flow direction at a large depth, and flows back up to the surface. The hydrostatic head pressurizes the bubbles and increases the dissolved oxygen deficit by increasing the saturation concentration, thus increases

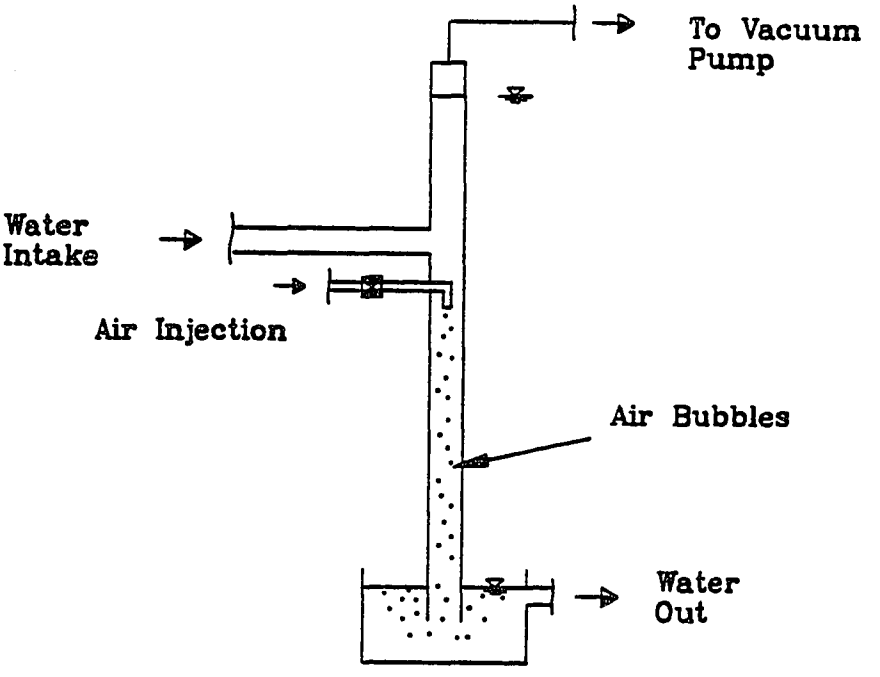

Figure 6.7 Schematic of Air Compression System (from [47])

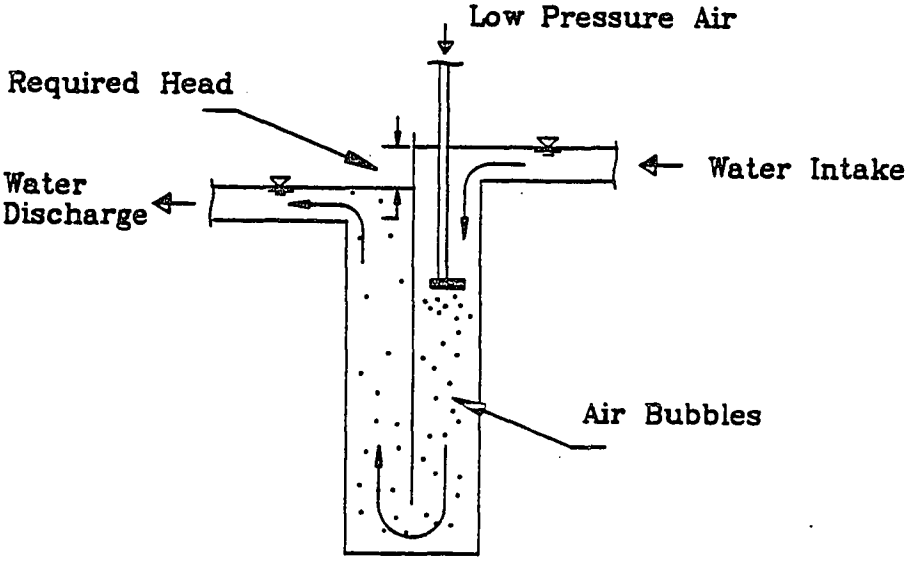

Figure 6.8 Principle of U-Tube Aerator

the driving force for absorption. The buoyant force of the bubble causes turbulence at the bubble surface which effectively increases the transfer coefficient.

The total head loss across the system is the sum of the headlosses due to air injection and due to the water flow alone. Results showed that headloss due to air injection increased with lower water flow rates at constant ratio of injected air to water.

The change in dissolved oxygen, and therefore the effectiveness of the aeration process, was increased with lower water velocities at equal air-water ratios. Both the required hydraulic head and the change in dissolved oxygen increased when the percentage of injected air in the water stream was increased.

6.2 Review of Sampling Procedures

Procedures to collect samples for gas analysis are well established for applications at atmospheric pressure. Standard procedures for obtaining water samples from low pressure vessels have not been established to date. There has been a considerable controversy about the reliability of the sampling procedures used in OC-OTEC gas transfer experiments . In this chapter the sampling procedures applied in recent OC-OTEC gas transfer investigations are reviewed and compared with findings of

the present gas transfer experiments.

Golshani [34] reported that the performance of flow-through Clark-type oxygen sensors gave erroneous results in a vacuum environment . At low pressure conditions, the membrane was observed to fit only loosely against the gold cathode causing inaccurate readings of dissolved oxygen concentrations. The suggested remedy was to move the sensor to locations where it was exposed to positive pressures. Since continuous measurements at low pressure locations were impossible, water samples had to be extracted from low pressure system locations where the D.O. concentration was sought.

Golshani's sampling procedure [34] consisted of a 1-l flask connected to the top section of the barometric leg (see figure 6.2). The flask was also connected and valved to the vacuum system, the atmosphere and a B.O.D. bottle drain port. The vacuum line equalized the pressure of the flask with that of the barometric riser. Upon opening a valve, water from the barometric leg flowed into the flask. Once full, the flask was vented and the collected sample transferred to a B.O.D. bottle by means of a valved drain.

Lindenmuth [84] employed a similar sampling technique. He, however, reported that this sampling procedure induced errors which he attributed to two factors, namely a sampling time effect and the magnitude of the vacuum

pressure in the barometric leg where the sample was taken.

Instead of an extraction technique, Lindenmuth adopted in-situ measurements of the dissolved oxygen. Since, as mentioned, present oxygen sensors fail in vacuum environments, the water flow had to be stopped and the system vented before the probe could be inserted.

In gas desorption experiments conducted by Fournier [37] the amount of evolved gas was assessed by comparing dissolved oxygen concentrations of the feed and discharge tanks, which were both at atmospheric pressure. Thus, the problems of sampling from a subatmospheric vessel were not encountered in this study.

Seawater experiments conducted by Krock and Zapka [76] employed an extraction procedure. Samples were extracted from the barometric leg by means of an upstream facing orifice, which was located in the pipe center. From there the water flowed to a sampling device which was designed to minimize barometric changes and sample contamination. The sample device is shown in figure 6.9.

The sample device was made of a 25 cm long, 10 cm diameter pipe which was flanged at one end. The other end was machined to accommodate an O-ring seal. A 300 ml B.O.D. bottle was placed on a bottle support in the device. A plexiglass cover was connected to two sample tubes. One of the tubes led to the valved sample port in the barometric leg; the other connected the sample device

to vacuum, thereby equalizing the pressure in the device with that in the barometric leg. A thin walled tube protruded from the underside of the cover plate. This tube was inserted into the sample bottle when the cover plate was placed on the O-ring seal. The vacuum line was opened and the pressures equilibrated. The water sample was admitted by opening the liquid valve (not shown in figure 6.9) and water overflowed the containing bottle. The volume of the sampling device was such as to allow flushing of the sample line and overflowing of the B.O.D. bottle by three bottle volumes. After sampling was completed the device was vented and the bottle removed. Measurements of dissolved oxygen were carried out by means of a oxygen sensor. The azide modification of the Winkler method was used to periodically check results obtained with the oxygen sensor.

Since transparent Tygon tubing was used for the sample lines, the sample water stream leading from the sample port on the barometric leg to the sampling device could be observed. At the beginning of tests [76] an elbow tube (inside the barometric intake pipe) facing upstream was used as the sampling port. At high vacuum pressures vigorous cavitation was observed in the main water flow in the barometric riser downstream of the intruding tube. Additionally, fairly numerous bubbles could be seen emerging from the tubing connector of the sampling port

and flowing with the sample water to the sampling device. The intruding sample tube in the barometric leg was removed and water was extracted from the flow pipe through an orifice which was flush with the interior wall of barometric pipe. Consequently, far fewer bubbles were visible entering the sample line, and also less cavitation was observed in the barometric leg.

It was further observed that bubbles emerged downstream of the sample valve. The number of bubbles decreased as the system pressure was increased and the flow in the sample line decresed. In addition to bubble generation by the sample valve, sample line components such as tubing connectors induced bubbles in the sample line. The magnitude of the generation of these bubbles decreased again with higher pressures and smaller flow.

Efforts were made to minimize the occurrences of bubbles in the sample line by improving the sample port configuration and avoiding flow obstructions in the sample line. However, the presence of bubbles could never be entirely avoided.

In addition to those previously mentioned, sampling procedures of other investigations, concerned with vacuum desorption, were reviewed as part of the present study [e.g. 74, 105, 114, 126]. From the reviewed references and personal observations by this author, the following

conclusions were drawn, which address sample extraction from low pressure vessels:

1) Bubbles in the sample line deaerate water if exposed to low pressure, and aerate samples with low gas concentrations at higher pressures.

2) Entrainment of bubbles into the sample line has to be avoided.

3) Bubbles can be generated in the sample line, particularly at low pressures. Flow obstructions such as tubing connectors and valves contribute substantially to bubble generation. The generation of bubbles in the sample line is more vigorous the faster the sample is extracted.

4) If bubbles are not entrained nor originate from leaks, but are solely generated in the line, bubbles should not be separated before the sample is pressurized to atmospheric conditions.

5) Some tubing material is gas permeable (e.g. Tygon and, particularly, silicon) and should not be used. Better materials are gas impermeable butyl rubber hoses or glass tubing.

In order to assess the effects of bubble generation in the sample line on the oxygen concentration of extracted water, the following test was conducted. The debubbler vessel of a previous experimental set-up (see figure 6.5) was filled with seawater. As shown in figure 6.10, the

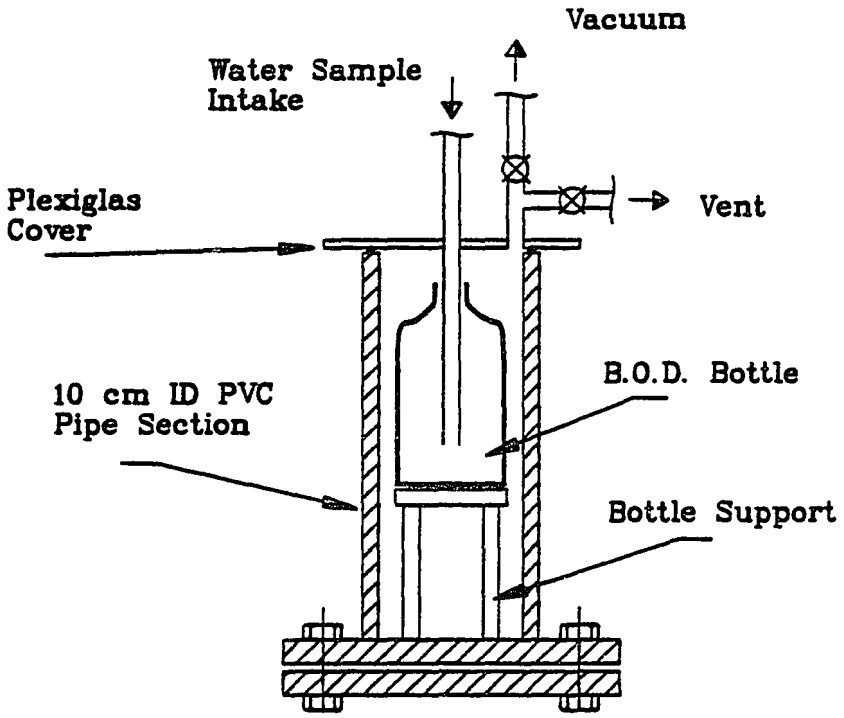

Figure 6.9 Sampling Device (from [76])

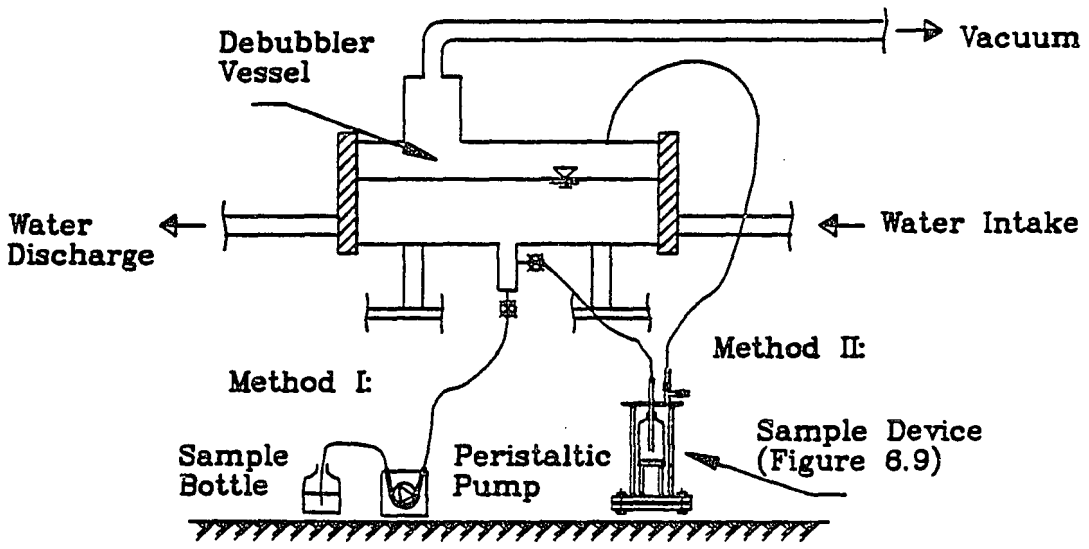

Figure 6.10 Comparison of Sampling Techniques

sampling device (figure 6.9) was connected to the debubbler. In addition a new sampling apparatus was constructed, which simply consisted of a peristaltic pump discharging water into a B.O.D. bottle. A 1.9 cm ID transparent PVC pipe was attached to the debubbler; the sample valves I and II were alternatively opened to either of the sampling devices. The debubbler was set to the desired vacuum pressure, and samples were collected alternatively in B.O.D. bottles using the two methods. After collection the debubbler was vented and the samples were drawn under atmospheric pressure by both methods.

The results of the test are shown in figure 6.11. The dissolved oxygen concentration of samples which were extracted at atmospheric pressure were averaged and are denoted B (for background) in figure 6.11. It is obvious that sampling at low vacuum with method II produces D.O. concentrations significantly lower than the background. Method I gave values which were close to the background readings. It should be noted that the background D.O. decreased with increasing pressure. This was due to the fact that the water standing in the debubbler was outgassing during the period of the test.

Sampling with method II was also done while deliberately increasing the amount of bubble generation in the sampling line, e.g. high flow rate and two redundant tubing connectors. As a consequence numerous bubbles could

be observed downstream of flow obstructions, particularly downstream of the sample valve, which connected the sampling line to the debubbler vessel. Sampling with method I was done with a relatively low flow rate. (approx. 200 ml/min). Bubbles were observed to emerge downstream of this sample valve, but the amount was considerably less than downstream of the sample valve used with method II. Bubbles carried into the sample line passed though the tubing pump. Downstream of the tubing pump no bubbles could be seen.

As evident from results in figure 6.11 water extracted with the new sampling method (method I) gave concentrations close to those extracted under atmospheric conditions. The older method (method II) resulted in too low concentrations. It should be pointed out that conditions under which water was extracted by means of method II were quite different from the sampling procedures of previous experiments [76]. During those gas transfer experiments bubble generation in sample line was less, due to lower flow rates and lesser flow obstructions. Furthermore, during those previous experiments water was extracted from the flow in a barometric leg. A correlation of test results between the recent method described above and those from previous experiments [76] is not attempted due to the different experimental conditions.

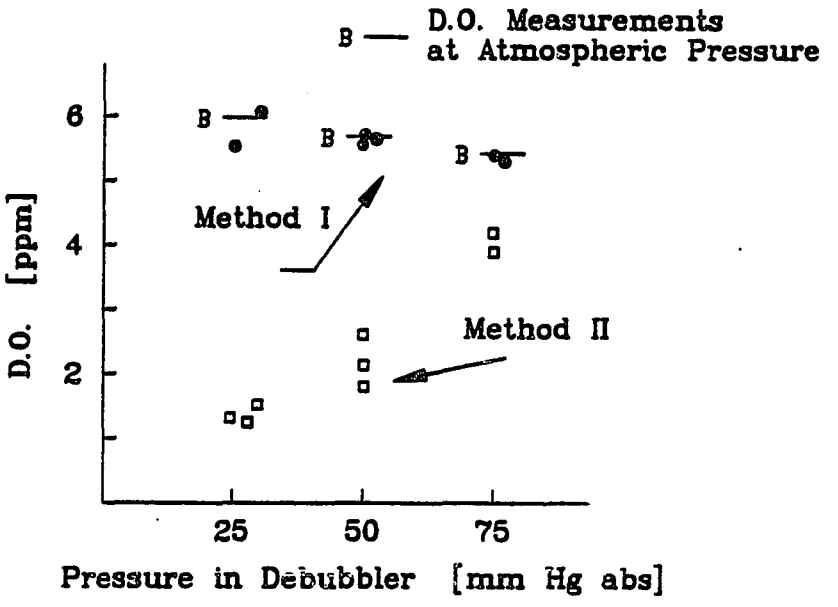

Figure 6.11 Results of Tests of Sampling Techniques

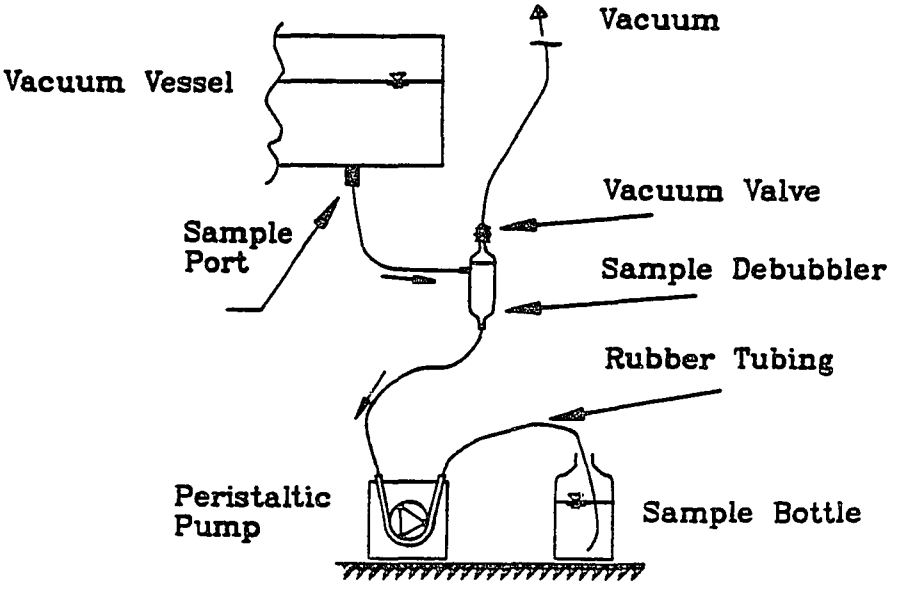

Figure 6.12 Sample Procedure for Gas Transfer Experiments

Further development of sample method II produced the sampling technique which was used for the gas transfer experiments of the present study. This method is illustrated in figure 6.12. Water in a subatmospheric pressure vessel is extracted by means of a peristaltic pump. Sample water should preferably be extracted downward to avoid bubbles entrainment. Shortly after exiting the vessel, the water passes through a glass sample debubbler, where bubbles can be separated from the flow.

The sample debubbler is connected to the vacuum source and valved with a glass stopcock. Bubbles contained in the sample line rise to the top of the sample debubbler, from which they are periodically removed by opening the vacuum stopcock. All tubing, except that in the pump head of the pump are butyl rubber (or glass). Tubing connectors should have a large internal diameter. It is better to use plastic connectors which are one size too large for the tubing size and force the tubing over them, than to use connectors with the same I.D. as the tubing.

It was generally observed that sampling downward from a vessel, with small flow through the sample port, did not entrain bubbles. Sampling, however, from a horizontal sample port caused entrainment of bubbles, even if the flow rate in the sample line was fairly small. The bubbles then had to be separated in the sample debubbler. It seems that vertical sampling from a vessel with relatively

little flow velocity across the mouth of the sample port is the preferable method.

The peristaltic pump used was a Masterflex (standard drive) with a continuous 6 to 600 rpm speed control. The Tygon tubing was Masterflex No.24 with an inside diameter of 6.3 mm and a wall thickness of 2.9 mm. The maximum vacuum against which pumping is possible was specified by the manufacturer as 150 mm Hg abs. (24" Hg Vac.). Pumping tests revealed that water can be extracted even against 75 mm (27" Hg. Vac.), provided fairly new tubing is used. The recommended water flow rate should not exceed 250 ml/min with the equipment described above.

6.3 Gas Transfer Experiments

6.3.1 Scope of Work

The gas transfer experiments were grouped into three segments which addressed different aspects of gas evolution and resorption in the OC-OTEC scheme. These three segments were:

1) Phase I: Deaeration due to air injection into barometric intake. Deaeartion in the upcomer was investigated in an effort to determine the effectiveness of the barometric leg in terms of gas desorption.

2) Phase II: Deaeration resulting from air injection into

deaerator vessel. The desorption of a reservoir at low pressure was investigated to assess potential increments in degasification with increasing residence time of water in a low pressure environment.

3) Phase III: Reaeration of process water in the system downcomer. Experiments with air injection into the deaerated discharge were intended to render preliminary assessments of feasibility of such a concept.

6.3.2. Overall Experimental Set-up

The experimental apparatus is shown in figure 6.13. Water was held in two tanks. When the system was running water was pumped from tank I into well II, from where it flowed back into tank I after completing the supply cycle. Tanks I and II were the same tanks as previously used for the packed column experiments.

Two pipe units were suspended by winches and served as supply and discharge wells. Due to overflow, these wells had constant water levels. The wells were made of 15 cm ID PVC pipe, closed and valved at one end and open at the other end. Both were 4.3 m long. The distance from the open top to the horizontal 7.5 cm ID overflow was 60 cm.

Water flow was measured with a flow meter used. The flow meter was located some 7 m below the deaerator in the barometric intake.

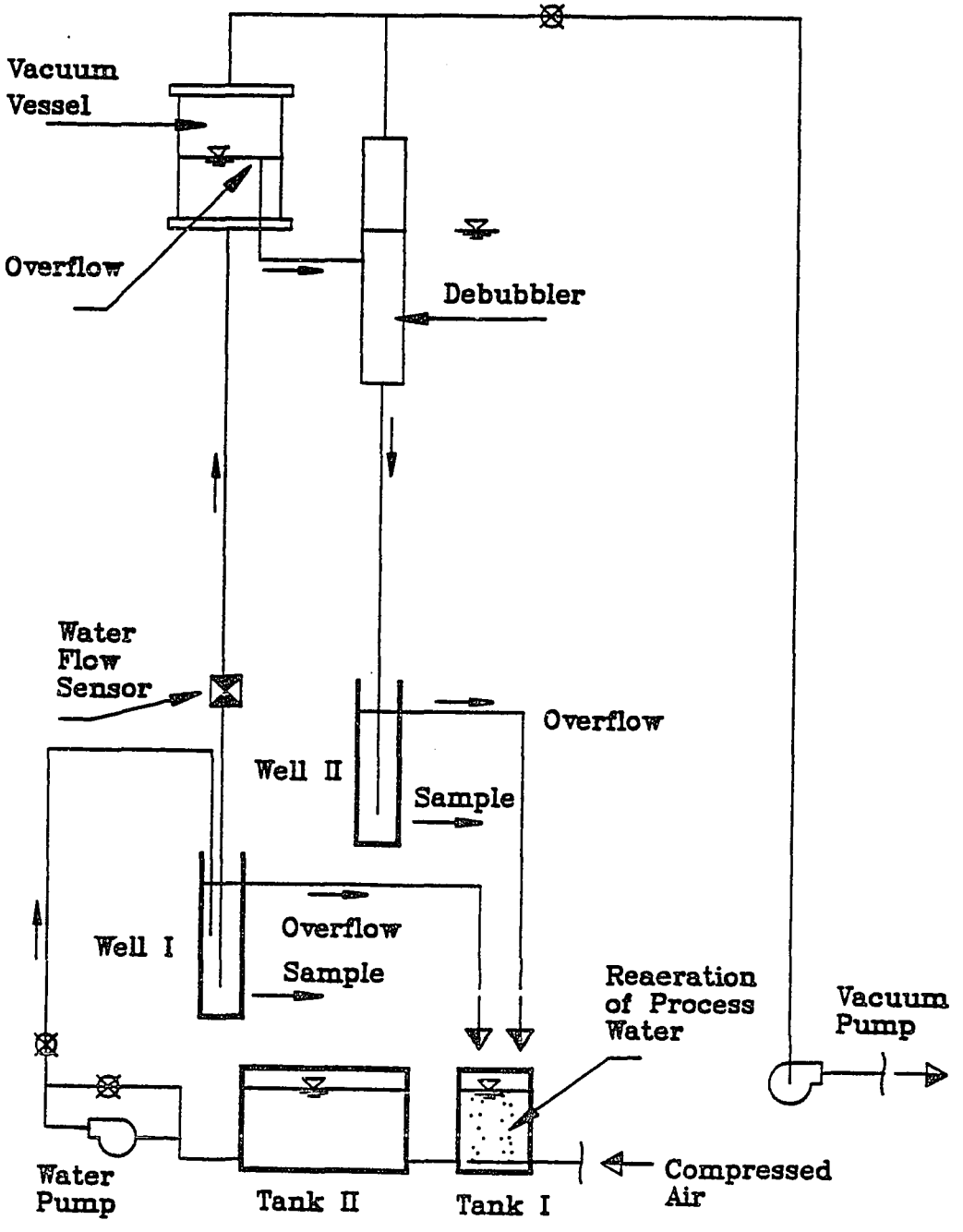

Figure 6.13 Overall Test Set-Up

The vacuum vessel (figure 6.14) was a 30.5 cm ID pipe section of 1.2 m length. It was flanged at both end and sealed with O-rings. The top blindflange was made of plexiglas and allowed observation of the vessel interior. Two orifices were drilled in the top flange, one to connect a mercury manometer, the other to connect to the vacuum line. The lower flange accommodated orifices for the intake and discharge water lines. The discharge port had an overflow which provided a constant water level. The connection from the deaearator to discharge debubbler was made of 7.5 cm ID pipe. Vacuum pressure in the vessel was adjusted by a ball valve and a needle valve. The ball valve was used for initial evacuation of the system; the needle valve was used during experiments to fine-tune the vacuum level.

The debubbler vessel was made of a 15 cm ID PVC pipe 2 m long. The discharge from the vacuum vessel entered the debubbler at its midpoint elevation. The pressure in the deaerator and the debubbler was kept equal. The function of the debubbler was to maintain a standing water column above the discharge port. Water discharged from the vacuum vessel entrained air which could thus be separated in the debubbler before entering the discharge downcomer. Water levels in the deaerator and the debubbler were monitored using two standpipes.

Three sample ports were built in the supply and insert

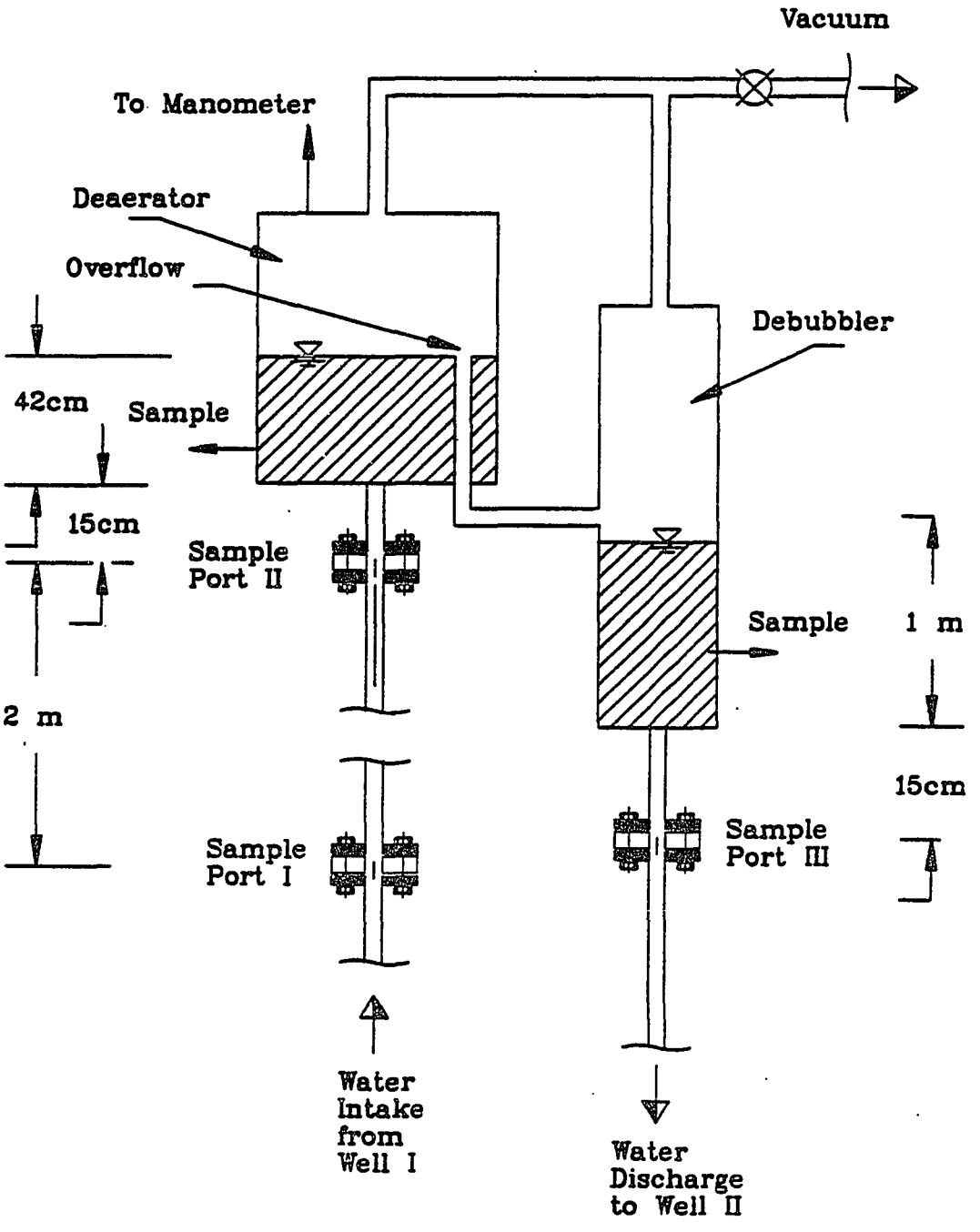

Figure 6.14 Deaerator and Debubbler Configuration

discharge pipes by sandwiching plexiglas blocks between flanges. The plexiglas blocks were machined to fit the dimensions of the pipe flanges. Two O-rings located between the flanges and the plexiglass sealed the assembly. The sampling port could accommodate plexiglas blocks which served several functions, namely air injection and sampling. If air injection occurred at the sampling port, the air injector shown in figure 6.15 was inserted.

A plexiglas block was machined to hold the fritted disk used in bubble deaeration and aeration experiments. The mount for the fritted disk was fabricated to give a fairly flush fit with the pipe walls. The fritted disk was connected to a rotameter to allow gas flow measurements. The rotameter scale read volumetric flow in l/min at 21.1 ^{0}C and 760 mm Hg abs. Atmospheric pressure was sufficient to supply the required air injection rate.

Water discharged from the debubbler flowed to well II from where it overflowed to tank I. A bubble aerator previously used in the packed column experiments provided bubble aeration in tank I.

Water used in the experiments was held in tanks I and II. As with the packed column experiments, filtered seawater was obtained from a nearby coastal facility. Seawater was replenished every four days to avoid algal growth. Fresh water came from the municipal water supply.

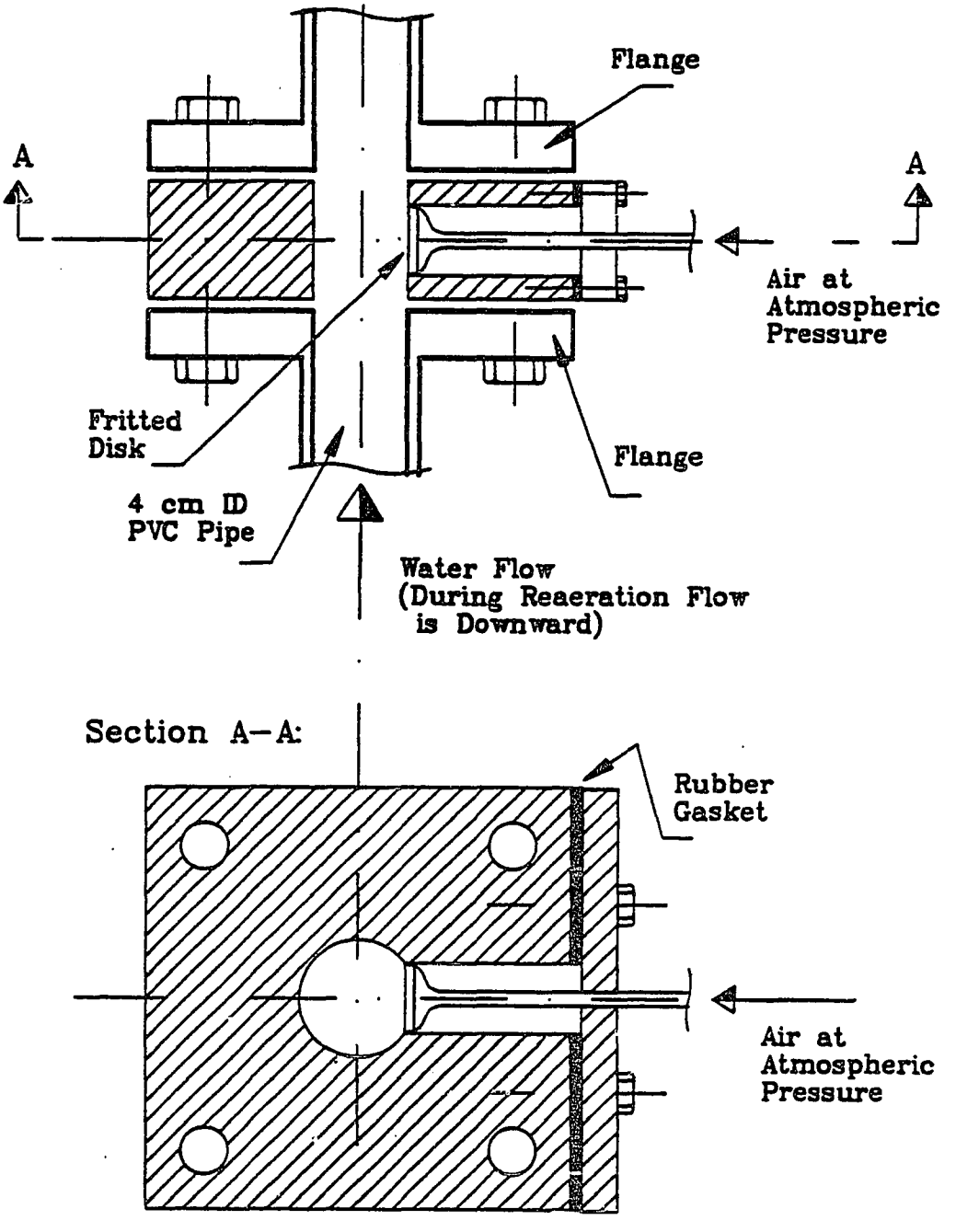

Figure 6.15 Air Injector Configuration

6.4 Phase I: Deaeration in the Up-comer

6.4.1. Test Procedure

For this test sequence the air injector was located at sample port I. Sample port II was equipped with a plexiglas block type which had one opening for sample withdrawal. Sample port III had a block without openings.

In order to start a test run, water was circulated from tank II to well I to provide a constant supply water level. Using a priming pump, water was also lifted from tank II into the discharge well. With both wells filled and constantly provided with excess water, vacuum was drawn at the deaerator and the debubbler. Water was thereby lifted slowly through the intake and discharge pipes. After water had filled the deaerator, the water flow increased to a magnitude which balanced the hydraulic head and pressure in the deaerator vessel. With the desired vacuum pressure adjusted intake well I was raised or lowered to that level which resulted in the target water flow rate. Generally, it was possible to maintain the flow rate within +- 1.2 l/min of the desired rate. Small fluctuations in the flow rate were typically observed even if the water level and vacuum pressure were constant over a considerable time.

Deaeration experiments in this research segment were

conducted with and without air injection. The rate of air injection was held constant at 1.0 l/min (21.1^{0}C, 760 mm Hg abs.). Different water flow rates were utilized to determine effects of residence time in both the barometric riser and the deaerator vessel. The vacuum pressure in the deaerator was changed to assess the pressure effect on deaeration. Samples were extracted from sample port II on the barometric leg and from a bottom orifice in the deaerator vessel.

6.4.2. Results and Discussion

Initial fresh water tests served to fine-tune the sampling technique and the overall test procedure. Initially, three sample bottles were obtained per setting. Due to data scatter the number of samples was increased to seven per setting. Although the repeatability improved substantially after modifications of sampling technique (outlined in chapter 6.2), seven samples were still collected per setting.

It was observed that during sample extraction from the barometric leg (sample port II) relatively large numbers of bubbles were entrained in the sample line. Bubble entrainment was observed with and without air injection. The magnitude of bubble entrainment was larger in the case of seawater than fresh water. Although various

modifications were tried bubble entrainment could not be avoided.

Sample extraction from the deaerator vessel was bubble-free with or without air injection. Because of the inherent difficulties encountered in sampling the barometric leg, later sample withdrawal was exclusively done from the deaerator.

The deaeration rate was calculated as follows:

$$\frac{C_o - C}{C_o} * 100 \quad [\ \% \ ] \tag{6.1}$$

where: C_o = dissolved oxygen concentration of background water, measured in well I; C = dissolved oxygen concentration following deaeration.

Equation (6.1) expresses the percentage of oxygen removed from the water. The fact that it is not possible to remove more oxygen than allowed by equilibrium conditions is incorporated in the expression of normalized deaeration:

$$\frac{C_o - C}{C_o - C_S} * 100 \quad [\ \% \ ] \tag{6.2}$$

where: C_S = saturation dissolved oxygen concentration.

As an overall assessment of gas evolution, deaeration (6.1) was used. If the effectiveness of the deaeration process was of interest, the normalized deaeration (6.2)

concept was adopted since it refers to the percentage of practically removable gas.

Fresh water tests were conducted with a flow rate of 55 l/min and three vacuum pressures, namely 50,70, and 100 mm Hg abs. The results are given in figure 6.16. The deaeration rate was an inverse function of vacuum pressure. The deaeration rates measured in the barometric leg indicated lesser differences between flow with and without air injection, than did rates measured in the deaerator vessel. A maximum deaeration rate of 36% was obtained in the deaerator at 50 mm Hg abs. pressure with air injection.

Seawater tests were carried out with the same system settings but with two flow rates, namely 30 and 75 L/min. Test results are given in figure 6.17. Due to the difficulties of sampling the barometric leg only one experimental run was conducted for this setting. An average deaeration rate of 4% was determined in the barometric leg without air injection.

Deaeration in the deaerator without air injection was higher for larger flow rates. Although the residence time was 2.5 times smaller for 75 l/min flow, larger turbulence in the deaerator contributed to an increase in the renewal of exposed water surfaces. It was unfortunate that the deaerator vessel was not transparent because visual inspection would have revealed to what extend cavitation

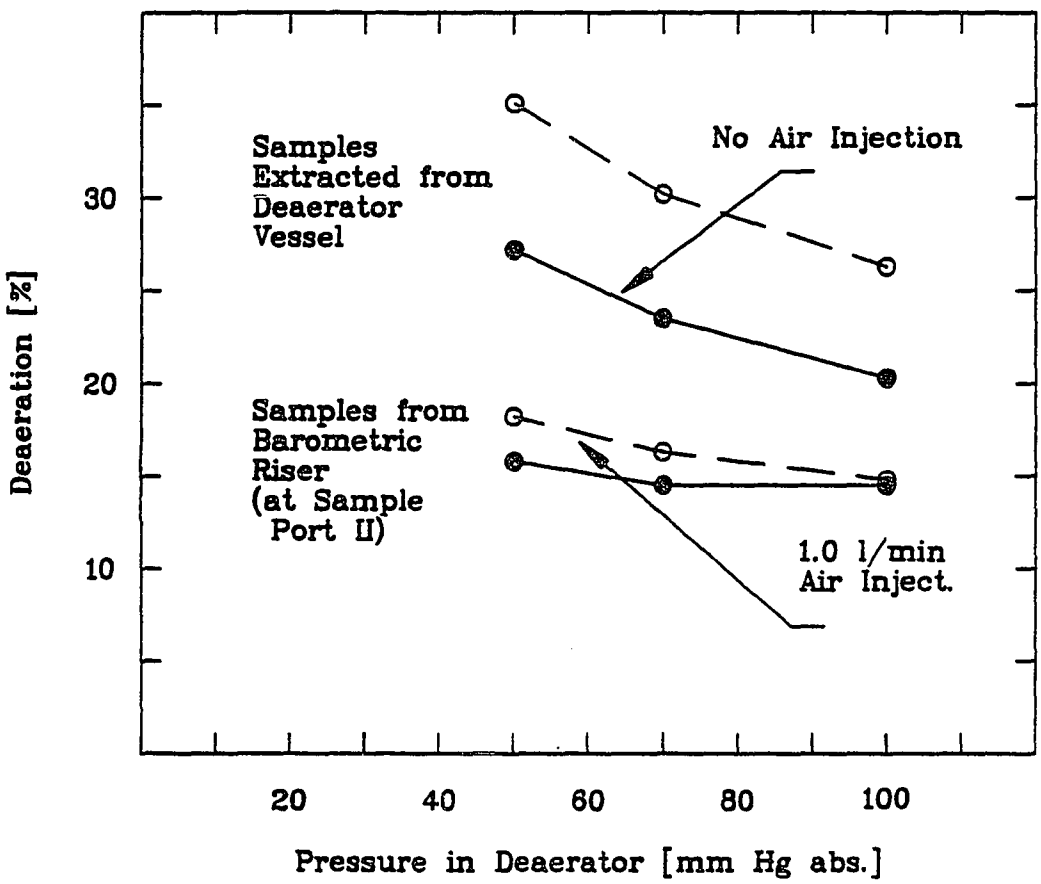

Figure 6.16 Phase I Fresh Water Results

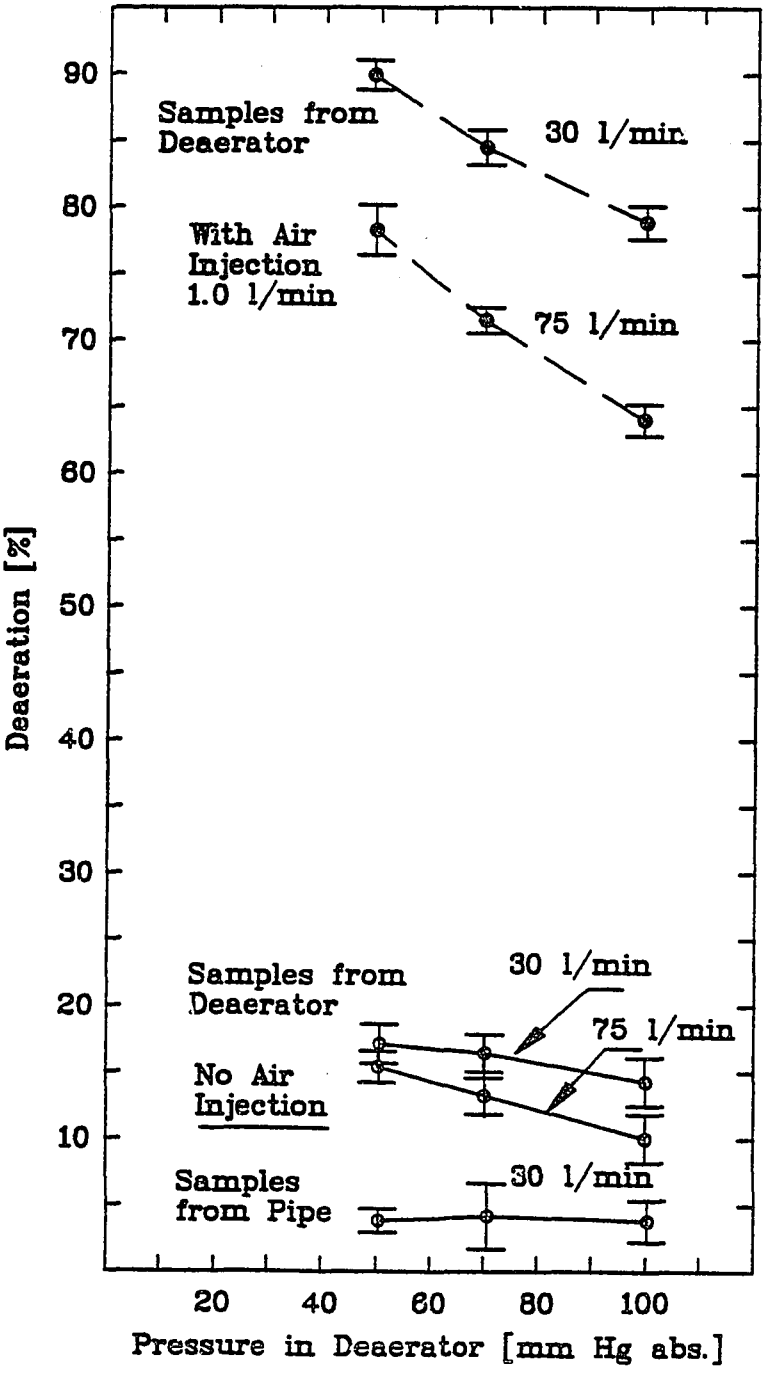

Figure 6.17 Phase I Seawater Results

at the entrance port of deaerator was responsible for desorption.

Deaeration with air injection was significantly higher than without. Deaeration rates with air injection increased more with increased vacuum than they did without air injection.

The maximum deaeration rate for fresh water was about 40% of the comparable value for seawater. This value is close to the ratio of fresh water and surface seawater deaeration determined in a previous investigation [76] (refer to figure 1.5).

Visual observation revealed that bubbles downstream of the air injector were smaller in seawater than in fresh water. A quantitative assessment of bubbles size distribution was not attempted for these experiments.

6.5 Phase II: Deaeration in Deaerator Vessel

6.5.1. Experimental Procedure

For this test sequence the air injector was alternatively located at sample ports I and II. Sample port III had a plexiglas block without openings. Overall test procedure was the same as in phase I. Air injection rate was used as a variable.

The purpose of the this sequence was to determine the

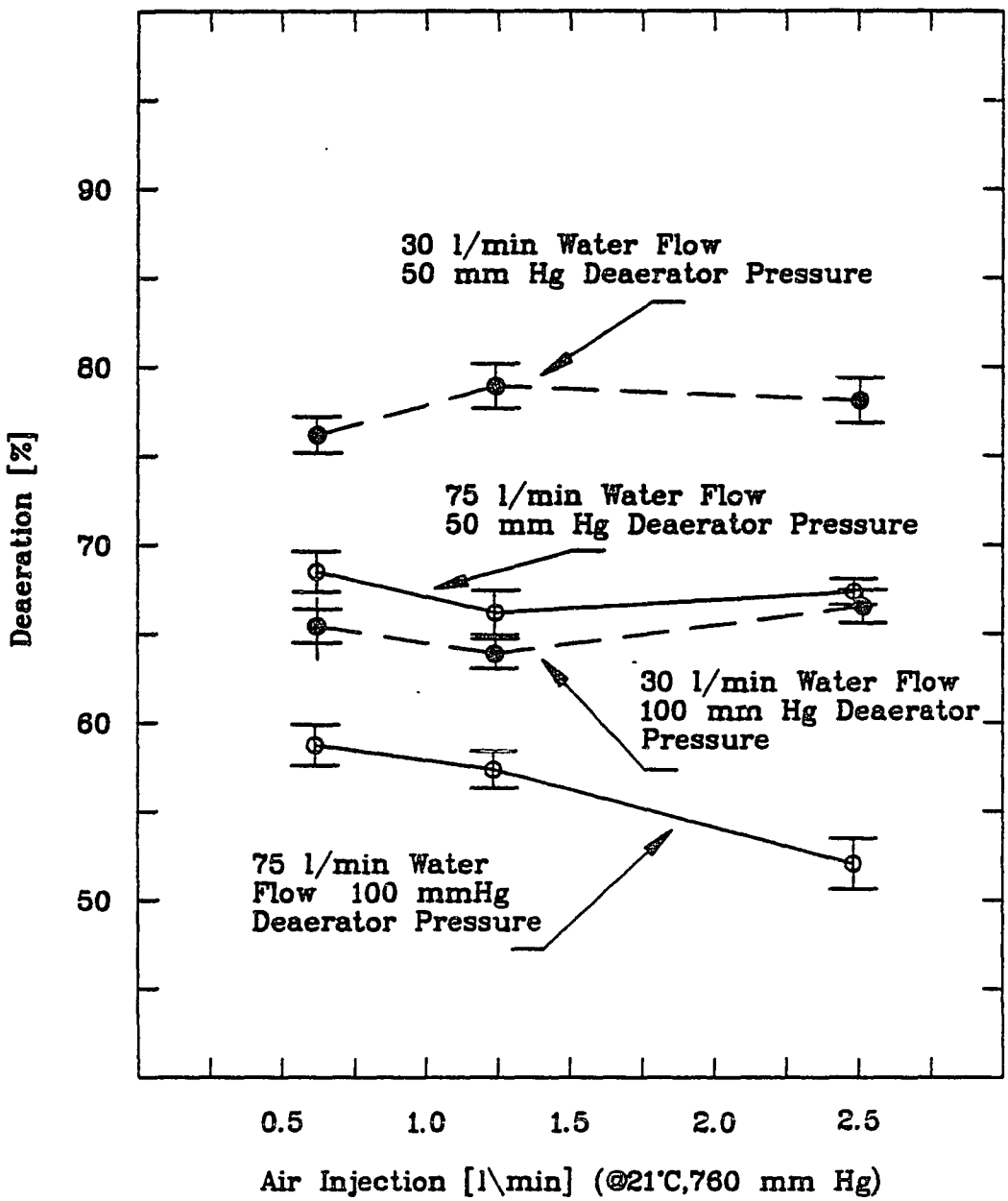

Figure 6.18 Phase II Air Injection at Sample Port II (Seawater)

effects of air injection rate and air injection location on deaeration efficiency. Three air injection rates were used, namely 0.5,1, and 2 l/min (@21.1^{0}C, 760 mm Hg abs.). Air injection at sample port I occurred at only one pressure setting, 50 mm Hg. Only seawater was used for the experiments.

6.5.2. Results and Discussion

Results of experiments with air injection at sample port II are shown in figure 6.18. As is apparent, the deaeration rates increased with lower pressures in the deaerator vessel. The deaeration rates did not vary significantly with increasing air injection.

Deaeration associated with air injection at sample ports I and II are compared in figure 6.19 . Deaeration rates resulting from injection at port I were noticeably higher than those from injection at port II. This fact revealed an interesting phenomenon. From the results (in figure 6.18) it can be inferred that deaeration effectiveness increased with residence time in the deaerator. With the water level in the deaerator constant at 43 cm, the volume of the water reservoir was 30.5 l. Thus, residence times of water in the deaerator were approximately one minute and 24 seconds for 30 and 75 l/min, respectively. Residence times of water in the

section of barometric leg downstream of sample port I were 1-4 sec, depending on the liquid flow rate, the air injection rate and the vacuum pressure in the deaeartor. Comparing the contribution of the residence time in the pipe section to the total residence time, it seems unlikely that changes in the deaeartion rates were solely caused by residence time contributions. Furthermore, it must be considered that the identical air injection rates at ports I and II, measured at atmospheric pressure, resulted in a higher bubble volume at port II because of the lower hydraulic pressure. It is suggested that the high turbulence in the barometric leg, with related high shear and mixing, contributed significantly. Furthermore, it is assumed that, if injection occured at port I, bubbles were more uniformly distributed in the water flow when water entered the deaerator. Therefore, better distribution of bubbles in deaerator vessel and more effective liquid-air contact could occur. Again, the presence of viewing ports in the deaerator would have helped to confirm this assumption.

The deaeration for one test run was compared with the normalized deaeration (figure 6.20), as defined in equation (6.2). The assumption of saturation oxygen concentration is of prime importance when calculating normalized deaeration . In the present case two conditions were used for determining the saturation values, namely

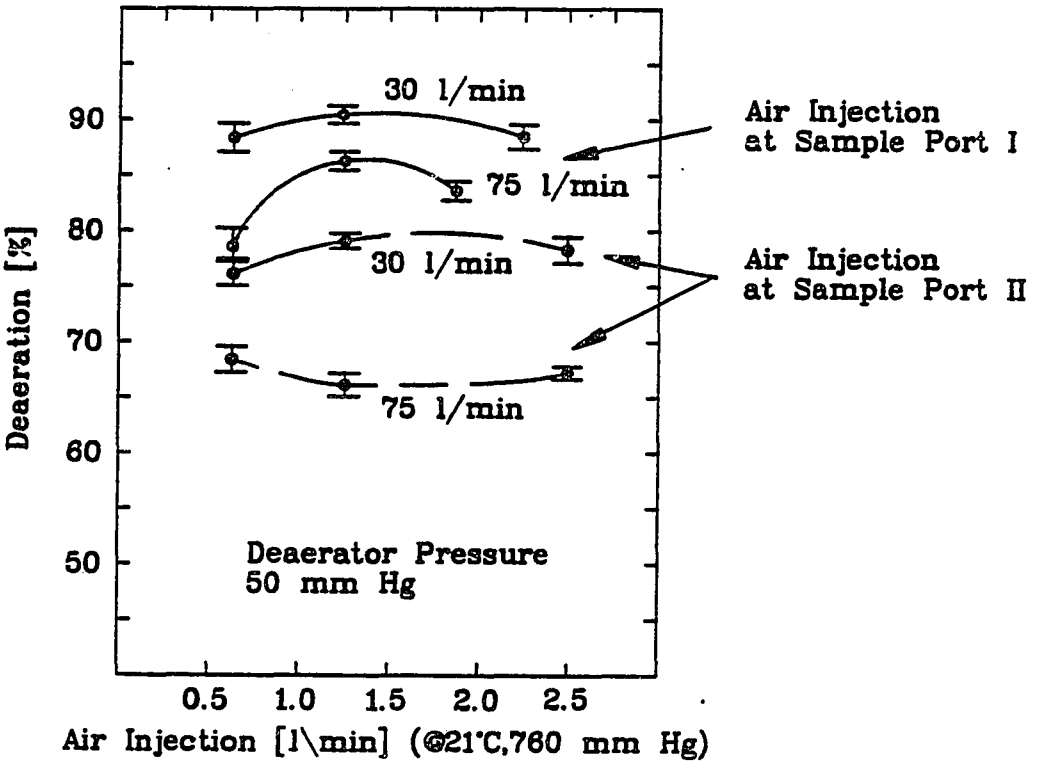

Figure 6.19 Phase II Comparison of Air Injection Locations

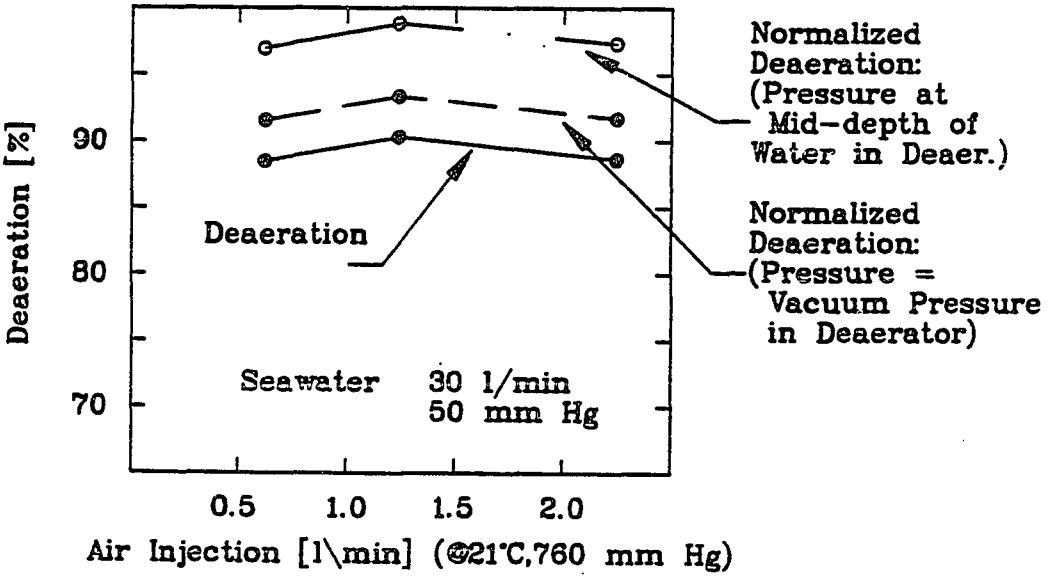

Figure 6.20 Phase II Deaeration Effectiveness

the pressure at the water surface and the pressure at the deaerator reservoir's mid-depth. In figure 6.20 the three assessments of desorption occurrences are shown. Whereas approximately 90% deaeration was measured, normalized deaeration approached 99% in the case of the saturation concentration was calculated for the mid-point of reservoir. The choice of this approach for calculation of saturation concentration seems appropriate as it was used for the batch experiments in chapter 4.3. The high normalized deaeration rates indicate that the desorption process can be deemed very effective.

Estimating the void ratio in the barometric leg and deaerator vessel was made difficult because the system pressure in the water column could not be determined. Inferring a hydraulic pressure distribution would give erroneous pressure magnitudes because of the relatively large fraction of injected volume. A qualitative assessment was tried for air injection at sample port II, which resulted in higher computed void ratios. The pressure at sample port I was assumed to be 36 mm Hg higher than the pressure above the water surface in the deaeartor. Volume ratios of air to water were calculated for different liquid flow rates, air injection rates, and vacuum pressures. Obtained results indicated maximum void ratios of about 25% and 13% for 30 and 75 l/min water flow, respectively, at 50 mm Hg abs.

It is expected that the generation of large bubble aggregates and the relative reduction of the small bubble fraction was responsible for the somewhat constant deaeration rate with increasing air injection rate.

6.6 Phase III: Reaeration in System Downcomer

6.6.1. Experimental Procedure

For this test sequence sample port II had a plexiglass block without openings. The air injector was located at sample port III. In order to strip the water of gases an additional air injector device was built. A coarse aeration stone held by an appropriate mount served as the sparging device. This assembly was located at sample port I. The air flow rate passing through the sparger was not measured volumetrically. Visual observation of the entrained bubbles was applied to estimate the maximum air flow rate which could be accommodated by the intake pipe. Water samples were extracted from the lower portion of the discharge debubbler vessel.

The system was operated as follows.The pressure in the deaerator and debubbler vessels was lowered and the water flow commenced. Well I was adjusted in height according to the desired water flow rate . Since high deaeration rates were desired, the pressure in the deaerator vessel was

low. It was held at 50 mm Hg for all reaeration tests. Air was permitted to enter the intake pipe through the sparging device.

With the water feed constant, adjustments were made on the discharge side. Without injection into the downcomer the water level in the debubbler was maintained at about 50 cm above its discharge opening. This water height was required to avoid bubbles, created by the overflow from the deaerator to the debubbler, being sucked into the discharge pipe. With a residual water level of 50 cm, the debubbler successfully separated the bulk of these bubbles from the discharge water stream. Adjustments of the water level in the debubbler were made by either lowering or raising the discharge well.

Water samples in well II were extracted through an orifice in the pipe wall. A rubber hose transported the sample water to a B.O.D. sample bottle.

Without air injection into the discharge pipe, a test sequence was carried out to determine the amount of indigenous reaeration, which is possibly due to small bubbles not separating in the debubbler and therefore becoming entrained in the discharge stream. In addition, the water level in the debubbler was recorded. For this to be done correctly it was important that the pressure in the deaerator and the connected debubbler be held constant during the entire test.

Several samples, usually six each, were withdrawn from the debubbler and well II. After collecting data with the initial setting, air was injected into the discharge using different air flow rates. It was observed that there was a maximum air flow rate which could be accommodated by the 3.8 cm pipe without significant water flow disturbances. Above this critical air injection rate the water flow in the downcomer separated downstream of the injection point. A flow pattern similar to a hydraulic jump developed. In addition, the water level in the debubbler rose significantly. After determining the critical air injection rates for the prevailing water flow, a range of suitable air injection rates was identified and tests with these air flow rates were carried out.

6.6.2. Results and Discussion

Experiments were conducted with fresh water and seawater. For seawater three water flow rates were used, namely 30, 55, and 75 l/min. Fresh water experiments were done with a flow rate of 55 l/min.

Calculation of reaeration rate was done using the following relationship:

$$\text{Reaeration} = \frac{C_W - C_D}{C_S - C_D} * 100 \ [\ \% \ ] \qquad (6.3)$$

where: C_W = dissolved oxygen concentration in the discharge well; C_D = concentration in debubbler.

Equation (6.3) simply compares the amount of oxygen added to the water to the amount which could be ideally added. It is obvious that the equilibrium concentration is dependent on the pressure of interest. In the present case the saturation concentration at atmospheric conditions was used. This provided a readily imaginable equilibrium state.

In figure 6.21 the dissolved oxygen concentrations measured in well -I are shown. For seawater the oxygen concentration in the discharge water increased with the amount of air injected at sample port III. The concentrations were higher for low water flow rates. The dissolved oxygen concentration of the fresh water effluent was fairly constant over the entire range of injection rates. Because there were relatively small experimental errors it can be assumed that fairly little oxygen was added to the fresh water flow. Figure 6.22 shows the reaeration rates calculated with equation (6.3).

The additional height required to compress the air in the effluent is given in figure 6.23 as a function of the air injection rate. The required height increased with higher injection rates, but decreased with high flow rates. Evidently fewer bubbles per unit volume were held in the pipe so that the required power for compressing the

bubbles was less for higher flow rates. Fresh water required more compression power than seawater at the same water flow rate. The reason for this may be the larger bubble sizes formed in fresh water due to coalescence. Larger bubbles have a greater rise velocity and therefore a longer residence time in the counter-current bubbly flow.

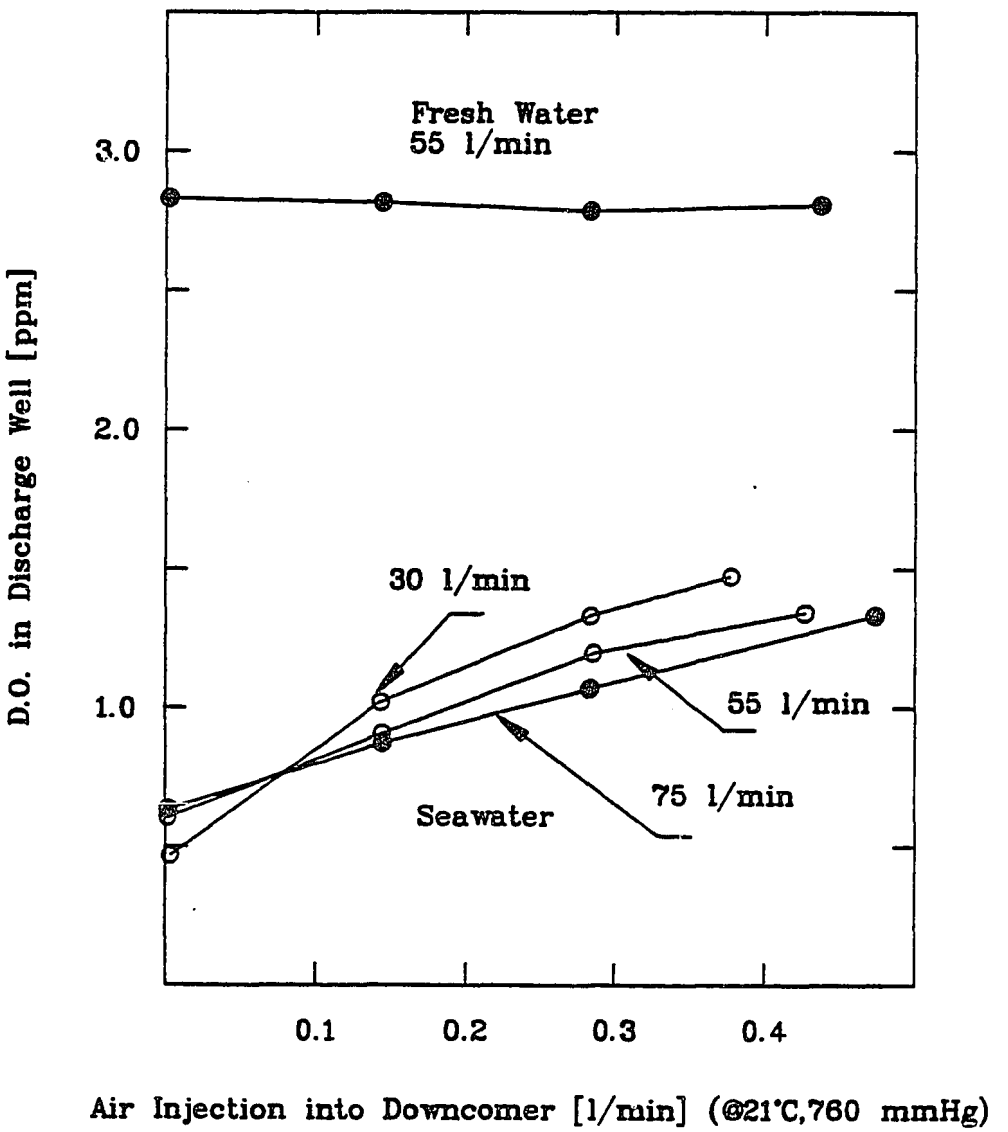

Figure 6.21 Phase III Reaeration in System Downcomer

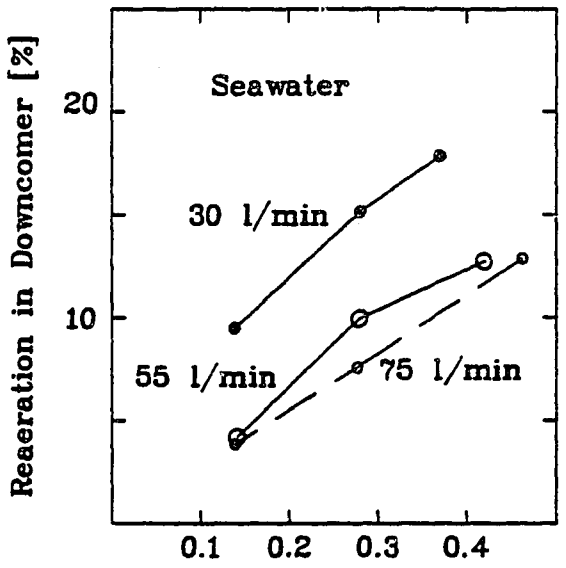

Figure 6.22 Phase III Reaeration Percentage in Downcomer

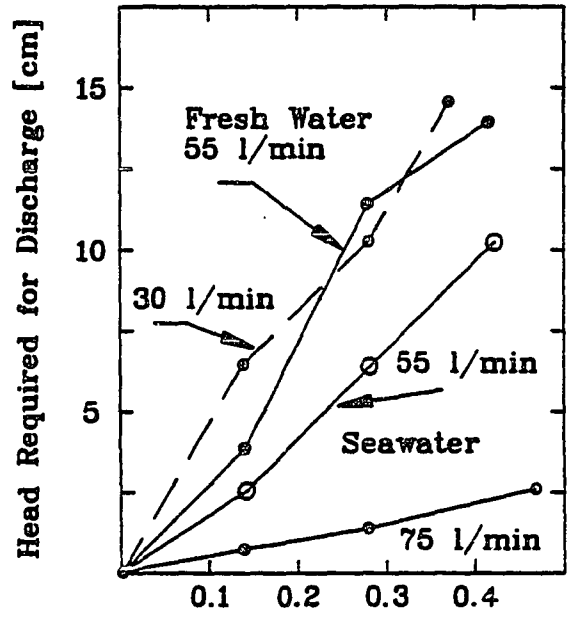

Figure 6.23 Phase III Additional Hydraulic Head for Discharge in Downcomer

CHAPTER VII

CONCLUSIONS AND RECOMMENDATIONS

7.1 Summary of Findings

Pertinent findings of the present experimental study are summarized as follows:

1) Single bubble aeration:

1.1. The experimental procedures used in this portion of the study resulted in good repeatability (generally within 5%).

1.2. The observed values for the liquid film transfer coefficient, k_L, were close to those reported in the literature [119], when small and medium bubble sizes were tested. For larger size bubbles and higher air flow rates the observed values for the transfer coefficient deviated from the literature values. Wall effects are probably responsible for this deviation.

1.3. Pressure pulses produced by a peristaltic pump caused considerable variations in transfer rates and resulted in greater than usual data scatter. Gas transfer rates generally increased when vibrations occurred during aeration.

1.4. The photographic procedure used in this portion of the study produced good measurements of bubble size and bubble residence time in the aeration column.

1.5. Identical settings controlling volumetric air injection rates and similar bubble sizes resulted in longer residence times of bubbles in the aeration column when using seawater than with fresh water. Thus, the speed of ascending bubbles is less in seawater than in fresh water.

1.6. the rise velocities of a string of single bubbles was measured to be approximately 10% smaller in seawater than in fresh water.

1.7. The overall transfer coefficient, K_L*a, for aeration was measured to be larger in seawater than in fresh water for small bubbles. When larger bubbles were used (4mm) the overall transfer coefficient was smaller in seawater than in fresh water.

1.8. The liquid film transfer coefficient, K_L, of seawater is smaller than or equal to that of fresh water.

2) Bubble swarm aeration:

2.1. The test procedures used in this portion of the study resulted in good repeatability of the test data (generally within 5%).

2.2. In order to study the effects of coalescence, the test set-up involved the use of an air stone which promoted multiple bubble formation at small distances, which resulted in bubble collisions.

2.3. The overall transfer coefficient for seawater , k_L*a, was measured to be between 2.7 to 3.7 times larger than

that for fresh water, for the range of air injection rates tested.

2.4. Offshore seawater, which is characterized by its relatively low surfactant content, had the same overall transfer coefficient, k_L*a, as filtered seawater, which was obtained from the Pacific Biomedical Research Center nearshore system. The transfer coefficient of this unfiltered coastal seawater was lower than for offshore or for filtered coastal seawater. Suspended matter and especially surfactants in these and other coastal waters apparently resulted in an increase in resistance to gas transfer.

2.5 Bubble coalescence was significantly less in seawater than in fresh water, thereby providing much larger liquid-gas interfacial area for gas transfer in seawater for the same gas flow.

2.6. A photographic procedure was the basis for estimating bubble size distributions in the plumes produced by air stone injection. Bubble coalescence was prominent in fresh water at higher air injection rates. Increased coalescence could also be observed in seawater at higher air injection rates. In this case, however, maximum sizes of bubbles were significantly smaller than in fresh water.

3) Bubble swarm deaeration:

3.1. The test procedure used in this portion of the study

resulted in good repeatability of test data (generally smaller than 6%).

3.2. The general air injection configuration was designed to minimize bubble coalescence. For the ranges of system test pressures and air injection rates, the overall transfer coefficients, k_L*a, for seawater was 8-14 times higher than that for fresh water.

3.3. Degasification was strongly dependent on the pressure exerted on the water surface in the vacuum vessel.

3.4. With appropriate system settings and a proper design, a deaeration rate of 85% is achievable with an injected air contact period of about 25 sec.

4) Single bubble deaeration:

4.1. Air injection during this portion of the study was conducted using capillary tubes. Bubbles were not brought into close contact with each other, and therefore no bubble coalescence occurred.

4.2. The overall transfer coefficient, k_L*a, for this test set-up was measured to be very similar for fresh water and seawater.

4.3. The overall transfer coefficient, k_L*a, for nitrogen was measured to be very similar to that for oxygen.

5) Bubble rise:

5.1. The terminal speeds of individual bubbles rising in

fresh water and in offshore seawater were determined to be similar. However, seawater bubbles showed slightly higher velocities.

5.2. Comparisons with literature values [24] suggested that the types of fresh water and seawater used in this study fall in the category of partially contaminated water.

5.3. The drag coefficients of bubbles rising in fresh water and seawater were determined to be similar. Drag coefficients in fresh water were found to have slightly higher values than seawater at higher Reynolds numbers.

5.4. Bubble rise velocities were observed to decrease from the time of detachment until terminal speed was reached. The distance required to attain terminal velocity was longer for bigger bubble sizes.

5.5. The rise distance required to attain terminal speed was measured to be shorter in natural waters, such as tapwater and seawater, than in the distilled water used in previous investigations [34].

6) Packed column deaeration experiments:

6.1. The test procedures and sampling methods used in this portion of the study resulted in good repeatability (generally within about 6%).

6.2. Heights of transfer unit, HTU, was found not to be a function of the vacuum pressure. HTUs were randomly distributed between upper and lower limits for all vacuum

pressures investigated. Upper and lower limits were 0.7 and 0.55 m for fresh water and 0.58 and 0.48 for seawater.

6.3. Comparing the median values of both HTU ranges, seawater HTUs were approximately 20% smaller than those of fresh water.

7) Gas transfer in the OC-OTEC test facility:

7.1. Extracting samples from a low pressure vessel requires a special sampling procedures to avoid aeration or deaeration of the sample water.

7.2. Previous OC-OTEC gas transfer investigations may have reported deaeration efficiencies which were biased by less than optimum sampling procedures.

7.3. An appropriate sampling procedure was conceived and tested in conjunction with the present deaeration and reaeration tests. This sampling technique allowed the extraction of water from subatmospheric pressures without inducing sample contamination. Conditions which affected sampling efficiency and which could result in erroneous readings were identified.

7.4. Deaeration rates observed in the barometric upriser without imposed bubble nucleation were in the range of 5% to 12%. Under these conditions the deaeration rates in seawater were measured to be less than in fresh water. (However, these results might be biased due to initial difficulties with the sampling procedure.)

7.5. Deaeration efficiencies in a water reservoir subjected to low system pressure without nuclei injection was dependent on the rate of renewal of the free surfaces. Deaeration was greater for higher flow rates due to increased turbulence, although the residence time of water in the reservoir was actually smaller for higher flow rates.

7.6. Deaeration rates increased significantly if bubble nuclei were injected into the reservoir. The amount of deaeration was greatly affected by the pressure in the reservoir.

7.7. Given the same bubble nuclei injection conditions, the maximum deaeration for fresh water was only approximately 40% of that for seawater.

7.8. Bubble nuclei injection into the upcomer pipe about 2m below the deaerator vessel increased the deaeration performance compared to air injection into the deaerator. Better mixing of the air and water in the upcomer was likely to be the responsible mechanism.

7.9. The deaeration process in the deaerator with air injection was very effective. Assuming the hydrostatic pressure at mid-depth in the deaerator indicated equilibrium conditions, the normalized deaeration approached 99%. This means that 99% of practically-achievable degasification occured.

7.10. Reaeration of previously degassed water in the 11 m

long barometric discharge pipe by means of air injection was observed to be possible for seawater. For fresh water no detectable increase of dissolved oxygen could be measured in the discharge of the downcomer.

7.11. Rates of reaeration increased with lower sea water flow rates due to the longer residence time of bubbles in the downcomer.

7.12. Maximum reaeration rates, expressed as a percentage of atmospheric conditions, were observed to be in the range of 12-18% for the liquid flow velocity range of 0.4-1.0 m/sec in the 11 m pipe section.

7.13. The power required to compress the injected air to form bubble nuclei was expressed as an additional water head of the discharge water column. Given the same conditions, fresh water requires more power than seawater to compress the injected air due to the increased residence time of the larger fresh water bubbles in the downcomer.

7.2 General Conclusions

General conclusions from all of the experiments conducted in this study can be summarized as follows:

1. Bubble coalescence is significantly less in seawater than in fresh water. Bubbles coalesce in seawater to a limited extend if flow conditions promote bubble

collisions; the magnitude of coalescence increases with the frequency and intensity of collisions

2. Gas transfer in seawater exceeds that of fresh water due primarily to the increased liquid-gas interfacial area resulting from the different coalescence behaviors.

3. Gas transfer rates in bubble aeration are the same in offshore and filtered Hawaiian coastal seawater. Suspended matter and surfactants in unfiltered coastal seawater reduce the overall transfer coefficient.

4. If bubbles do not coalesce, the magnitude of gas transfer is similar in fresh water and in seawater.

5. The liquid film transfer coefficient k_L in seawater is smaller than or equal to that of fresh water.

6. The overall transfer coefficient, k_L*a, for nitrogen in seawater and fresh water is similar to that of oxygen

7. Gas transfer in a packed column indicates a higher liquid film transfer coefficient for seawater. This higher transfer coefficient suggests that, under relatively uncontaminated conditions, seawater interfaces offer less resistance to gas transfer than do fresh water surfaces.

8. The terminal velocities of bubbles rising in seawater and fresh water are similar. The observed values are typical for bubbles rising in natural waters.

9. Rise speeds decrease as bubbles ascend and contaminants accumulate on bubble surfaces. The required

distance for the bubble to rise to reach terminal speed increases with bubble size and is substantially shorter in natural waters than in distilled water.

10. The rise speed of a bubble in the presence of other bubbles is higher than the rise speed of that bubble by itself. The difference is larger for fresh water than for seawater.

7.3. Design Recommendations for an OC-OTEC Deaerator

Design recommendations for an OC-OTEC deaeration process are summarized below:

1) Dearation effectiveness is strongly dependent on the pressure in the deaerator vessel. With low pressures the saturation concentration of dissolved gases is low which gives rise to a high driving force for gas transfer.

2) Deaeration rates are low if no bubble seeding occurs in the intake water. With air injection the degree of deaeration increases up to a point with the volume of injected air, provided that optimum air injection conditions prevail.

3) Deaeration rates in the barometric upcomer alone are insufficient for optimum OC-OTEC applications. A water reservoir has to be incorporated in the deaeration system to allow for a longer residence time of water at low pressure.

4) Injection of air should occur in the low pressure water reservoir and not in the barometric upriser. The observed increased deaeration effectivness due to injection into the barometric intake rather than injection into the reservoir, has to be regarded as specific for this experimental setting. Air injection into the barometric leg is likely to stimulate bubble coalescence because the injection procedure is likely to resemble flow characteristics of point injection.

5) Air injection should produce small bubbles. Air injection from widely separated stone injectors would avoid high concentrations of injected air and the resulting formation of larger size air slugs.

6) A preferable source for bubble nuclei for injection is the exhaust of the vacuum pumps. This procedure would have the advantage of discharging the air to a low pressure environment, and would thereby significantly reduce the power requirements for the vacuum compressor system.

7) The choice of the optimum depth of the water reservoir depends on two conflicting criteria: a) the water column has to be deep enough to provide sufficient residence time for rising bubbles ; b) the water column should not be too deep since the pressure exerted on bubbles would increase, thereby decreasing the deaeration performance of the system and requiring higher pressure at the injector.

8) The water reservoir is the main component of the

recommended deaeration process and serves the following functions: a) it allows a longer residence time of the intake water in a low pressure environment; b) it allows air injection to take place at low pressure; c) it provides a water body in which injected bubbles remain suspended for an adequate time for deaeration to occur; d) it provides a water body in which bubbles can rise to the surface and be separated from the process water before it enters the evaporator or the condenser (if direct contact condensation is used).

The recommended deaeration system is shown in figure 7.1.

For structural dimensioning the water flow rate is assumed to be in the order of 10 m^3/sec, which corresponds to a 5 MW power plant [19]. The residence time of water in the low pressure reservoir is assumed to be 25 sec. In the batch deaeration experiments this duration resulted in an 85% reduction of the dissolved gas content at a system pressure of 50 mm Hg.

As water rises through the upcomer its flow speed decreases as it enters an upcomer pipe section where the diameter gradually increases. The water is then guided to the outer reservoir by means of a large baffle plate.

Air stone injectors are located in a concentric pattern on the bottom of reservoir. The spacing of these injectors allows uniform air injection and avoids point

sources of high volume injection.

Vertical baffles are placed to separate the surface layers of the inner and the outer portions of the reservoir, in order to minimize the entrance of suspended bubbles to the inner portion of water reservoir, from which water enters the evaporator (or the direct contact condenser).

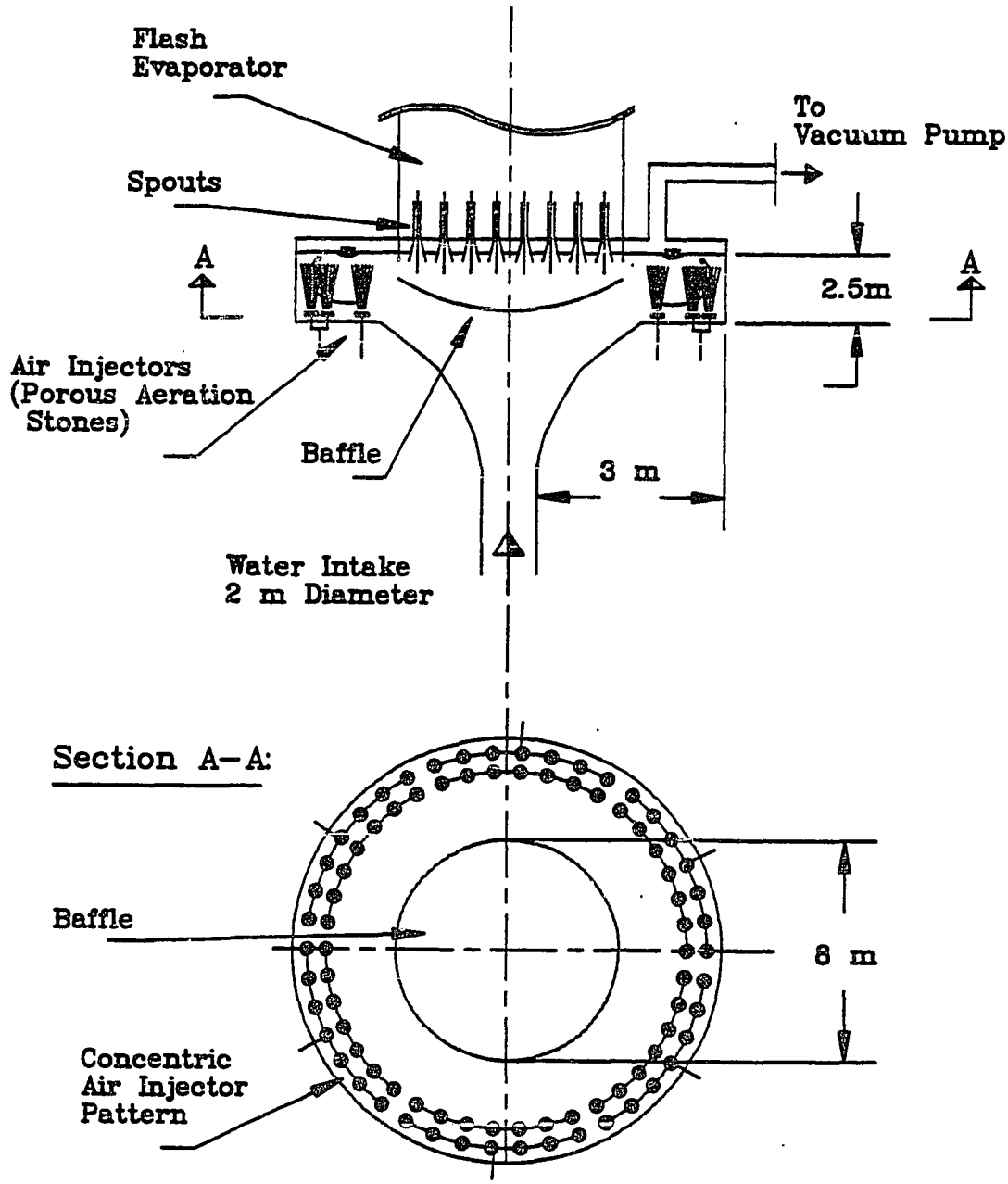

Figure 7.1 Prototype for Deaerator Device for a 5 MW OC-OTEC Plant

REFERENCES

1) Aieta, E.A. and Roberts, P.V. (1986) "Application of Mass-Transfer Theory to the Kinetics of Fat Gas-Liquid Reaction" Environmental Science Technology, Vol. 20, pg. 44-50

2) Akita, K. (1981) "Diffusivities of Gases in Aqueous Electrolyte Solutions" Ind. Eng. Chem. Fundam., Vol. 20, pg 89-94

3) Au-Yeung, P.H. and Ponter, A.B. (1983) "Estimation of Liquid Film Mass Transfer Coefficient for Randomly Packed Absorption Columns" The Canadian Journal of Chemical Engineering, Vol. 61, August 1983

4) Barczewski, B. (1979) "Innovative Measurements Techniques for Water-Air Mixtures and Their Application in Two-Phase Plumes" (in German) Institut fuer Wasserbau, University of Stuttgart, Stuttgart, West Germany

5) Barnhart, E.L. (1969) "Transfer of Oxygen in Aqueous Solutions" Journal of the Sanitary Engineering Division Proceedings of ASCE, June 1969, pg. 645-661

6) Benedek, A. and Heideger, W.J. (1971) "Effect of Additives in Turbine Aeration" Biotechnology and Bioengineering, Vol. 13, pg. 663-684

7) Benson, B.B. and Krause, D. (1980) "The Concentration and Isotopic Fractioning of Gases in Freshwater in Equilibrium with the Atmosphere: 1. Oxygen" Limnology and Oceanography, Vol. 25, No. 4, pg. 662-671

8) Betzer, P.R. (1984) "The Oceanic Carbonate System: A Reassessment of Biogenic Controls" Science, Vol. 226, pg. 1074-1077, November 1984

9) Bird, R.B., Steward, W.E. and Lightfoot, E.N. (1960) Transport Phenomena , John Wiley & Sons, New York

10) Bharathan, D. (1984) "Heat and Mass Transfer in Open-Cycle OTEC Systems" Heat Transfer Engineering, Vol. 5, No. 1, pg. 17-30

11) Bharathan, D. and Althof, J. (1984) "An Experimental Study of Steam Condensation on Water in Countercurrent Flow in the Presence of Inert Gases" Journal of ASME

12) Bilstad, T. and Lightfoot, E.N. (1984) "Simultaneous In-Situ Determination of Dissolved Gases by Gas Chromatography" in Gas Transfer at Water Surfaces, edit. by Brutsaert, W., D. Reidel Publishing Company

13) Blanchard, D.C. and Woodcock, A.H. (1957) "Bubble Formation and Modification in the Sea and its Meteorological Significance" Tellus, Vol. 9, No. 2, pg. 145-158

14) Blanchard, D.C. (1963) "The Electrification of the Atmosphere by Particles from Bubbles in the Sea" in Oceanography, Vol. I, edit. by Sears, M., The Macmillan Company

15) Blanchard, D.C. and Syzdek, L.D. (1972) "Concentration of Bacteria in Jet Drops from Bursting Bubbles" Journal of Geophysical Research, Vol. 77, No. 27, pg. 5087-99

16) Blanchard, D.C. and Syzdek, L.D. (1977) "Production of Air Bubbles of a Specified Size" Chemical Engineering Science, Vol. 32, pg. 1109-12

17) Blanchard, D.C. (1982) "The Production, Distribution, and Enrichment of the Sea-salt Aerosol" in Air-Sea Exchange of Gases and Particles, edit. by Liss, P.S. and Slinn, W.G.N., D. Reidel Publishing Company

18) Blanchard, D.C. (1986) Personal Correspondence with M.Zapka

19) Block, D.L. et al (1984) "Thermoeconomic Optimization of OC-OTEC Electricity and Water Production" Florida Solar Energy Center, Cape Canaveral, Florida

20) Broecker, W.S. and Peng, T.-H. (1984) "Gas Exchange Measurements in Natural System" in Gas Transfer at Water Surfaces, edit. by Brutsaert, D.R., D. Reidel Publishing Company, Boston

21) Burden, R.L. and Faires, J.D. (1981) Numerical Analysis, Third Edition, Prindle, Weber&Schmidt, Boston

22) Carlson, T.C.G. (1980) "OTEC - A Comprehensive Analysis" Mechanical Engineering, Vol.102, No.1, pg. 32-39

23) Claude, G. (1930) "Power from the Tropical Sea" Mechanical Engineering, Vol. 52, No. 12, pg. 1039-44

24) Clift, R., Grace, J.R. and Weber, W.E. (1978) Bubbles, Drops and Particles, Academic Press

25) Cohen, R. (1978) "An Overview of the U.S. OTEC Development Program" Proceedings of the ASME Energy Technology Conference, Houston

26) Cohen, R. (1980) "Energy from the Ocean Thermal Gradients" Oceans, Vol. 22, No. 4

27) Coppock, P.D. et. al. (1951) "The Behaviour of Gas Bubbles in Relation to Mass Transfer" Trans. Chem. Engrs., Vol. 29, pg. 75-86

28) Craver, C.E.Jr. (1975) "Absorption of Oxygen in Bubble Aeration" in Biological Treatment of Sewage and Industrial Wastes, edit. by McCabe, J. and Eckenfelder, W.W., Rheinhold Publishing Company, New York

29) Danckwerts, P.V. (1951) "Significance of Liquid-Film Coefficients in Gas Absorption" Industrial and Engineering Chemistry, Vol. 43, No. 6, pg. 1460-66

30) Danckwerts, P.V. (1970) Gas-Liquid Reactions, McGraw-Hill Book Company, New York

31) Dacies, R.M. and Taylor, Sir G. (1950) "The Mechanics of Large Bubbles Rising through Extended Liquids and through Liquids in Tubes" Proceedings of the Royal Society, Ser. A 200, pg. 375-390

32) Deckwer, W.-D. (1977) "Absorption and Reaction of Isobutene in Sulfuric Acid III" Chemical Engineering Science, Vol. 32, pg. 51-57

33) Detwiler, A. and Blanchard, D.C. (1978) "Aging and Bursting Bubbles in Trace-Contaminated Water" Chemical Engineering Science, Vol. 33, pg. 9-13

34) Detwiler, A. (1979) "Surface-Active Contamination on Air Bubbles in Water" in Surface Contamination, Vol.2, edit. by Mittal, K.L., Plenum Press, New York

35) Emmert, R.E. and Pigford, R.L. (1954) "A Study of Gas Absorption in Falling Liquid Films" Chemical Engineering Progress, Vol. 50, No. 2, pg. 87-93

36) Epstein, P.S. and Plesset, M.S. (1947) "On the Stability of Gas Bubbles in Liquid-Gas Solutions" The Journal of Chemical Physics, Vol. 18, No. 11

37) Fournier, T. (1985) "Open-Cycle Ocean Therma Energy Conversion: Experimental Study of Flash Evaporation" Proceedings of the 7th Conference OCEANS '85, Washington, D.C.

38) Fox, F.E. and Herzfeld, K.F. (1954) "Gas Bubbles with Organic Skin as Cavitation Nuclei" The Journal of the Acoustic Society of America, Vol. 26, No. 6, pg. 984-989

39) Fujie, K., Ishihara, N. and Kubota, H. (1980) "Mass Transfer Coefficient in Electrolyte Solutions" Journal of Ferment. Technology, Vol. 58, No. 5, pg. 477-484

40) Garrettson, G.A. (1973) "Bubble Transport Theory with Application to the Upper Ocean" Journal of Fluid Mechanics, Vol. 59, Part 1, pg. 187-206

41) Giles, R.V. (1962) Theory and Problems of Fluid Mechanics and Hydraulics, McGraw-Hill Book Company, New York

42) Goldberg, R. (1978) "Some Effects of Gas-Supersaturated Seawater on Spisula Solidissima and Argopecten Irradians" Aquaculture, Vol. 4, pg. 281-287

43) Goldman, J. and Dennett, M.R. (1983) "Carbon Dioxide Exchange Between Air and Seawater: No Evidence for Rate Catalysis" Science, Vol. 226, pg. 199-201

44) Golanty, E. (1984) "The Global Experiment: Carbon Dioxide and Ocean Temperature" Oceans, Vol. 1,pg. 66-69

45) Golshani, A. and Chen, F.C. (1980) "Ocean Thermal Energy Conversion Gas Desorption Studies: Vol. 1. Design of Experiments" Oak Ridge National Laboratory, Report ORNL/tm-7438/v1

46) Golshani, A. and Chen, F.C. (1981) "Ocean Thermal Energy Conversion Gas Desorption Studies: Vol. 2. Deaeration in a Packed Column and a Barometric Intake System" Oak Ridge National Laboratory, Report ORNL/tm-7438/v2

47) Golshani, A. and Chen, F.C. (1983) "A Study of Hydraulic Air Compression for Ocean Thermal Energy Conversion Open Cycle Applications" Oak Ridge National Laboratory, Oak Ridge

48) Gucinski, H. (1986) "Bubble Coalescence in Seawater and Freshwater: Requisites for an Explanation" in Oceanic Whitecaps and their Role in Air-Sea Exchange Processes, edit. by Monahan, E.C., D. Reidel Publishing Company, Boston

49) Guinasso, N.L. and Schink, D.R. (1973) "A Simple Physicochemical Acoustic Model of Methane Bubbles Rising in the Sea" Department of Oceanography, Texas A&M University

50) Gurol, M.D. and Nekouinani, S. (1985) "Effect of Organic Substances on Mass Transfer in Bubble Aeration" Journal WWPCF, Vol. 57, No. 3, pg. 235-240

51) Haberman, W.L. and Morton, R.K. (1956) "An Experimental Study of Bubbles Moving in Liquids" Transactions of the American Society of Civil Engineering, Vol. 121, pg. 227-250

52) Hanbury, W.T. and McCartney, W. (1973) "Nucleation in the Flash Boiling of Sea Water" Desalination, Vol. 14, pg. 217-228

53) Haney, P.D. (1954) "Theoretical Principles of Aeration" Journal of American Water Works Association, Vol. 46, April 1954, pg. 353-376

54) Harbaum, K.L. and Houghton, G. (1962) "Effects of Sonic Vibration on the Rate of Absorption of Carbon Dioxide in Gas Bubble-Beds" Journal of Applied Chemistry, Vol. 12, pg. 234-240

55) Hentschel, W. and Lauterborn, W. (1985) "High Speed Holographic Movie Camera" Optical Engineering, Vol. 24, No. 4, pg. 687-691

56) Hewitt, G.F. (1970) Annular Two-Phase Flow, Pergamon Press, Oxford

57) Himmelblau, D.M. (1964) "Diffusion of Dissolved Gases in Liquids" Chemical Review, Vol. 64, pg. 527-550

58) Himmelblau, D.M. (1972) Basic Principles and Calculations in Chemical Engineering, 2nd edition, Prentice-Hall, Englewood, New Jersey

59) Hitchman, M.L. (1978) Measurement of Dissolved Oxygen, John Wiley & Sons, New York

60) Ho, K.W.A. and Benedek, A. (1975) "Effect of Electrolytes on Aeration" in Chemistry and Physics of Aqueous Gas Solutions, edit. by, Adams, W.A., The Electrochemical Society

61) Homan, J.P. (1981) Heat Transfer, 5th edition, McGraw Hill, New York

62) Horne, R.A. (1969) Marine Chemistry: The Structure of Water and the Chemistry of the Hydrosphere, John Wiley&Sons, New York

63) Houghton, G.R. and Thompson, J.A. (1957) "Velocity of Rise of Air Bubbles in Seawater and their Types of Motion" Chemical Engineering Science, Vol. 7, pg. 111-112

64) Hunter, J.A. (1967) Research and Development Report No. 34, Office of Saline Water

65) Hwang, H.J. and Stenstrom, M.K. (1985) "Evaluation of Fine-Bubble Alpha Factors in Near Full-Scale Equipment" Journal WPCF, Vol. 57, No. 12, pg. 1142-1151

66) Ippen, A.T. and Carver, C.A. (1954) "Sewage Works: Basic Factors of Oxygen Transfer in Aeration Systems" Sewage and Industrial Wastes, Vol. 26, No. 7, pg. 813-827

67) Ito, F. (1986) "Operational Experiences of Nauru 100 kW OTEC and its Subsequent Research" Personal Correspondence with M. Zapka

68) Johnson, B.D. and Cook, R.C. (1979) "Bubble Populations and Spectra in Coastal Waters: A Photographic Approach" Journal of Geographic Research, Vol. 84, No. C7, pg. 3761-3765

69) Johnson, B.D. and Cook, R.C. (1980) "Organic Particle and Aggregate Formation Resulting from the Dissolution of Bubbles in Seawater" Limnology and Oceanography, Vol. 25, No. 4, pg. 653-661

70) Johnson, B.D. and Cook, R.C. (1981) "Generation of Stabilized Microbubbles in Seawater" Science, Vol. 213, July 1981

71) Johnson, D.H. (1982) "The Exergy of the Ocean Thermal Resource and the Second-Law Efficiency of Idealized Ocean Thermal Energy Conversion Power Cycles" Solar Energy Research Institute, Golden, Colorado

72) Johnson, P.A. and Babb, A.L. (1956) "Liquid Diffusion of Non-Electrolytes" Chemical Reviews, Vol. 56, pg. 387-453

73) M.W. Kellogg Company (1975) "Saline Water Conversion Engineering Data Book - 1975" Office of Water Research and Technology, October 1975

74) Knoedler, E.L. and Bonilla, C.F. (1954) "Vacuum Degasification in a Packed Column" Chemical Engineering Progress, Vol. 50, No. 3, pg. 125-133

75) Krock, H.-J. (1981) "Gas Analysis of Water Samples for OTEC Program" J.K.K. Look Laboratory, Technical Report No. 51, Dept. of Ocean Engineering, University of Hawaii

76) Krock, H.-J. and Zapka, M.J. (1986) "Gas Evolution in Open-Cycle OTEC" Proceed. of 5th Symposium of Offshore Mechanics and Arctic Engineering, Tokyo, Japan

77) Larsen-Basse, J., Sonwalkar, N. and Seki, A. (1986) "Preliminary Seawater Experiments with OC-OTEC Spout Evaporator" Oceans' 86, Washington D.C.

78) LeBlond, P.H. (1969) "Gas Diffusion from Ascending Gas Bubbles" Journal of Fluid Mechanics, Vol. 35, No. 4

79) Lee, J.C. and Meyrick, D.L. (1970) "Gas-Liquid Interfacial Areas in Salt Solutions in an Agitated Tank" Trans. Instn. Chem. Engrs., Vol. 48, pg. 37-45

80) Lessard, R.R. and Zieminski, S.A. (1971) "Bubble Coalescence and Gas Transfer in Aqueous Electrolytic Solutions" Ind. Eng. Chem. Fundam., Vol. 10, No. 2, pg. 260-268

81) Lewis, W.K. and Whitman, W.G. (1924) "Principles of Gas Absorption" Industrial and Engineering Chemistry, Vol. 16, No. 12, pg. 1215-1220

82) Lewis, G.N. and Randall, M. (1961) Thermodynamics, 2nd edition, McGraw-Hill Book Company, New York

83) Liebermann, L. (1957) "Air Bubbles in Water" Journal of Applied Physics, Vol. 28, No. 2, pg. 205-210

84) Lindenmuth, W. et. al. (1982) "Seawater Deaeration in OC-OTEC Risers" Technical Report 3031-1, Hydronautics, Inc., Laurel, MD

85) Liu, J.L. (1970) "The Determination of the Rate of Diffusion of Dissolved Gases in Saline Waters" Master of Science Thesis, Dept. of chemical Engineering, University of Maine, Orono

86) Loeb, L.B. (1931) Nature of a Gas, John Wiley & Sons, New York

87) Macdonald, R.W. and Wong, C.S. (1975) "Factors Influencing the Degree of Saturation of Gases in Seawater" in Chemistry and Physics of Aqueous Gas Solution, edit. by, Adams, W.A., The Electrochemical Society

88) Mancy, K.H. and Okun, D.A. (1960) "Effects of Surface Active Agents on Bubble Aeration" Journal of Water Pollution Control Federation, Pg. 351-364, April 1960

89) Mancy, K.H. and Barlage, W.E. Jr. (1974) "Mechanism of Interference of Surface Active Agents with Gas Transfer in Aeration Systems" in Advances in Water Quality Improvements, Water Resources Symposium No. I, edit. by Gloyna, E.F. and Eckenfelder, W.W., University of Texas Press, Austin

90) Mason, E.A. and Monchick, L. (1962) "Transport Properties in Polar-Gas Mixtures" The Journal of Chemical Physics, Vol. 36, No. 10, pg. 2746-2757

91) Martin, C.S. (1976) "Vertical Downward Two-Phase Slug Flow" Journal of Fluid Engineering, Vol. 98, No. 12, pg. 715-722

92) Medwin, H. (1977) "In-Situ Acoustic Measurements of Microbubbles at Sea" Journal of Geophysical Research, Vol. 82, No. 6, pg. 971-976

93) Merlivat, L. and Memery, L. (1983) "Gas Exchange Across an Air Water Interface: Experimental Results and Modeling of Bubble Contribution to Transfer" Journal of Geophysical Research, Vol.88, No. C1, pg. 707-724

94) Miyagi, O. (1925) "On Air Bubbles Rising in Water" Phil. Mag. S., Vol. 50, No. 295, pg. 113-141

95) O'Brian, R.N. and Hyslop, W.F. (1975) "A Fabry-Perot Interferometer for Monitoring Gas-Liquid Exchange" in Chemistry and Physics of Aqueous Gas Solutions, edit. by, Adams, W.A., The Electrochemical Society

96) Panchal, C.B. and Bell, K.J. (1986) "Simultaneous Production of Desalinated Water and Power Using a Hybrid-Cycle OTEC plant" Argonne National Laboratory, Argonne

97) Parson, B.K. and Link, H.F. (1985) "System Studies of Open-Cycle OTEC Components" Proceedings of OCEANS '85, Vol. 2, Washington, D.C.

98) Parson, B. (1984) "Open-Cycle OTEC Thermal-Hydraulic Systems Analysis and Parametric Studies" Proceedings of OCEAN '84, Washington, D.C.

99) Pasveer, A. (1955) "Research on Activated Sludge; VI. Oxygenation of Water with Air Bubbles" Sewage and Industrial Wastes, Vol. 27, No. 10, October 1955, pg. 1130-1146

100) Penney, T. and Shelpuk, B. (1981) "An Overview and Recent Progress on Open-Cycle OTEC Power Systems" Proceedings of the 8th Ocean Energy Conference, Washington, D.C.

101) Penney, T. et. al. (1984) "Open-Cycle Ocean Thermal Energy Conversion (OTEC) Research: Progress and a Design Study" Journal of the ASME

102) Penney, T.R. and Bharanthan, D. (1987) "Power from the Sea" Scientific America, pg. 86-92, January 1987

103) Pijanowski, B.S. (1975) "Dissolved Oxygen Sensors-Theory of Operation, Testing and Calibration Techniques" in Chemistry and Physics of Aqueous Gas Solutions, edit. by, Adams, W.A., The Electrochemical Society

104) Pouder, C. (1986) "Sodium Chloride and Water Temperature Effects on Bubbles" in Oceanic Whitecaps and their Role in Air-Sea Exchange Processes, edit by, Monahan,E.C., D. Reidel Publishing Company, Boston

105) Rasquin, E.A., Lynn, S. and Hanson, D.N. (1977) "Vacuum Degassing of Carbon Dioxide in Packed Columns" Ind. Eng. Chem. Fundam., Vol. 16, No. 1, pg. 103-108

106) Ratcliff, G.A. and Holdcroft, J.G. (1963) "Diffusivities of Gases in Aqueous Electrolyte Solutions" Trans. Instn. Chem. Engrs., Vol. 41, pg. 315-318

107) Reith, T. and Beek. W.J. (1970) "Bubble Coalescence Rates in a Stirred Tank Contractor" Trans. Instn. Chem. Engrs., Vol. 48, pg T63-67

108) Resch, F.J. Darrozes, J.S. and Afeti, G.M. (1986) "Marine Liquid Aerosol Production From Bursting of Air Bubbles" Journal of Geophysical Research, Vol. 91, No. C1, pg. 1019-1029, January 1986

109) Rey, M., Lecoffre, Y. and Poux, J. (1981) "Open-Cycle Seawater Evaporation and Gas Venting Studies" NEYRTEC, Div. of Alstrom-Atlantique, Grenoble, France

110) Rice, W. (1976) "Performance of Hydraulic Gas Compressors" Journal of Fluid Engineering, Vol. 98, No. 12

111) Rietema, K. and Ottengraf, S.P.P. (1970) "Laminar Liquid Circulation and Bubble Street Formation in a Gas-Liquid System" Trans. Instn. Chem. Engrs., Vol. 48, pg. 54-62

112) Ridgeway, S.L. (1975) "The Mist Flow Ocean Thermal Energy Conversion Plant" Proceedings of the Fourth Ocean Thermal Energy Conversion Conference, New Orleans

113) Rowlingson, J.S. (1963) The International Encyclopedia of Physical Chemistry and Chemical Physics: Volume 5, The Perfect Gas, The MacMillan Company, New York

114) Sherwood, T.K. and Holloway, F.A.L. (1940) "Performance of Packed Towers - Liquid Film Data for Several Packings" Chemical Engineering Progress, Vol. 36, No. 21, pg. 39-70

115) Sonwalkar, N. (1986) "Preliminary Thermal Hydraulic Studies on Spout Evaporator for Open-Cycle Ocean Thermal Energy Conversion Application" M.S. Thesis, Dept. of Mechanical Engineering, University of Hawaii, Honolulu, Hawaii

116) Speece, R.E., Adams, J.L. and Wcolridge, C.B. (1969) "U-Tube Aeration Operation Characteristics" Journal of the Sanitary Engineering Division, Proc. of the ASCE, No. 95, pg. 563-574, June 1969

117) Streeter, V.L. (1966) Fluid Mechanics, fourth edition, McGraw-Hill Book Company, New York

118) Stuart, R.V. (1983) Vacuum Technology, Thin Films and Sputting, Academic Press, New York

119) Valentine, F.H.H. (1967) Absorption in Gas-Liquid Dispersion, E.& F.N. Spon, Ldt., London

120) Wassel, A.T., Bugby, D.C. and Mills, A.F. (1982) "Bubble Nucleation and Growth in Open-Cycle Ocean Thermal Energy Conversion Subsystems" Science Application International, El Segundo, California

121) Weiss, R.F. (1970) "The Solubility of Nitrogen, Oxygen and Argon in Water and Seawater" Deep-Sea Research, No. 17, pg. 721-735

122) Wolf, K.L. (1957) Physics and Chemistry of Interfaces (in German) Springer Verlag, Berlin

123) Woodcock. A.H. (1955) "Bursting Bubbles and Air Pollution" Sewage and Industrial Wastes, Vol. 27, No. 10, pg. 1189-1192

124) Wylen, G.J. and Sonntag, R.E. (1978) Fundamentals of Classical Thermodynamics, John Wiley & Sons, New York

125) Wyman, J. (1952) "On the Stability of Gas Bubbles in Seawater" Journal of Marine Research, Vol. 11, pg. 47-62

126) Yoshida, F. and Tanaka (1951) "Air-Water Contact Operations in a Packed Column" Industrial and Engineering Chemistry, Vol. 43, No. 6, pg. 1467-1473

127) Young, H.D. (1962) Statistical Treatment of Experimental Data, McGraw-Hill Book Company, New York

128) Zieminski, ,S.A., Goodwin, C.C. and Hill, R.L. (1960) "The Effect of Some Organic Substances on Oxygen Absorption in Bubble Aeration" Tappi, Vol. 43, No. 12, pg. 1029-1034